Functional and structural characterisation of the Eop1 effector from *Erwinia amylovora* and related species

A thesis submitted to Massey University for the degree of

Master of Science

in

Plant Breeding

MASSEY
UNIVERSITY
TE KUNENGA KI PŪREHUROA
UNIVERSITY OF NEW ZEALAND

School of Agriculture and Environment

Vishant Tomar

December 2022

Abstract

Erwinia amylovora is the etiologic agent of the fire blight disease of apples (*Malus* species), pears (*Pyrus* species), and many other members of the Rosaceae family. Fire blight affects virtually all pome species and encompasses major pome fruit-producing countries worldwide. Moreover, it is gradually progressing into the far east Asian countries, which hold a prime position in the pome fruits production.

Management of the fire blight disease is challenging due to the lack of effective control measures capable of suppressing its necrogenic effects in the diseased plants or restricting the pathogen's spread. Using resistant cultivars for pome fruit production is one of the most environmentally friendly and sustainable methods. However, it is not a permanent solution due to the pathogen's ability to evolve and overcome host resistance by employing proteinaceous virulence factors termed 'effectors' and restoring host susceptibility. This dynamism of host-pathogen molecular interactions and their role in disease development in the host plant and eliciting an immune response in the non-host plant necessitates a thorough understanding of pathogen-delivered effectors, their mechanisms, and host targets.

In this study, non-host resistance was used to decipher the activity, molecular mechanism, and potential host targets of Eop1, one of the effectors secreted by *E. amylovora* and many other related species during pathogenesis. Firstly, it is demonstrated that Eop1 and its sequence homologs function as a 'putative' avirulence factor in the non-host plant *Nicotiana tabacum*. Following that, evidence was produced to show that the effector utilises an enzymatic mechanism for its activity; additionally, Eop1s' tertiary structure and catalytic motif were also examined using *in-silico* protein modelling. Moreover, it was discovered that RIN4, a plant immune regulator, and an R-protein, RPA1, are crucial for the Eop1s' recognition in the tobacco plant. Finally, by

connecting all the aforementioned pieces of evidence, a model for Eop1s' activity and its recognition in the host and non-host plants is proposed, which follows the 'guard' paradigm of effector recognition.

A thorough understanding of the Eop1 effectors, including their structure, activity mechanism and host targets, would contribute to a better understanding of host-pathogen interaction in the *Erwinia*-Rosaceae pathosystem, ultimately assisting in the delivery of elite cultivars with durable resistance.

Acknowledgements

"If I have seen further, it is by standing on the shoulders of Giants."

Sir Isaac Newton (1642-1727)

The aforementioned quote by Sir Isaac Newton (1675) summarises the fundamental foundation of all scientific endeavours ever made by any human. Also, it signifies that no piece of scientific work is complete without acknowledging the work and effort of those "*Giants*". Similarly, the work conducted in this research would only be 'complete' after recognising the efforts of the people who have contributed to this work directly or indirectly.

First and foremost, I would like to thank my supervisors: Dr. Erik HA Rikkerink[1], Dr. Svetla Sofkova-Bobcheva[2], and Dr. Vincent GM Bus[3], for their absolute support and unshakable belief in me and my work, especially when I was struggling to believe in my own abilities (thanks to imposter syndrome!). I am also grateful to my lab mentors, Dr. Jay Jayaraman[1] and Dr. Minsoo Yoon[1], for not only mentoring me in the lab but also answering all my scientific and 'not-so-scientific' queries with incredible patience and enthusiasm.

I'd also like to thank the Plant and Food Research (PFR) MARC level-6 team for a friendly and supportive environment and for making the MSc journey a 'life-changing' experience. Additionally, I extend my special thanks to Lauren Hemara[4], Erin Stroud[4], and Liz Florez[4] for the excellent and informative lab-tutorial sessions. Moreover, I also appreciate the PFR's plant team:

[1] Plant and Food Research, Mount Albert, Auckland, New Zealand, 1025.
[2] Massey University, School of Agriculture and Environment, Tennent Drive, Palmerston North, New Zealand, 4410.
[3] Plant and Food Research, Havelock North, Hawkes Bay, New Zealand, 4130.
[4] Ph.D. students at Plant and Food Research, Mount Albert, Auckland, New Zealand, 1025.

Monica Dragulescu[1], G. Wadasinghe[1], and Sumathi Tomes[1], for providing the plant material used in the study.

I acknowledge and appreciate the Pear Research Institute of the Rural Development Administration (RDA), Republic of Korea, for the funding, without which this research endeavour would not have been possible. I would also take this opportunity to show my gratitude and appreciation to Dr. Janghoon Song[5] for his interest in the Eop1 research and for providing insight into relations between overseas research organisations.

I am also grateful to my family, friends and well-wishers who supported me during my 'thick and thin'. Finally, and perhaps most importantly, I express my deepest gratitude to all the researchers whose preceding work I have used directly and indirectly in the presented research.

I would also like to put forward a verse from the Hindu scripture: Bhagavad Gītā (Chapter 2, Verse: 47), that provided me with much necessary strength during tough times:

कर्मण्येवाधिकारस्ते मा फलेषु कदाचन।

मा कर्मफलहेतुर्भूर्मा ते सङ्गोऽस्त्वकर्मणि॥ २-४७

The translation:

"You have the right to work only but never to its fruits. Let not the fruits of action be your motive, nor let your attachment be to inaction."

[5]Pear Research Institute, Rural Development Administration (RDA), Republic of Korea, 58216.

A note to the reader

Firstly, thanks for your interest in the science of host-microbe interaction, fire blight disease, and resistance breeding strategies and for referring to this research work. I hope it provides you with the insight you seek. This thesis has been designed to provide a comprehensive understanding of the researched topic; consequently, you will find that the thesis has been broadly divided into 3 major sections, which are as follows:

I. The first section begins with a 'General Introduction' (Chapter 1), reviewing the contemporary literature on the researched topic. It aims to provide the necessary background knowledge, which is crucial to understand the subsequent research. This section ends by pointing out some significant findings from the literature that form the basis of the 'central research theme' under investigation, finally culminating with the 'research questions'.

II. The second section focuses on specific chapters (Chapters 2, 3 and 4) that address one or two 'research questions' by formulating the hypotheses and their testing via experimentation. These 'specific chapters' are further divided into 5 sub-sections: (1) Introduction, (2) Material and Methods, (3) Results, (4) Conclusion and (5) Discussion. The chapter-specific 'Introduction' section was included to address the 'Why and how' questions of the central research theme under investigation in each chapter. The procedure of the experiments is included in the 'Material and Methods' section. The results obtained from the experiment are presented in the 'Result' section, the analysis of which is presented in the 'Discussion' section. Finally, the 'Conclusion' section focuses on comprehending and threading the obtained results with the previous experimental results and forming the platform for the subsequent research work.

III. The third section, ‘Discussion of the Research’ (Chapter 5), thoroughly summarises all the results obtained from the experiments conducted in the study and talks about their significance. The research findings are then woven together to expound further on the ‘future research prospects’ and ‘potential challenges’ and to ‘propose models’ for the molecular recognition mechanism of the Eop1 effectors and potential durable resistance in pome fruits.

In addition to the sections mentioned above, the thesis also incorporates a section titled ‘Additional Research’ (Chapter 6) to include the research work that was conducted in line with the thesis but was not finished due to the limited time frame. Furthermore, at the end of the thesis, an ‘Appendix’ section has been included to contain all of the supplementary research material. Also, ‘footnotes’ were put forward to explain concepts or provide additional information wherever deduced necessary, which can be found at the foot of the corresponding pages. (See footnote ‘6’ for the information on the font style and size convention used in the thesis).

I wish you a very happy reading.

Thanks and regards,

Vishant Tomar (The Author).

[6] Font style and font size convention used in the thesis: Thesis body = Times New Roman (12) with double Spacing; Images and tables = Arial (11) with a Spacing of 1.5; Footnote = Calibri (10) with Spacing of 1.

List Of Contents

List Of Figures

List of figures in the Appendix section

Supplementary Figures: Chapter 2

Supplementary Figures: Chapter 3

Supplementary Figures: Chapter 4

Supplementary Figures: Chapter 5

Supplementary Figures: Chapter 6 (Additional research)

Plasmid map of the vectors

List of TABLES

Abbreviations

General Abbreviations

aa	Amino acid
ABG	Adelaide Botanic Gardens
AcCoA	Acetyl coenzyme A
AI	Artificial intelligence
AVP	Adenoviral protease
Avr	Avirulence
B&S	Bait-and-switch model
BLAST	Basic local alignment search tool
bp	Base pair(s)
CaMV	Cauliflower mosaic virus
ccdB	Control of cell death B
CE	Christian Era
CFU	Colony forming unit
Co-IP	Co-immunoprecipitation
CSI	Conserved signature indels
CTR	Catalytic triad residues
DH	Decoy hypothesis
DNA	Deoxyribonucleic acid
DNase	Deoxyribonuclease
dNTPs	Deoxynucleotide triphosphates
dpi	Days-post infiltration
dsDNA	Double-stranded DNA
EDTA	Ethylenediaminetetraacetic acid
EF-Tu	Elongation factor thermal unstable Tu
EGTA	Ethylene glycol-bis(β-aminoethyl ether)-N,N,N′,N′-tetraacetic acid

Eop1	*Erwinia* outer protein 1
EPPO	European and Mediterranean Plant Protection Organization
ETI	Effector-triggered immunity
ETS	Effector-triggered susceptibility
EV	Empty Vector
Fb	Fire blight
G-F-G	Gene-For-Gene
GH	Guard hypothesis
hp	hairpin (silencing construct)
hpi	Hours post infiltration
HR	Hypersensitive response
IAA	Indole-3-acetic acid
IP6	Inositol hexakisphosphate
LB	Lysogeny broth
LG	Linkage group
LRR	Leucine-rich repeat
MAMP	Microbe-associated molecular patterns
MAPK	Mitogen-activated protein kinases
MES	2-(N-morpholino) ethanesulfonic acid
MLSA	Multilocus sequence analysis
*Mr*5	*Malus robusta* 5
MSRE	Methylation-sensitive restriction enzyme
NB	Nucleotide-binding
NB-LRR	Nucleotide-binding and leucine-rich repeat
*Nb*RIN4	*Nicotiana benthamiana* RIN4
NEB	New England Biolabs
NMR	Nuclear magnetic resonance
NRC	NLR required for cell-death

*Nt*RIN4	*Nicotiana tabacum* RIN4
OD_{600}	Optical density (measured at a wavelength of 600 nm)
ORF	Open reading frame
PCR	polymerase chain reaction
PFR	Plant and Food research
PRR	Pattern recognition receptors
Psa	*Pseudomonas syringae* pv. actinidiae
Psy	*Pseudomonas syringae* pv. syringae
PTI	Pattern-triggered immunity
RBGM	Royal Botanic Gardens of Melbourne
RCF	Relative centrifugal force
RDA	Rural development administration
RIN4	RPM1-Interacting protein 4
RLCK	Receptor-like cytoplasmic kinase
RNA	Ribonucleic acid
RNAi	RNA interference
RNase	Ribonuclease
RPA1	Resistance to *Pseudomonas syringae* pv. actinidiae 1
RPM	Revolutions per minute
RPM1	Resistance to *Pseudomonas syringae* pv. maculicola 1
R-gene/s	Resistance gene/s
R-protein/s	Resistance protein/s
RPS2	Resistance to *Pseudomonas syringae* protein 2
rRNA	ribosomal RNA
RT-PCR	Reverse transcription PCR
SDM	Site-directed mutagenesis
SNP	Single nucleotide polymorphism
ssDNA	single-stranded DNA

T3SE/s	Type-III secretion system effector/s
T3SS	Type-III secretion system
TAE	1X Tris-Acetate-EDTA
UK	United Kingdom
Ulp1	Ubiquitin-like protease 1
USA/US	United States of America
UTR	untranslated region
WGD	Whole genome duplication
WT	Wildtype
WUI	Web user interface
YopJ	*Yersinia* outer protein J

Abbreviations for general and SI units

$	Dollar
%	Percentage
°C	Degrees Celsius
µF	Microfarad
µS	Microsiemens
cm	Centimeter(s)
g	Gram(s)
L	Litre(s)
mL	Millilitre(s)
mM	Millimolar
ng	Nanogram(s)
V	Volt(s)
v/v	Volume per volume
w/v	Weight per volume
µg	Microgram(s)

μL	Microlitre(s)
μM	Micromolar
Ω	Ohm(s)

1 Chapter 1: General Introduction

1.1 Introduction to *Erwinia amylovora*

The fire blight disease, caused by the gram-negative bacterial pathogen *Erwinia amylovora* (Burrill) (Winslow et al., 1920), is one of the most destructive necrogenic diseases of apple and pear. It also causes disease in many other wild and cultivated members of the Rosaceae family (Khan et al., 2011; Malnoy et al., 2012; Vanneste, 2000). Characteristically, *E. amylovora* is a rod-shaped, facultatively anaerobic, non-sporulating bacterium that employs peritrichous flagella for its motility (Figure 1.1) (Paulin, 2000). Furthermore, it is the first bacterial pathogen that was demonstrated to cause disease in plants via Koch's postulate (Baker, 1971; Oh & Beer, 2005).

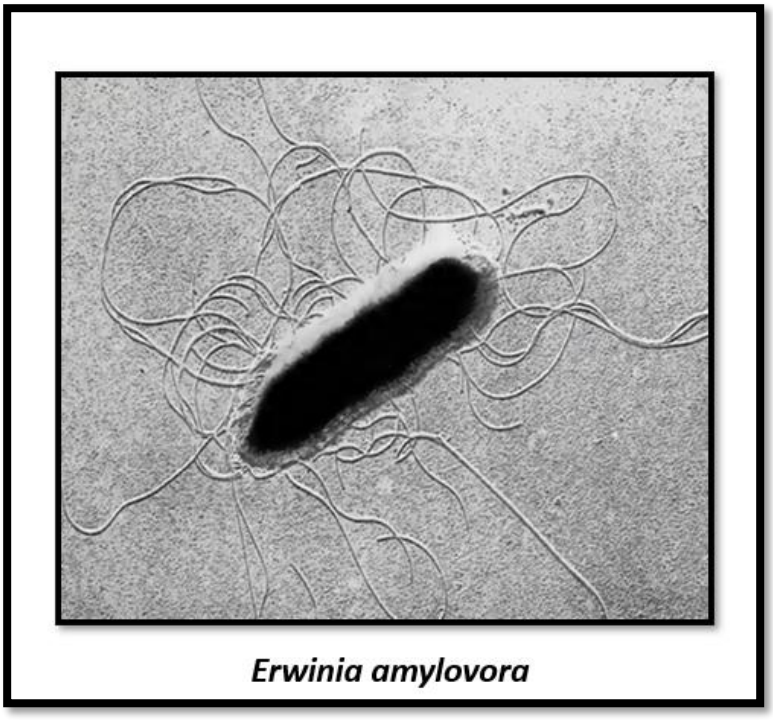

Figure 1.1: An individual capsulated cell of *E. amylovora* with peritrichous flagella (X 18,000). The figure is adapted from Van Der Zwet & Beer (1999).

1.1.1 History and spread of *Erwinia amylovora*

Since its discovery, the fire blight disease has gradually spread globally, encompassing North America, Europe, the Middle East, Asia, and Oceania countries, including New Zealand (Figure 1.2). The following sections aim to account the history and spread of the fire blight disease, which is divided into three-time frames: (1) discovery and early spread, (2) spread in the 20th century CE, and (3) current scenario and forecast.

1.1.1.1 Discovery and early spread

The symptoms of the fire blight disease were first discovered in the late 18th century CE (1780) in the Hudson Valley of New York, located on the east coast of the USA (Bonn & Zwet, 2000; Denning, 1794). With the planting of fruit orchards by early settlers, the disease quickly spread to the south and west territories of the country, causing significant losses in pome fruit production. Fire blight-like symptoms first appeared on the west coast in California in 1882, where its causal agent was discovered as *E. amylovora* (Pierce, 1902). From 1901 to 1910, the fire blight disease instigated substantial economic losses in California (Peil et al., 2009; Wilson, 1906). Gradually, the pathogen spread northward into Oregon and Washington State, covering almost every region of the USA over the subsequent century (Bonn & Zwet, 2000; Zwet & Keil, 1979).

1.1.1.2 Spread in the 20th century

By the beginning of the first decade of the 20th century CE, the disease had spread far beyond the North American continent. The first report of fire blight outside of North America came from Japan (Uyeda, 1903), followed by New Zealand (Campbell, 1920), with its initial outbreak reported in 1919 in the Auckland region of North Island (Cockayne, 1921). The primary source material for the disease in both countries is believed to have come from imported plant material, presumably from the USA (Bonn & Zwet, 2000; Zwet & Keil, 1979).

The first outbreak of fire blight disease in the United Kingdom was reported in 1958 (Crosse et al., 1958); however, disease symptoms in mainland Europe were observed in the mid-1960 (Bonn & Zwet, 2000; Peil et al., 2009; Zwet & Keil, 1979). Based on the similarity of *E. amylovora* strains from New Zealand and Europe, the fire blight disease in Europe is believed to have been introduced from plant material imported from New Zealand (Jock et al., 2002).

From the 1960s to the 1990s, the disease spread throughout Europe and the nearby region, covering Denmark (Klarup, 1969; van der Zwet et al., 2016a), Germany (Fischer & Meyer, 1972; Peil et al., 2009), Belgium (Veldeman, 1972), France (Callu, 1984), Czech Republic (Kůdela, 1988), Switzerland (Grimm & Vogelsanger, 1989), and Austria (Keck et al., 1996). At the same time, reports of the disease spreading throughout the Middle East nations began to emerge, including Cyprus (Psallidas & Dimova, 1986), Israel (Shabi & Zutra, 1987), Turkey (1985), Lebanon (1988), Jordan (Tehabsim et al., 1992), Armenia (1990) and Iran (Afunian & Rahimian, 1996). By the late 1990s, the disease had spread to Italy (Calzolari et al., 1999), Spain (De la Cruz Blanco, 1996; van der Zwet et al., 2016a), and south-eastern Hungary (Hevesi, 1996; van der Zwet et al., 2016a; VÉGh & Palkovics, 2013), before reaching northward into mainland Greece (Psallidas, 1990). The disease then spread further northward into Eastern Europe, gradually establishing in Macedonia, Bulgaria, Romania, Serbia, Bosnia, Herzegovina, Croatia, and Albania (Bonn & Zwet, 2000; Peil et al., 2009; van der Zwet et al., 2016b).

Interestingly, the first report of the fire blight disease from Australia came at the end of the 20th century CE (1997) when symptomatic plants from the Royal Botanic Gardens of Melbourne (RBGM) and the Adelaide Botanic Gardens (ABG) were sampled. The two plants from the RBGM were determined to be positive for *E. amylovora* and were subsequently eradicated (Jock et al., 2000). Extensive surveys conducted since the first outbreak have revealed no evidence of the

disease or the pathogen, making Australia the only country to eradicate the pathogen species successfully (Vieira et al., 2020).

1.1.1.3 Current scenario and forecast

Since the beginning of the 21st century CE, the disease has spread rapidly throughout central and far-east Asian countries. In the last decade, the disease symptoms have been reported from Kyrgyzstan (Doolotkeldieva & Bobusheva, 2016) and Kazakhstan, the germplasm centre for the apple, consequently posing a threat to the susceptible members of the *Malus* germplasm (Drenova et al., 2013; Maltseva et al., 2022). The latest report of the fire blight disease came from South Korea, where the disease was discovered in 2015 (Wilson & Seller, 1977; Zhao et al., 2019), with the most recent outbreak reported in 2020. Moreover, due to the disease's expansion in Asian countries, it is forecasted by experts that a fire blight epidemic in China is only a matter of time. Although China is currently devoid of the fire blight disease, it concerns the nation's phytopathologists and pome fruit growers as the disease has already reached its borders (Wilson & Seller, 1977; Zhao et al., 2019).

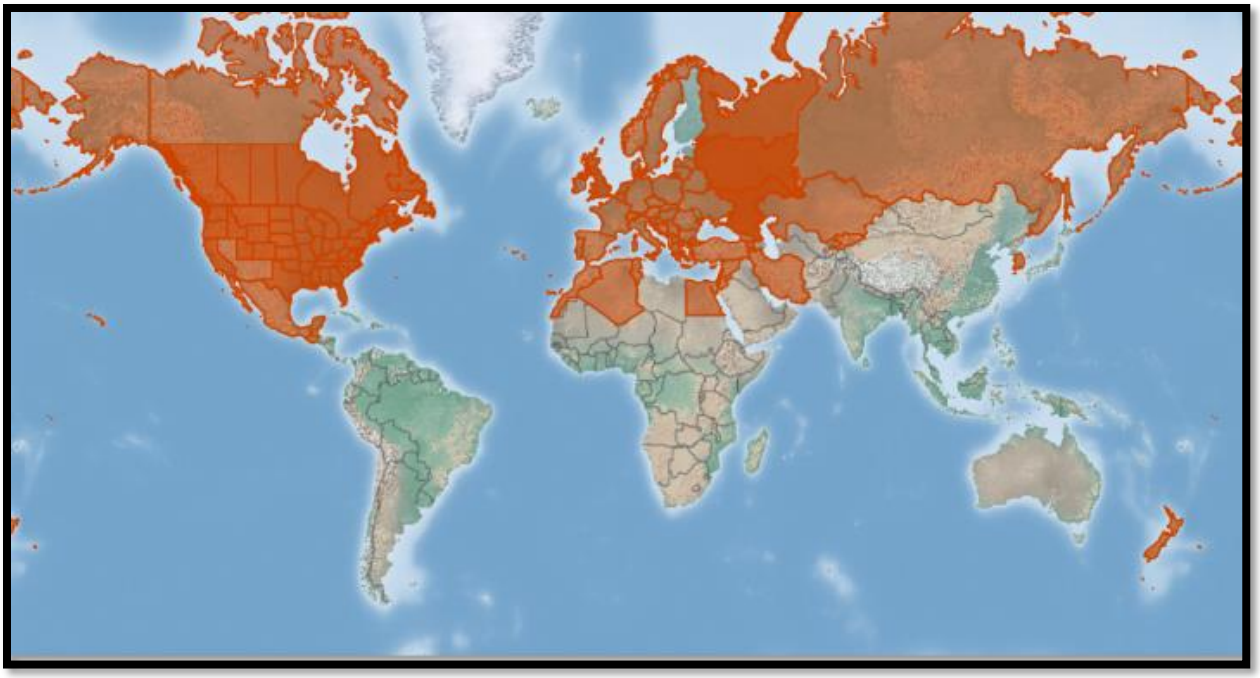

Figure 1.2: Global distribution map of the fire blight disease. The coloured region (red) in the map represents the presence of fire blight disease in the countries[7].

1.1.2 The economic impact of fire blight disease in Rosaceae

In the discipline of molecular plant pathology, *E. amylovora* is considered one of the top 10 plant pathogenic bacteria. One main reason for this status is its economic impact on the pome fruit and ornamental plants industry (Mansfield et al., 2012). Interestingly, accurate estimation of the losses instigated by the fire blight disease is challenging as the economic impact of the disease is usually accounted during the initial outbreak, whereas its repercussions persist for several succeeding years (Vanneste, 2000). Furthermore, the costs of post-outbreak remedial treatments[8] further add to the losses (Malnoy et al., 2012). Therefore, the following paragraph aims to provide insight into

[7] The image has been adapted from the CABI database: https://www.cabi.org/isc/datasheet/21908#toDistributionMaps

[8] The post-outbreak remedial measures include practices such as chemical treatment, diseased plant eradication, and orchard replanting.

the pathogen's ability to cause economic damage by summarising severe outbreaks that have occurred in different countries in the last five decades.

According to a study conducted by Norelli et al. (2003), in the USA alone, the fire blight disease causes an annual economic loss of about US$100 million to the pome fruit sector. For instance, significant fire blight outbreaks in the southwestern state of Michigan during 1991 and 2000 were reported to have incurred estimated losses of US$3.8 million and US$42 million, respectively. During the same duration, a loss of US$68 million was recorded in Washington and Northern Oregon due to fire blight (Bonn & Zwet, 2000; Peil et al., 2009). Furthermore, the disease has caused economic damages of millions of US dollars in European nations wherever documented (Bonn & Zwet, 2000; Peil et al., 2009). Moreover, the fire blight epidemic in New Zealand reported in the early 2000s from the Hawke's Bay region incurred an estimated loss of NZ$10 million.

1.1.3 Fire Blight Symptomology

The fire blight disease manifests with wilting and necrosis of the infected region, giving the infected parts of the plant a scorched and burnt appearance, which led William Coxe to coin the term "fire blight" for the disease in 1817 (Burrill et al., 2003; Zhao, 2014). In nature, the symptoms of the fire blight disease can be observed virtually on all aerial parts of the plants, including inflorescence, fruits, leaves, shoots, and rootstock. Therefore, based on the infected plant part, the disease symptoms are categorised into four distinct categories, namely: (1) blossom blight, (2) fruit blight, (3) twig or shoot blight, and (4) rootstock blight.

The blossom blight is the first symptom of the disease observed early in the spring. The flowers of the infected inflorescence become water-soaked, gradually shrivel, and turn brownish-black (Figure 1.3 A), adversely affecting the crop yield of the current season (Agrios, 2005b; Peil et al., 2009; Van Der Zwet & Beer, 1999).

Fruit blight occurs when the young fruits in or near the infected inflorescence also become infected. The immature fruit initially appears water-soaked, turns black and mummifies progressively (Figure 1.3 B). The leaves near the diseased inflorescence can also get infected and develop brownish-black blotches. The blotch size gradually increases, making the leaves shrivel and hang downward while remaining intact with the twig (Figure 1.3 D) (Agrios, 2005b).

The infected twigs wilt from the tip downwards and curl with a hooked tip giving a typical 'shepherd's crook' like appearance (Figure 1.3 C) and culminating in twig blight[9] (Peil et al., 2009; Zhao, 2014). Interestingly, the disease can also spread from the diseased twig into the branches and trunk, causing canker in the woody tissues. Occasionally, the canker encircles the whole branch killing any part above the canker (Figure 1.3 E). Furthermore, the pathogen can move further down into the trunk and infect the susceptible rootstock, causing rootstock blight (Figure 1.3 F) (Agrios, 2005b).

[9] Twig blight also increases losses for the following seasons by damaging the annual wood that generates the fruit spurs.

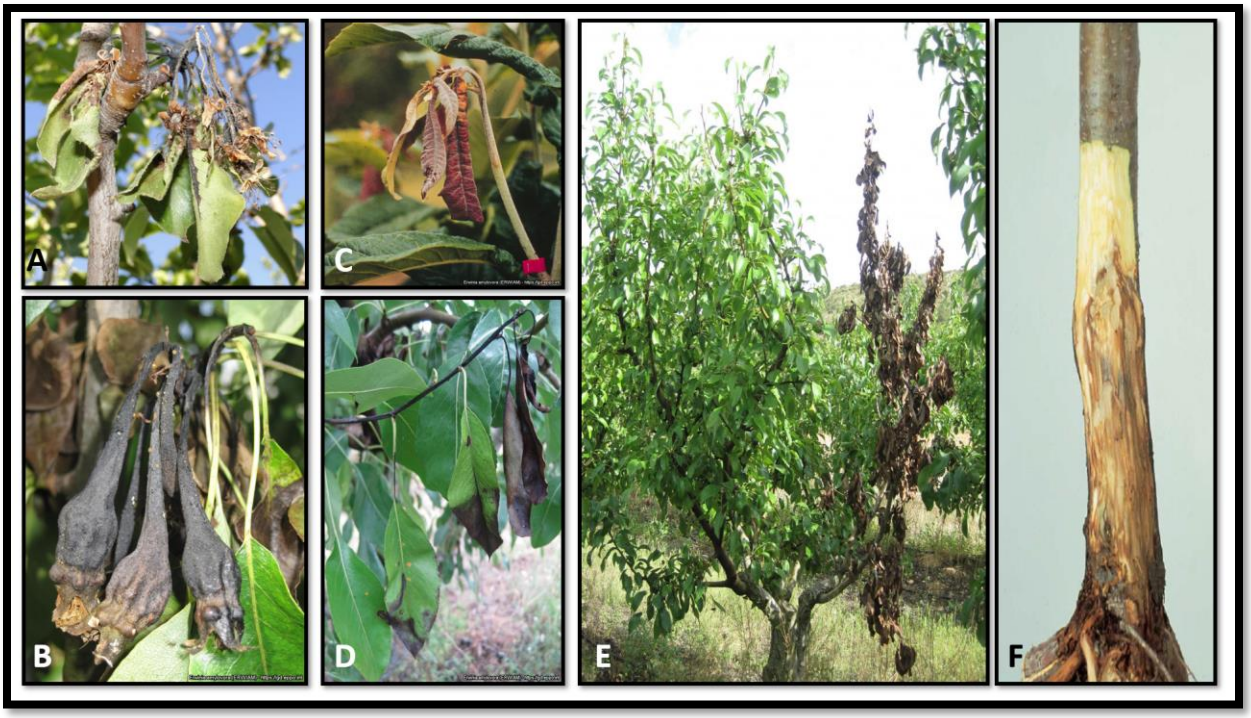

Figure 1.3: Typical symptoms of the fire blight disease in the Rosaceae members. (A) blossom blight on the inflorescence of a pear plant of the 'Shah' cultivar, (B) mummified infected pear fruits with ooze droplets on pedicel, (C) shepherd's crook on a loquat shoot, (D) necrosis of infected pear leaves, (E) blight of the pear shoot, and (F) rootstock blight in the pear crown. The images were adapted from EPPO Global Database[10] and Agrios (2005).

1.1.4 The life cycle of *E. amylovora*

The life cycle of *E. amylovora* (Figure 1.4) begins with canker tissues acting as a primary source of inoculum. The bacteria overwinter in the canker's margins and become active during the spring. Bacterial ooze begins to exude from the plant's cracks and lenticels during the blooming period. Insects like ants, bees, and flies are drawn to the ooze and aid in spreading the inoculum from the ooze or canker to the blooming flowers. Furthermore, wind and rain splash also assist in pathogen dispersal (Agrios, 2005b; Thomson, 1986; van der Zwet et al., 2016b).

[10] The sub-figures from 'A' to 'E' were adapted from EPPO Global Database: https://gd.eppo.int/taxon/ERWIAM/photos#

The bacteria multiply in the nectar of the blooming flower before entering the flower tissues via the nectarthode. Soon, it spreads intercellularly deep into the fruit spur, causing the surrounding cells to collapse, resulting in blossom and fruit blight. Next, the disease slowly spreads into the bark tissues, causing shoot blight and forming new cankers in which the pathogen again overwinters (Agrios, 2005b; Thomson, 1986; Zhao, 2014).

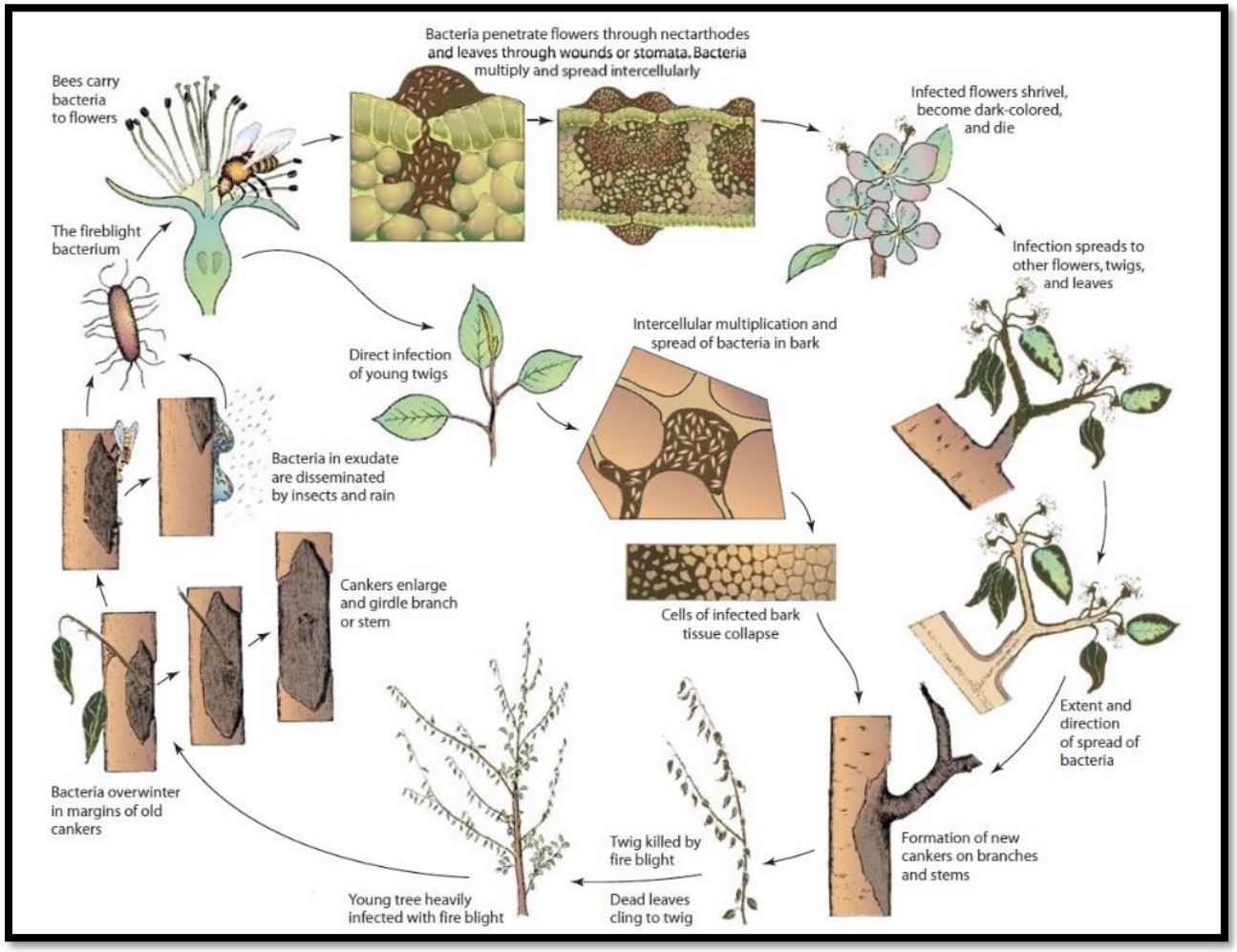

Figure 1.4: The life cycle of *E. amylovora.* The figure was reproduced from Agrios, 2005b.

1.2 *E. amylovora* and other related species: General description and taxonomy

Several bacterial species related to *E. amylovora* have been discovered in the last three decades. These bacterial species are either ecologically associated or pathogenic to the pome fruits. The pathogenic species cause symptoms similar to the fire blight disease in the infected host plants (Zhao, 2014); however, some related species have also been discovered to infect members of plant families other than Rosaceae (Olawole et al., 2021). Therefore, contemplating this, the following sections attempt to put forward a brief review of the description of species closely associated with *E. amylovora* and the taxonomy of the *Erwinia* genus.

1.2.1 A classic to modern mini-review of the taxonomy of the *Erwinia* genus

The genus *Erwinia*, named after the phytobacteriologist Erwin F. Smith, was first created in the family Enterobacteriaceae in 1920 to encompass all Enterobacteriaceae members that were either ecologically associated or pathogenic to the plants (Gardner & Kado, 1972; Hauben et al., 1998; Paulin, 2000; Zhang & Qiu, 2015). However, this categorisation was non-scientific and lacked any genetic or phylogenetic relatedness, thus limiting its application. Gardner and Kado (1972) first proposed to regroup the Enterobacteriaceae family into pre-existing and new genera based on DNA relatedness (Paulin, 2000). Since, the genus *Erwinia* has been reviewed several times (Dye, 2012; Holt et al., 1994; Lelliott, 1984; Mergaert et al., 1984). Interestingly, until the last decade, the most widely accepted phylogenetic classification of the *Erwinia* genus and other related Enterobacteriaceae members was proposed by Hauben and colleagues (Hauben et al., 1998). The proposed classification utilised sequence differences in the 16S rRNA to delineate species into four taxonomic clusters. Cluster 1 included all the true *Erwinians*, encompassing species such as *E. amylovora*, *E. persicina*, *E. psidii*, and *E. tracheiphila*. Clusters 2 and 3 encompassed

Pectobacterium spp. and *Brenneria* spp., respectively. Finally, cluster 4 included members from the *Pantoea* spp., which were distinct but phylogenetically related to the *Erwinia* species (Adeolu et al., 2016; Hauben et al., 1998; Janda & Abbott, 2021; Paulin, 2000).

A remarkable phylogenetic classification, succeeding the previous classification by Hauben et al., was proposed by Adeolu and associates in 2016. The phylogenetic classification was based on the analysis of conserved signature indels (CSI), shared core, ribosomal and MLSA proteins from 179 members of the Enterobacteriales order. The authors also recommended renaming the order from "Enterobacteriales" to "Enterobacterale" and classifying it into seven novel monophyletic families, including "Erwiniaceae" as a separate family containing six genera: *Erwinia*, *Buchnera*, *Pantoea*, *Phaseolibacter*, *Tatumella*, and *Wigglesworthia* (Adeolu et al., 2016). Moreover, Janda and Abbott (2021) have recently proposed categorising the "Enterobacteriaceae" family into nine groups based on evolutionary relatedness, with the "*Erwinia-Pantoea*" group[11] as a distinct group encompassing all the *Erwinia* and other closely related species.

1.2.2 *Erwinia-Pantoea* group: A general description

Like *E. amylovora*, species in the "*Erwinia-Pantoea"* group are members of the Enterobacteriaceae family (Table 1.1) and include both phytopathogenic and non-phytopathogenic species (Janda & Abbott, 2021; Zhao, 2014). In addition, *E. amylovora* acts as a type species for the group, with virtually all the *Erwinia*-related species sharing multiple morphological and physiological features with *E. amylovora* (Palacio-Bielsa et al., 2011; Zhao, 2014). However, despite various similarities, some *Erwinia*-related species differ in a few characteristics, such as

[11]"*Erwinia-Pantoea*" group is a convention that is frequently used in this work to represent all the *Erwinia* and related species. This convention has been adopted based on the classification scheme proposed by Janda and Abbott (2021).

host range, symptoms incurred on the host, tissue preference, and virulence factors repository (Mizuno et al., 2009; Rhim et al., 1999; Roselló et al., 2006; Shrestha et al., 2003; Zhao, 2014). *Erwinia pyrifoliae*, *E. tracheiphila*, *E. piriflorinigrans*, *E. tasmaniensis*, *E. billingiae*, and *P. vagans* are some important notable species related to *E. amylovora* (Table 1.1) (Palacio-Bielsa et al., 2011; Zhao & Qi, 2011). The following paragraph aims to provide a general description of the aforementioned 'notable' species.

E. amylovora is the causal agent of fire blight disease, which infects more than 200 species across all the Rosaceae sub-families (Palacio-Bielsa et al., 2011; Van Der Zwet & Keil, 1979) (See footnote '12' for the taxonomical classification of the Rosaceae family and the convention used in the current study). Contrastingly, in nature, *E. pyrifoliae* is primarily known to cause 'bacterial shoot blight' disease on Asian pear (*Pyrus pyrifolia*) cultivars, producing symptoms resembling the fire blight disease. Interestingly, it can also produce symptoms in apple (*Malus domestica* cv. Idared) and European pear cultivars (*Pyrus communis*) upon artificial inoculation (Kim, Hildebrand, et al., 2001). *E. tracheiphila* is the etiological agent of the bacterial wilt disease of cucurbits, which is limited to the temperate regions of North America (Shapiro et al., 2018). *E. piriflorinigrans* is a unique species as it contrasts *E. amylovora* and *E. pyrifoliae* regarding tissue preference and symptomology produced in different host species. Interestingly, it can only cause necrosis on pear blossoms but not on any other plant part or Rosaceae species (Lopez et al., 2011; Roselló et al., 2006). *E. tasmaniensis* and *E. billingiae* are non-pathogenic *Erwinia* species, which

[12] As described by Zhao (2014), the family Rosaceae is traditionally divided into four subfamilies based on fruits type: "Amygdaloideae (syn. Prunoideae), Maloideae (syn. Pomoideae), Rosoideae, and Spiraeoideae". Potter and colleagues (2007) revised Rosaceae taxonomy and proposed three sub-families based on phylogenetic analyses of four chloroplast and six nuclear genes; the proposed classification is as follows: (1) Spiraeoideae (encompassing formerly classified sub-families: Amygdaloideae, and Maloideae), (2) Dryadoideae, (3) and Rosoideae. (For ease of comprehension, the presented work follows the Rosaceae classification scheme proposed by Potter and colleagues (2007) with three sub-families).

are considered as the deemed members of apple and pear microbiota and potential biocontrol agents against *E. amylovora* (Palacio-Bielsa et al., 2011). *Pantoea* species harbours some notable antagonists, such as *P. agglomerans* strain P10c and E325 (Johnson et al., 2004; Pusey, 2002; Smits et al., 2019), and *P. vagans* strain C9-1 (Ishimaru et al., 1988), which are used as biocontrol agents against *E. amylovora* in New Zealand[13] and other North American and European countries (Malnoy et al., 2012; Stockwell et al., 2011).

Table 1.1: Taxonomic classification of some notable plant-associated members of the "*Erwinia-Pantoea*" group[14].

Domain	Bacteria
Phylum	Proteobacteria
Class	Gammaproteobacteria
Order	Enterobacteriales
Family	Enterobacteriaceae
Genus	*Erwinia; Pantoea*
Species	*E. amylovora; E. pyrifoliae; E. tracheiphila; E. piriflorinigrans; E. tasmaniensis; E. billingiae; P. vagans; and P. agglomerans*

[13] BlossomBless® is a widely popular biocontrol product against fire blight disease in New Zealand, which contains *P. agglomerans* str. P10c in the form of a wettable powder.
[14] The information was acquired from the NCBI taxonomy browser: https://www.ncbi.nlm.nih.gov/Taxonomy/Browser/wwwtax.cgi?id=2

1.3 Population structure within *E. amylovora* species

E. amylovora, as a species, is capable of infecting more than 200 species in the Rosaceae family; however, its strains are known to be host-specific (Malnoy et al., 2012; Palacio-Bielsa et al., 2011; Zhao, 2014; Zwet & Keil, 1979). Based on their ability to infect different Rosaceae members (host range), *E. amylovora* strains are divided into two major groups: Spiraeoideae isolated strains (hereafter called 'Spiraeoideae isolates') and Rubus isolated strains (hereafter called 'Rubus isolates') (Asselin et al., 2011). The Spiraeoideae isolates have a broad host range and are capable of infecting multiple members of the economically important horticulture crops from the Spiraeoideae sub-family, such as pear (*Pyrus* spp.), apple (*Malus* spp.), plum (*Prunus* spp.), and Hawthorns (*Cartages* spp.); in contrast, the Rubus isolates are highly-selective and naturally infects hosts only from the Rosoideae sub-family (Asselin et al., 2011; Mohan & Bijman, 1999; Potter et al., 2007; Zhang & Geider, 1997). Interestingly, results from artificial inoculation of both isolates suggest that some Spiraeoideae isolates are indeed capable of causing disease in some Rubus hosts. Conversely, the Rubus isolates repeatedly failed to cause disease on the apple shoots; however, a few strains were observed to cause disease on immature apple and pear fruit (Asselin et al., 2011; Braun & Hildebrand, 2005; Triplett et al., 2006).

The exact molecular mechanism underlying this phenomenon of host specificity in Spiraeoideae and Rubus isolates remains unknown. However, research indicates that both isolate types differ in various features, including serological properties, exopolysaccharide structure, carbon source preference and RNA expression (Asselin et al., 2011; Braun & Hildebrand, 2005; Maes et al., 2001; Mizuno et al., 2002; Triplett et al., 2006). Interestingly, *Erwinia* outer protein 1

(Eop1), a widely conserved effector[15] in *E. amylovora* and related species (X. C. Yuan et al., 2021), has been shown as a 'potential' host specificity determinant factor (Asselin et al., 2011; Asselin et al., 2008).

1.4 Host-Pathogen Interaction

Host-pathogen interaction can be defined as a highly dynamic interaction between microbial pathogens and their corresponding hosts, determining the host's reaction to the pathogen invasion. Furthermore, it establishes a basis for co-evolution between the host's defence system and the pathogens' defence-suppressing machinery.

1.4.1 Plant immunity in a nutshell

Self-defence against biotic stresses is crucial for the survival of all biological organisms. However, being sessile, unlike other organisms, plants cannot avoid these stresses via locomotion. Nevertheless, plants evolved with an intricate defence system that extends beyond the physical barriers and turns every plant cell capable of performing a complex immune activity and executing self-defence.

1.4.1.1 The concept of 'pattern' and 'effector' triggered immunity

The plant immune system is generally classified into a two-tier system: (1) pattern-triggered immunity (PTI) and (2) effector-triggered immunity (ETI) (Jones & Dangl, 2006). PTI is plants' first tier of active defence against microbes, which relies on a set of transmembrane proteins known as pattern recognition receptors (PRRs) (Afzal et al., 2011; Rathore & Ghosh, 2018). PRRs perceive microbes (including pathogens) by recognising their conserved signature molecules,

[15] Dodds & Rathjen (2010) describes 'Effectors' as unique proteins secreted by the pathogens into the host cells to aid virulence in the host plant by suppressing the plant's basal defence response.

collectively termed microbe-associated molecular patterns (MAMPs) (Ausubel, 2005; Cook et al., 2015; Rathore & Ghosh, 2018). The MAMPs include macromolecules such as prokaryotic EF-Tu, bacterial flagellin, chitin, lipopolysaccharide, peptidoglycan (Zipfel, 2014), and bacterial RNA (Lee et al., 2016). ETI, the second tier of plant immunity, in contrast to PTI, relies on intracellular polymorphic proteins termed 'resistance proteins' (R-proteins), which are a translated product of the 'resistance genes' (R-genes) (Dodds & Rathjen, 2010). Interestingly, the R-genes encode approximately 6 classes of R-proteins (Agrios, 2005a), of which nucleotide-binding (NB) leucine-rich repeat (LRR), collectively acronymised as NB-LRR, is the most predominant class of R-protein in the plants (Glowacki et al., 2011; Kourelis & van der Hoorn, 2018).

The NB-LRR proteins perceive pathogen-delivered effectors, either directly or indirectly (Dodds & Rathjen, 2010; Jones & Dangl, 2006); (the direct and indirect modes of effector recognition by NB-LRRs are covered in Chapter 4's introduction (Section 4.1 and Figure 4.1). Overall, PTI and ETI trigger similar downstream responses, resulting in triggered immunity (Dodds & Rathjen, 2010; Tao et al., 2003). However, ETI induced immune response is more robust due to the development of hypersensitive response (HR), a form of localised cell death aimed at limiting pathogen development at the site of infection (Balint-Kurti, 2019; Dodds & Rathjen, 2010). Moreover, pieces of evidence supporting the theory that both tiers of plant immunity are interrelated with mutual potentiation, forming a PTI-ETI continuum, are gradually accumulating (Chang et al., 2022; Naveed et al., 2020; Ngou et al., 2021; Tian et al., 2021; M. Yuan et al., 2021).

1.4.1.2 The "Zig-Zag" model of pathogen detection

The concept connecting the MAMPs' perception by PRRs, the role of effectors in pathogenesis and its interaction with other components of the plant immune system, such as NB-LRRs, is defined via an infographic (Figure 1.5). The infographic also attempts to pictorially explain the

"zig-zag" model of the plant immune system initially proposed by Jones and Dangl (2006), which aims to connect PTI and ETI and explain the fundamental basis of co-evolution between the host and its corresponding pathogen.

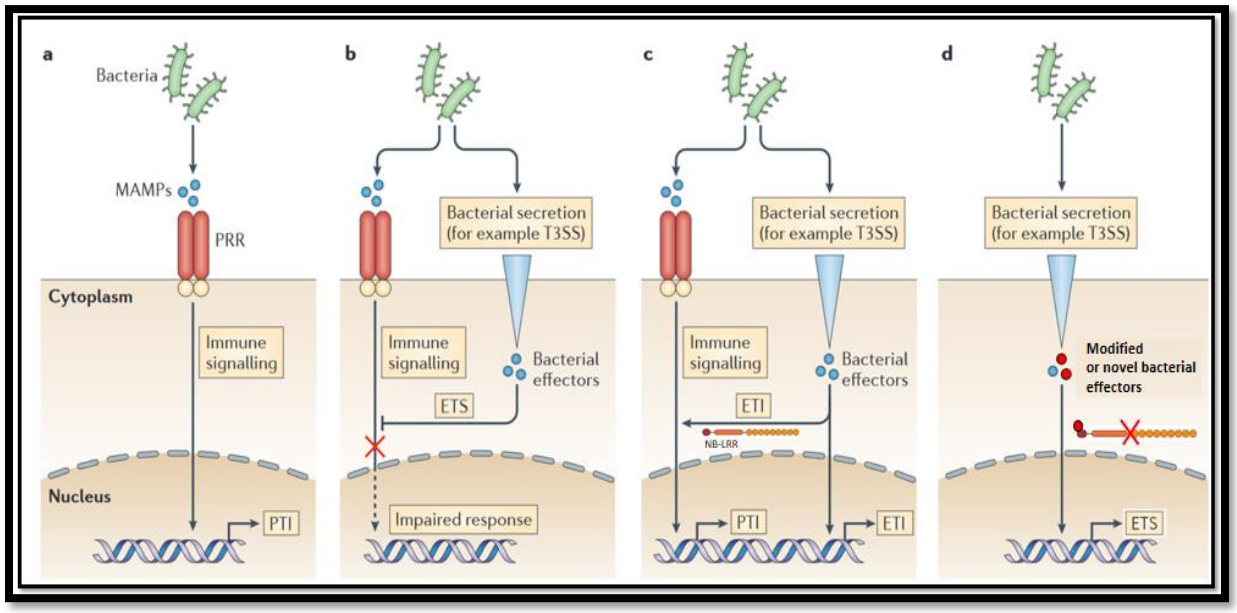

Figure 1.5: Pictorial representation of the "Zig-Zag" model of plant immunity. (a) During bacterial infection, plant cells' pattern recognition receptors (PRRs) bind to the microbe-associated molecular patterns (MAMPs), activating immune signalling and resulting in pattern-triggered immunity (PTI). (b) Adapted bacterial pathogens suppress PTI by delivering effectors into host-plant cells via the T3SS, promoting infection and resulting in effector-triggered susceptibility (ETS). (c) To combat ETS, resistant plants employ R-proteins (usually NB-LRRs) which perceive the pathogen effectors and trigger a more robust form of plant immunity known as effector-triggered immunity (ETI). (d) Pathogens, in turn, respond to ETI by introducing novel effectors or mutations in the pre-existing effectors to escape recognition, which again results in ETS. (The figure was adapted from Stuart et al. (2013) and slightly modified to exemplify the "zig-zag" model using a bacteria-host pathosystem).

1.4.2 Pathogenicity and Virulence factors in *E. amylovora*

Decades of research devoted to the understanding of the molecular mechanisms underlying *E. amylovora* pathogenicity have yielded several 'virulence factors' such as type III secretion system

(T3SS), type III secretion system effectors (T3SE), exopolysaccharides (amylovoran and levansucrase), biofilm, motility apparatus, and iron scavenging siderophores (Pique et al., 2015). Many of these identified factors provide *E. amylovora* with an advantage in causing disease in the host plants; however, only three virulence factors have been demonstrated to act as 'pathogenicity factors'[16], namely 'hypersensitive response and pathogenicity-type III secretion system' (*hrp*-T3SS) (Oh & Beer, 2005), 'DspA/E' effector (Bogdanove, Bauer, et al., 1998; Boureau et al., 2006), and exopolysaccharide (amylovoran) (Koczan et al., 2009). Furthermore, *E. amylovora* mutants carrying the deletion of the aforementioned pathogenicity factors remain unable[17] to cause disease in the host plant (Boureau et al., 2006; Koczan et al., 2009; Oh & Beer, 2005). Therefore, the following section addresses the *E. amylovora* hrp-T3SS, its encoded effectors and their importance in pathogenicity. A summary of the other mentioned virulence factors can be found in Piqué et al. (2015).

1.4.2.1 hrp-pathogenicity Island, T3SS and effectors in *E. amylovora* and related species

T3SS, a needle-like structure traversing bacterial membranes, is a vital pathogenicity factor in many gram-negative bacterial pathogens (Buttner & He, 2009; Galan et al., 2014). T3SS allows the pathogen to deliver T3SEs, which are proteins with a potential virulence or pathogenic function, directly into the protoplasm of the host's cell (Coburn et al., 2007; Galan et al., 2014). The genes encoding for the structural and regulatory components of the T3SS and T3SE are highly

[16] 'Pathogenicity factors' refers to the pathogen-associated components without which the pathogen remains unable to cause disease; in contrast, the 'virulence factors' refers to the components which determine the severity of the disease.

[17] It is important to note that the three virulence factors identified as 'pathogenicity factors' were identified using contemporary screening techniques, which only account the gross changes in the pathogen's disease-causing ability upon its mutation; however, other virulence factors may have subtler effects that are yet to be discovered but could be essential for the pathogen to cause disease.

conserved across and within the bacteria species[18]. Interestingly, these genes are usually present on a discrete segment of the bacterial genome termed 'pathogenicity island' (Galan et al., 2014; Hacker & Kaper, 2000).

The 'pathogenicity island' in *E. amylovora* is widely known as the 'hypersensitive response and pathogenicity island' (hrp-pathogenicity island or PAI1[19]) because of its importance in causing disease in the host plants and triggering the hypersensitive response in host and non-host plants (Oh & Beer, 2005). Genomic and secretome analysis suggests that *E. amylovora* secretes at least five effectors via its hrp-T3SS, namely, DspA/E, Eop1, Eop3, Eop4 ($AvrRpt2_{Ea}$), and $HopPtoC_{Ea}$ (Nissinen et al., 2007; X. C. Yuan et al., 2021; Zhao, 2014); (Table 1.2 summarise the essential characteristics of the aforementioned T3SEs, including the effectors' family, homolog proteins from other bacterial species, proposed virulence function, and the effect of the effector gene deletion on *E. amylovora* strains on infecting Spiraeoideae hosts).

The sequence homologs of the aforementioned *E. amylovora* effectors have also been observed in several members of the "*Erwinia-pantoea*" group (summarised via a heatmap in 'Figure 1.6'). Interestingly, a pattern of co-existence between *dspA/E* and *eop1* effector genes was also observed, which was attributed to two possibilities; First, both the effectors may have a form of linkage effect as they share the same pathogenicity island: PAI1, and consequently exhibit high proximity on the genomic scale (Figure 1.7); second, Eop1 protein has a crucial but subtle function that is yet to be identified, explaining its high conservation with a vital pathogenicity factor 'DspA/E'.

[18] It is important to note that despite wide conservation, the genes repository encoding for various T3SEs usually varies between species.

[19] Khan et al. (2012) suggest that the genome of *E. amylovora* contains three pathogenicity islands: PAI1, PAI2, and PAI3, however, only 'PAI1' contains the virulence-associated genes, while the other two are non-functional in virulence.

1.5 Gene-For-Gene interactions in *Malus* - *E. amylovora* pathosystem

'Gene-For-Gene' relationship (hereafter, G-F-G), a theory proposed by HH Flor, suggests that for every dominant host-resistance gene in the resistant host, there is a corresponding single dominant avirulence (Avr) gene expressed by the pathogen (Cook et al., 2015; Flor, 1971). This theory parallels the avirulence activity of effectors and its recognition by the R-proteins, as proposed in the "zig-zag" model (Jones & Dangl, 2006). Interestingly, of the five T3SEs delivered by *E. amylovora*, only two effectors, AvrRpt2$_{Ea}$ (Vogt et al., 2013) and Eop1 (Wöhner et al., 2018), have been discovered to have a G-F-G relationship with *Malus* cultivars.

AvrRpt2$_{Ea}$ is the first *E. amylovora* effector for which a G-F-G phenomenon was observed and verified in a crab apple species, *Malus robusta* 5 (*Mr*5). The observation was made when an AvrRpt2$_{Ea}$ mutant strain, ZYRKD3-1, and four other strains with a single nucleotide polymorphism (SNP), resulting in C156S mutation in AvrRpt2$_{Ea}$ protein were able to overcome the *Mr*5 resistance (Broggini et al., 2014; Emeriewen et al., 2019; Vogt et al., 2013; Zhao et al., 2006). Subsequent experiments later attributed the *Mr*5 resistance to the 'Fb_MR5' R-protein (Fahrentrapp et al., 2012). Likewise, by employing T3SE-knock-out strains of *E. amylovora* in artificial inoculation experiments, Wöhner et al. (2018) discovered that Eop1 has a G-F-G relationship with an ornamental (*Malus* 'Evereste') and a wild cultivar (*Malus floribunda* 821) of the *Malus* species; however, the R-protein responsible for this Eop1-*Malus* G-F-G phenomenon is still unknown.

Table 1.2: Summary of the essential characteristics of the type III secretion system effectors (T3SEs) from *E. amylovora*.

T3SS* effectors *of* *Erwinia amylovora	**Effector's family**	**Homologous proteins present in other species**	**Proposed virulence Function**	**Effect of the 'effector gene deletion' on *E. amylovora* strains on infecting Spiraeoideae hosts**	**References**
DspA/E	AvrE	AvrE1, HopR1 (*P. syringae*) PopS (*Ralstonia* spp.) WtsE (*Pantoea* spp.) XopAM (*Xanthomonas spp.*)	Suppression of Salicylic Acid mediated defences, callose deposition, and actin remodelling, vesicular traffic disruption.	Non-pathogenic on immature pear fruits.	(Bogdanove, Bauer, et al., 1998; Bogdanove, Kim, et al., 1998; Degrave et al., 2015; Laflamme et al., 2020; Xin et al., 2015)
Eop1 (Formerly known as EopB or OrfB)	YopJ/ AvrRxv	HopZ (*P. syringae*) PopP, RipAE, RipJ (*Ralstonia* spp.) XopJ (*Xanthomonas* spp.)	Acetylation of a host-substrate(s); Interference with the host's immune signalling and isoflavonoid biosynthesis pathway; cytoskeleton perturbation via acetylation. *	No effect on virulence in immature pear fruit or apple shoots.	(Asselin et al., 2011; Lee et al., 2015; Lewis et al., 2014; Lewis et al., 2010; Tasset et al., 2010; Wöhner et al., 2018; Zhou et al., 2011)
$HopPtoC_{Ea}$	YopT	HopC1, AvrPphB/HopAR1, HopAY1, HoAW1, HopN1 (*P. syringae*) RipT (*Ralstonia* spp.) HopAY1 (*Pantoea* spp.)	Disruption in immune signalling, most likely via cleavage of plasma membrane-associated proteins. *	No effect on virulence in immature pear fruits.	(Arnold et al., 2001; Baltrus et al., 2012; Dowen et al., 2009; Nissan et al., 2018; Russell et al., 2015; Zhao et al., 2005)
Eop3	HopX/AvrPphE	HopX1/AvrPphE (*P. syringae*), RipE (*Ralstonia* spp.) XopE1 (*Xanthomonas* spp.)	Degradation of JAZ transcriptional repressors consequently activating jasmonate signalling. *	No effect on virulence in immature pear fruits and apple shoots.	(Bocsanczy et al., 2012; Gimenez-Ibanez et al., 2014; Laflamme et al., 2020; Mansfield et al., 1994; Nimchuk et al., 2007; Sang et al., 2020; Thieme et al., 2007)
Eop4 ($AvrRPt2_{Ea}$)	C70 family of peptidases, and CA clan of papain-like peptidases.	AvrRpt2 (*P. syringae*) RipBN (*Ralstonia* spp.) AvrRpt2 (*Acidovorax* spp.)	Degradation of the Aux/IAA repressor 'AXR2' altering auxin signalling. MAPK pathway repression. *	Reduced virulence on immature pear fruits.	(Axtell et al., 2003; Chen et al., 2007; Chisholm et al., 2005; Coaker et al., 2006; Cui et al., 2013; Eschen-Lippold et al., 2016; Vogt et al., 2013; Zhao et al., 2006)

Note: (1) The asterisk (*) indicates the 'putative virulence function of the *E. amylovora* effectors', proposed based on the activity of the homolog proteins from other plant-pathogenic bacteria. (2) The information was adapted from Yuan et al. (2021).

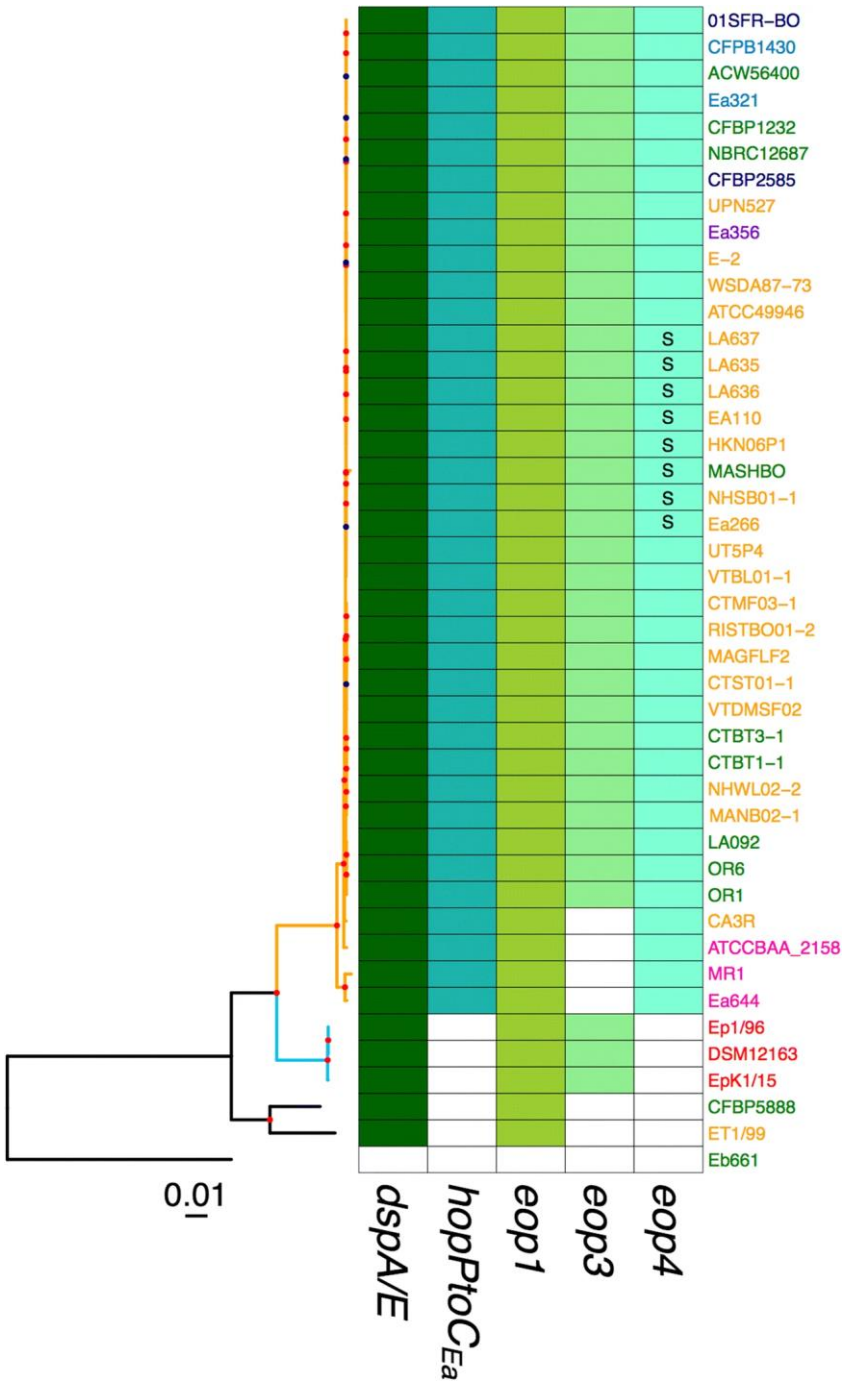

Figure 1.6: A heatmap accounting the presence and absence of the known type III secretion system effectors (T3SEs) in *E. amylovora* strains and related species. The coloured cells represent the presence of a full-length sequence homolog in each strain, whereas the unfilled cell represents the lack of the effector. The colour code of the dendrogram's branches represents the following: orange = *E. amylovora* strains; blue = *E. pyrifoliae* strains; black = other related epiphyte species. Black and red dots on the dendrogram's branches represent > 80% and > 50%

phylogenetic support, respectively. Bacterial strains are also colour coded based on a host of isolation: dark blue = *Sorbus* spp.; light blue = *Crataegus* spp.; green = *Pyrus communis*; purple = *Cotoneaster* spp.; orange = *Malus domestica*; pink = *Rubus idaeus*; red = *Pyrus pyrifolia*. The letter '**S**' in the "*eop4*" column represents *E. amylovora* strains with the known C156S mutation in Eop4 (AvrRPt2$_{Ea}$). (Note: Effector homologs scoring > 60% identity and > 40% query length were concluded to be putatively present by the authors. The image was reproduced from Yuan et al. (2021)).

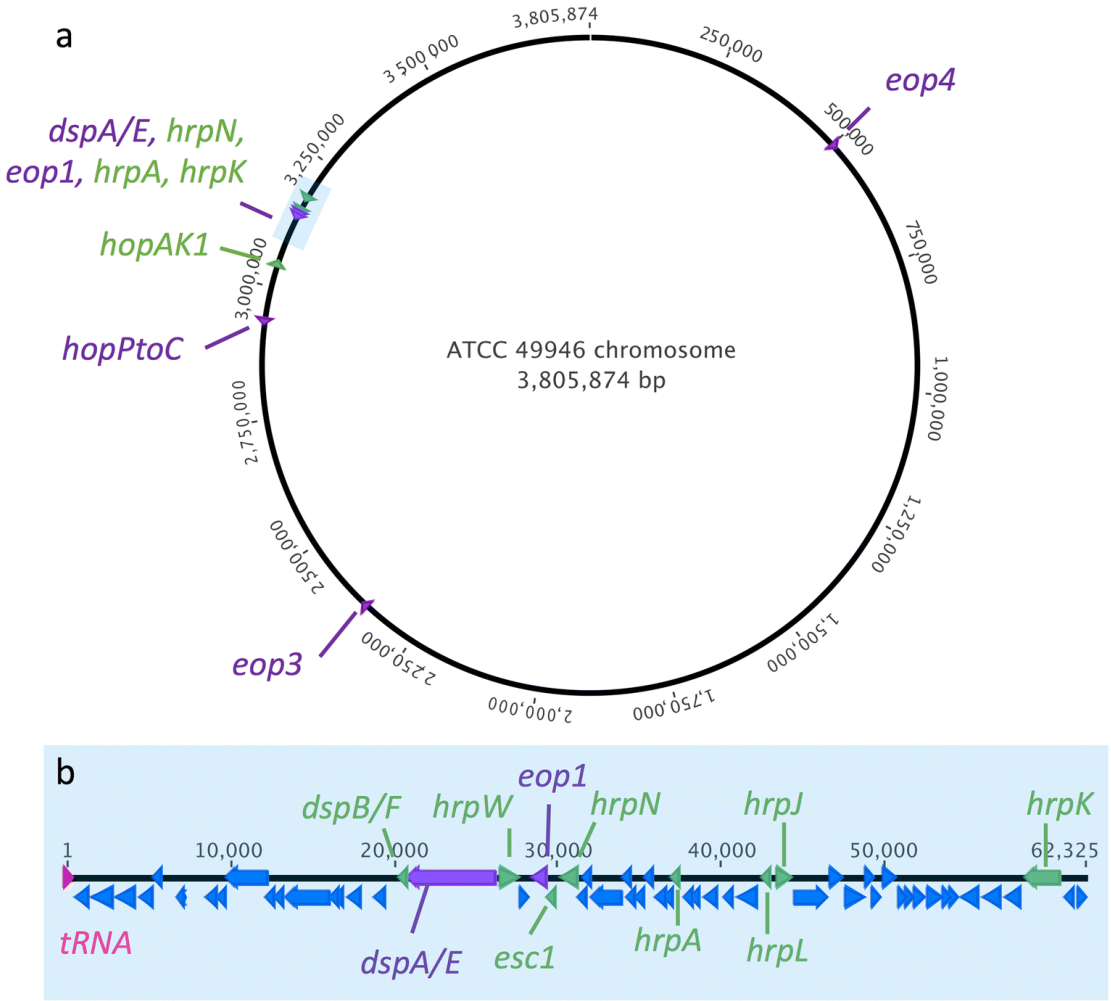

Figure 1.7: Genome map of *Erwinia amylovora* strain ATCC 49946 (*Ea*273), representing the location of the 'hypersensitive response and pathogenicity island' (*hrp*-pathogenicity island or PAI1), type III secretion system (T3SS) and T3SS effectors (T3SEs) genes on the genomic scale. (a) Circular view of *Ea*273 genome; (b) Enlarged view of the *hrp*-pathogenicity island. The colour codes are as follows: purple = T3SEs encoding genes, and green = genes encoding for other T3SS components. The image was adapted from Yuan et al. (2021).

1.6 The theme of investigation in the current research

1.6.1 Basis of research questions

A number of significant observations from the aforementioned review of the literature form the basis of the investigation in this study. The pertinent points are as follows:

(1) The T3SS effector 'DspA/E' is a vital pathogenicity factor for the pathogen. Studies suggest that *E. amylovora* strains with the *dspA/E* gene deletion are unable to cause disease in the *Malus* and *Pyrus* cultivars (Bogdanove, Bauer, et al., 1998; Boureau et al., 2006). In contrast, *eop1* deletion does not affect the pathogenicity or virulence of the pathogen, yet it is roughly as broadly conserved in the *E. amylovora* strains and related species as *dspA/E* (Figure 1.6). Interestingly, the coexistence of the *eop1* and *dspA/E* also indicates that the two genes may be genetically linked (Figure 1.7) or that the Eop1 protein may have a crucial but 'subtle' function that is yet to be discovered. Furthermore, the genomic region surrounding the *eop1* gene contains genes for virulence factors such as '*hrpA*' (Oh & Beer, 2005), the loss of which has been proven to have a detrimental effect on the pathogen's virulence.

(2) Contemporarily available research data, majorly based on phenotypic analysis, suggests that Eop1 is not 'directly' involved in pathogenesis or virulence; however, it is deduced that it has a subtler function yet to be examined. An available example of one such 'subtle function' is based on the notable research conducted by Asselin et al. (2011), which suggests that Eop1 could be a potential host-specificity factor in the *E. amylovora* population (refer to section 1.3), partly explaining its high conservation across *E. amylovora* strains and other members of "*Erwinia-Pantoea"* clade (Olawole et al., 2021; Shapiro et al., 2018).

(3) Research conducted by Wöhner and associates (2018) led to the discovery of a G-F-G relationship in two fire blight-resistant apple cultivars, namely, *Malus* 'Evereste' and *Malus floribunda* 821, with resistance based on the Eop1 recognition, indicating the potential existence of an R-gene encoded R-protein recognising Eop1 in both species.

(4) Lastly and perhaps most importantly, the breakdown of the Fb_MR5 R-protein imparted resistance by *E. amylovora* strains carrying an SNP in the effector $AvrRpt2_{Ea}$ (Broggini et al., 2014; Vogt et al., 2013; Zhao et al., 2006), indicate the need for more durable fire blight resistance in apple cultivars. Therefore, a thorough understanding of the pathogen-delivered effectors and their interactions with their target host-proteins is necessary to tackle similar situations in the future and build more durable resistance cultivars.

1.6.2 Research questions[20]

Considering the abovementioned factors, it was hypothesised that resistance based on Eop1 recognition, in conjunction with gene pyramiding with other resistance genes (such as *Fb_MR5*), could provide more durable resistance to pome fruits, specifically apples. Additionally, a G-F-G relationship for Eop1 indicates the potential existence of an R-gene encoded R-protein recognising Eop1. However, due to its lack of direct involvement in pathogenesis or virulence, little is known or researched about Eop1. Regardless, the preceding points lay a solid foundation for the investigation of the following questions:

a) What is/are Eop1's function(s) and mechanism(s)?
b) What is/are Eop1's host target(s)?
c) Can we utilise the non-host resistance (NHR) to answer the abovementioned questions?

[20] Note: The above section (Research question) informs about the 'central theme' of the research. The chapter-specific 'introduction sections' cover the specific questions under investigation in each study.

d) What R-protein(s) is/are driving the recognition of Eop1s in *Malus* ‘Evereste’ and *Malus floribunda* 821, and what could its mechanism be?

The following chapters attempt to address these above-stated questions.

2 Chapter 2: Recognition of Eop1 effector from *E. amylovora* and related species in the non-host plant *Nicotiana tabacum*

2.1 Introduction

When introduced into the host plants, pathogen-delivered effectors act as a virulence factor, assisting the pathogen in successfully invading the host plant by modulating its innate immune system (Panstruga & Moscou, 2020; Toruno et al., 2016a). However, when delivered in the non-host plants, the same effectors can serve as an avirulence factor and trigger HR through specific recognition via NB-LRR type immune receptors, imparting non-host resistance[21] (Panstruga & Moscou, 2020; Vleeshouwers et al., 2008). The YopJ family effectors and homologs of Eop1 (Ma & Ma, 2016), HopZ5, HopZ3 and HopZ1a from *Pseudomonas syringae* pathovars[22] are classic examples of NHR, as they trigger HR when introduced or expressed in the non-host plant, *Nicotiana benthamiana* (Jayaraman et al., 2017), *Nicotiana tabacum* (Vinatzer et al., 2006) (unpublished data from Yoon & Rikkereink[23]) and *Arabidopsis thaliana* (Zhang et al., 2016), respectively.

Erwinia amylovora, like many other gram-negative bacterial pathogens, delivers effectors through T3SS, which triggers HR in non-host plants such as *Arabidopsis* and *N. tabacum* (Buttner & He, 2009; Degrave et al., 2008; Oh & Beer, 2005; Zhao et al., 2006). DspA/E (Boureau et al., 2006) and Eop3 (Bocsanczy et al., 2012) are two of the five T3SEs delivered by *E. amylovora* that

[21] Non-host resistance (NHR) is generally defined as "the ability of all genotypes of a plant species to confer resistance to all genotypes of a pathogen species" (Panstruga & Moscou, 2020). The plants exhibiting NHR against a microbe are termed 'non-host plants' corresponding to that particular species.

[22] HopZ5 from *P. syringae* pv. actinidiae (*Psa*); HopZ3 from *Psa* and *P. syringae* pv. syringae (*Psy*); and HopZ1a from *Psy.*

[23] All the unpublished data from Yoon and Rikkerink was conveyed through personal communication and will be referred to as 'unpublished data from Yoon & Rikkerink' or simply as 'unpublished data' in this study.

have been shown to elicit HR in *N. tabacum*; in contrast, Eop2 has been identified not contributing to the HR (Bocsanczy et al., 2012). Furthermore, a thorough review of the literature for Eop1, $AvrRPt2_{Ea}$, and $HopPtoC_{Ea}$ effectors interaction in *N. tabacum* reveals that they have not been adequately investigated. Nonetheless, the $AvrRPt2_{Ea}$-RPS2 interaction via RIN4 perturbation in *Arabidopsis* has been comprehensively characterised and explains the reason behind the HR-triggering phenomenon by *E. amylovora* in *Arabidopsis* (Mooney et al., 2021; Vogt et al., 2013; Zhao et al., 2006).

Agrobacterium-mediated transient expression of the T3SEs is a powerful tool for studying and characterising individual effectors. In this method, *Agrobacterium* harbouring a gene-of-interest (which in this instance is an effector encoding gene) in a binary plasmid vector under an appropriate promoter (such as 35S promoter) is infiltrated into plant leaves (Kapila et al., 1997). Once infiltrated into the plant, the *Agrobacterium* cells adhere to the plant cells. Upon sensing the plant cells, a cascade of signal transduction starts within the *Agrobacterium* cells, which culminates with the transfer of the 'transfer-DNA' (T-DNA), carrying the gene-of-interest, from the bacterial into the plant cells, where it is integrated into the plant genome via “illegitimate recombination” (Mayerhofer et al., 1991), and expressed by the plant's protein translation machinery (Gelvin, 2003; Kapila et al., 1997).

Using *Agrobacterium*-mediated transient expression in combination with RNAi-induced silencing, Yoon and Rikkerink (2020) discovered an R-protein of NB-LRR class, namely Resistance to *Pseudomonas syringae* pv. actinidiae 1 (RPA1), resident to *N. tabacum* cv. Samsun. RPA1 was found to trigger HR upon recognising the AvrRpm1 effector from *Psa*_V3 (Yoon & Rikkerink, 2020). Interestingly, the transient expression analysis of HopZ3 effector from *Psa* biovar_1 (hereafter, HopZ3*psa*_V1) and Eop1 from *E. amylovora* (*Ea*246), conducted by Yoon

and Rikkerink, also triggered HR in the same *N. tabacum* cultivar (Unpublished data). Furthermore, a subsequent study conducted by the same group discovered that RPA1 and RPM1-Interacting protein 4 (RIN4), an intrinsically disordered hub-protein (Sun et al., 2014), are crucial for the HopZ3*psa*_V1 triggered HR in *N. tabacum*, as silencing of either of the two resulted in the significant reduction in HR (unpublished data).

Considering the ability of Eop1 (*Ea*246) to trigger HR in *N. tabacum* cv. Samsun and its phylogenetic relation with HopZ3 (Ma & Ma, 2016), with HopZ3 being a putative functional homolog of the Eop1 effector (Ma et al., 2006), it was hypothesised that the Eop1 from *E. amylovora* strains and its sequence homologs from the "*Erwinia-Pantoea*" group members would likewise use the similar effector recognition mechanism and trigger HR in *N. tabacum* cv. Samsun. Therefore, an attempt was made to test the proposed hypothesis by transiently expressing the Eop1 variants via *Agrobacterium* in *N. tabacum* 'Samsun' (Figure 2.1).

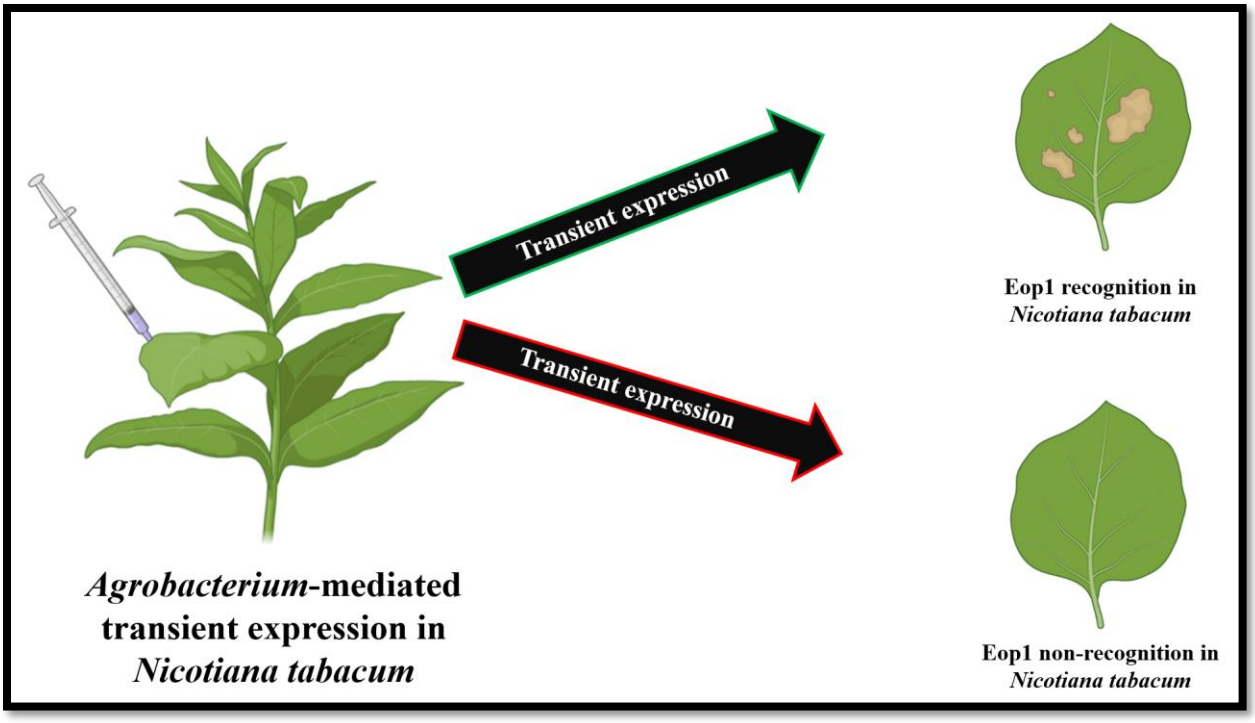

Figure 2.1: Anticipated phenotype of the Eop1 effector recognition and non-recognition in *Nicotiana tabacum*. The induction of the hypersensitive response in the *N. tabacum* leaf infiltrated with the *Agrobacterium* strain carrying an expression clone harbouring the *eop1* gene construct indicates recognition and vice versa for non-recognition.

2.2 Materials and Methods

2.2.1 Bioinformatics Methods

2.2.1.1 Protein sequence alignment

The protein sequences were aligned using bioinformatics software: Genious 2018: Version 10.2.5 [Dotmatics, Boston, USA]. The following parameters were used for the alignments: Geneious alignment algorithm; Alignment type: Global alignment with free end gaps; Cost matrix: Blosum62; Gap open penalty: 12; Gap extension penalty: 3; and Refinement iterations: 2 (Supplementary Figure C2S1).

2.2.1.2 Selection of Eop1 variants

The Eop1 variants from *E. amylovora* and other related species from the "*Erwinia-Pantoea"* group were selected for the transient expression analysis based on differences in the protein sequence identity (in %) and associated host plants. The primary objective of this strategy was to include a diverse set of Eop1 variants from the plant-pathogenic bacteria while excluding those from an animal-pathogenic background, such as *Pantoea agglomerans*, *Serratia marcescens* and members of *Yersinia* species.

2.2.2 Preparation of electrocompetent cells

2.2.2.1 Preparation of *Escherichia coli* (TOP10) electrocompetent cells

Escherichia coli (*E. coli*) TOP10 (see footnote '24' for the genotype) was streaked out from glycerol stock stored at -80℃ freezer and incubated at 37℃ for 24 hours. A single colony from the streaked plate was then used to inoculate a 25 mL starter culture of Lysogeny broth (LB) liquid

[24] Genotype of the *E. coli* (TOP10): [F– mcrA Δ(mrr-hsdRMS-mcrBC) Φ80lacZΔM15 ΔlacX74 recA1 araD139 Δ(araleu) 7697 galU galK rpsL (StrR) endA1 nupG].

medium (Bertani, 1951) in a 50 ml Falcon® tube. The inoculated culture was incubated overnight in a shaking incubator at 37℃ and 200 RPM [Infors HT (Ecotron), NZ]. The following day, 10 mL aliquots of starter culture were used to inoculate two Erlenmeyer flasks, each containing 250 mL of autoclaved LB liquid medium. The growth of cells (cell density) in LB medium was intermittently monitored by measuring the optical absorbance of light at 600 nm wavelength (OD_{600}) using a spectrophotometer [Global Science, NZ].

Once an approximate OD_{600} value of 0.4 (equivalent to $5x10^8$ CFU/mL) was obtained, the cultures were removed from the incubation shaker. The *E. coli* cell cultures were then chilled on ice for 30 minutes by continuous swirling. The cells were then poured into pre-chilled 500 mL centrifuge bottles and centrifuged for 20 minutes at 1542 RCF and 4°C in a Sorvall RC6 Plus™ centrifuge [Thermo Scientific, Langenselbold, Germany]. Next, the supernatant was discarded, and the cell pellets were gently resuspended into a chilled 200 mL 10% (v/v) glycerol solution; the resulting cell suspension was centrifuged again at the same RCF, temperature, and duration. After discarding the supernatant, the pellets were resuspended in 100 mL of 10% glycerol solution. Both bottles' cell suspensions were combined and centrifuged for 20 minutes at 1542 RCF and 4°C. Next, the supernatant was discarded, and a new cell suspension was made by resuspending the cell pellet in 50 mL 10% glycerol solution; the cell suspension was again centrifuged under the same centrifuge conditions described above. Finally, the supernatant was discarded again, and the cell pellet was gently resuspended in 1 mL chilled 10% glycerol solution by gentle pipetting (Figure 2.2 illustrates the schematic representation of the process).

After final resuspension, 1mL of competent cells were divided evenly into twenty-five aliquots of 40 µL volume. The aliquots were snap-frozen by immersing them in liquid nitrogen. The competency of the *E. coli* electrocompetent cells was assessed by transforming one aliquot

with pUC-19 plasmid DNA (Yanisch-Perron et al., 1985) and plating 100 µL of 10X and 100X dilutions of the transformed culture on LB agar plates containing Carbenicillin (50 µg/ml) [Duchefa Biochemie; Haarlem, The Netherlands].

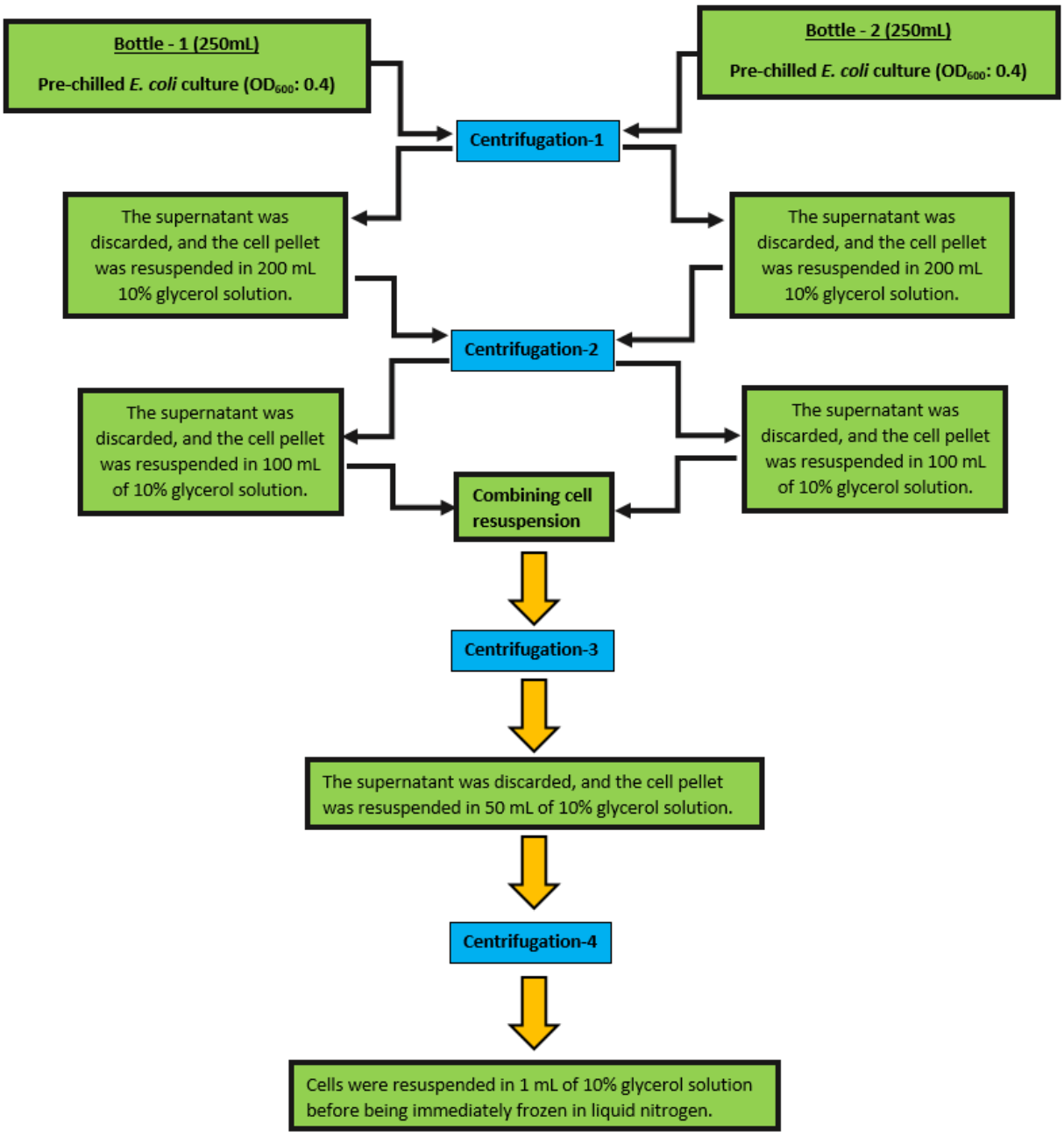

Figure 2.2: Schematic representation of the steps involved in the preparation of *E. coli* (TOP-10) electrocompetent cells.

2.2.2.2 Preparation of *Agrobacterium tumefaciens* (GV3101) electrocompetent cells

Agrobacterium tumefaciens (GV3101) (see footnote '25' for genotype) was streaked out from glycerol stock stored at a -80℃ freezer and incubated for 36 hours at 28℃. A single colony from the streaked plate was used to inoculate a 25 mL starter culture of LB liquid medium containing selective antibiotics: Gentamicin (20 µg/mL) [Duchefa Biochemie; Haarlem, The Netherlands] and Rifampicin (10 µg/mL) [Duchefa Biochemie; Haarlem, The Netherlands] in a 50 ml Falcon® tube. The inoculated culture was then incubated overnight in a shaking incubator at 28℃ and 200 RPM [Infors HT (Ecotron), NZ]. The following day, 10 mL aliquots of the starter culture were used to inoculate two Erlenmeyer flasks, each carrying 250 mL of LB broth containing the aforementioned antibiotics. The cultures were then incubated at 28℃ and 200 RPM.

The cultures were taken out of the incubator at approx. OD_{600} value of 0.4. Following that, the *Agrobacterium* cells were made electrocompetent by multiple centrifugations at 1542 RCF for 20 minutes at 4°C and 10% glycerol washes (by employing the same workflow as described for making *E. coli* electrocompetent cells in 'Figure 2.2'). Finally, 40 µL aliquots of *Agrobacterium* electrocompetent cells were snap-frozen in liquid nitrogen.

The competency of the *Agrobacterium* electrocompetent cells was assessed by transforming one aliquot with pUC-19 and plating 100 µL of 10X and 100X dilutions of the transformed culture on LB agar plates containing selective antibiotics: Carbenicillin (50 µg/mL), Gentamicin (20 µg/mL), Rifampicin (10 µg/mL).

[25] Genotype of the *Agrobacterium tumefaciens* (GV3101): [C58 (rif R) Ti pMP90 (pTiC58DT-DNA) (gentR/strepR) Nopaline].

2.2.3 Molecular cloning

2.2.3.1 Introduction to Twist technology of gene synthesis

The Twist technology, developed by Twist Bioscience [South San Francisco, California, USA], entails the artificial synthesis of the desired gene into an entry or expression vector (Figure 2.3).

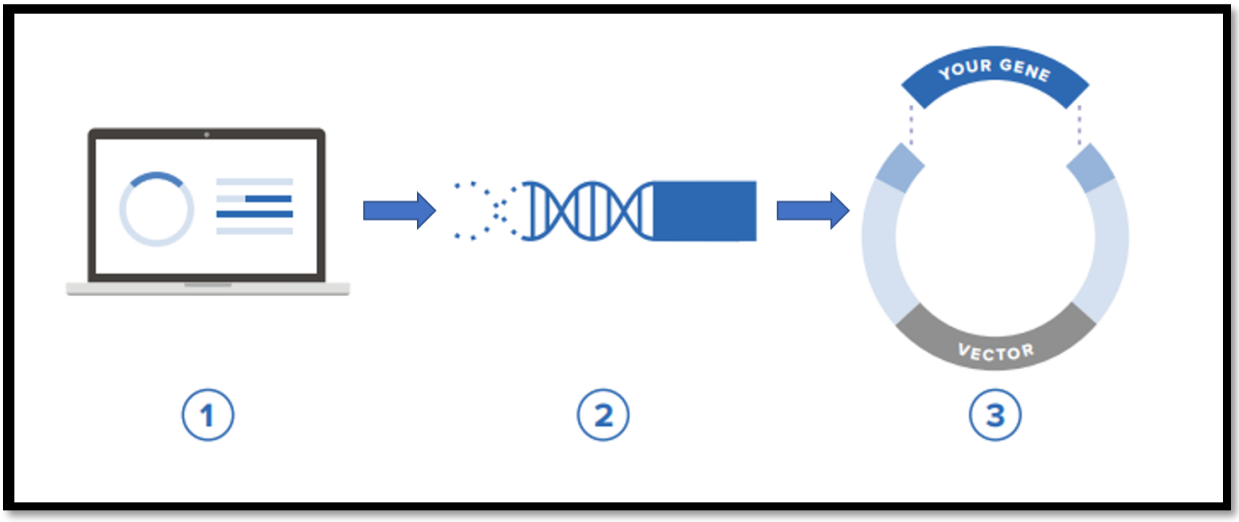

Figure 2.3: An outline of the steps involved in 'Twist technology' of gene synthesis. (1) The database is first queried for the DNA sequence of the targeted gene; (2) The gene is then artificially synthesised using Twist technology; (3) The newly synthesised gene is inserted into a cloning or expression vector for subsequent usage[26].

2.2.3.1.1 Synthesis of the gene-of-interest in entry vector using Twist technology

First, the FASTA DNA sequence[27] of the 'gene-of-interest' was retrieved from the NCBI database. A tag sequence[28] was then added to the selected genes. Next, Twist Bioscience synthesised and cloned the selected genes separately into a Kanamycin-resistant and Gateway™ cloning compatible

[26] The figure is obtained from the TwistGenes_Twist Vectors_ProductSheet. The URL for the same is as follows: https://www.twistbioscience.com/assets/media/Twist_Genes_TwistVectors_ProductSheet.pdf
[27] The FASTA DNA sequence of the selected sequences is provided in the appendix section.
[28] The Eop1 variants were HA-tagged at the C-terminus, while the RIN4 variants were FLAG-tagged at the N-terminus.

entry vector. The entry clones harbouring the selected gene were then used in the downstream Gateway® cloning process.

2.2.3.2 Introduction to Gateway Cloning

The Gateway® cloning System, developed by Invitrogen in the late 1990s, is a two-step high throughput cloning system which utilises 'site-specific recombination' properties of lambda bacteriophage in molecular cloning (Chiew Foan Chin, 2015). This cloning system incorporates 'BP' and 'LR' reactions (Figure 2.4).

The 'BP' cloning reaction involves an excision-recombination reaction between a PCR-amplified or synthesised gene flanked with cloning sites 'attB' and a donor vector with 'attP' sites. These sites are interchanged in a recombination reaction catalysed by BP clonase, yielding an entry clone containing the gene-of-interest along with 'attL' cloning sites. Similar to the 'BP' cloning reaction, in the 'LR' cloning reaction, a Gateway® cloning compatible destination vector (e.g., pHEX2) with 'attR' sites is used in an excision-recombination reaction with the entry clones developed in the preceding BP reaction. The LR cloning reaction is led by LR clonase and results in an expression clone harbouring the gene-of-interest, ready for *in-planta* expression post-*Agrobacterium* delivery (Figure 2.4) (Chiew Foan Chin, 2015; Dubin et al., 2008; Earley et al., 2006). In addition, to eliminate negative clones (clones not carrying the gene-of-interest), a 'control of cell death B' (ccdB) gene cassette coding for the 'ccdB toxin' protein is used (Earley et al., 2006; Lemieux, 2016).

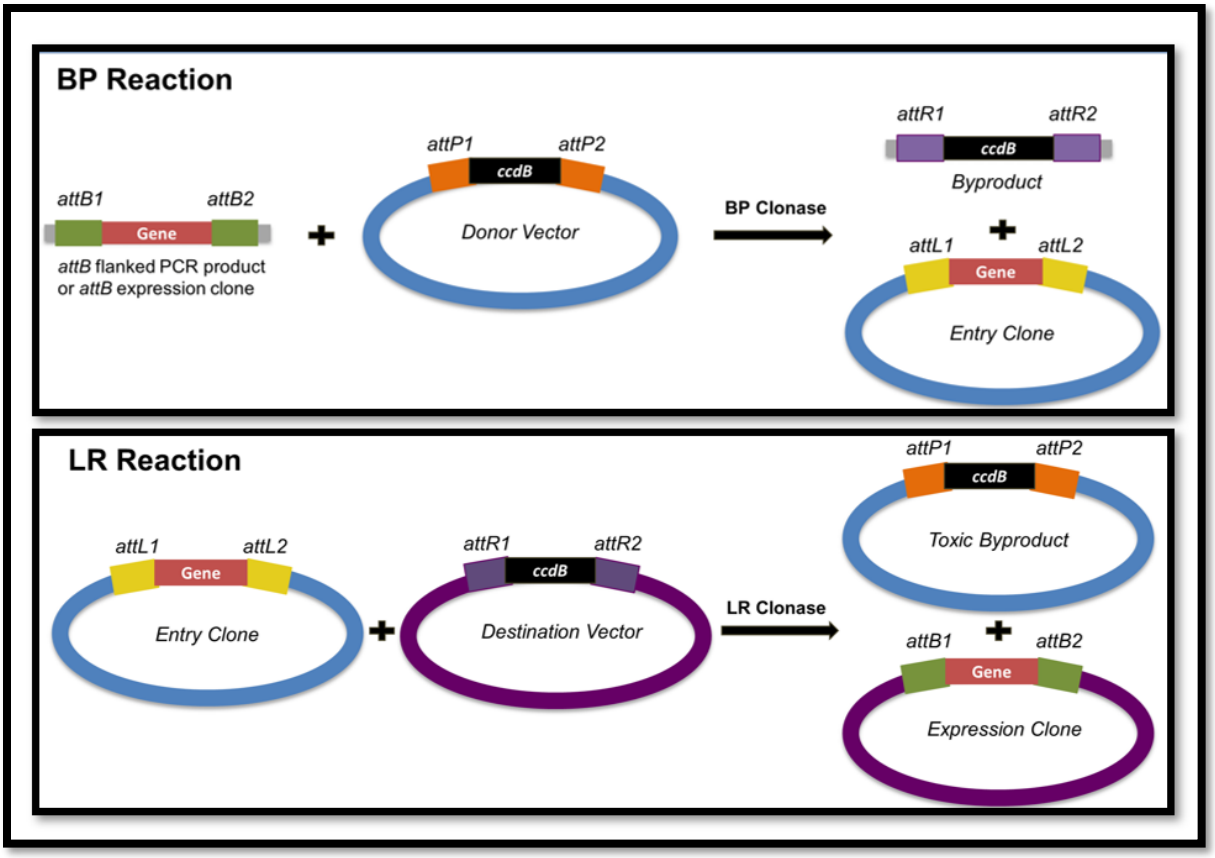

Figure 2.4: An outline of the steps involved in Gateway molecular cloning[29].

2.2.3.2.1 LR reaction in Gateway cloning

For LR cloning reactions[30], 1.5 µL (100-150 ng) of entry clone carrying the gene-of-interest was first put in a 1.5 mL Eppendorf® tube; to this, 1.5 µL (150-175 ng) of destination vector: pHEX2, 7 µL of TE buffer, and 2 µL of Gateway™ LR Clonase™ II Enzyme Mix [Life Technologies, CA, USA] was mixed and incubated at 25°C for 2 hours. The LR cloning reaction was then terminated by adding 1 µL (2 µg) of Proteinase K solution [Life Technologies, CA, USA], followed by gentle

[29] The image was adopted from: https://blog.addgene.org/plasmids-101-gateway-cloning

[30] In the Gateway® cloning performed in this study, the 'BP' reaction was not performed as the sequences were synthesised using Twist Technology (see section 2.2.3.1.1). Consequently, only the 'LR' reaction was required and performed.

vortexing and incubation at 37℃ for 15 minutes. The cloning product was then used to transform 40 µL of *E. coli* electrocompetent cells, prepared as described in section 2.2.2.1.

2.2.4 Electroporation assisted transformation of electrocompetent cells

E. coli and *Agrobacterium* electrocompetent cells were transformed through electroporation. Frozen aliquots of electrocompetent cells (40 µL) were first thawed on ice for 20 minutes. Next, 1 µL (100-150 ng) of plasmid DNA was added to the cells and mixed gently by pipetting, followed by ice incubation for 10 minutes. Finally, the mixture was carefully transferred to a pre-chilled sterile electroporation cuvette of 0.1 cm gap width [Bio-Rad, NZ], gently tapped for even distribution and placed in an electroporator.

The cells were electroporated using a Bio-Rad X-cell GenePulser® electroporator [Bio-Rad, NZ] at 1800 kV voltage, 200 Ω resistance, and 25 µF capacitance. Following electroporation, the cells were immediately inoculated with 1 mL of antibiotic-free LB liquid medium and incubated for 1 to 2 hours at the optimum temperature, i.e., 37℃ for *E. coli* and 28℃ for *A. tumefaciens*. Next, 100 µL cells were plated on an LB agar plate containing the appropriate selective antibiotics to obtain transformants carrying the gene-of-interest.

2.2.5 Plasmid DNA isolation

E. coli culture was grown overnight in LB liquid medium containing appropriate antibiotics, i.e., Kanamycin (50 µg/mL) and Spectinomycin (50 µg/mL) for the *E. coli* carrying entry and expression clone, respectively. Next, the plasmid DNA from the overnight cultured *E. coli* cells was harvested using materials and instructions guided by the Zyppy® Plasmid Miniprep Kit®

[Zymo Research, CA, USA]. In addition, the harvested plasmid DNA was checked for quality and integrity using Nanodrop® ND-1000 Spectrophotometer[31] [Thermo Fisher Scientific, USA].

2.2.6 Gel Electrophoresis

For gel electrophoresis, 1% (w/v) agarose gel was prepared by mixing 1 gram of Agarose powder in 100 mL of 1X Tris-Acetate-EDTA (TAE) buffer in a 250 mL flask and microwaved until a clear homogeneous solution was obtained. To this, 5 µL of Redsafe™ nucleic acid staining solution (20,000X) [iNtRON BIOTECHGNOLOGY, Cat. No. 21141] was added and mixed by continuous swirling. Once adequately cooled, the agarose gel was poured into a tray with the well-comb and allowed to solidify. The gel was then immersed in TAE buffer in an electrophoresis box. Next, the gel was loaded with a maximum volume of 15 µL of the PCR or restriction digest product mixed with gel loading dye (6X) [Invitrogen, NZ], mixed in a ratio of 5:1 (v/v), respectively. The gel was then run at 110 volts for 40-80 minutes. Finally, the gel was visualised under UV and captured into an image using GelDoc XR+ [Bio-Rad; Hercules, CA, USA].

2.2.7 Restriction enzyme digest

In a 1.5 mL Eppendorf® tube, a master mix comprised of 2.5 µL of 10X CutSmart® Buffer [NEB, B7204S], 0.5 µL (5 units) *Pst*I-HF® [NEB, #R3140S] or *Eco*RV-HF® [NEB, #R3195S] restriction enzyme, and 12 µL of PCR grade water was prepared first. To this, 1 µg (4-5 µL) of plasmid DNA was added and incubated at 37℃ for 2-3 hours. The restriction digest result was then visualized on a 1% agarose gel and compared to the template produced through the *in-silico* restriction digest.

[31] Nanodrop® ND-1000 is a full-spectrum spectrophotometer that evaluates 1 µl samples to provide information on the quality and concentration of the DNA or RNA in a given sample.

2.2.8 *In-silico* Gateway cloning and restriction digest

First, using Geneious software V10.2.5, virtual entry clones containing the gene-of-interest were created by inserting the gene-of-interest individually in the virtual entry vector between the 'attL1' and 'attL2' sites (Figure 2.5). The entry clones were then Gateway® cloned with the virtual destination vector (pHEX2) using the default parameters in the software, resulting in virtual expression clones. The expression clones were then virtually digested with the *Pst*I-HF® restriction enzyme, and the bands were viewed on a virtual gel. The result was then used to compare *in-vitro* restriction digests and select positive expression clones.

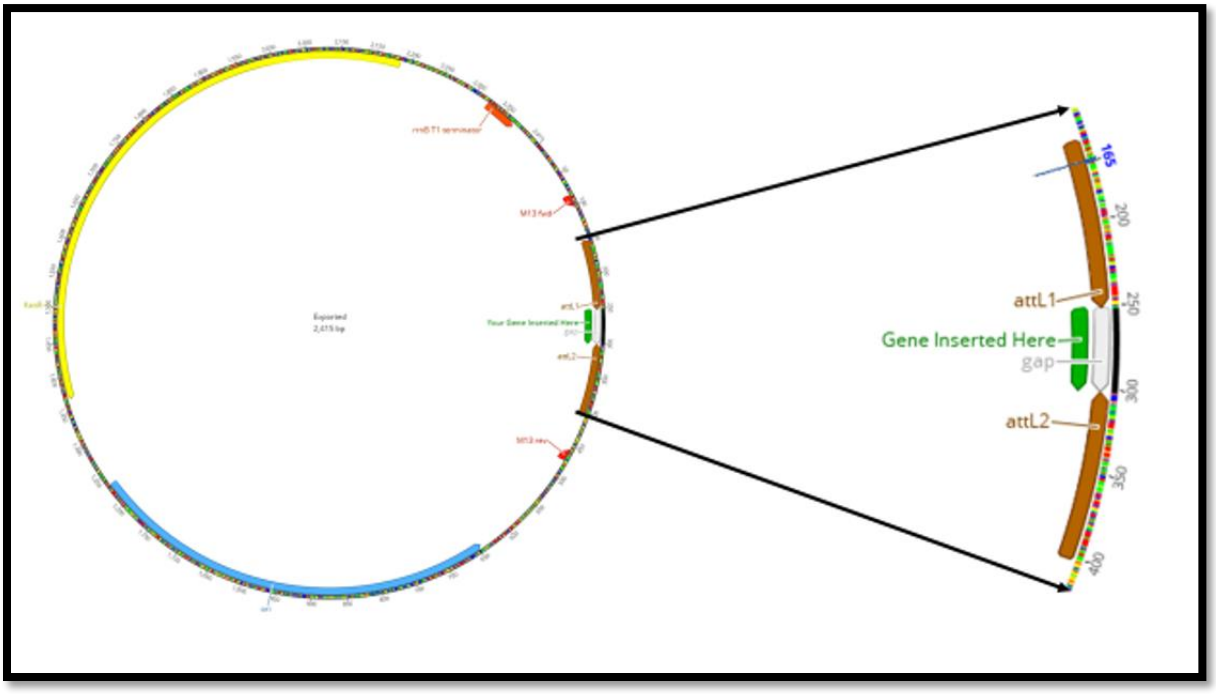

Figure 2.5: Site of gene insertion in the virtual entry vector, pTwist+ENTR.

2.2.9 Colony PCR

First, a single *Agrobacterium* colony from the LB plate was resuspended in 50 µL of PCR-grade water. Next, 19 µL PCR master mix was separately prepared in a 0.2 mL PCR tube by combining 2 µL 10X PCR buffer [Invitrogen, NZ], 1µL (2.5 mM) MgCl2 [Invitrogen, NZ], 1 µL (0.5 mM)

dNTPs mix [Invitrogen, CA, USA], 1 µL (0.5 mM) of each forward and reverse M13 primers, 12.5 µL PCR grade water, and 0.5 µL of Platinum™ Taq DNA Polymerase [Invitrogen, CA, USA]. To this master mix, 1 µL of *Agrobacterium* cell resuspension made previously was added.

The PCR mix was then run in an Eppendorf™ Mastercycler X50s thermal cycler for gene amplification via a three-step PCR protocol. First, initial denaturation was performed at 95℃ for 4 minutes, followed by 45 sequentially run consecutive cycles of denaturation at 95℃ for 30 seconds, annealing at 58℃ for 30 seconds, and extension at 68℃ for 2 minutes; a final extension was carried out at 68℃ for 30 minutes followed by a final hold of the samples at 4℃. The PCR product was then visualised by running on 1% agarose gel.

2.2.10 Glycerol stocks

Glycerol stock was prepared from the *Agrobacterium* culture grown overnight in an LB liquid medium containing selective antibiotics: Spectinomycin (50 µg/ml) [Duchefa Biochemie; Haarlem, The Netherlands], Gentamicin (20 µg/ml), Rifampicin (10 µg/ml). In a 1.5 mL Eppendorf® tube, 1 volume of overnight-grown culture was combined with 1 volume of sterile 50% glycerol. The mixture was thoroughly mixed through pipetting and stored in a -80 freezer for long-term storage. When required, the bacteria were recovered by thawing the glycerol stock on ice for 10 minutes and streaking an LB plate containing the aforementioned antibiotics with a sterile loop dipped in the glycerol stock.

2.2.11 Plants associated material and methods

2.2.11.1 Plant material

Nicotiana tabacum cv. Samsun plants were grown in the controlled environment of a glass house and provided by PFR, Auckland. The controlled environment was maintained at 22℃, with long-day conditions of 16:8 hours of light and darkness, under unregulated but optimal humidity.

2.2.11.2 *Agrobacterium*-mediated transient expression in *Nicotiana tabacum*

Agrobacterium tumefaciens (GV3101) harbouring Empty Vector (EV) or expression clones carrying the gene-of-interest were first grown on LB solid media containing selective antibiotics: Gentamicin (20 µg/mL), Rifampicin (10 µg/mL) and Spectinomycin (50 µg/mL), at 28℃ for 36 hours. Next, a single colony from the plate was used to inoculate 20 mL LB broth containing the aforementioned antibiotics and incubated in a shaker incubator at 28°C and 200 RPM to prepare an overnight culture.

The *Agrobacterium* cells for infiltration were freshly grown by inoculating a 25 mL LB liquid medium containing the aforementioned antibiotics with 1 mL of overnight culture. The cells were then incubated in a shaker incubator at 28℃ and 200 RPM for 6-7 hours (approx. OD_{600} of 0.3 to 0.4). Next, the cells were centrifuged for 15 minutes at 2100 RCF, and the cell pellet was resuspended in 10 mL of infiltration buffer comprised of 10 mM MES (pH 7.2) and 10 mM MgCl2. Finally, the cell-containing infiltration solution was diluted to the desired OD_{600} range and hand-infiltrated in 3-3.5 weeks-old fully expanded leaves of *N. tabacum* using a 1mL needleless syringe.

2.2.11.3 Electrolyte leakage assay

Twenty-one to Twenty-five days old *N. tabacum* ‘Samsun’ leaves were infiltrated with *A. tumefaciens* (GV3101) using the protocol described in section 2.2.11.2. Then, leaf discs of 10 mm

diameter were collected from leaves on different plants for each infiltrated construct on the days indicated on the graph plots. Next, the leaf discs were gently washed in 25 mL MQ water in a Falcon® tube by shaking them on a rocker [TLS, NZ] for 10 minutes. The leaf discs were then strained, washed thoroughly, and placed in a small container filled with 50 mL MQ water. For each sample, two leaf discs were fished out of the water using inoculation loops, put in 2 mL MQ water, and shaken for 2 hours at 150 RPM; 4 replicates of each sample were measured for each day. Finally, electrolyte leakage was measured using a conductometer [Horiba Scientific, Stanmore, UK]. The reading was taken by pipetting 80 µL of water from the 2 mL MQ-water used to collect the leakage. The graph for each tested sample was generated using Microsoft Excel 2019 (clustered and line chart) based on the replicates' mean value from 4 replications for each day, with error bars indicating the standard error.

2.3 Results

2.3.1 Identification of Eop1 variants with high protein sequences identity

The protein sequences of the Eop1 variants (cordially provided by Erik HA Rikkerink) were first aligned and analysed using the parameters described in sections 2.2.1.1 and 2.2.1.2, respectively. The protein sequence identity[32] (in %) between the Eop1 variants in the alignment ranged from 55% to 100%. Following the analysis, three clusters with more than 94 % sequence identity and two clusters with more than 80% sequence identity were identified (marked in red and yellow boxes, respectively, in 'Figure 2.6').

Given the high level of protein sequence identity within the identified clusters and the low level of identity between them, a single Eop1 variant representing each cluster was selected for the transient expression analysis. Moreover, Eop1 from *E. tracheiphila* (EtrEop1), placed outside the identified clusters, was also chosen for testing based on the bacterium host plant (infects non-*Malus* hosts). In totality, six Eop1 variants were selected for the transient expression analysis (see 'Table 2.1' for the 'resident species' of the selected Eop1 variants and associated host plants), along with HopZ3*psa*_V1 as a positive control for HR. The selected Eop1s were HA-tagged at the C-terminus end of the sequence and sent for synthesis in entry vectors via Twist technology, as described in section 2.2.3.1

[32] As determined by sequence alignment, a statistically significant identity between two or more polynucleotide or polypeptide sequences are termed as sequence homologs; similar functions often accompany sequences sharing high identity (Koonin & Galperin, 2003; Pearson, 2013).

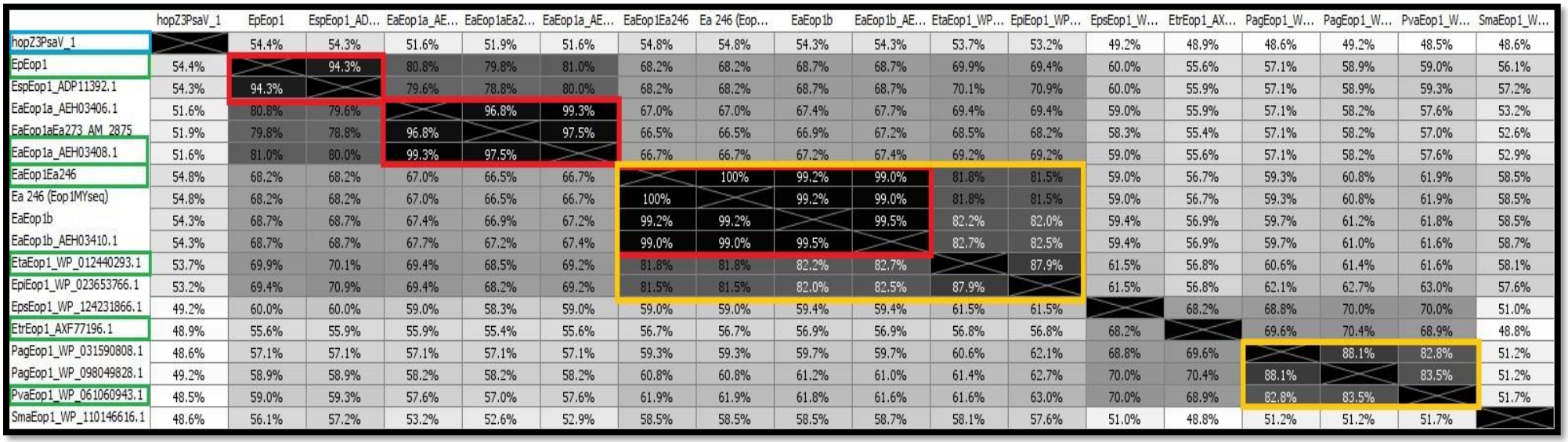

	hopZ3PsaV_1	EpEop1	EspEop1_AD...	EaEop1a_AE...	EaEop1aEa2...	EaEop1a_AE...	EaEop1Ea246	Ea 246 (Eop...	EaEop1b	EaEop1b_AE...	EtaEop1_WP...	EpiEop1_WP...	EpsEop1_W...	EtrEop1_AX...	PagEop1_W...	PagEop1_W...	PvaEop1_W...	SmaEop1_W...
hopZ3PsaV_1		54.4%	54.3%	51.6%	51.9%	51.6%	54.8%	54.8%	54.3%	54.3%	53.7%	53.2%	49.2%	48.9%	48.6%	49.2%	48.5%	48.6%
EpEop1	54.4%		94.3%	80.8%	79.8%	81.0%	68.2%	68.2%	68.7%	68.7%	69.9%	69.4%	60.0%	55.6%	57.1%	58.9%	59.0%	56.1%
EspEop1_ADP11392.1	54.3%	94.3%		79.6%	78.8%	80.0%	68.2%	68.2%	68.7%	68.7%	70.1%	70.9%	60.0%	55.9%	57.1%	58.9%	59.3%	57.2%
EaEop1a_AEH03406.1	51.6%	80.8%	79.6%		96.8%	99.3%	67.0%	67.0%	67.4%	67.7%	69.4%	69.4%	59.0%	55.9%	57.1%	58.2%	57.6%	53.2%
EaEop1aEa273_AM_2875	51.9%	79.8%	78.8%	96.8%		97.5%	66.5%	66.5%	66.9%	67.2%	68.5%	68.2%	58.3%	55.4%	57.1%	58.2%	57.0%	52.6%
EaEop1a_AEH03408.1	51.6%	81.0%	80.0%	99.3%	97.5%		66.7%	66.7%	67.2%	67.4%	69.2%	69.2%	59.0%	55.6%	57.1%	58.2%	57.6%	52.9%
EaEop1Ea246	54.8%	68.2%	68.2%	67.0%	66.5%	66.7%		100%	99.2%	99.0%	81.8%	81.5%	59.0%	56.7%	59.3%	60.8%	61.9%	58.5%
Ea 246 (Eop1MYseq)	54.8%	68.2%	68.2%	67.0%	66.5%	66.7%	100%		99.2%	99.0%	81.8%	81.5%	59.0%	56.7%	59.3%	60.8%	61.9%	58.5%
EaEop1b	54.3%	68.7%	68.7%	67.4%	66.9%	67.2%	99.2%	99.2%		99.5%	82.2%	82.0%	59.4%	56.9%	59.7%	61.2%	61.8%	58.5%
EaEop1b_AEH03410.1	54.3%	68.7%	68.7%	67.7%	67.2%	67.4%	99.0%	99.0%	99.5%		82.7%	82.5%	59.4%	56.9%	59.7%	61.0%	61.6%	58.7%
EtaEop1_WP_012440293.1	53.7%	69.9%	70.1%	69.4%	68.5%	69.2%	81.8%	81.8%	82.2%	82.7%		87.9%	61.5%	56.8%	60.6%	61.4%	61.6%	58.1%
EpiEop1_WP_023653766.1	53.2%	69.4%	70.9%	69.4%	68.2%	69.2%	81.5%	81.5%	82.0%	82.5%	87.9%		61.5%	56.8%	62.1%	62.7%	63.0%	57.6%
EpsEop1_WP_124231866.1	49.2%	60.0%	60.0%	59.0%	58.3%	59.0%	59.0%	59.0%	59.4%	59.4%	61.5%	61.5%		68.2%	68.8%	70.0%	70.0%	51.0%
EtrEop1_AXF77196.1	48.9%	55.6%	55.9%	55.9%	55.4%	55.6%	56.7%	56.7%	56.9%	56.9%	56.8%	56.8%	68.2%		69.6%	70.4%	68.9%	48.8%
PagEop1_WP_031590808.1	48.6%	57.1%	57.1%	57.1%	57.1%	57.1%	59.3%	59.3%	59.7%	59.7%	60.6%	62.1%	68.8%	69.6%		88.1%	82.8%	51.2%
PagEop1_WP_098049828.1	49.2%	58.9%	58.9%	58.2%	58.2%	58.2%	60.8%	60.8%	61.2%	61.0%	61.4%	62.7%	70.0%	70.4%	88.1%		83.5%	51.2%
PvaEop1_WP_061060943.1	48.5%	59.0%	59.3%	57.6%	57.0%	57.6%	61.9%	61.9%	61.8%	61.6%	61.6%	63.0%	70.0%	68.9%	82.8%	83.5%		51.7%
SmaEop1_WP_110146616.1	48.6%	56.1%	57.2%	53.2%	52.6%	52.9%	58.5%	58.5%	58.5%	58.7%	58.1%	57.6%	51.0%	48.8%	51.2%	51.2%	51.7%	

Figure 2.6: Protein sequence alignment matrix of the Eop1 variants. The figure presents the identified clusters with high-sequence identity and Eop1 variants selected for the HR assay in *N. tabacum*. The boxes' colour codes are as follows: red boxes = Eop1 clusters with >94% sequence identity; yellow boxes = Eop1 clusters with 80 % and above sequence identity; green boxes = Eop1 variants selected for HR assay; blue box = HopZ3*psa*_V1 (positive control for HR in the study).

Table 2.1: An overview of the essential details of the Eop1 variants selected for the HR assay in *N. tabacum*.

Annotation in the protein sequence alignment	Accession No. in NCBI database	Resident species of the Eop1 variant	In the current study, referred as	Associated host plants
EpEop1	WP_012669297.1	*Erwinia pyrifoliae* str. Ep1/96	*Ep*1/96	Pathogenic to Asian pear (*Pyrus pyrifoliae)* but also infects some cultivars of apple (Kim, Jock, et al., 2001; Lee et al., 2020).
Eop1Ea246	AAF63400.1	*Erwinia amylovora* str. Ea246	*Ea*246	Rubus infecting strains of *E. amylovora*, particularly raspberry and blackberry (Asselin et al., 2011).
EaEop1a	AEH03408.1	*Erwinia amylovora* str. Ea262	*Ea*262	Spiraeoideae infecting strain of *E. amylovora*, particularly apple and pear (Asselin et al., 2011).
EtaEop1	WP_012440293.1	*Erwinia tasmaniensis* str. Et1/99	*Et*1/99	An epiphytic and a putative non-phytopathogenic relative of *E. amylovora* (Kube et al., 2008).
EtrEop1	AXF77196.1	*E. tracheiphila* str. MDcuke	*E. tr_MDcuke*	The etiological agent of the bacterial wilt disease in Cucurbitaceae, mainly infecting *Cucurbita* and *Cucumis* species. Localised to the Midwest, Mid-Atlantic, and Northeast regions of the USA, along with extreme southern portions of Canada (Rojas et al., 2015; Shapiro et al., 2018).
PvaEop1	WP_061060943.1	*Pantoea vagans* str. C9-1	*P. va_* C9-1	*P. vagans* (formerly *Erwinia herbicola)* is a non-phytopathogenic epiphyte species which is used as an antagonistic biocontrol agent against *E. amylovora* (Walterson & Stavrinides, 2015).

2.3.2 Cloning of the Eop1 variants' gene in the expression vector for HR assays

The Twist technology (section 2.2.3.1) was used to synthesise the selected Eop1 variants' gene[33]; consequently, the 'BP' cloning reaction in the Gateway® cloning was not required and the expression clones carrying the *eop1* gene in the expression vector: pHEX2 was generated via LR cloning reaction as described in section 2.2.3.2.1. Following that, electrocompetent *E. coli* cells (prepared via the method described in section 2.2.2.1) were transformed with 1 µL of the LR cloning reaction product by employing the protocol described in section 2.2.4. Afterwards, the transformed cells were grown for 24 hours at 37°C on LB solid medium containing Spectinomycin (50 µg/mL).

The plasmid expression clones from the transformed *E. coli* cells were harvested using the method described in section 2.2.5. The expression clones were then restriction digested with the *Pst*I-HF® restriction enzyme (via the protocol described in section 2.2.7) to select expression clones carrying the *eop1* gene (i.e., positive expression clones). Finally, *in-silico* Gateway® cloning and *Pst*I-HF® restriction digest were also performed using the Geneious software V10.2.5 (by employing the method described in section 2.2.8) to create a template for comparing and selecting positive expression clones. The *in-vitro* restriction digest result of the expression clones perfectly matched the *in-silico* generated restriction digest template, suggesting positive cloning of the *eop1* variants' gene in the expression clones (Figure 2.7).

[33] The FASTA DNA and protein sequence of the selected Eop1 variants is provided in the 'appendix' section.

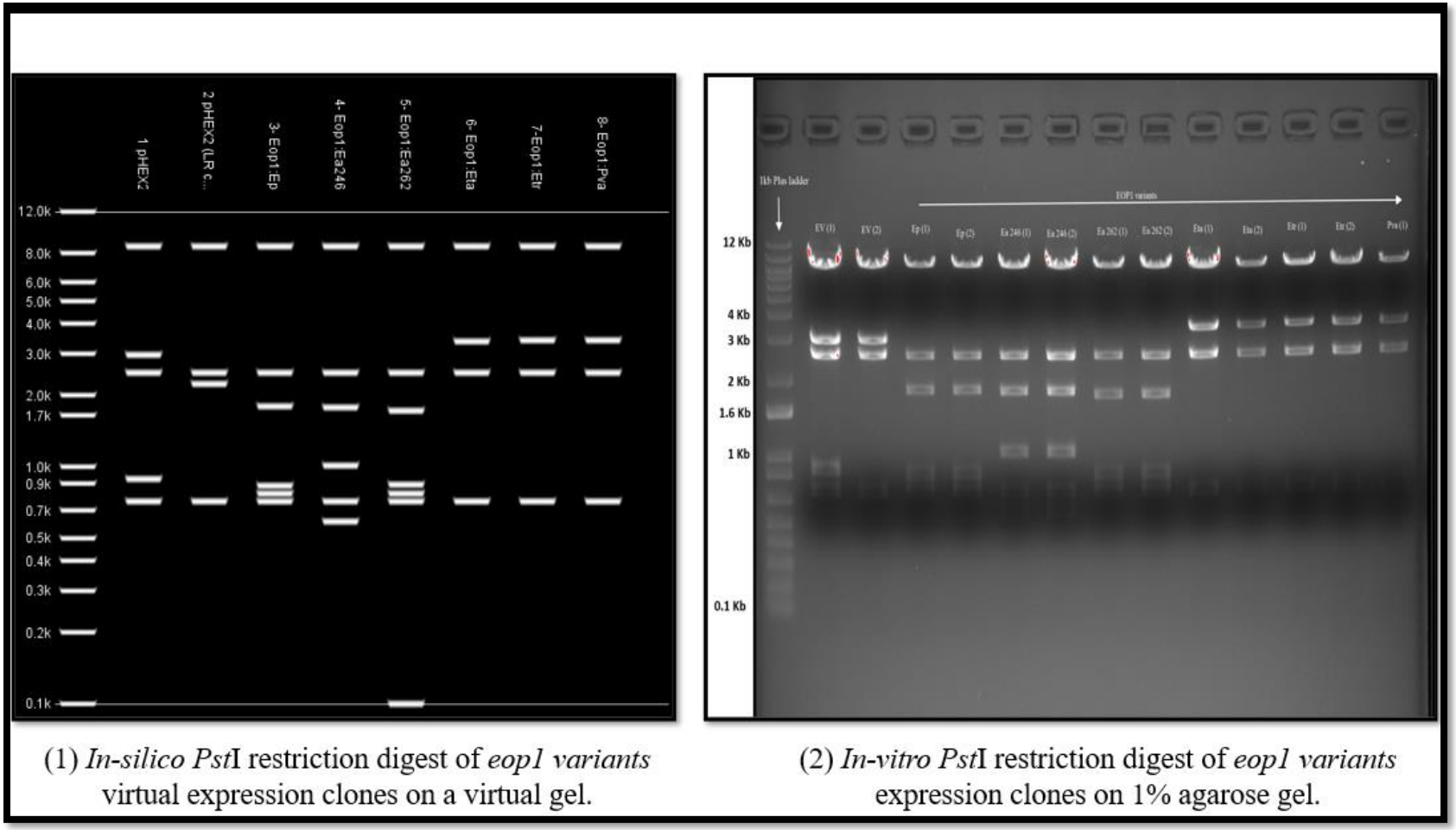

(1) *In-silico Pst*I restriction digest of *eop1 variants* virtual expression clones on a virtual gel.

(2) *In-vitro Pst*I restriction digest of *eop1 variants* expression clones on 1% agarose gel.

Figure 2.7: Comparison of the *in-vitro* restriction digest result of Eop1 variants' expression clones with *in-silico* generated restriction digest template. The remarkable similarity confirms the positive cloning of *eop1* variants in the expression clone: pHEX2. (Note: For each sample presented in the *in-silico* restriction digest template, expression clones from two separate *E. coli* colonies were harvested and tested in the *in-vitro* restriction digest).

The expression clones that passed the *Pst*I-HF® restriction digestion analysis were used to transform the *Agrobacterium* electrocompetent cells (prepared as described in section 2.2.2.2) by employing the method described in section 2.2.4. The Colonies were then grown on an LB solid medium containing appropriate selective antibiotics. Next, positive transformants were verified using M13 universal primers driven colony PCR (Figure 2.8), using the protocol described in section 2.2.9. Finally, using the protocol described in section 2.2.10, glycerol stocks were prepared from the colonies that passed the colony PCR check and subsequently tested in the HR assay.

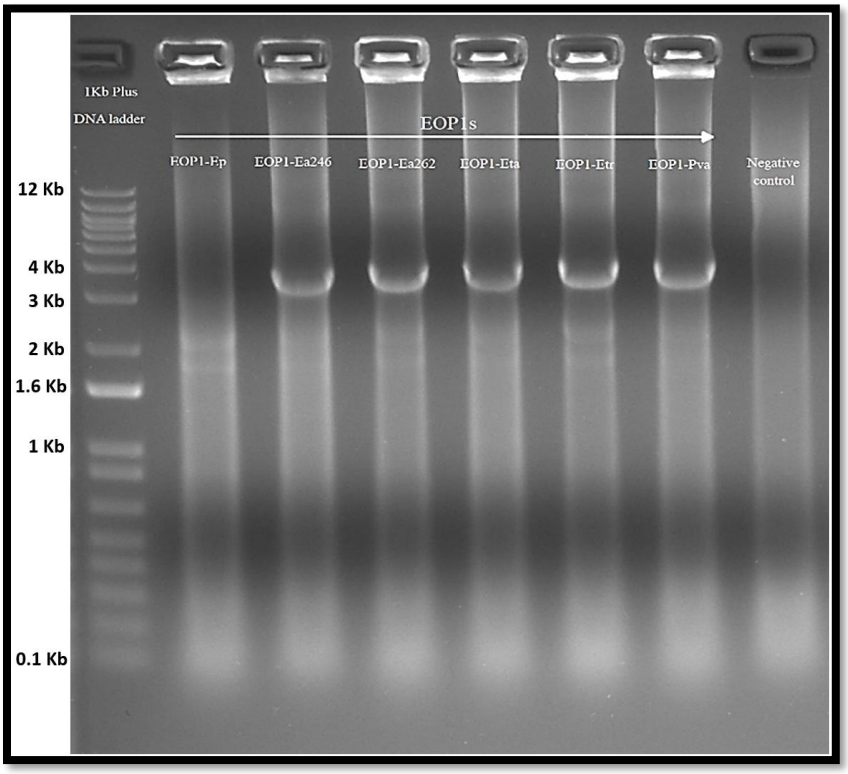

Figure 2.8: M13-universal primers driven colony PCR of *Agrobacterium* colonies harbouring expression clones carrying the *eop1* variants' gene. The bands on the agarose gel image confirm the presence of the *eop1* gene in the corresponding *Agrobacterium* colony[34].

[34] Note: "Eop1–Ep" (referred to as '*Ep*1/96' in the text) in the gel electrophoresis (Figure 2.8) shows a negative cloning result. However, a positive clone was later confirmed by testing a different colony using the same protocol.

2.3.3 Eop1 effector from *E. amylovora* and other related species from the "*Erwinia-Pantoea*" clade elicits HR-like cell death in *N. tabacum*

The primary objective of this experimental study was to test the HR-eliciting ability of Eop1 effector from *Erwinia amylovora* and its sequence homologs from other related species from the "*Erwinia-Pantoea*" group in the non-host plant *N. tabacum* cv. Samsun (See footnote '35' for details on the Eop1s' reaction in *N. tabacum* cv. W38). Therefore, *Agrobacterium* cells carrying an expression clone harbouring the gene of the selected Eop1 under 35S promoter were infiltrated into 3-3.5 weeks old *N. tabacum* leaves by employing the method as described in section 2.2.11.2. Furthermore, *Agrobacterium* cells harbouring Empty Vector (EV) and expression clones for HopZ3*psa*_V1 were infiltrated as negative and positive controls, respectively, for the HR phenotype. The obtained results are as follows:

2.3.3.1 Transient expression analysis of Eop1 variants in *N. tabacum*

HR in the plant leaf, characterised by rapid necrosis followed by gradual mummification of the infiltrated region, was observed in 5 out of 6 tested Eop1s in the HR assay (Figure 2.9). However, a difference in the time of HR elicitation was observed for different Eop1 variants (Figure 2.10). Three Eop1 variants, namely, *Ea*246, *Et*1/99, and *P.va*_C9-1, along with the positive control (HopZ3*psa*_V1), triggered a strong HR in *N. tabacum* after 24-26 hours post-infiltration (hpi) (or 1dpi [36]). Eop1 from *Ep*1/96 and *Ea*262, on the other hand, triggered the HR 46-48 hours post infiltration (2 dpi). Interestingly, no cell death was observed in the leaf segments infiltrated with *Agrobacterium* harbouring EV and *E. tr*_MDcuke Eop1 expression clones (Figure 2.9).

[35] The HR assay of the Eop1 variants was also performed in *N. tabacum* cv. W38 (Supplementary Figure C2S3),yielding similar results as shown in section 2.3.3.1. However, for the subsequent experiments, *N. tabacum* cv. Samsun was used as 'RPA1' R-protein was primarily discovered in the 'Samsun' cultivar.

[36] dpi (in text) / DPI (in figures) = days post-infiltration.

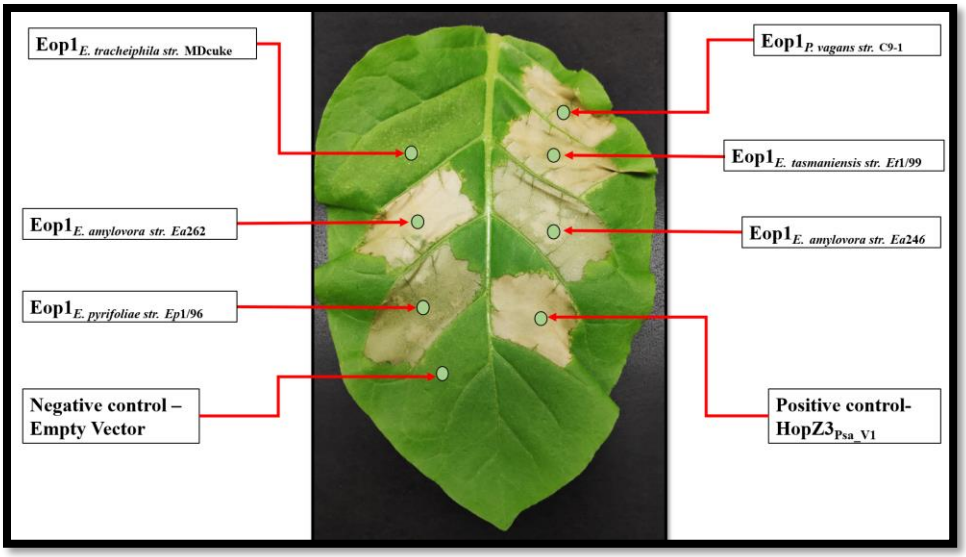

Figure 2.9: HR-elicitation activity of the Eop1 effector from *E. amylovora* and its sequence homologs from other related species in the non-host plant *N. tabacum*. The annotations on both sides of the leaf image represent the transient expression of the annotated *eop1* gene in the corresponding leaf segment delivered via *Agrobacterium* (OD_{600}: 0.1) and expressed under 35S promotor. Circular green dots represent the infiltration site within the leaf. The image was taken at 4 dpi. The experiment was repeated 10 times with similar results.

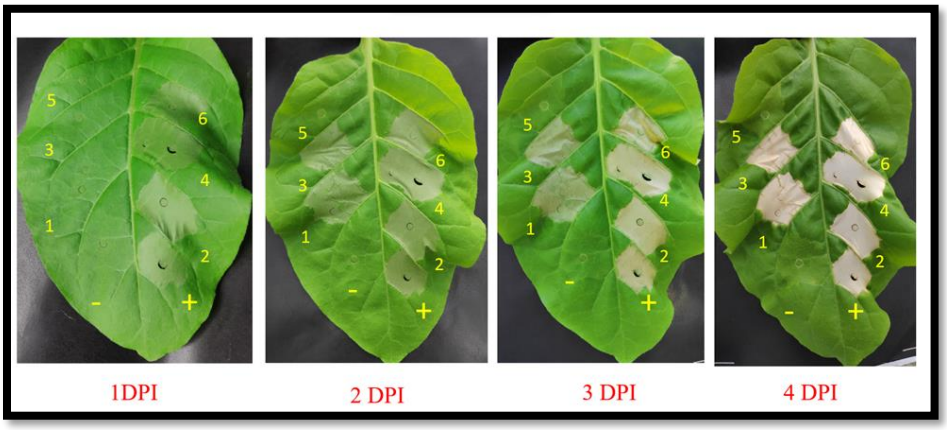

Figure 2.10: An account of the time difference observed in the HR elicitation with the expression of *eop1* variants in *N. tabacum*. The numeric annotations on the leaf segments are as follows: '+' = HopZ3*psa*_V1 (positive control); '-' = Empty Vector (negative control); 1 = Eop1: *E. pyrifoliae* str. *Ep*1/96; 2 = Eop1: *E. amylovora* str. *Ea*246; 3 = Eop1: *E. amylovora* str. *Ea*262; 4 = Eop1: *E. tasmaniensis* str. *Et*1/99; 5 = Eop1: *E. tracheiphila* str. MDcuke; 6 = Eop1: *P. vagans str. C9-1.* The images were taken on consecutive days, as indicated below the images.

2.3.3.2 Electrolyte leakage assay reinforces the Eop1 variants-induced HR phenotype

A unique characteristic of HR is the leakage of electrolytes from stressed and dying plant cells (Demidchik et al., 2014; Murray et al., 1989). Therefore, an electrolyte leakage assay was performed to quantify the observed phenotype of Eop1 variants induced HR in *N. tabacum* at the physiological level by employing the protocol described in section 2.2.11.3.

An anticipated trend of ion leakage paralleling the visual HR phenotype was observed. Based on the analysis of mean value from four replicates for individual tested Eop1 each day, it was observed that three Eop1s, namely, *Ea*246, *Et*1/99, and *P. va*_C9-1 along with the positive control (HopZ3*psa*_V1) exhibited strong ion leakage at 1dpi and had an electrolyte leakage peak value of more than 150 µS/cm (Figure 2.11). Similar ion leakage values were observed at 36-48 hpi for the Eop1s that triggered HR on 2 dpi, namely *Ep*1/96 and *Ea*262; moreover, no significant ion leakage, i.e., a peak value of less than 50 µS/cm, was observed in *E. tr*_MDcuke, EV, and 'non-infiltrated' region (Figure 2.11).

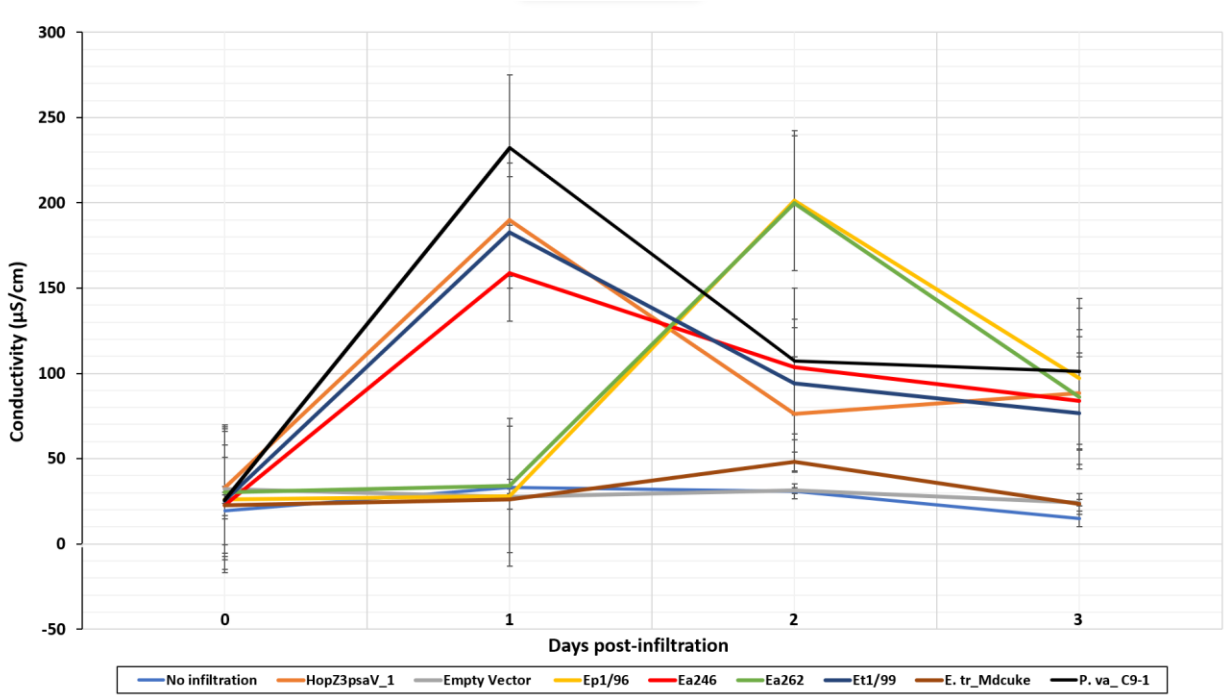

Figure 2.11: Electrolyte leakage data from *N. tabacum* leaf discs infiltrated with *A. tumefaciens* (OD_{600}: 0.1) carrying the *eop1* gene expression clones. The graph is plotted based on the mean value from four replicates on the indicated days for each sample (see section 2.2.11.3 for the detailed procedure); error bars indicate the standard error from the replicates. A complimentary bar plot with data plotted for each day is presented in 'Supplementary Figure C2S2'.

2.4 Discussion

2.4.1 The Eop1 effector from the "*Erwinia-Pantoea"* group members act as a 'putative' avirulence factor in *N. tabacum*

T3SE-induced HR in the host and non-host plants is a hallmark of the effector-triggered immune response (Henry et al., 2013; Senthil-Kumar & Mysore, 2013). ETI also indicates the potential involvement of one or more corresponding R-genes encoded R-proteins (Cook et al., 2015; Jones & Dangl, 2006). Additionally, as suggested by Jones and Dangl (2006), the effectors recognised by the R-protein(s) are referred to as avirulence proteins; however, the pathogen harbouring and expressing the gene for the Avr protein must also render the pathogen avirulent in the resistant host (Bliven & Maurelli, 2012).

The experiments conducted in this study discovered that when transiently expressed in the non-host plant *N. tabacum* cv. Samsun, Eop1 from *E. amylovora* and four of its sequence homologs from related species from the "*Erwinia-Pantoea"* group trigger HR-like cell death, consequently serving as a 'putative' avirulence factor. Moreover, as the tested Eop1s were initially selected as representative of Eop1 homolog clusters (identified as described in section 2.3.1), other members from the same cluster are likely to react similarly and trigger HR in *N. tabacum*.

E. tracheiphila pathovars induce HR in the non-host plant *N. tabacum* (Nazareno et al., 2016); however, the Eop1 effector from *E. tr*_MDcuke tested in the current study failed to elicit HR or any other phenotypic change upon transient expression in *N. tabacum* cv. Samsun. This implies that the *E. tracheiphila* Eop1 effector, unlike Eop1 from *E. amylovora* and *E. pyrifoliae* pathovars, does not contribute to the elicited HR in *N. tabacum*. Furthermore, the *E. tr*_MDcuke Eop1 was chosen based on the criteria of infected host (cucurbit species) and was not a member

of the Eop1 clusters identified in section 2.3.1; thus, it is likely that it may have escaped recognition due to polymorphism in the polypeptide sequence, which requires further investigation.

2.5 Conclusion

The putative avirulence activity of Eop1 variants in *N. tabacum* raises three critical questions that need to be addressed to understand the effectors thoroughly: (1) What is the function of the Eop1 effectors that results in its recognition in *N. tabacum*? (2) What effectors' molecular host target(s) could be? (3) Which cognate R-protein(s) drive Eop1s' recognition that ultimately results in HR in *N. tabacum*?

To look for the clues to answer the aforementioned questions, the Eop1's closest homologs from other species with verified *in-planta* activity were critically analysed (Table 1.2). Based on the analysis, it was observed that the HopZ3 effector, also a putative functional homologue of Eop1 (Ma et al., 2006), interacts with several kinases of the receptor-like cytoplasmic kinase (RLCK) family, such as RIPK, BIK1, PBS1, PBL1, and also acetylates RIN4 (Lee et al., 2015). Interestingly, Yoon & Rikkerink also discovered that RIN4 and RPA1 are crucial for the HopZ3*psa*_V1-induced HR in *N. tabacum* (see section 2.1: paragraph 4). Thus, considering all the aspects mentioned above, it was proposed that similar to HopZ3, Eop1 could interact with RLCK kinases and possibly acetylate RIN4. Furthermore, it was also proposed that RPA1 could be the R-protein driving Eop1 elicited HR in the Samsun cultivar of *N. tabacum.* To test the proposed hypothesis, the functional mechanism of the Eop1 effector was investigated in Chapter 3, and in Chapter 4, the potential involvement of RPA1 and RIN4 proteins in Eop1-triggered HR in *N. tabacum* was researched.

3 Chapter 3: Characterisation of Eop1: *Ea*246 induced HR in *Nicotiana tabacum* and structural and catalytic motif analysis of Eop1 variants via *in-silico* protein modelling

3.1 Introduction

Yersinia outer protein J (YopJ) is a superfamily of evolutionarily conserved bacterial protein effectors whose members are found in animal and plant pathogens and symbionts (refer to 'Supplementary Figure C3S1' for YopJ family effectors phylogeny) (Lewis et al., 2011; Ma & Ma, 2016; Orth et al., 2000). As Ma and Ma (2016) describe, the catalytic activity of the YopJ effectors relies on a conserved 'catalytic triad' present in the effectors' "central region". The catalytic triad typically comprises three amino acid residues: histidine (H), glutamic acid (E), and cysteine (C) (Ma & Ma, 2016; Orth et al., 2000). However, a few exceptions to this have been discovered, such as PopP2, a *Ralstonia solanacearum* YopJ effector, in which aspartate (D) was found to substitute for glutamic acid (E) in the catalytic triad (Tasset et al., 2022). Moreover, mutations in catalytic triad often perturb the enzyme and result in loss of activity (Carter & Wells, 1988); for example, a catalytic cysteine to alanine (C216A) mutant of HopZ1a, a *P. syringae* YopJ effector, fails to trigger HR in *Arabidopsis* eco. Col-0 (Zhang et al., 2016).

The YopJ effectors were initially assumed to have a cysteine protease-like activity because of their structural and topological similarity to the members of the C55 family of cysteine proteases, such as ubiquitin-like protease 1 (Ulp1) and adenoviral protease (AVP) (Orth et al., 2000). However, several YopJ effectors were later discovered to modify their host targets post-translationally via acetylation (Ma & Ma, 2016). The acetylation activity allowed the pathogen to disrupt the stability, subcellular localisation, and enzymatic activity of host-target proteins,

ultimately facilitating the suppression of innate plant immunity (Ma & Ma, 2016). Examples of YopJ effectors from plant pathogens with validated acetyltransferase activity include PopP2 (Le Roux et al., 2015; Sarris et al., 2015); AvrBsT (Cheong et al., 2014); HopZ1a (Jiang et al., 2013; Lee et al., 2012; Lewis et al., 2013; Lewis et al., 2010); and HopZ3 (Lee et al., 2015). Interestingly, modest protease activity of less than 10% compared to archetypal proteases, such as trypsin or proteinase K, has also been observed in *P. syringae* (HopZ1a, HopZ2, and HopZ3) (Ma et al., 2006) and *X. campestris* pv. vesicatoria (AvrBsT and XopJ) YopJ effectors (Szczesny et al., 2010; Ustun & Bornke, 2015).

The YopJ family effectors are distinguished from other acetyltransferases by a unique activation and functional mechanism. Unlike other acetyltransferases, YopJ effectors require a eukaryote-specific co-factor, inositol hexakisphosphate (IP6), for its activation (Mittal et al., 2010). IP6 activates the YopJ effector by inducing a conformational change, forming an 'Acetyl coenzyme A-binding pocket' adjacent to the catalytic motif (Ma & Ma, 2016; Zhang et al., 2016). The binding of Acetyl coenzyme A (AcCoA) to the YopJ effector is considered a critical step for its function as it provides the 'acetyl' functional group for the acetylation activity (Ma & Ma, 2016). The "ping-pong" model (Mukherjee et al., 2006) explains the most widely accepted catalytic mechanism of the YopJ effectors (Ma & Ma, 2016). The model proposes a two-step mechanism involving effectors' autoacetylation and the trans-acetylation of their corresponding substrates (Figure 3.1) (Cheong et al., 2014; Jiang et al., 2013; Lee et al., 2012; Ma & Ma, 2016; Mittal et al., 2010; Trosky et al., 2007; Zhang et al., 2016).

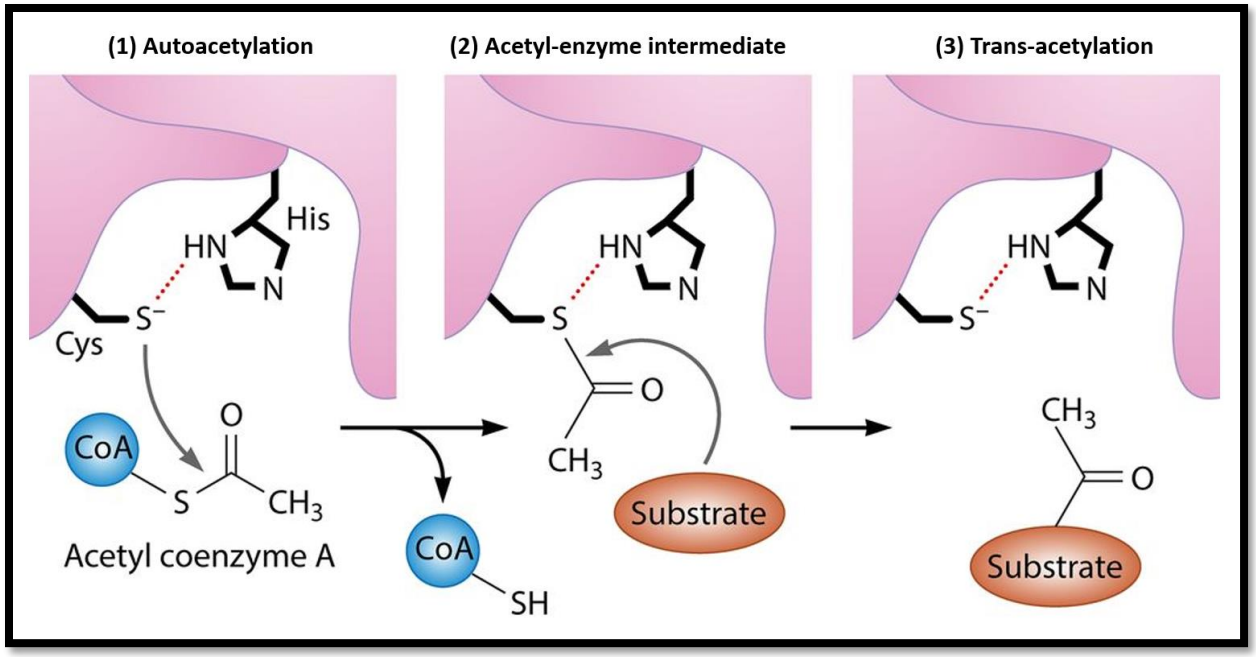

Figure 3.1: Ping-pong model for YopJ effectors induced acetylation. (1) First, the YopJ effector undergoes an autoacetylation process by interacting with AcCoA; (2) Next, the autoacetylated effector, designated as 'acetyl-enzyme intermediate', interacts with the host-substrate; (3) the host-substrate is then trans-acetylated completing the acetylation process. The image was adapted from Ma & Ma (2016).

Eop1, a T3SS effector from *E. amylovora*, is a member of the YopJ family and, consequently, a putative acetyltransferase. As per the phylogenetic classification of YopJ effectors by Ma & Ma (2016), Eop1 is classified in the "group III" of YopJ effectors (Supplementary Figure C3S1), with HopZ effectors from *P. syringae* sharing the same group and HopZ3 as its closest homolog.

The previous experiments discovered that Eop1 from *E. amylovora* and its sequence homologs from other related species act as a putative avirulence factor and trigger HR in the non-host plant *N. tabacum*. Therefore, considering the Eop1s' phylogenetic relationship with the YopJ family effectors and the HR as a consequence of the recognition of Eop1-induced catalytic activity in the *N. tabacum*, it was hypothesised that the tested Eop1 variants possess a catalytic triad (H/E/C) that allows it to modify, perhaps acetylate, the plant's molecular target(s). First, however,

the putative catalytic triad residues site in the Eop1 of *Erwinia amylovora* str. Ea246 (hereafter referred to as Eop1: *Ea*246; the archetype of the Eop1 variants in the current study) was identified to verify the proposed hypothesis. Next, a catalytic triad residues conservation analysis in Eop1 sequence homologs was conducted. Finally, Eop1: *Ea*246 catalytic triad mutants were generated using site-directed mutagenesis (SDM), which were then characterised using a combination of HR and electrolyte leakage assays in *N. tabacum* (Figure 3.2). In addition, *in-silico* protein models of all the tested Eop1 variants were also generated to analyse their structural and catalytic motif homology with the recently deciphered tertiary structure of HopZ1a (Zhang et al., 2016).

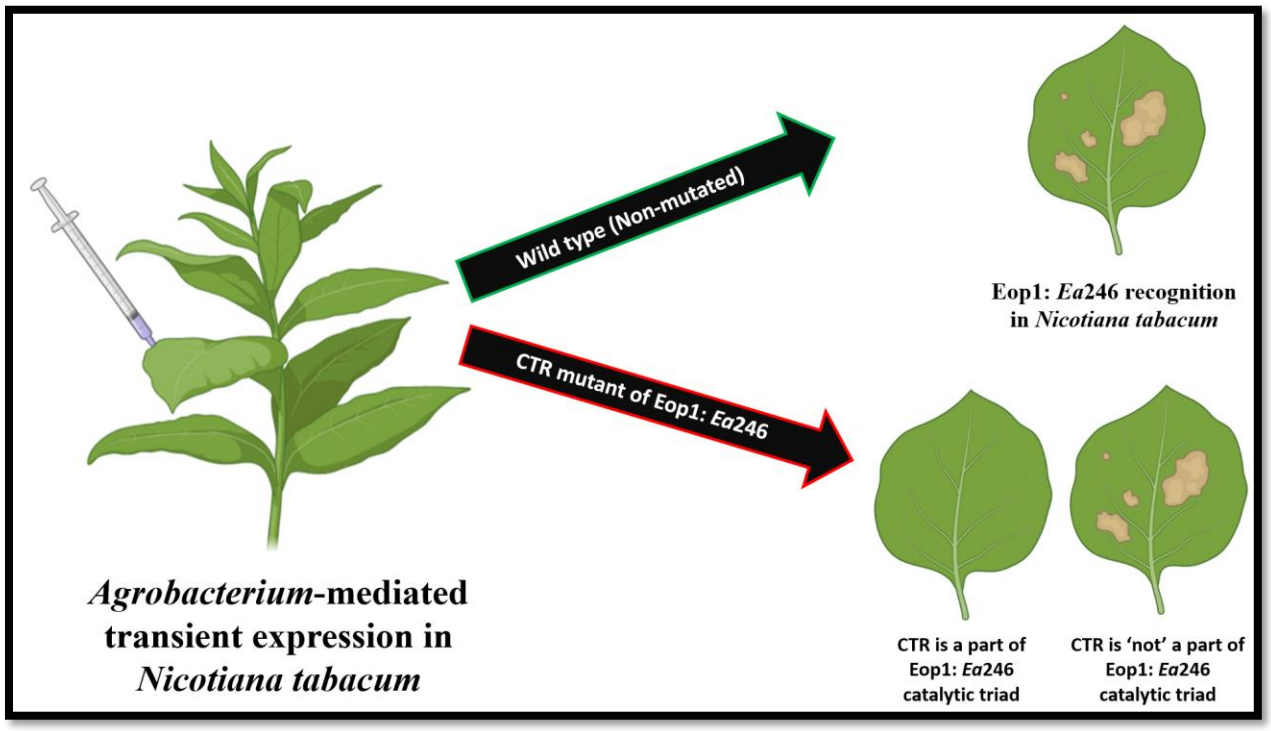

Figure 3.2: Analysis of putative catalytic triad residues (CTR) involvement in Eop1: *Ea*246 induced HR in *N. tabacum*. The screening process relies on the lack of HR in the *N. tabacum* leaf infiltrated with *Agrobacterium* cells harbouring the expression clone carrying *eop1: Ea246* gene with catalytic triad mutation, suggesting the potential involvement of the corresponding residue in the catalytic activity and vice versa for non-involvement.

3.2 Materials and Methods

3.2.1 Bioinformatics methods

3.2.1.1 Protein sequence alignment

The protein sequences in the current study were aligned using Genious 2018: V10.2.5, using the parameter described in section 2.2.1.1.

3.2.1.2 Identification of putative catalytic triad residues site in Eop1: *Ea*246

The catalytic triad residues site in Eop1: *Ea*246 (AAF63400.1) were identified by aligning its protein sequence with the HopZ1a sequence (AAR02168.1) (Sundin et al., 2004) using parameters described in section 3.2.1.1.

3.2.1.3 Catalytic triad residues conservation analysis in Eop1: *Ea*246 protein sequence homologs

The conservation of the catalytic triad residues in Eop1: *Ea*246 protein sequence homologs were evaluated in two phases. First, the Eop1: *Ea*246 protein sequence was used as a 'query sequence' in a BLASTp search to find the sequence homologs in the NCBI database. The search yielded 100 homolog protein sequences, which were aligned with the catalytic triad residues annotated protein sequence of Eop1: *Ea*246 using Geneious 2018: V10.2.5 by employing the parameters described in section 3.2.1.1. However, 15 of the 100 sequences were partial and consequently removed from the alignment. The remaining 85 sequences were then analysed to assess the catalytic triad residues conservation level, completing the phase 1 study. Then, in Phase 2, a similar sequence alignment strategy was used to evaluate the catalytic triad residues conservation level in the 6 Eop1 variants tested in the HR assay.

3.2.2 Molecular methods

3.2.2.1 Introduction to site-directed mutagenesis

For decades, gene mutation analysis has been a powerful tool that enabled researchers to study and characterise the function of genes, proteins, and even specific amino acid residues. These mutations can be incorporated randomly or at specific sites using *in-vitro* mutagenesis techniques (Carrigan et al., 2011; Strachan & Read, 1999). Several strategies for *in-vitro* mutagenesis have been published; however, many of these strategies utilise time-consuming and technically labour-intensive methods (Carrigan et al., 2011). In addition, these methods primarily utilise single-stranded DNA (ssDNA) as a template and involve prerequisite steps such as subcloning and ssDNA rescue (Kunkel, 1985; Sugimoto et al., 1989; Taylor et al., 1985; Vandeyar et al., 1988). The QuikChange™ system, in contrast to other approaches, provides a simple three-step SDM protocol for *in-vitro* mutagenesis (Carrigan et al., 2011; Manual).

The QuikChange™ system of *in-vitro* SDM (Figure 3.3), developed by Stratagene [San Diego, California, USA], is a PCR-based protocol that allows researchers to mutate the 'site-of-interest' virtually in any double-stranded DNA (dsDNA) plasmid in three simple steps. The first step encompasses all conventional PCR steps: denaturation of plasmid DNA template, annealing of the mutagenic primers carrying the desired mutation, and extension of the primers via DNA polymerase. *Dpn*I endonuclease is used to digest parental methylated and hemimethylated plasmid DNA templates in the second step. The final step involves transforming the competent cells with the mutated DNA molecule for nick repair and plasmid amplification (Carrigan et al., 2011; Manual).

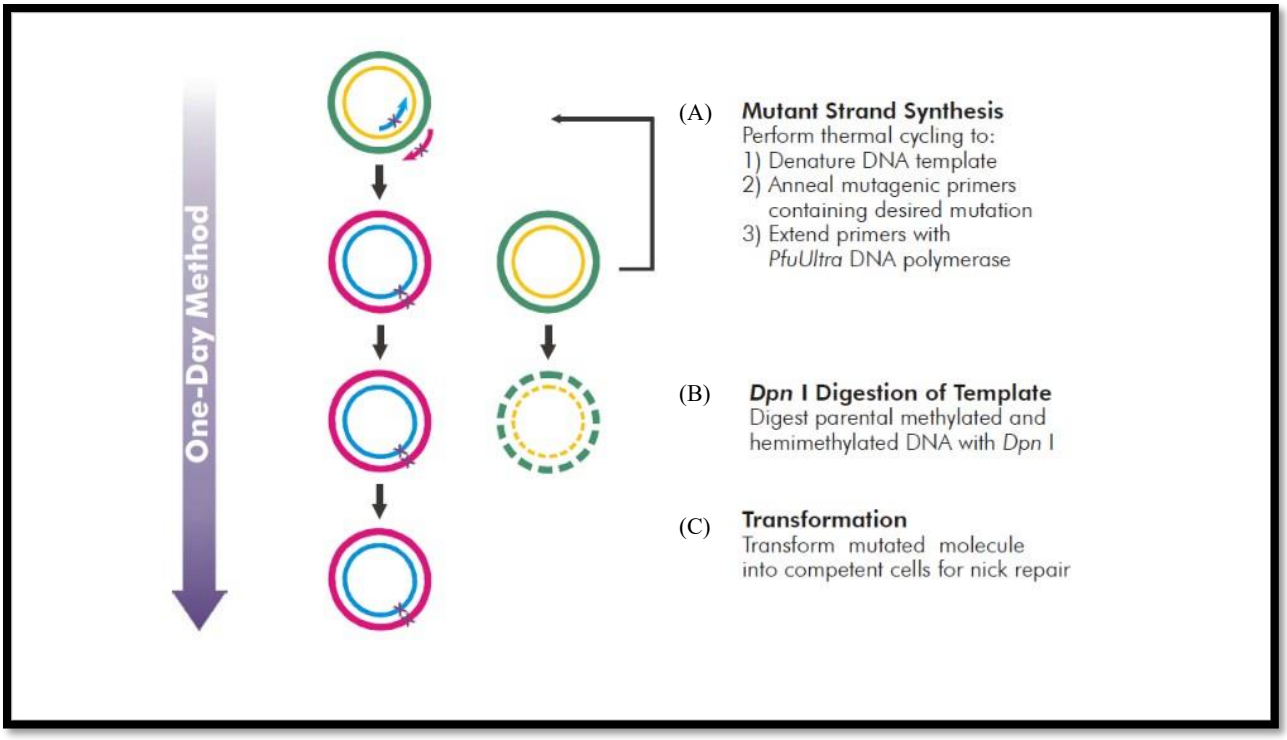

Figure 3.3: An outline of the QuikChange™ system of site-directed mutagenesis[37].

3.2.2.2 Generating Eop1: *Ea*246 catalytic triad mutants through SDM

The Eop1: *Ea*246 catalytic triad mutants were generated using the QuikChange™ system of *in-vitro* SDM with slight modifications, i.e., using different enzyme and PCR conditions. Separate PCR reactions were set up to obtain mutants for each catalytic triad residue, i.e., histidine to alanine (*Ea*246: H228A), glutamic acid to alanine (*Ea*246: E248A), and cysteine to alanine (*Ea*246: C285A). The mutagenic primer pairs used to generate the mutants are presented in Table 3.1.

[37] The image was adapted from the QuikChange™ site-directed mutagenesis kit manual. The link for the same is as follows: https://www.agilent.com/cs/library/usermanuals/Public/200523.pdf

Table 3.1: Mutagenic primers used to generate mutations in the catalytic triad of Eop1: *Ea*246.

S. No	Catalytic triad residues	Primer type	Primers sequence
1.	Ea246: H228A	Forward	5‘—ATCCCCCTTTTATAGGCATGCCTGAC**GC**CCATATCGCCCTGGACATTCATC—3’
		Reverse	3’—GATGAATGTCCAGGGCGATATGG**GC**GTCAGGCATGCCTATAAAAGGGGGAT—5‘
2.	Ea246: E248A	Forward	5‘—CTTCGATTGTCGGTTTTG**C**GTCGGCGCTGGGGCATATGGTCGA—3’
		Reverse	3’—TCGACCATATGCCCCAGCGCCGAC**G**CAAAACCGACAATCGAAG—5‘
3.	Ea246: C285A	Forward	5‘—CAGGATTCAAAATTCCGAGTGGGAC**GC**CATCATGTACTCGTTGAACAATGCCT—3’
		Reverse	3’—AGGCATTGTTCAACGAGTACATGATG**GC**GTCCCACTCGGAATTTTGAATCCTG—5‘
Note: The bold and highlighted letters in the primer pair sequences represent the introduced mutations.			

To generate catalytic triad mutants, first, in a 0.2 mL PCR tube, a master mix was prepared by combining 10 µL of Q5® Reaction Buffer [NEB, B9027S], 2µL (2 mM) MgCl2, 2.5µL (0.5 mM) dNTPs mix, 2.5 µL (0.5 µM) of each forward and reverse primer, 26.5 µL PCR grade water, and 2 µL (4 units) of Q5® High-Fidelity DNA Polymerase [NEB, M0491S]. To this master mix, 2 µL (100-150 ng) of *eop1: Ea246* harbouring entry clones (harvested from *E. coli*) were added as a parental plasmid DNA template, making the final PCR reaction-mix volume 50 µL.

The PCR mix was then run in a Mastercycler® X50s thermocycler to generate mutation using two-step PCR. First, initial denaturation was performed at 95℃ for 4 minutes, followed by 18 sequentially run consecutive cycles of denaturation at 95℃ for 1 minute, and a combined annealing and extension step at 72℃ for 11 minutes; final extension was carried out at 72℃ for 10 minutes followed by a final hold of the samples at 4℃. The PCR product was then analysed by running on 1% agarose gel.

3.2.2.2.1 *Dpn*I restriction digest

Plasmid DNA amplified in *E. coli* (TOP10) cells is methylated and can be digested with methylation-sensitive restriction enzyme (MSRE), such as *Dpn*I (Marinus & Lobner-Olesen, 2014).

The PCR product obtained from the SDM procedure in section 3.2.2.2 was a combination of non-methylated mutagenised plasmid DNA generated through PCR and methylated plasmid DNA used as a template for the PCR. Therefore, the PCR product was treated with *Dpn*I restriction enzymes to retrieve the non-methylated mutagenised plasmid entry clones.

In a 1.5 mL Eppendorf® tube, 3 µL of 1X rCutSmart® Buffer [NEB, B7204S], 1 µL (20 units) *Dpn*I restriction enzyme [NEB, R0176S], and 20 µL of PCR product from SDM procedure were gently mixed and incubated at 37°C for 1 hour. The restriction digest reaction was then terminated by incubating the reaction mix at 80°C for 20 minutes. 5 µL of the mix was then visualised on a 1% agarose gel. The remaining sample was cleaned using DNA Clean & Concentrator™-25 kit [Zymo Research, USA]. The cleaned PCR product was then used for *E. coli* transformation.

3.2.2.2.2 Transformation of *E.* coli with SDM-generated plasmid entry clones harbouring *eop1: Ea246* gene

E. coli electrocompetent cells were transformed with PCR-generated and *Dpn*I-treated and cleaned entry clones harbouring mutated *eop1: Ea246* gene by employing the protocol described in section 2.2.4. 100 µL of the transformed cells were then plated on an LB solid medium containing Kanamycin (50 µg/mL). Finally, colonies harbouring the mutated version of the *eop1: Ea246* gene were grown overnight in an LB liquid medium containing Kanamycin (50 µg/mL) for plasmid extraction.

3.2.2.2.3 Plasmid DNA isolation through a miniprep kit

Plasmid DNA from the overnight cultured transformed *E. coli* cells was harvested using the protocol described in section 2.2.5.

3.2.2.2.4 Validation of positive catalytic triad mutants through sequencing

The plasmid DNA was sequenced by Macrogen (Seoul, South Korea) using M13F and M13R-pUC universal primers. The sequencing results were analysed in the Geneious 2018: V10.2.5 by framing the sequenced mutated residue site with the catalytic triad annotated Eop1: *Ea*246 sequence. The point mutation, i.e., 'H/E/C' to 'A', was first validated separately (Supplementary figures Figure **C3S5**' and Figure **C3S6**'), and then the entire sequence was examined for unwanted mutations. Finally, the plasmid DNA with the desired single catalytic triad mutation in the Eop1: *Ea*246 backbone were used for further experiments, while the versions containing additional unwanted mutations were discarded.

3.2.2.3 Molecular cloning

3.2.2.3.1 Gateway cloning of the Eop1: *Ea*246 mutants

To generate *Agrobacterium*-compatible expression clones for *in-planta* transient expression, entry clones harbouring mutated *eop1: Ea246* (H/E/C to A; with each mutated residue in separate entry clones) were Gateway® cloned separately with the destination vector (pHEX2). LR reaction of the Gateway® cloning system was employed for the task. The LR reaction was performed by employing the protocol described in section 2.2.3.2.1, followed by the transformation and plating of the *E. coli* cells. Finally, *E. coli* colonies from the plate were cultured overnight in LB liquid medium containing Spectinomycin (50 µg/mL). High-quality expression

clones for *Agrobacterium* transformation were obtained by harvesting overnight cultured cells using a Zyppy® Plasmid Miniprep Kit.

3.2.3 Plant expression studies

3.2.3.1 *A. tumefaciens* (GV3101) electrocompetent cells transformation with Eop1: *Ea*246 catalytic triad mutant expression clones

A. tumefaciens (GV3101) electrocompetent cells were transformed with the expression clones harbouring a 'catalytic triad mutant version' of *eop1: Ea246*, using the same protocol described in section 2.2.4. Next, 100 µL of the transformed cell culture was plated on LB solid medium containing selective antibiotics: Gentamicin (20 µg/ml), Rifampicin (10 µg/ml), and Spectinomycin (50 µg/ml).

3.2.3.2 Colony PCR and Glycerol stocks of Eop1: *Ea*246 mutants

The Colony PCR was performed via the method described in section 2.2.9 on the colonies selected from the plate to confirm the presence of the mutated *eop1: Ea246* gene in *Agrobacterium* cells. Following that, glycerol stocks were prepared (as described in section 2.2.10) from the *Agrobacterium* colony that passed the colony PCR check.

3.2.3.3 *Agrobacterium*-mediated transient expression of Eop1: *Ea*246 catalytic triad mutants in *N. tabacum*

The *Agrobacterium* harbouring expression clones for Eop1: *Ea*246 catalytic triad mutants were transiently expressed in *N. tabacum* using the procedure described in section 2.2.11.2.

3.2.3.4 Eop1: *Ea*246 mutants electrolyte leakage assay

Electrolyte leakage assay for Eop1: *Ea*246 mutants was performed using the method described in section 2.2.11.3.

3.2.4 AI systems used to generate tertiary structure models of Eop1s

Three-dimensional (3D) tertiary structure models of the Eop1 variants and Eop1: *Ea*246 mutants were developed using AlphaFold_V2.2.4 (AlphaFold2 or AF2) and Phyre2[38] AI systems. For this, the amino acid sequence of Eop1s was put as a query on the web interface of AlphaFold2[39] and Phyre2. The web user interface (WUI) links of AlphaFold2 and Phyre2 are as follows:

(1) AlphaFold_V2.2.4 open-source code:

https://github.com/deepmind/alphafold

(2) A simplified AlphaFold2 WUI that was used to obtain the predicted Eop1 variant models:

https://colab.research.google.com/github/deepmind/alphafold/blob/main/notebooks/AlphaFold.ipynb#scrollTo=pc5-mbsX9PZC

(3) Phyre2 (Version 2.0) web interface:

http://www.sbg.bio.ic.ac.uk/~phyre2/html/page.cgi?id=index

The AlphaFold2 predicted molecular models were visualised and analysed using a molecular visualisation system, PyMOL Version 1.2r3pre [Schrödinger, Inc., USA]. The obtained tertiary structure was first transformed into a 'ribbon cartoon' structure to highlight the protein's overall 'path and backbone' organisation; next, the catalytic triad residues were shown through 'sticks'. Additionally, the unconserved disordered tail at the N-terminal region was removed prior to analysis.

[38] Only Eop1: *Ea*246 model was produced using the Phyre2 WUI, as presented in 'Supplementary Figure C3S4'. Due to the unreliable structure prediction parameters of Phyre2 WUI, other Eop1 variants were not produced.
[39] The AlphaFold2 open-source WUI was accessed via Colab notebook (a Google Product).

3.3 Results

In the previous experimental study, 5 Eop1 variants out of 6 examined in the HR assay induced strong HR in the non-host plant *N. tabacum*, including Eop1 from Rosoideae and Spiraeoideae infecting pathovars of *E. amylovora*: *Ea*246 and *Ea*262, respectively. Interestingly, HR elicited by Eop1: *Ea*262 was comparatively slower than Eop1: *Ea*246 as Eop1: *Ea*246 triggered HR 24 hours prior to its homolog Eop1: *Ea*262. Hence, due to its robust activity, Eop1: *Ea*246 was chosen as a candidate to characterise the Eop1-induced HR in *N. tabacum* through catalytic triad mutation analysis.

3.3.1 Sequence alignment with HopZ1a unravels putative catalytic triad residues site in Eop1: *Ea*246

The knowledge of the functionally important catalytic triad residues site is one of the criteria required for the YopJ effector's characterisation through mutation. Consequently, the site of the putative catalytic triad residues in Eop1: *Ea*246 were first determined.

The catalytic triad residues site in the Eop1: *Ea*246 sequence was identified by aligning its protein sequence with the sequence of another well-studied YopJ acetyltransferase, HopZ1a. HopZ1a was chosen as a reference sequence since it is the only homolog of Eop1 from "group III", as classified by Ma & Ma (2016), whose protein and catalytic motif structure has been deciphered and validated through X-ray crystallography and NMR spectroscopy; resulting in the identification of HopZ1a catalytic triad residues site as H150, E170, and C216 (Zhang et al., 2016). Moreover, the catalytic residue (C216) involvement in the HopZ1a catalysis was validated through mutation analysis in *Arabidopsis* eco. Col-0 (Zhang et al., 2016).

The protein sequence of Eop1: *Ea*246 was aligned with the HopZ1a sequence by employing the method described in section 3.2.1.1, revealing the putative catalytic triad residues

site in Eop1: *Ea*246 as H228, E248, and C285 (Figure 3.4). Eop1: *Ea*246 protein sequence, annotated with the sites of the putative catalytic triad residues, was then used for further investigations in catalytic triad residues conservation analysis and SDM.

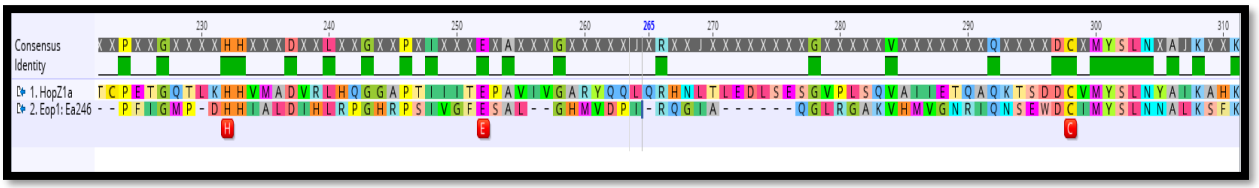

Figure 3.4: Identification of the catalytic triad residues site in the Eop1: *Ea*246 protein sequence via protein sequence alignment with HopZ1a. The catalytic triad residues are annotated below the alignment in the red box from left to right as H/E/C, respectively.

3.3.2 The catalytic triad residues (H/E/C) are substantially conserved across Eop1: *Ea*246 sequence homologs

The catalytic triad residues (H/E/C) are considered functionally important and highly conserved in the YopJ family of plant and animal pathogenic bacterial effectors (Ma & Ma, 2016; Orth et al., 2000). To verify this, a catalytic triad residues conservation study in Eop1: *Ea*246 homologs was performed in two phases. The first phase focused on the 'widescale' conservation analysis of the catalytic triad residues in the 85 homolog sequences retrieved from the NCBI database using BLASTp search (by employing the method described in section 3.2.1.3). The second phase, however, encompassed the conservation analysis of the catalytic triad residues in the 6 Eop1s tested in the HR assay in the previous experiment (Table 2.1).

The phase one study discovered that the catalytic triad residues were substantially conserved in the Eop1: *Ea*246 homologs obtained from the BLASTp search. The catalytic residues: histidine (H), glutamic acid (E) and cysteine (C) were determined to be 100 %, 96.4%

and 98.8% conserved (see footnote '40' for the equation), respectively, in 85 homolog protein sequences, thus, confirming the broad conservation of catalytic triad residues in Eop1: *Ea246* homologs (Figure 3.5). In phase two study, the conservation of the catalytic triad residues was assessed in 6 Eop1 variants tested in the HR assay experiment by employing the same method used in the 'phase one' study. As anticipated, the catalytic triad residues were discovered to be conserved in all 6 Eop1s (Table 3.2). Next, mutation analysis was conducted to test the involvement of the predicted catalytic triad residues in Eop1: *Ea*246 induced HR in *N. tabacum.*

Table 3.2: Conservation analysis of catalytic triad residues (H/E/C) in 6 Eop1 variants tested in HR assay in *N. tabacum*.

Eop1 variants tested in HR assay	**Protein sequences**
Eop1: *E. amylovora* (*Ea*246) (Annotated reference sequence)	MPD**H**HIALDIHLRPGHRPSIVGF**E**SALGHMVDPIRQGIAQGLRGAKVHMVGNRIQNSEWD**C**IMYSL ----(228) ----------(248) ----------(285) -----
Eop1: *E. pyrifoiliae* (*Ep*1/96)	ARD**H**RVALDIQFRPGHRPSIVGF**E**SAPGNLAELLQHELEHALRGAKVQVVENTIQNSLRG**C**SMFAL
Eop1: E. amylovora (*Ea*246)	MPD**H**HIALDIHLRPGHRPSIVGF**E**SALGHMVDPIRQGIAQGLRGAKVHMVGNRIQNSEWD**C**IMYSL
Eop1: *E. amylovora* (*Ea*262)	MSD**H**RVALDIQFRPGHRPSVVGY**E**SAPGNLAEHLKYGLEHGLRGAKVQVVANTIQNSVRG**C**SMFAL
Eop1: *E. tasmaniensis* (*Et*1/99)	MPD**H**HIALDIQLRPGHRPSIVGF**E**SALGHMVEHLKQGIAEGVRGAKVHMVGNTIQNSQWD**C**TMYSL
Eop1: *E. tracheiphila* (*E. tr*_MDcuke)	IPDH**H**VALDVQLRPGHHPSVVCF**E**SALWGMMNEIRQGIEHGLKESKVKLIGNFVQASDWD**C**AMFAL
Eop1: *Pantoea vagans* (*P. va*_C9-1)	MPD**H**HIALDIQLRPGHRPSIVCF**E**SALGNMMDPIKQGIEQGLKGARVKMVGNFIQASSWD**C**AMFAL
HopZ3*psa*_V1	AKD**H**HVTLDIQMRPGHRPSIVMF**E**SAEADLLMYARGTLASALPRAKIKVDGSFIQRSKYD**C**IMYSL
Note: The bold and highlighted letters in the table represent the catalytic triad residues, H/E/C, respectively. (See supplementary Figure C3S2 for the protein sequence alignment).	

[40] The equation used to calculate the level of residue conservation (in %): [sequences with conserved residues / total no. of sequences X 100]; Sequences with Conserved residues = 'Total number of sequences' – 'sequences with unconserved residues'.

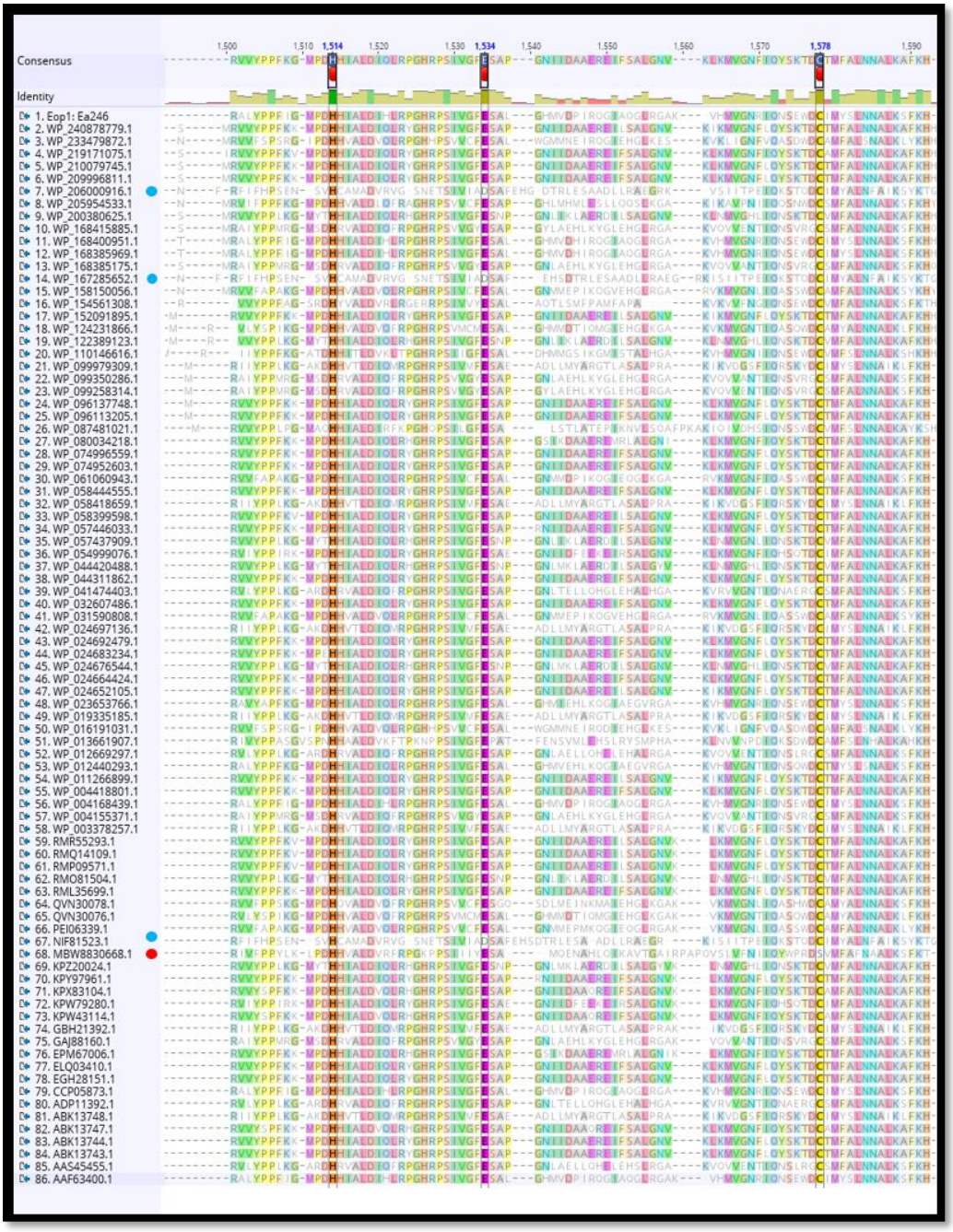

Figure 3.5: Conservation analysis of the catalytic triad residues in the Eop1: *Ea*246 protein sequence homologs retrieved from the NCBI database through BLASTp search. The catalytic residue annotations are as follows: histidine (H), glutamic acid (E), and cysteine (C). The catalytic triad residues (H/E/C) were determined to be 100%, 96.4% and 98.8% conserved, respectively. Additionally, in a few sequences, aspartic acid (D) (presented as a blue dot) and serine (S) (presented as a red dot) were also discovered to substitute glutamic acid and cysteine residues, respectively.

3.3.3 Characterisation of Eop1: *Ea*246 induced HR in *Nicotiana tabacum*

The Eop1: *Ea*246 activity was characterised through mutation analysis of the catalytic triad residues. The catalytic triad mutants were generated through site-directed mutagenesis (SDM) and tested via HR and electrolyte leakage assay. In addition, the wildtype (WT) was maintained as a contrast to the mutants for comparing the phenotype.

3.3.3.1 Catalytic triad mutants of Eop1: *Ea*246 generated through the SDM method

The catalytic triad mutants of Eop1: *Ea*246: (*Ea*246: H228A, *Ea*246: E248A, and *Ea*246: C285A) were generated by employing the method described in section 3.2.2.2. Interestingly, only two catalytic triad residues mutant: *Ea*246: H228A and *Ea*246: C285A, were obtained, whereas glutamic acid to alanine mutant (*Ea*246: E248A) was not recovered (Figure 3.6).

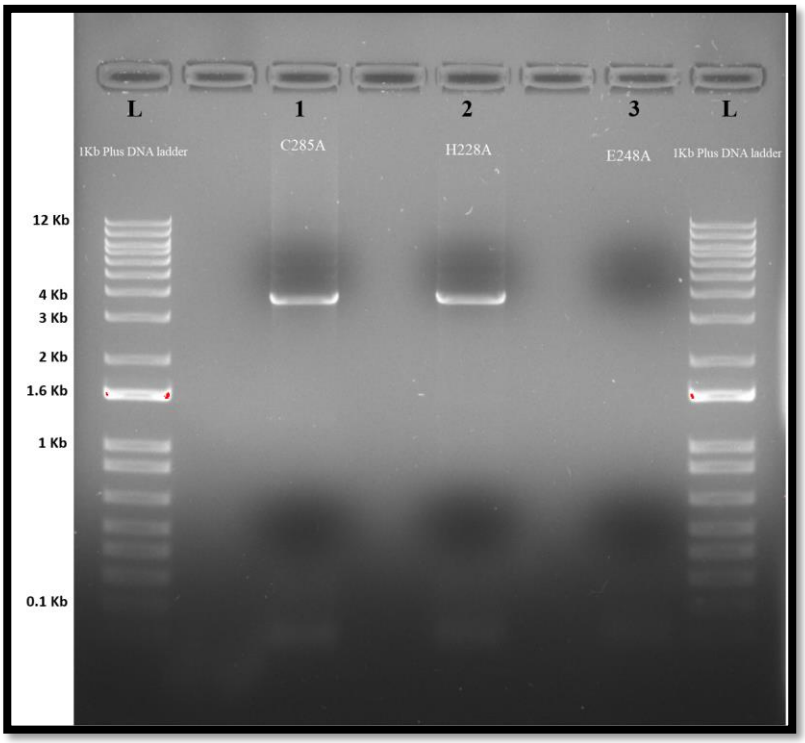

Figure 3.6: Gel electrophoresis of entry clones harbouring the catalytic triad mutant of *eop1*: *Ea*246 gene generated through SDM. The annotations are as follows, L = 1 Kb plus ladder [Invitrogen; USA]; 1 = *Ea*246: C285A; 2 = *Ea*246: H228A; 3 = *Ea*246: E248A.

Further investigation revealed that a high GC-rich region surrounded the glutamic acid residue (*Ea*246: E248) (refer to 'Supplementary Figure C3S3'). As a result, methods recommended by Assal & Lin (2021) and Sahdev et al. (2007) to amplify high GC-rich regions were employed for the SDM PCR in combination with the GC enhancer. Unfortunately, despite multiple attempts, the mutation was still not recovered. Finally, another primer pair (Table 3.3) was designed to anneal with the DNA template at a high temperature to counteract the temperature required to denature the GC-rich region. However, the *Ea*246: E248A mutation remained unrecovered.

Table 3.3: Set two of *Ea*246: E248A mutagenic primers. The bold and highlighted letters in the primer sequences represent the introduced nucleotide mutations.

Catalytic triad residue	Primer type	Primers sequence
*Ea*246: E248A (Primer set 2)	Forward	5'—CATCGCCCTTCGATTGTCGGTTTTG**C**GTCGGCGCTGGGGCATATGGTCGATCCTATCA—3'
	Reverse	3'—TGATAGGATCGACCATATGCCCCAGCGCCGAC**G**CAAAACCGACAATCGAAGGGCGATG—5'

The obtained mutants were treated with *Dpn*I restriction enzyme (section 3.2.2.2.1) to remove the parental plasmid DNA template from the PCR mix and checked for PCR-generated DNA plasmid through gel electrophoresis (Figure 3.7). The desired catalytic triad residue mutation was then confirmed through sequencing (refer to section 3.2.2.2.4). Following that, the *Agrobacterium* electrocompetent cells were transformed with the expression clone harbouring catalytic triad mutated version of *eop1: Ea246* using the protocol described in section 3.2.3.1.

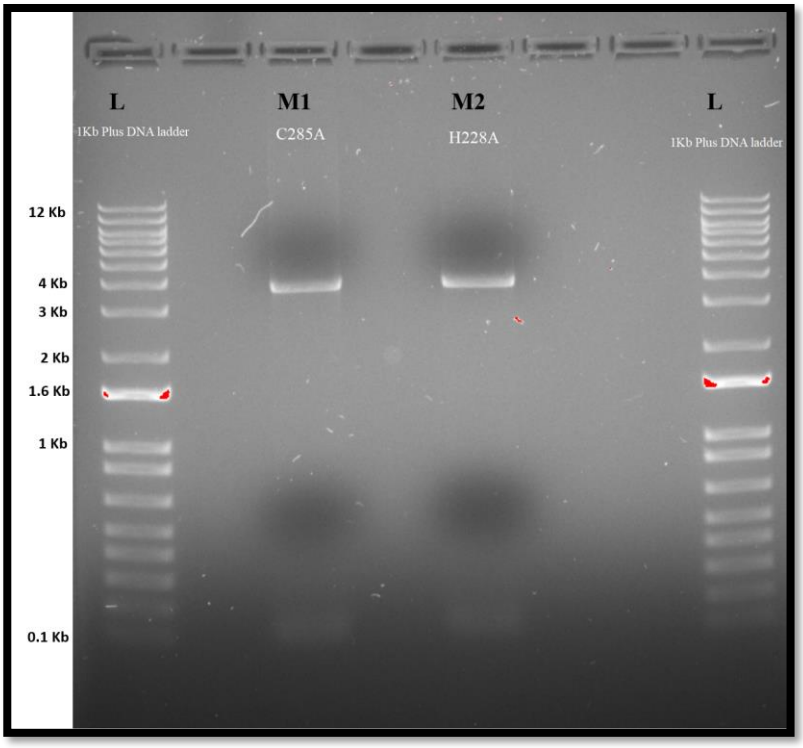

Figure 3.7: Gel electrophoresis of *Dpn*I-treated entry clones harbouring the catalytic triad mutant of *eop1*: *Ea*246 gene generated through SDM. The annotations are as follows, L = 1 Kb plus ladder (Invitrogen; USA); M1 = *Ea*246: C285A; M2 = *Ea*246: H228A.

3.3.3.2 HR and electrolyte leakage assay of Eop1: *Ea*246 catalytic triad mutants

Eop1: *Ea*246 catalytic triad mutants were characterised through HR and electrolyte leakage assay in *N. tabacum. Agrobacterium tumefaciens* carrying the mutant version of *eop1: Ea246* gene in an expression clone was infiltrated in 3-4 weeks old fully expanded leaves of *N. tabacum.*

As observed in the previous experiment, the Wildtype (Eop1: *Ea*246) triggered a strong HR at 24 hpi; in contrast, no HR-induced cell death was observed in the histidine mutant (*Ea*246: H228A) infiltrated region (Figure 3.8). Interestingly, in contrast to the wildtype, the transient expression of cysteine mutant (*Ea*246: C285A) elicited an HR that developed over 6 days. The cell death began to develop in small patches at 2 dpi and gradually grew to encompass approximately the entire infiltrated region by the 6th day (Figure 3.8 and Figure 3.9).

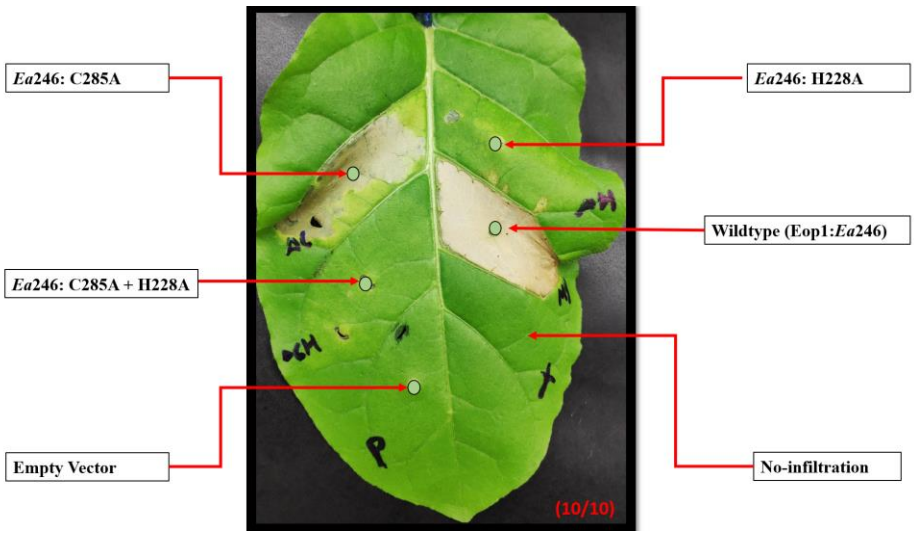

Figure 3.8: Eop1: *Ea*246 catalytic triad mutants HR assay. The annotations are as follows: Empty Vector = pHEX2: EV; Wildtype = Eop1: *Ea*246; *Ea*246: H228A = histidine to alanine mutant; *Ea*246: C285A = cysteine to alanine mutant; *Ea*246: H228A + C285A = double mutant. The image was taken at 6 dpi. The ratio (10/10) indicates the number of leaves with the presented phenotype/total number of conducted replications. The experiment was repeated thrice with similar results.

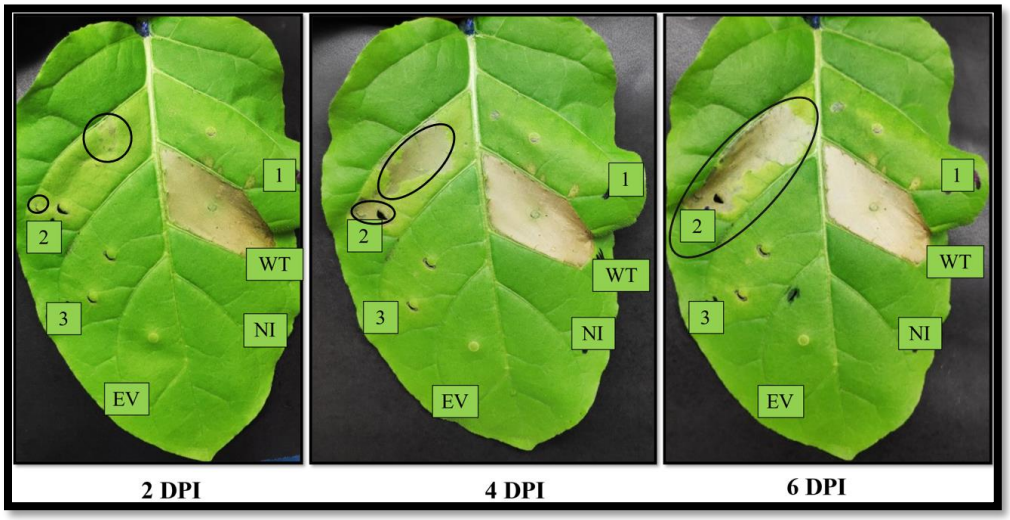

Figure 3.9: Cysteine mutant (*Ea*246: C285A) induced progressive HR in *Nicotiana tabacum*. The encircled regions represent the HR-induced cell death by *Ea*246: C285A. The annotations are as follows: EV = Empty Vector; WT = Wildtype (Eop1: *Ea*246); NI = non-infiltrated region; 1 = Histidine mutant (*Ea*246: H228A); 2 = Cysteine mutant (*Ea*246: C285A); 3 = Double mutant (*Ea*246: H228A + C285A).

To further validate the activity of cysteine and histidine mutants, a double mutant with C285A and H228A mutations combined in the *eop1: Ea246* backbone was generated. The double mutant (*Ea*246: C285A + H228A) was created using the methods described in section 3.2.2.2. However, *Ea*246: C285A entry clones were used as plasmid DNA template in the SDM procedure with *Ea*246: H228A primers (as mentioned in Table 3.1) to incorporate the H228A mutation in *Ea*246: C285A. As anticipated, the double mutant did not trigger HR in the HR assay (Figure 3.8 and Figure 3.9).

An electrolyte leakage assay was also performed to quantify and substantiate the Eop1: *Ea*246 catalytic triad mutants HR assay result. As anticipated, electrolyte leakage data (Figure 3.10) corroborated the phenotypic data observed in the HR assay. At 24 hpi, leaf discs infiltrated with *Agrobacterium* carrying the expression clones for the wildtype (Eop1: *Ea*246) exhibited significant ion leakage, with an electrolyte leakage value of more than 150 µS/cm (mean value from 4 replicates). In contrast to the wildtype, no significant ion leakage was observed in the histidine mutant (*Ea*246: H228A), double mutant (*Ea*246: C285A+H228A), and the EV infiltrated leaf discs. However, progressive electrolyte leakage was detected in leaf discs infiltrated with cysteine mutant (*Ea*246: C285A). The electrolyte leakage value was observed to rise after 1 dpi, which gradually increased till the 4^{th} day and culminated with a peak value of 100 µS/cm on the 5^{th} day. The ion leakage trend of the cysteine mutant further supported the finding that the observed phenotype of progressive HR resulted from progressive cell death.

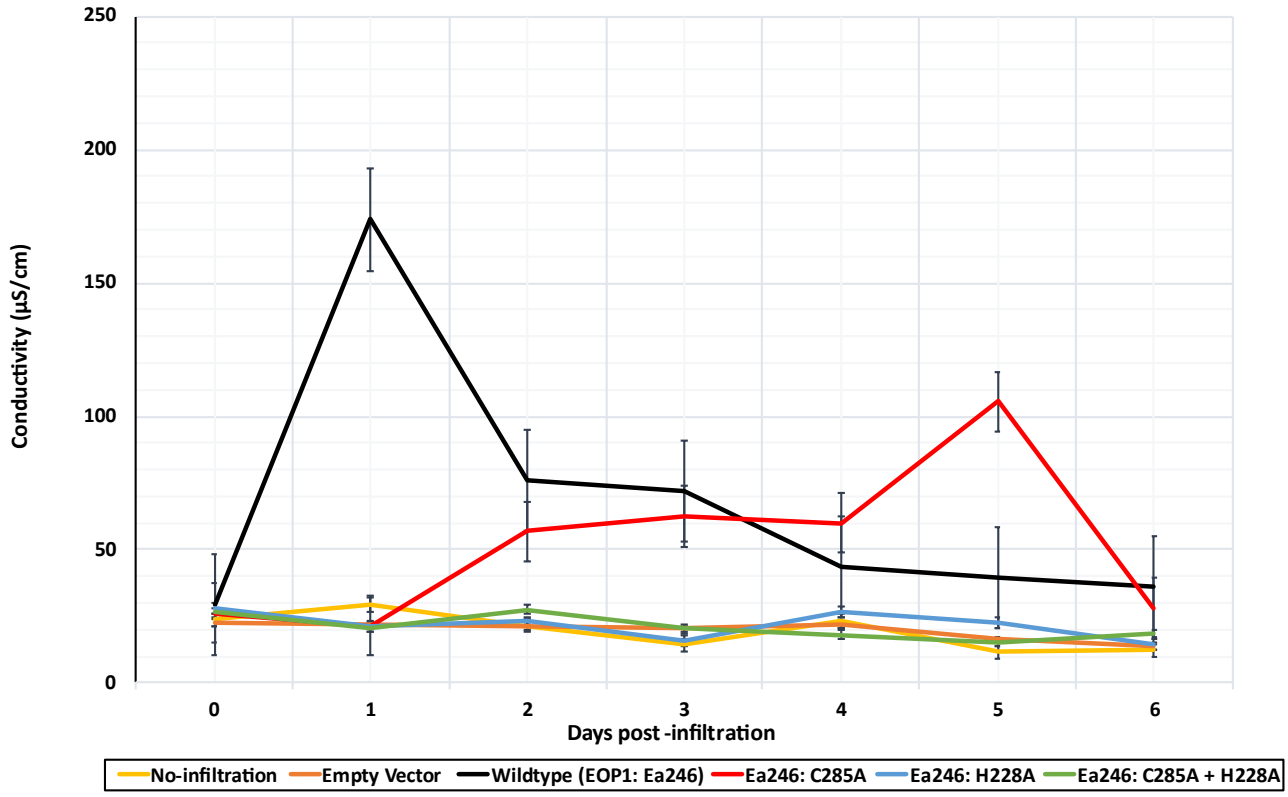

Figure 3.10: Electrolyte leakage data from *N. tabacum* leaf discs infiltrated with *Agrobacterium tumefaciens* harbouring the expression clones carrying the gene for *eop1*: *Ea*246 catalytic triad mutants (H/E/C) separately. *Agrobacterium* were infiltrated at the OD_{600} of 0.1 (approx. 1 x 10^8 CFU/mL). The graph was plotted based on the mean value from four replicates on indicated days for each sample (see section 2.2.11.3 for the detailed procedure); error bars indicate the standard error from the replicates. A complimentary bar plot with data plotted for each day is presented in 'Supplementary Figure C3S7'.

3.3.4 Eop1s structural and catalytic motif analysis through AI-predicted models

The HR assay of Eop1: *Ea*246 catalytic triad mutants revealed that the histidine mutant (*Ea*246: H228A) does not trigger HR, whereas the cysteine mutant (*Ea*246: C285A) induces progressive HR. In contrast, the glutamic acid mutant (*Ea*246: E248A) remained untested as it was not recovered due to technical difficulties. The results mentioned above raised the following questions concerning the catalytic motif and cysteine residue as follows:

1. Are all catalytic triad residues correctly oriented in the catalytic motif of Eop1: *Ea*246, as observed in the structure of its homolog, HopZ1a?
2. Does catalytic triad residues substitution with alanine induce effector perturbation or a conformation change in the catalytic motif that could affect the effector's activity?
3. Is there any other conserved residue that can substitute for cysteine while maintaining the integrity of the 3D conformation of the catalytic motif by being in proximity to the other two residues?

In-silico tertiary structure model of the Eop1variants, Eop1: *Ea*246 catalytic triad mutants, HopZ3*psa*_V1 and HopZ1a, were produced by AlphaFold2 using the protocol described in section 3.2.4 to answer the aforementioned questions.

3.3.4.1 Preliminary analysis of AlphaFold2 predicted models

The 3D models predicted by AlphaFold2 were predicted based on the predicted local distance difference test (pLDDT) score, which is a measure of estimating the per-residue confidence metric with a scale range from 0-100. A pLDDT score between 70 to 90 represents a confident model with accurate backbone prediction. In contrast, a score < 50% corresponds to a low-confidence model and is suggested not to be interpreted. Moreover, a score of 90 and above correspond to a high-confidence model with high accuracy (Jumper et al., 2021; Tunyasuvunakool et al., 2021).

Additionally, to provide a comprehensive view of the model's intra-domain confidence, the AlphaFold2-predicted models were colour coded based on the pLDDT score (as exemplified with the Eop1: *Ea*246 model[41] in 'Figure 3.11'). However, the predicted 'crude' models (as shown in Figure 3.11 'A') were hard to analyse for the overall conformation and catalytic motif analysis; Consequently, the models produced by Alphafold2 were further analysed in PyMOL, a molecular visualisation system. The observations made from the analysis are presented in the succeeding sections.

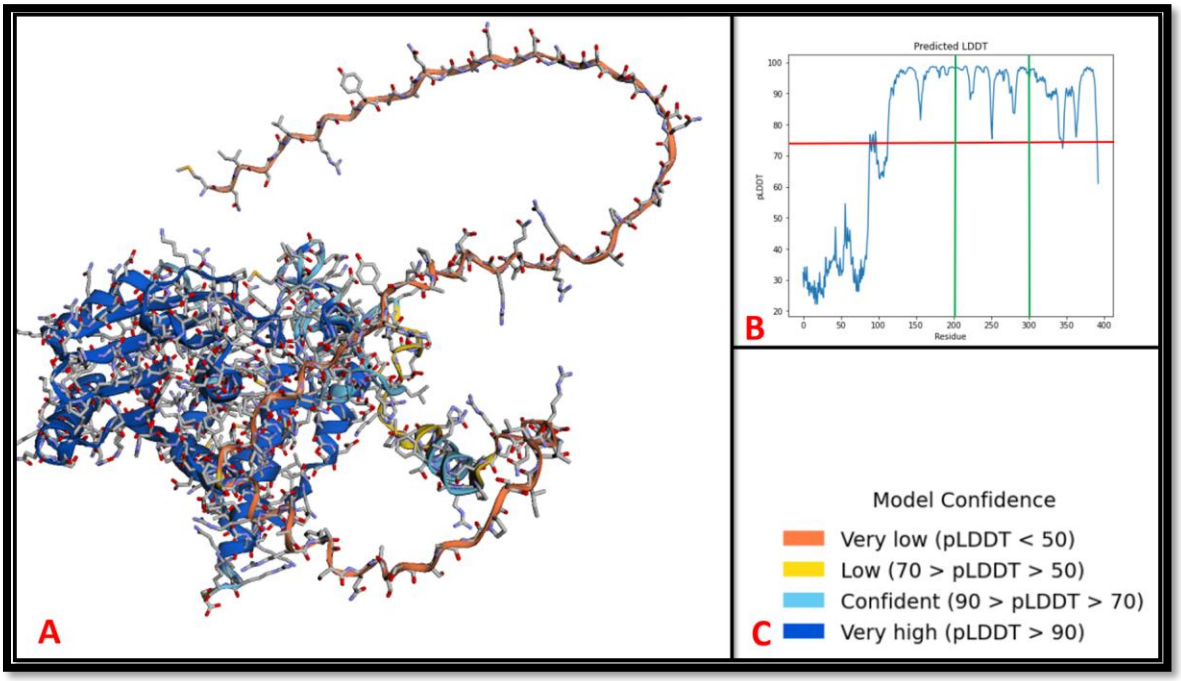

Figure 3.11: AlphaFold2 predicted 'crude' model of Eop1: *Ea*246 and the parameters used in the prediction. (A) AlphaFold2 predicted 'crude' model of Eop1: *Ea*246. (B) pLDDT score graph of Eop1: *Ea*246 representing the 'per-residue confidence estimate metric' (the residues between the green lines (residues 200-300) harbour the catalytic triad residues, and the intersecting 'red line' corresponds to the pLDDT score of 70 and above). (C) Colour codes employed in sub-figure 'A' to provide a comprehensive view of the intra-domain confidence of the Eop1: *Ea*246 AlphaFold2 predicted model.

[41] High confidence pLDDT score of >70% was observed in the 'conserved core folds' of all the tertiary structures (Figure 3.12 to Figure 3.18) predicted via AlphaFold2.

3.3.4.2 Eop1s from *E. amylovora* and related species exhibit high-structural and catalytic motif homology with HopZ1a

Overall, the comparative analysis discovered that the tertiary structure of HopZ1a, determined through NMR spectroscopy and X-ray crystallography (Figure 3.12; sub-figure 1) (Zhang et al., 2016), was highly similar to its AlphaFold2 predicted tertiary structure molecular model[42] (Figure 3.12; sub-figure 2). Moreover, despite low sequence identity (20.1%), the HopZ1a predicted tertiary structure was also discovered to be homologous to the Eop1: *Ea*246 model (Figure 3.13). Interestingly, the conserved catalytic and regulatory domains identified in the HopZ1a structure, including substrate-binding pockets for 'AcCoA' and 'IP6' in the regulatory domains, were also observed in the Eop1: *Ea*246 structure (Figure 3.12). Moreover, analysis of the 3D conformation of the catalytic residues in the catalytic motif of the two structures was also observed to share parallel similarities (Figure 3.14). Therefore, high homology of the overall structure, including the catalytic motif and residues conformation, solved the first question regarding the orientation of the catalytic triad residue in Eop1: *Ea*246.

In addition, the presence of the regulatory and the catalytic domains in the protein sequence (Table 3.4), along with the catalytic triad residues site (Table 3.5), were also identified using protein sequence alignment (Supplementary Figure C3S8) in all the tested Eop1s and the control HopZ3*psa*_V1. By utilising the data from Table 3.4 and Table 3.5, the *in-silico* models[43] were produced, which were also intriguingly similar to the HopZ1a structure (Figure 3.15 to Figure

[42] The AlphaFold2 predicted structure of HopZ1a was used as a control for the 'tertiary structure prediction' by AlphaFold2. It was discovered that the AlphaFold2 predicted structure of HopZ1a was nearly 100% homologous to the structure deciphered via NMR and X-ray crystallography, indicating that the Eop1 variants models produced using the AlphaFold2 AI system would also be highly reliable.

[43] pLDDT score graph of all the *in-silico* generated models are provided in 'Supplementary Figure C3S10'.

3.18). The structural and catalytic motif homology among the tested Eop1 variants was also analysed through a superimposition analysis, as shown in Figure 3.19.

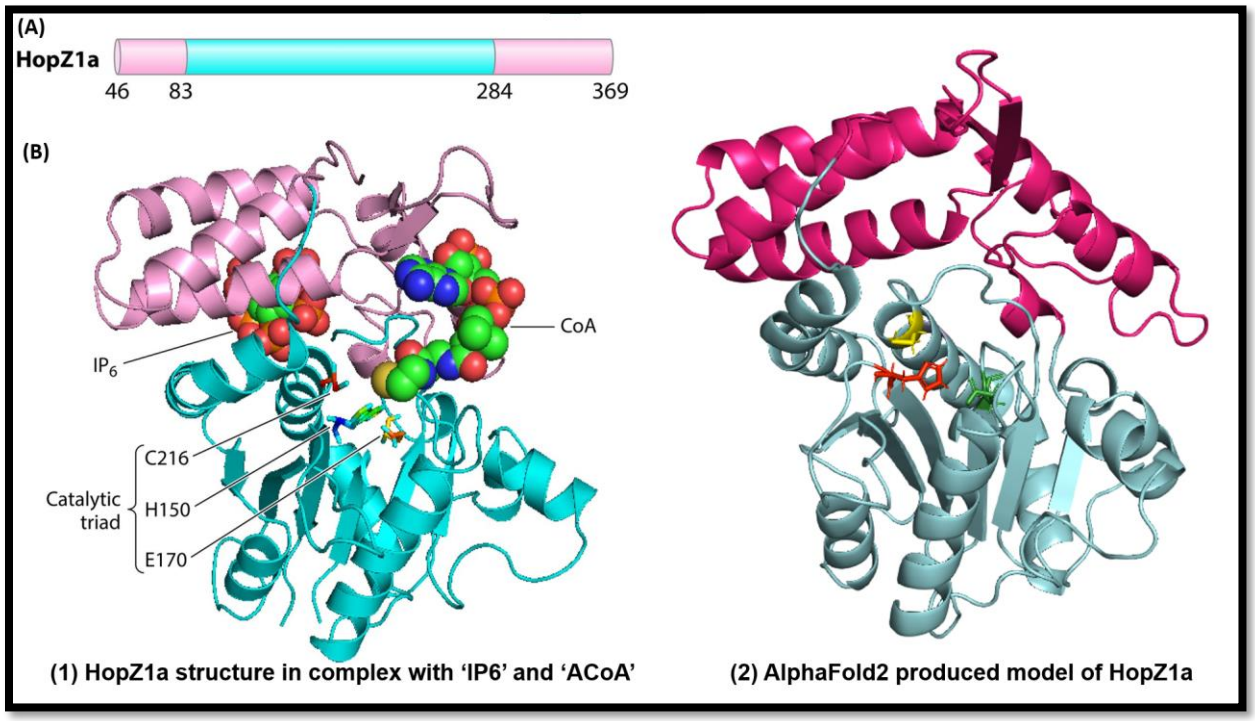

Figure 3.12: Analysis of HopZ1a structure. (1) HopZ1a structure in complex with eukaryote-specific activation co-factor 'inositol hexakisphosphate' (IP6) and the acetyl group donor 'acetyl coenzyme A (ACoA); (A) Linear representation of the HopZ1a protein sequence annotated with regulatory and catalytic domains via colour codes; (B) HopZ1a tertiary structure in complex with 'IP6' and 'AcCoA'; The image was adapted from Ma & Ma (2016). (2) AlphaFold2 predicted tertiary structure of HopZ1a (produced in the current study). The pink and cyan colours in sub-figures '1' & '2' correspond to the regulatory and catalytic domains, respectively.

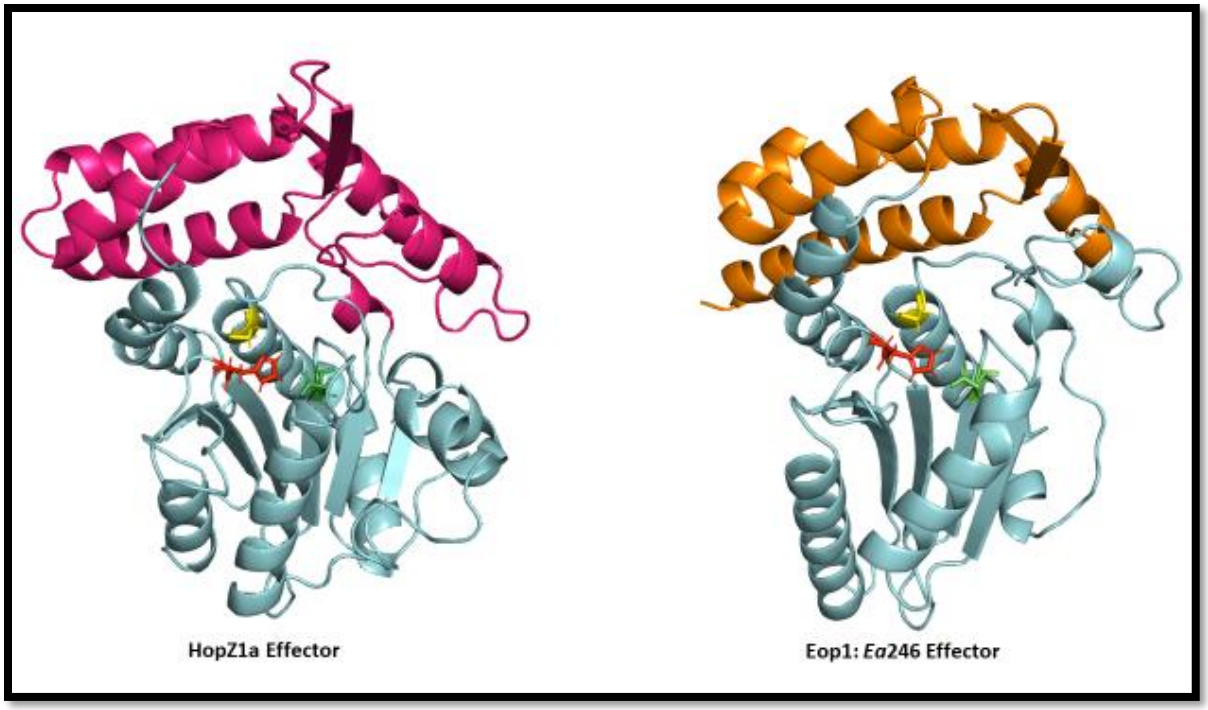

Figure 3.13: Analysis of the tertiary structure and catalytic motif identity between HopZ1a and Eop1: *Ea*246 effectors. The colour codes are as follows: regulatory domains = hot-pink (HopZ1a) and orange (Eop1: *Ea*246); catalytic domain = pale-cyan (in both structures). The catalytic triad residues in the structures' core are also colour-coded: histidine = red, glutamic acid = green, and cysteine = yellow.

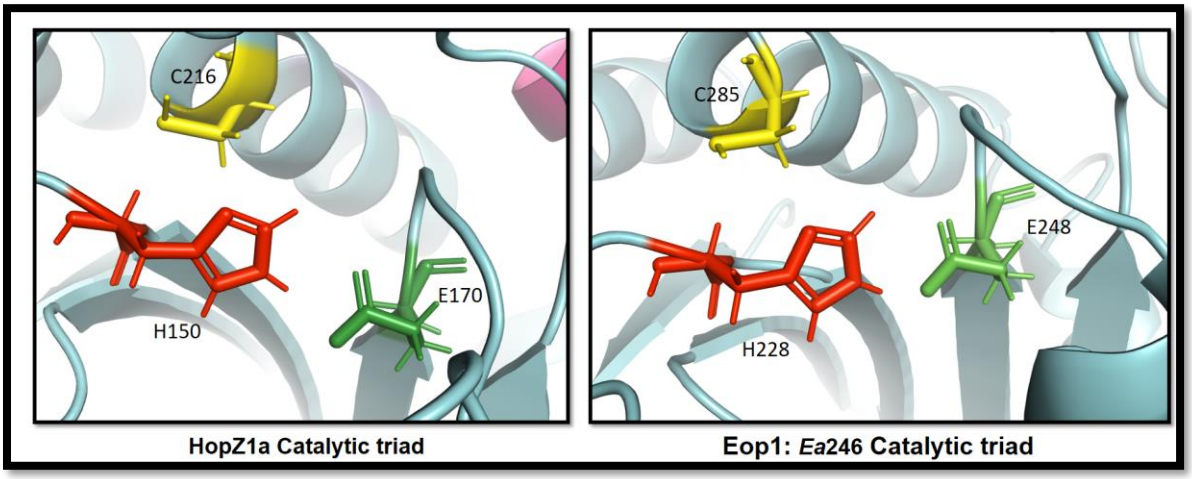

Figure 3.14: Analysis of catalytic triad residues identity between HopZ1a and Eop1: *Ea*246 catalytic motif. The predicted catalytic triad residues are annotated with their respective residue position and are colour-coded as: histidine = red, glutamic acid = green, and cysteine = yellow.

Table 3.4: Sequence length of the regulatory and catalytic domains in the protein sequence of tested Eop1 variants, HopZ1a and HopZ3*psa*_V1.

Effector	The seq. length of the N-terminus tail	Regulatory domain 1 Seq. length	Catalytic domain Seq. length	Regulatory domain 2 Seq. length	References
HopZ1a	1 - 45	46 - 83	84 - 284	285 - 369	(Zhang et al., 2016)
Eop1: *Ep*1/96	1 - 124	125 - 164	165 - 360	361 - 401	This study
Eop1: *Ea*246	1 - 117	118 - 157	158 - 352	353 - 393	This study
Eop1: *Ea*262	1 - 124	125 - 164	165 - 360	361 - 401	This study
Eop1: *Et*1/99	1 - 120	121 - 160	161 - 355	356 - 396	This study
Eop1: *E. tr*_MDcuke	1 - 132	133 - 172	173 - 368	369 - 409	This study
Eop1: *P.va*_C9-1	1 - 130	131 - 170	171 - 366	367 - 407	This study
HopZ3*psa*_V1	1 - 130	131 - 170	171 - 366	367 - 407	This study

Note: The sequence length of the regulatory and catalytic domains in the effectors mentioned above was predicted based on the protein sequence alignment with HopZ1a (refer to 'Figure C3S8'). The catalytic triad residues site for the same effectors is mentioned in Table 3.5. The tertiary structures deduced from this data are presented from Figure 3.15 to Figure 3.18. The models were predicted by AlphaFold2 and analysed via PyMOL. Also, the N-terminal disordered tail was removed before analysing the conserved and functionally important domains.

Table 3.5: Predicted catalytic triad residues site in the tested Eop1 variants and Sequence length.

Effector	**Catalytic histidine site in the sequence**	**Catalytic glutamate site in the sequence**	**Catalytic cysteine site in the sequence**	**References**
HopZ1a	150	170	216	(Zhang et al., 2016)
Eop1: *Ep*1/96	235	255	292	This study
Eop1: *Ea*246	228	248	285	This study
Eop1: *Ea*262	235	255	292	This study
Eop1: *Et*1/99	231	251	288	This study
Eop1: *E. tr*_MDcuke	243	263	300	This study
Eop1: *P.va*_C9-1	241	261	298	This study
HopZ3*psa*_V1	241	261	298	This study

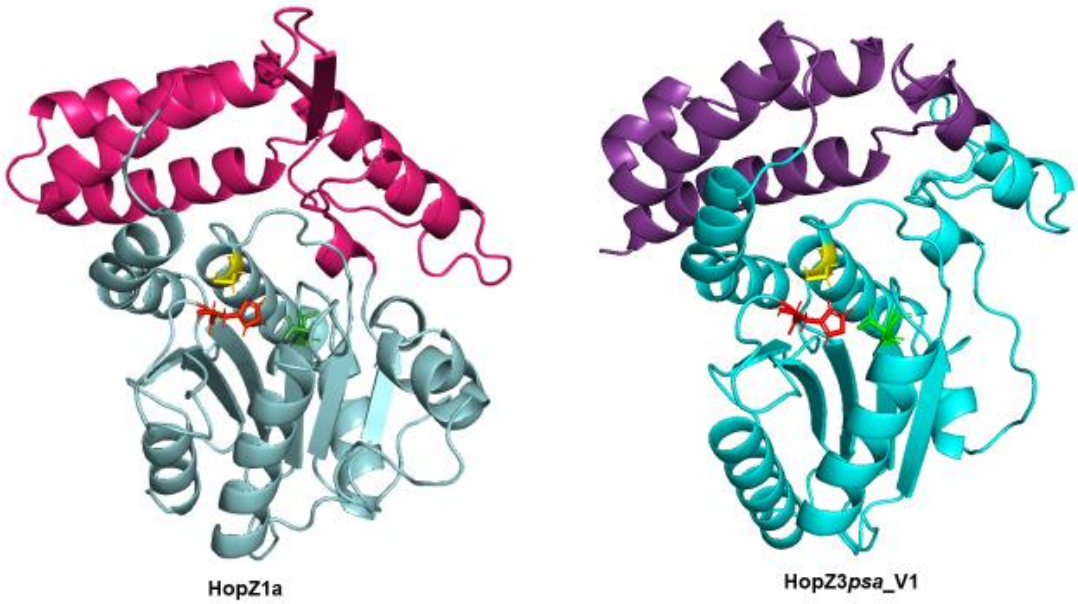

Figure 3.15: Tertiary structure and catalytic motif analysis of HopZ1a and HopZ3*psa*_V1 effectors. The colour codes are as follows: regulatory domains = hot-pink (HopZ1a) and purple (HopZ3*psa*_V1); catalytic domain = cyan (in both structures). The catalytic triad residues are colour-coded: histidine = red, glutamic acid = green, and cysteine = yellow.

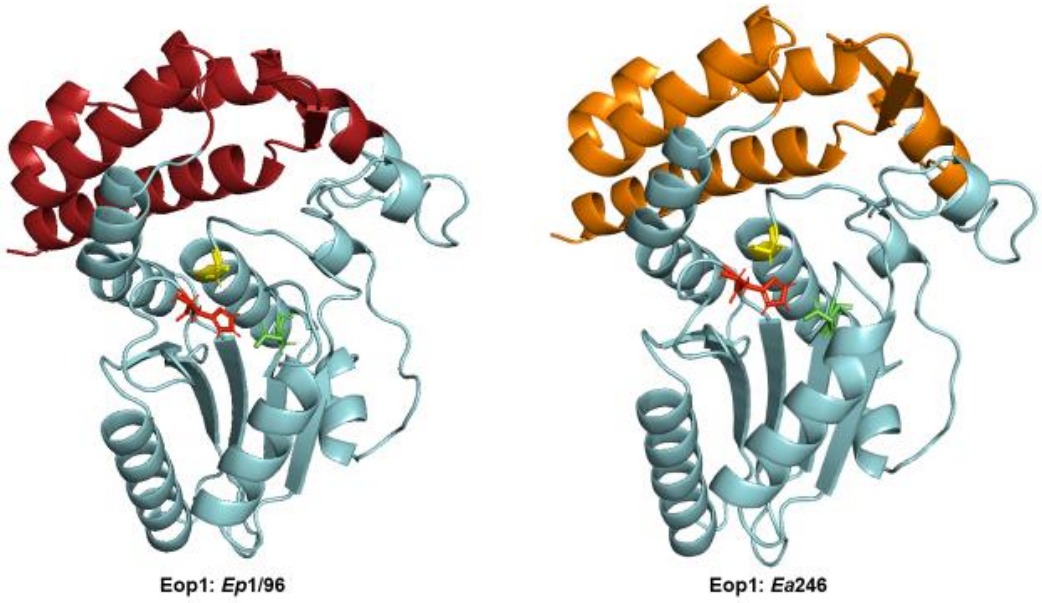

Figure 3.16: Tertiary structure and catalytic motif analysis of Eop1: *Ep*1/96 and Eop1: *Ea*246 effectors. The colour codes are as follows: regulatory domains = brick-red (Eop: *Ep*1/96) and orange (Eop: *Ea246*); catalytic domain = pale-cyan (in both structures). The catalytic triad residues are colour-coded: histidine = red, glutamic acid = green, and cysteine = yellow.

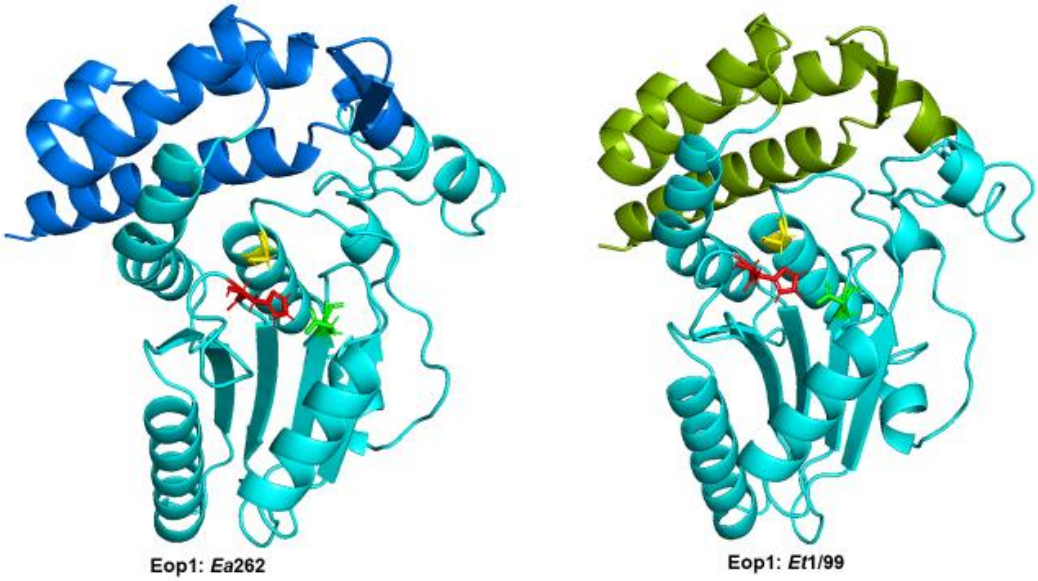

Figure 3.17: Tertiary structure and catalytic motif analysis of Eop1: *Ea*262 and Eop1: *Et*1/99 effectors. The colour codes are as follows: regulatory domains = marine-blue (Eop1: *Ea*262) and pea-green (Eop1: *Et*1/99); catalytic domain = cyan (in both structures). The catalytic triad residues are colour-coded: histidine = red, glutamic acid = green, and cysteine = yellow.

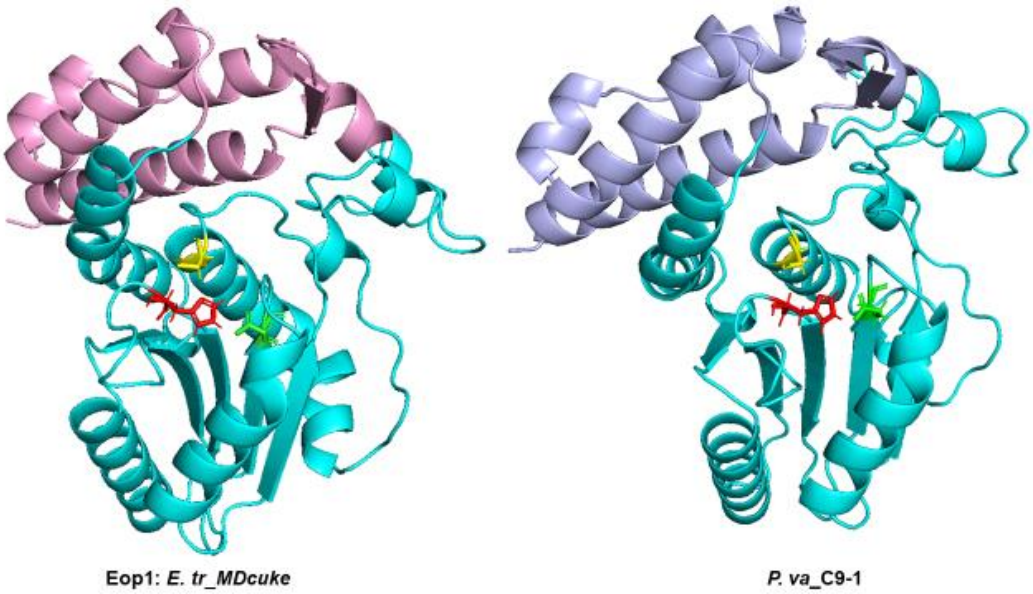

Figure 3.18: Tertiary structure and catalytic motif analysis of Eop1: *E. tr*_MDcuke and Eop1: *P. va*_C9-1 effectors. The colour codes are as follows: regulatory domains = pink (Eop1: *E. tr*_MDcuke) and slate-blue (Eop1: *P. va*_C9-1); catalytic domain = cyan (in both structures). The catalytic triad residues are colour-coded: histidine = red, glutamic acid = green, and cysteine = yellow.

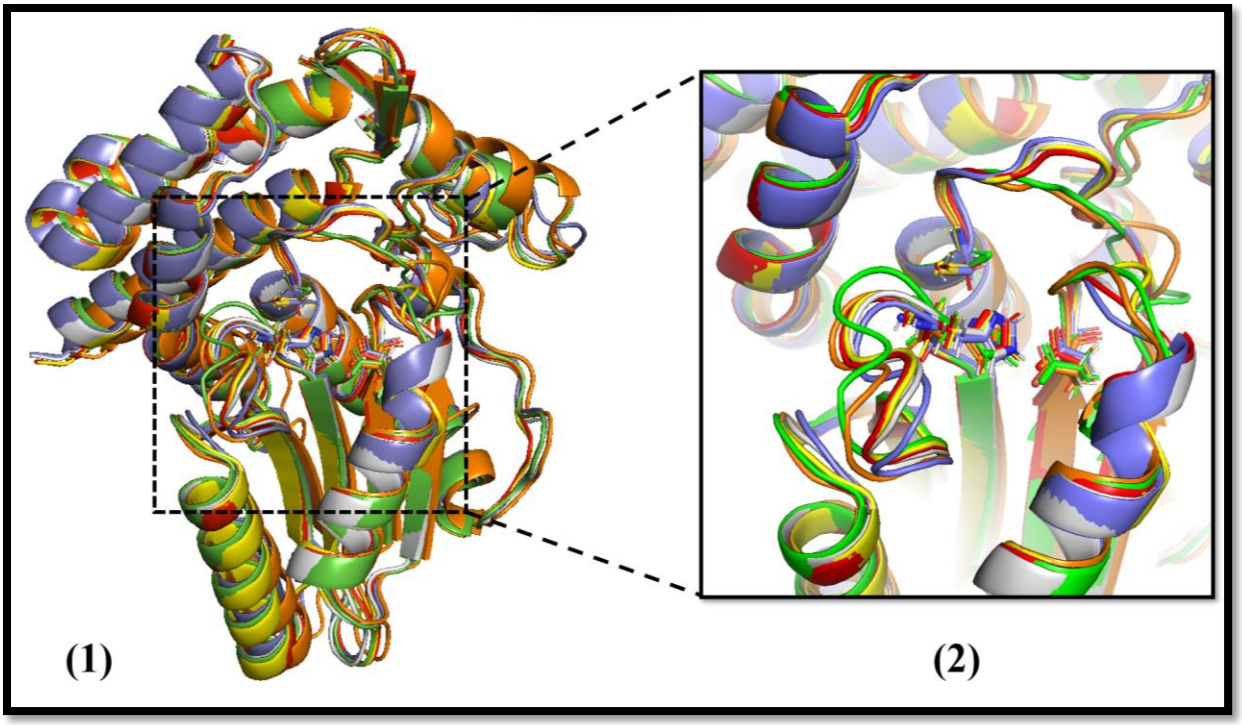

Figure 3.19: Superimposition analysis of all the Eop1 variants tested in the HR assay. (1) Superimposition of the tertiary structure of all Eop1 variants; (2) Superimposition of the catalytic motif and catalytic triad residues of Eop1s. The colour codes are as follows: red = Eop1: *Ea*246 (WT), green = Eop1: *Ep*1/96, yellow = Eop1: *Et*1/99, grey = Eop1: *P. va*_C9-1, orange = Eop1: *Ea*262, blue = Eop1: *E. tr*_MDcuke.

3.3.4.3 Catalytic triad mutation in Eop1: *Ea*246 does not induce any structural or catalytic motif perturbation

To answer the second question regarding potential mutation-induced effector structure perturbation and catalytic motif conformation change, the Eop1: *Ea*246 (wildtype) tertiary structure was superimposed on the catalytic triad residue mutated tertiary structures. The extent of deviation from the superimposition to the wildtype corresponded to the perturbation level.

Interestingly, the tertiary structure of the Eop1: *Ea*246 mutants was starkly similar to its wildtype structure, with mutants maintaining their domains' structural integrity (Figure 3.20). Additionally, the catalytic motif of the mutants was also analysed using a superimposition

approach, which followed a similar trend as mentioned above (Figure 3.21 and Figure 3.22). The analysis also suggested that the phenotype observed in the mutants' HR assay (Figure 3.8) is more likely to result from the induced catalytic triad mutation in Eop1: *Ea*246 rather than gross structural perturbation.

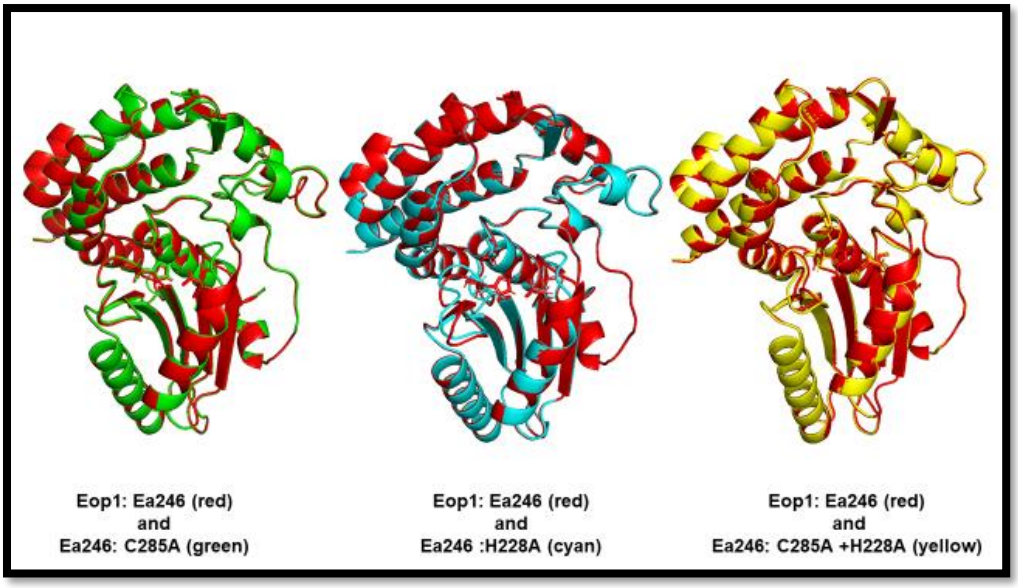

Figure 3.20: Tertiary structure superimposition analysis of Eop1: *Ea*246 and its catalytic triad mutants.

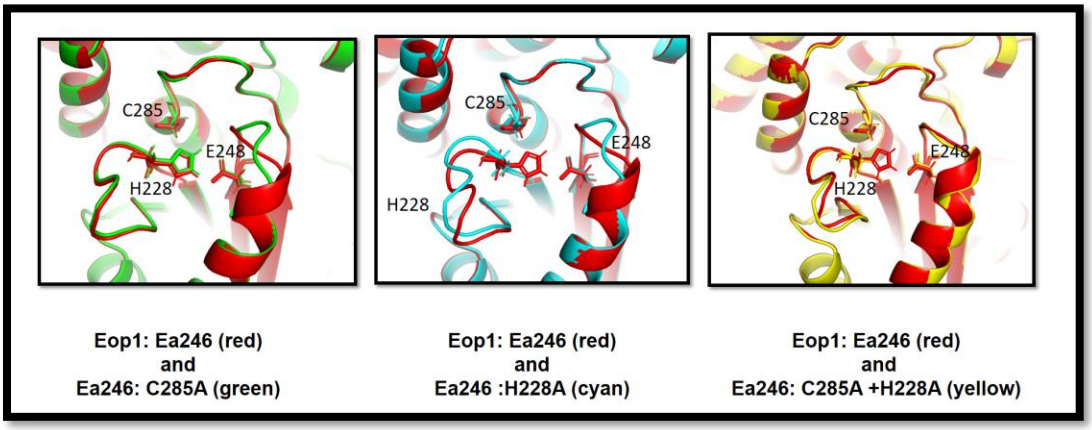

Figure 3.21: Catalytic motif superimposition analysis between Eop1: *Ea*246 and its catalytic triad mutants. The predicted catalytic triad residues are annotated with their respective position in the figure.

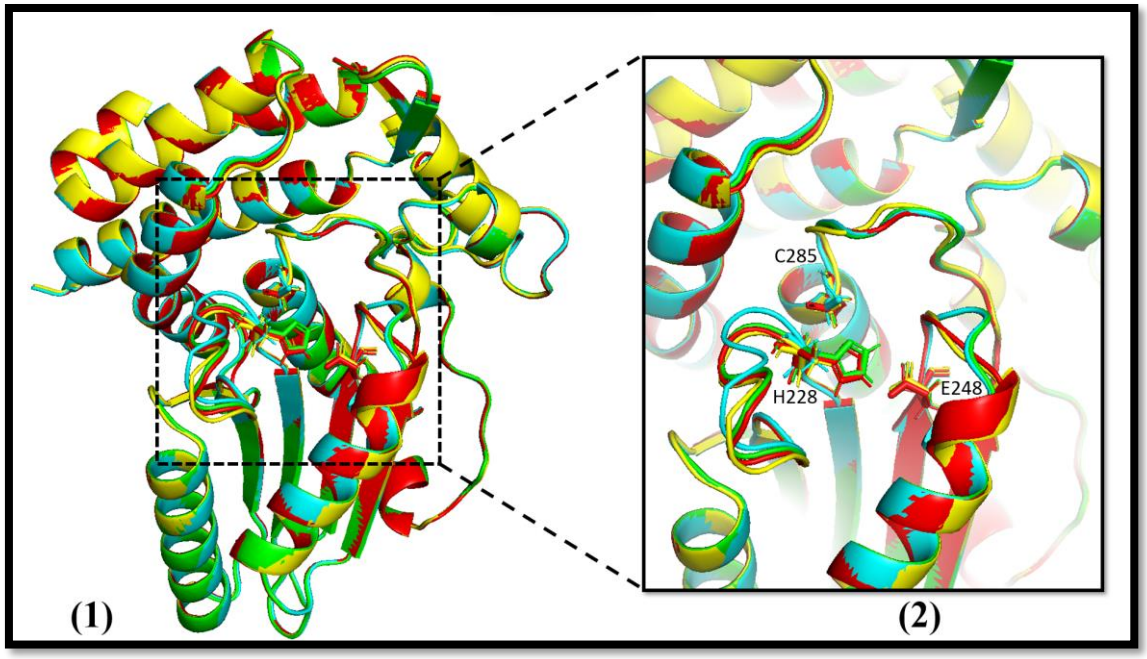

Figure 3.22: Superimposition analysis of Eop1: *Ea*246 catalytic triad mutants with Eop1: *Ea*246 (WT). (1) superimposition of the tertiary structure of Eop1: *Ea*246 with the tertiary structure of its catalytic triad mutants; (2) Superimposition of Eop1: *Ea*246 catalytic motif with the catalytic triad mutants' catalytic motif. The predicted catalytic triad residues are annotated with their respective position in the figure. The colour codes are as follows: red = Eop1: *Ea*246 (WT), green = *Ea*246: C285A, cyan = *Ea*246: H228A, Yellow = *Ea*246: C285A + H228A.

3.3.4.4 Serine residue in Eop1: *Ea*246 potentially substitute for cysteine's nucleophilic activity

As proposed in the "ping-pong" model, the cysteine residue in the catalytic triad of YopJ effectors functions as a nucleophile post-deprotonation of the thiol (SH) group. The nucleophile is considered crucial for catalysis as it attacks 'ACoA' to retrieve the 'acetyl group' for the catalytic process of acetylation (Ma & Ma, 2016). Therefore, to answer the third and final question, amino acids that can function as a nucleophile to replace cysteine in the catalytic triad, such as serine, and cysteine (other than *Ea*246: C285), were considered as 'potential substitute residues' for C285, and consequently 'putative secondary nucleophiles' as well. However, more emphasis was given to serine residues, as serine is known to function as a nucleophile in other enzymes that uses a

catalytic triad for their activity, such as serine protease (Carter & Wells, 1988); additionally, in the 'widescale conservation analysis' of the catalytic triad residues (section 3.3.2), serine was discovered as a substitute for the cysteine residue (Figure 3.5) in one of the Eop1: *Ea*246 protein sequence homologue.

A two-step procedure was employed to identify amino acid residues that could substitute for cysteine (C285) in Eop1: *Ea*246. In the first step, serine and cysteine residues (other than C285) with high conservation in 6 Eop1 variants tested in the HR assay were selected. Next, the proximity of the selected residues to the other two catalytic residues (H228 and E248) was evaluated through AlphaFold2 predicted 3D model. Additionally, particular care was taken in the second step to ensure that the catalytic motif confirmation remains undisturbed.

Three serine residues were identified using the abovementioned technique: S249, S281 and S289. S249 and S281 residues were conserved in the six Eop1 variants (Figure 3.23); however, S289 was only conserved in Eop1: *Ea*246 immediate homologue: Eop1: Et1/99 (See 'Supplementary Figure C3S9' for the phylogenetic tree of the tested Eop1 variants). Regardless, all the identified 'putative secondary nucleophile' residues shared high proximity to the other two catalytic residues: H228 and E248 (Figure 3.24). Interestingly, S249 and S289 were the two most promising candidates as they were comparatively closer to the catalytic histidine than the other residue: S281. The proximity of the 'nucleophile' residue to histidine is significant as histidine acts as a proton acceptor during the deprotonation of the residue functioning as a nucleophile (Ma et al., 2015; Ma & Ma, 2016; Zhang et al., 2016). However, further site-directed mutagenesis studies would be required to validate or dismiss the probable involvement of the selected residues in Eop1: *Ea*246 catalytic activity.

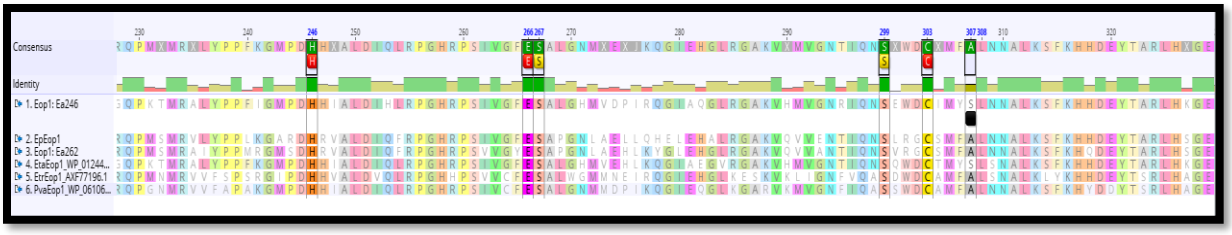

Figure 3.23: Conservation analysis[44] of putative cysteine-substituting serine residues (putative secondary nucleophiles) in Eop1 variants tested in the HR assay. The red boxes below the 'consensus sequence' represent the catalytic triad residues, H/E/C, respectively. The yellow boxes represent conserved 'putative secondary nucleophiles': 'S249' and 'S281'; the black box represents another potential but unconserved 'putative cysteine-substituting serine residue': S289. (See footnote '44' for information on wide-scale conservation analysis of the 'putative secondary nucleophiles).

[44]Note: a widescale conservation analysis of the 'putative secondary nucleophile' residues in 86 protein sequence homologs of Eop1: *Ea*246 was also performed (Supplementary Figure C3S11); the conservation rate of the residues from the analysis is as follows: S249 conservation rate: 97.6%; S281 conservation rate: 96.5%; S289 conservation rate: 22%.

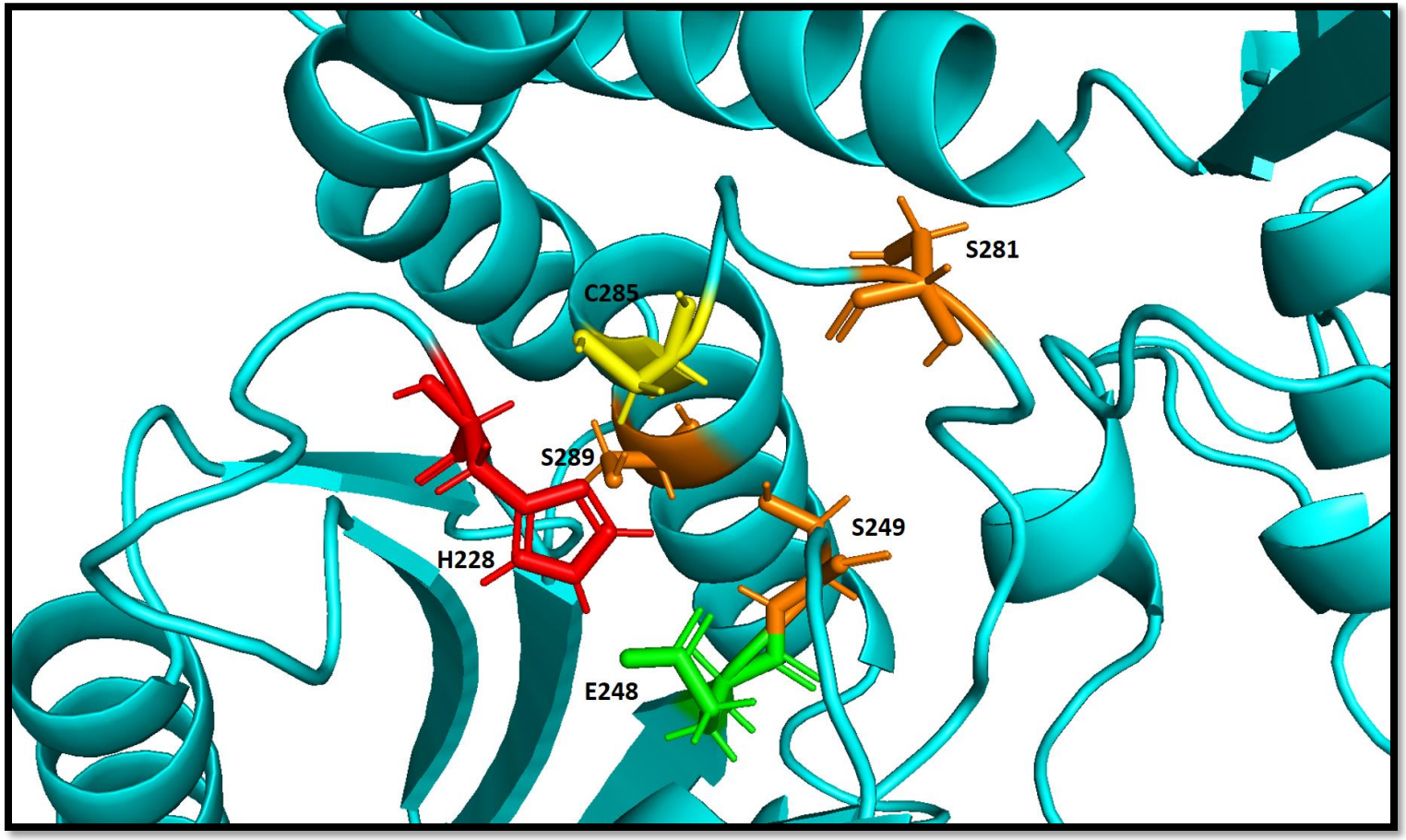

Figure 3.24: Proximity analysis of the putative 'secondary nucleophile' residues (S249, S281, and S289) to the other catalytic triad residues in the predicted catalytic triad of Eop1: *Ea*246. The Eop1: *Ea*246 catalytic triad residues' colour codes are: red = histidine: 228, green = glutamic acid: 248, and yellow = cysteine: 285. Serine residues identified as 'putative secondary nucleophiles' (S249, S281, and S289) are presented via orange colour. The cyan colour represents Eop1: *Ea*246 backbone.

3.4 Discussion

The previous study discovered that transient expression of Eop1 variants induces a strong HR in the non-host plant *N. tabacum*. The HR was proposed to result from the catalytic activity induced by Eop1s and its recognition by an NB-LRR plant receptor(s). Eop1 is a member of the YopJ family of bacterial effectors. The members of this family rely on a C55 family protease-like catalytic triad for its catalytic activity. The catalytic triad is evolutionarily conserved and consists of cysteine, histidine, and glutamic acid (Lewis et al., 2011; Ma & Ma, 2016; Orth et al., 2000). Thus, this study conducted a series of experimental and *in-silico* protein modelling to validate the conservation and involvement of the catalytic residues (H/E/C) in the HR activity induced by Eop1: *Ea*246 and other Eop1 variants in *N. tabacum*.

3.4.1 Unity in diversity: effectors employing similar catalytic triad residues can target different host substrates

The conservation study affirmed that the functionally important catalytic residues (H/E/C) are widely conserved in the Eop1s of "*Erwinia-Pantoea*" clade members. The evolutionary conservation of the catalytic triad signifies its potential significance in the Eop1s. It also indicates that catalytic triad residues could be the central driver of the catalytic activity in different Eop1 variants. However, various YopJ effectors utilising identical catalytic triad residues for catalysis do not imply targeting of the same host substrates or plant proteins. HopZ1a from *Psy*A2, and HopZ3 from *Psy*B728a, for example, are YopJ effectors that employ the catalytic triad residues for catalysis (Lee et al., 2015; Lewis et al., 2010); however, in the *Arabidopsis* plant, HopZ3 acetylates RIN4 (Lee et al., 2015), whereas HopZ1a acetylates ZED1 (Lewis et al., 2013). This suggests that despite sharing identical catalytic triad residues for catalysis, the YopJ effectors can target and potentially acetylate a diverse set of plant proteins. Additionally, it is equally important

to note that YopJ effectors utilise a protease-like catalytic triad and are capable of proteolytic activity (Orth et al., 2000).

3.4.2 Residue conservation may not necessitate its involvement in the catalysis process

The conservation of catalytic triad residues may not necessitate their participation in the catalysis process, an example of which is demonstrated in this study. Despite wide conservation of the putative catalytic cysteine residue in the Eop1 variants, the cysteine mutant (*Ea*246: C285A) was observed to elicit a progressive HR in *N. tabacum*, indicating that the residue C285 is probably not involved in Eop1: *Ea*246 catalytic activity in *N. tabacum*. However, the observed progressive HR can be attributed to two possibilities: (1) the actual residue acting as a nucleophile in the catalysis is proximal to the mutated C285 residue, and the C285A mutation interferes with and impedes the catalytic activity; (2) An alternate possibility could be, whenever present, the C285 residue acts as the 'primary' nucleophile; however, in its absence, the other nearby 'secondary' nucleophile with potentially weak nucleophilic activity functions as a primary nucleophile in the catalysis, or it could be a combination of both the possibilities. Regardless, the involvement of another residue functioning as a nucleophile apart from C285 in Eop1: *Ea*246 is highly likely.

Nucleophilic activity is of prime importance for catalysis in YopJ effectors (Ma & Ma, 2016). Thus, it is probable that a nearby amino acid residue capable of nucleophilic activity may have compensated for the C285 mutation in the Eop1: *Ea*246 catalytic triad. Interestingly, three serine residues, intrinsically capable of performing a nucleophilic activity (Cuesta et al., 2020), i.e., S249, S281 and S289, were discovered to be in proximity with the other two catalytic triad residues, making them potential substitutes for cysteine. However, more research is necessary to investigate the involvement of the proposed substitute residues.

3.4.3 Evidence of Eop1: *Ea*246 indirect recognition in *Nicotiana tabacum*

The Eop1: *Ea*246 catalytic triad mutation analysis revealed that, unlike the wildtype or cysteine mutant, the histidine mutant (*Ea*246: H228A) failed to trigger the HR-induced cell death in the non-host plant *N. tabacum*. The requirement of the predicted catalytic histidine residue 'H228' in Eop1: *Ea*246 induced HR in *N. tabacum* indicates that it functions through an enzymatic mechanism and is consequently more likely to be recognised indirectly through its enzymatic activity on the host target(s).

Even though YopJ family effectors can potentially target a wide variety of host substrates, Eop1 from *E. amylovora*, in particular, is more likely to target RIN4 because of its unique phylogenetic and evolutionary relationship with HopZ3. HopZ3 is also considered a putative functional homolog of Eop1 (Ma et al., 2006). Interestingly, HopZ3, unlike other HopZ1 effectors, is not ancestral to *P. syringae* and may have been acquired through horizontal gene transfer from other ecologically associated phytopathogenic species, such as *E. amylovora* (Ma et al., 2006).

3.4.4 The tertiary structure of Eop1 from *E. amylovora* and related species mimic the HopZ1a structure

Despite a low protein sequence identity (< 21.5%), a comprehensive *in-silico* structural analysis of the HopZ3 effector from *P. syringae* conducted by Chakraborty (2021) revealed that it fully adopts HopZ1a-like structural and catalytic motif conformation. Interestingly, a similar observation was made when the Eop1s from *E. amylovora* and related species *in-silico* tertiary structures were compared with the HopZ1a structure in this study. All the tested Eop1s share less than 25% protein sequence identity with HopZ1a; however, their *in-silico* tertiary structure models were intriguingly similar to the HopZ1a structure deciphered through X-ray crystallography and

NMR imaging (Zhang et al., 2016). Additionally, the structural and catalytic motif analysis further supported the finding that Eop1 variants will likely employ the catalytic triad for their activity.

Interestingly, substrate-binding pocket-like structures similar to the HopZ1a's IP6 and AcCoA binding sites in the regulatory and catalytic domain, respectively (Ma et al., 2015; Ma & Ma, 2016; Zhang et al., 2016), were also discovered in Eop1s during the analysis. The substrate-binding pockets in the Eop1 variants suggest that they would probably require the eukaryote-specific co-factor 'IP6' for activation and 'AcCoA' for catalysis. However, the involvement of IP6 and AcCoA in the YopJ effector's activation and function is not uncommon, as both have already been verified in HopZ1a (Zhang et al., 2016) and HopZ3 (Lee et al., 2015; Ma et al., 2015). However, a further investigation involving the mutation analysis of the regulatory domain potentially involved in the binding of IP6 is required to validate the IP6 requirement in Eop1s *in-planta* activity.

3.5 Conclusion

In conclusion, it is evident from the experiments that Eop1: *Ea*246 acts as a typical YopJ effector and utilises at least part of the predicted catalytic triad for its catalytic activity. However, the non-participation of the cysteine residue in the catalysis is an intriguing piece of evidence that opens new opportunities for investigating and reshaping our current understanding of the conserved residues and the residues involved in the catalytic activity in the YopJ effectors. Additionally, the evidence for Eop1's indirect recognition and Eop1's evolutionary relationship with HopZ3 strongly reinforce the idea of RIN4 participation in Eop1-induced activity in *N. tabacum*. Furthermore, analysis of the *in-silico* tertiary structure reveals that the activation and function of the Eop1s may necessitate the participation of IP6 and AcCoA. As a result, further experimentation-driven research would be necessary to characterise the Eop1 activity within the plant's biosystem thoroughly.

4 Chapter 4: RPA1 and RIN4 proteins are crucial for the molecular recognition of Eop1s in *Nicotiana tabacum*

4.1 Introduction

Throughout their lives, plants are constantly challenged by the microbes present in the environment. However, most microbes are neutralised by the plant's physical barriers or by its first layer of innate defence response, PTI (Serrano et al., 2014; Stuart et al., 2013; Zipfel & Robatzek, 2010). Adapted bacterial pathogens suppress PTI by secreting T3SE into the plant cells via T3SS (Macho & Zipfel, 2015; Toruno et al., 2016b). To combat the pathogen's effector-driven invasion efforts, plants evolved with R-proteins. The R-protein perceives the effectors and triggers ETI, which manifests as localised cell death (HR), limiting pathogen development at the site of infection (Cui et al., 2015; Jones & Dangl, 2006).

In the absence of the cognate R-protein in the susceptible host, the effectors' activity on the host target protein(s) goes unchecked, enabling the pathogen to manipulate the plant's innate immune system and infect it (Figure 4.1) (Stuart et al., 2013). However, in the resistant host plants, the effectors' activity is recognised directly or indirectly by its cognate R-proteins (Jones & Dangl, 2006). Direct recognition is described by a receptor-ligand model (Figure 4.1; sub-figure 1), in which the effector acting as a 'ligand' is recognised by its cognate R-protein acting as a 'receptor', culminating in immune signalling post-recognition (Dodds & Rathjen, 2010; Ellingboe, 1981). The indirect effector recognition encompasses multiple models (Figure 4.1; sub-figure 2), which are as follows:

a) Guard hypothesis (GH): In GH, the host-target (guardee) is 'guarded' by its cognate R-protein, which triggers an immune response by detecting effector-induced host target

perturbation (Dangl & Jones, 2001; Jones & Dangl, 2006). This phenomenon can occur via two mechanisms: (1) GH model 1: the interaction between the effector and its host target induces a modification in the host target which is recognised by the R-protein, resulting in immune response (Figure 4.1; sub-figure 2.1) (Dodds & Rathjen, 2010; Stuart et al., 2013); (2) GH model 2: the host target and R-protein co-exist coherently forming a 'guard-guardee' protein complex and suppressing the immune response. This 'guard-guardee' protein complex gets disturbed by host-target (guardee) interaction with the effector, resulting in the release of the R-protein and enabling it to engage in immune activation processes (Figure 4.1; sub-figure 2.2) (Dodds & Rathjen, 2010; Stuart et al., 2013).

b) Decoy hypothesis (DH): the DH proposes the existence of proteins that are 'decoys' (structural mimic proteins) of the effector target and function as a sentinel for the effector's perception (Figure 4.1; sub-figure 2.3). The decoy proteins' sole purpose is to recognise the effector and does not serve a primary function[45] in the host plant's physiology (Jones & Dangl, 2006; Stuart et al., 2013; van der Hoorn & Kamoun, 2008).

c) Bait-and-switch model (B&S): B&S is a unique modified version of the 'decoy' model, which involves a two-step recognition event. In the first step, the effector binds to the 'bait protein', which, if in association with the R-protein, leads to a secondary recognition event in which the R-protein interacts and recognises the effector but not through the effector-induced modification (Figure 4.1; sub-figure 2.4) (Collier & Moffett, 2009; Dodds & Rathjen, 2010; Stuart et al., 2013).

[45] The decoy proteins are believed to be the result of a gene duplication event or a "splice variant of the normal target" Stuart et al. (2013).

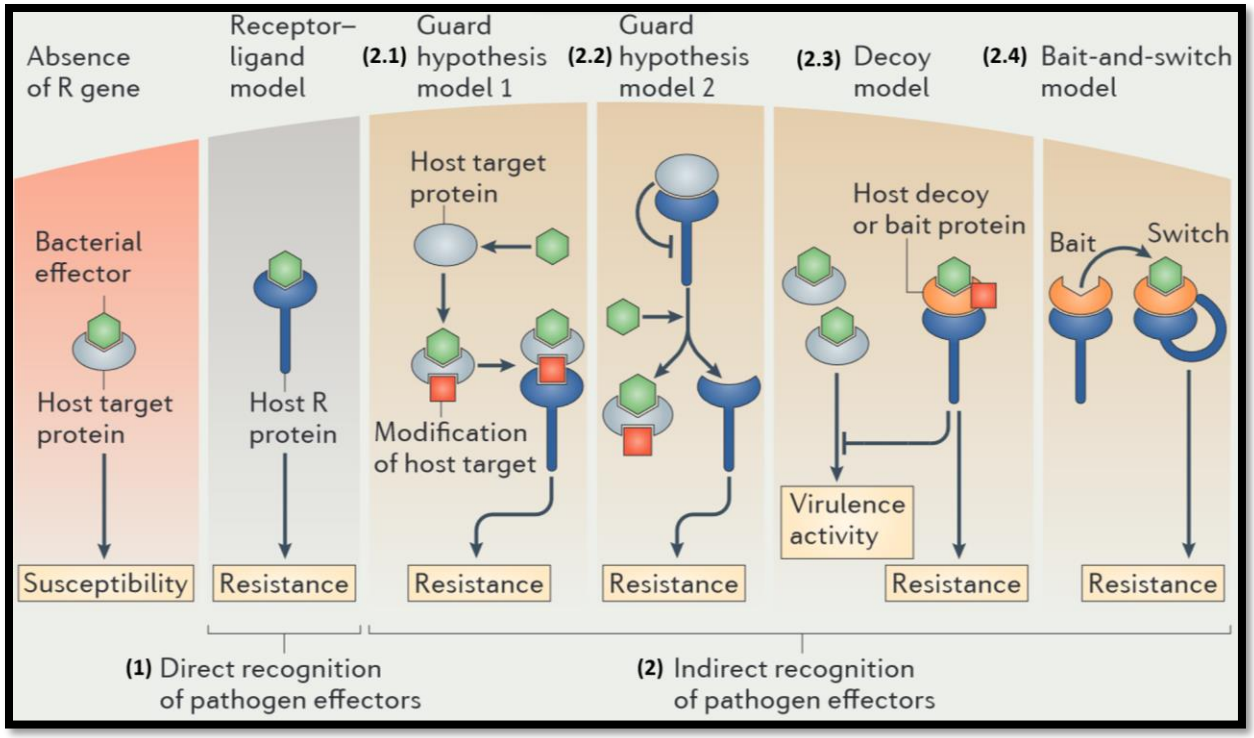

Figure 4.1: An overview of the mechanisms of effector-induced susceptibility (ETS) and its recognition by R-proteins resulting in effector-triggered immunity (ETI). The image was adapted from Stuart et al. (2013).

Upon encountering proteinaceous effectors from non-adapted bacterial pathogens, the non-host plants often express resistance in the form of HR, which can be attributed to specific R-proteins (Fonseca & Mysore, 2019; Lindgren et al., 1986; Panstruga & Moscou, 2020). Through forwards and reverse genetics screening techniques, the 'non-host resistance induced HR' can be used to characterise a specific effector or discover the R-gene encoded R-protein responsible for the HR (Senthil-Kumar & Mysore, 2013). These screening techniques either rely on the elicitation of HR or the absence/reduction of HR. The HR elicitation screening techniques involve the co-expression of the R-protein with pathogen origin Avr effector protein in the plant (Du & Vleeshouwers, 2014; Senthil-Kumar & Mysore, 2013), whereas the screening techniques based upon the absence or reduction of HR relies on virus-induced gene silencing (VIGS) (Anand et al.,

2007), or hairpin (hp)-based gene silencing of the targeted gene, delivered via *Agrobacterium* in the non-host plant (Brendolise et al., 2017; Senthil-Kumar & Mysore, 2013).

In the previous experiments, it was observed that the Eop1 effector from *E. amylovora* and its homologs from other related species trigger HR in the non-host plant *N. tabacum*. Additionally, Eop1 from *E. amylovora* '*Ea*246' was also demonstrated to employ an enzymatically important and conserved histidine residue: H228, to induce HR. Thus, suggesting the involvement of the hypothesised enzymatic role, probably acetylation of the targeted host protein(s). Interestingly, a putative functional homolog of the Eop1 effector (Ma et al., 2006), HopZ3, acetylates a plant immune regulator protein, RIN4 (Afzal et al., 2013). Moreover, the HopZ3$_{Psa}$_V1 effector requires RPA1 and RIN4 proteins to elicit HR in *N. tabacum*, as silencing of either of the two results in a significant reduction in HR (unpublished data from Yoon & Rikkerink). Therefore, considering all the aforementioned factors, it was hypothesised that Eop1s would probably require RPA1 and RIN4 proteins to trigger HR in the non-host plant *N. tabacum*. Consequently, the following chapter includes a series of experiments employing forward and reverse genetic approaches to test the proposed hypothesis.

4.2 Materials and Methods

4.2.1 Plant Material (*Nicotiana tabacum* and *Nicotiana benthamiana*)

Nicotiana tabacum cv. Samsun and *Nicotiana benthamiana* (unknown cultivar) plants used in this study were grown under the same conditions described in section 2.2.11.1.

4.2.2 Plant expression studies

4.2.2.1 *Agrobacterium*-mediated transient expression in *N. tabacum* and *N. benthamiana*

The transient expression of the desired gene via agroinfiltration in *N. tabacum* and *N. benthamiana* was performed by employing the protocol described in section 2.2.11.2. The HR-induced cell death was assayed after three days post-infiltration.

4.2.2.2 Sequential infiltration in *N. benthamina* and *N. tabacum*

The *Agrobacterium tumefaciens* (GV3101) cells were prepared and infiltrated in *N. benthamiana* and *N. tabacum* plants using the same methodology described in section 4.2.2.1. However, sequential infiltration encompassed two successive infiltrations, with the second infiltration delivered two days following the first. Also, additional infiltration descriptions are described along with the results for better comprehension.

4.2.2.3 Co-infiltration in *N. benthamiana* and *N. tabacum*

The *Agrobacterium tumefaciens* (GV3101) cells were infiltrated in *N. benthamiana* and *N. tabacum* plants using the same methodology described in section 4.2.2.1. However, in co-infiltration, a premix of *Agrobacterium* cells harbouring expression clones of different genes under investigation was suspended in 10 mL of infiltration buffer. Additionally, two distinct infiltration buffers: 10 mM MES (pH 7.2) + 10 mM $MgCl_2$ and 5 mM EGTA + 10 mM $MgCl_2$, were employed

in the experimental study in *N. tabacum*. Additional infiltration descriptions are described along with the results for better comprehension.

4.2.3 Development of a three-component co-infiltration combination system to investigate the participation of gene(s) involved in Eop1-triggered HR in *Nicotiana tabacum* via hairpin-induced silencing

The developed 'three-component co-infiltration system' comprised of an infiltration premix composed of *Agrobacterium* cells harbouring expression clones for (1) a replaceable component, (2) a hairpin-producing component for silencing, and (3) an HR elicitor component (refer to 'Figure 4.2' for infographic). The replaceable component was either an empty expression vector (pHEX2: EV or pTKO2: EV) or an expression vector containing GUS insert (pHEX2: GUS or pTKO2: GUS)[46]. Thus, it had no effect of its own and was consequently used to balance the *Agrobacterium* concentration (OD_{600}) in the co-infiltration combination premix and to test the system's efficacy (Figure 4.2; sub-figure 1). In contrast, the HR elicitor component involved the HR elicitation activity, which in this case was an Eop1 effector. Finally, the silencing component involved the production of the hairpin (hp) constructs, inducing the RNAi effect by silencing the gene under investigation (Figure 4.2; sub-figure 2).

Given the successful silencing of the gene-of-interest and reduction in HR, the replaceable component was replaced with *Agrobacterium* carrying an expression clone containing the functional form of the 'gene-of-interest' (or its allelic version). This step was explicitly included to restore HR via complementation, confirming the gene-encoded protein's participation in the HR (see Figure 4.2; sub-figure 3).

[46] The GUS expression vectors (pHEX2/pTKO2: *GUS*) were developed as described in section 4.2.4.1.

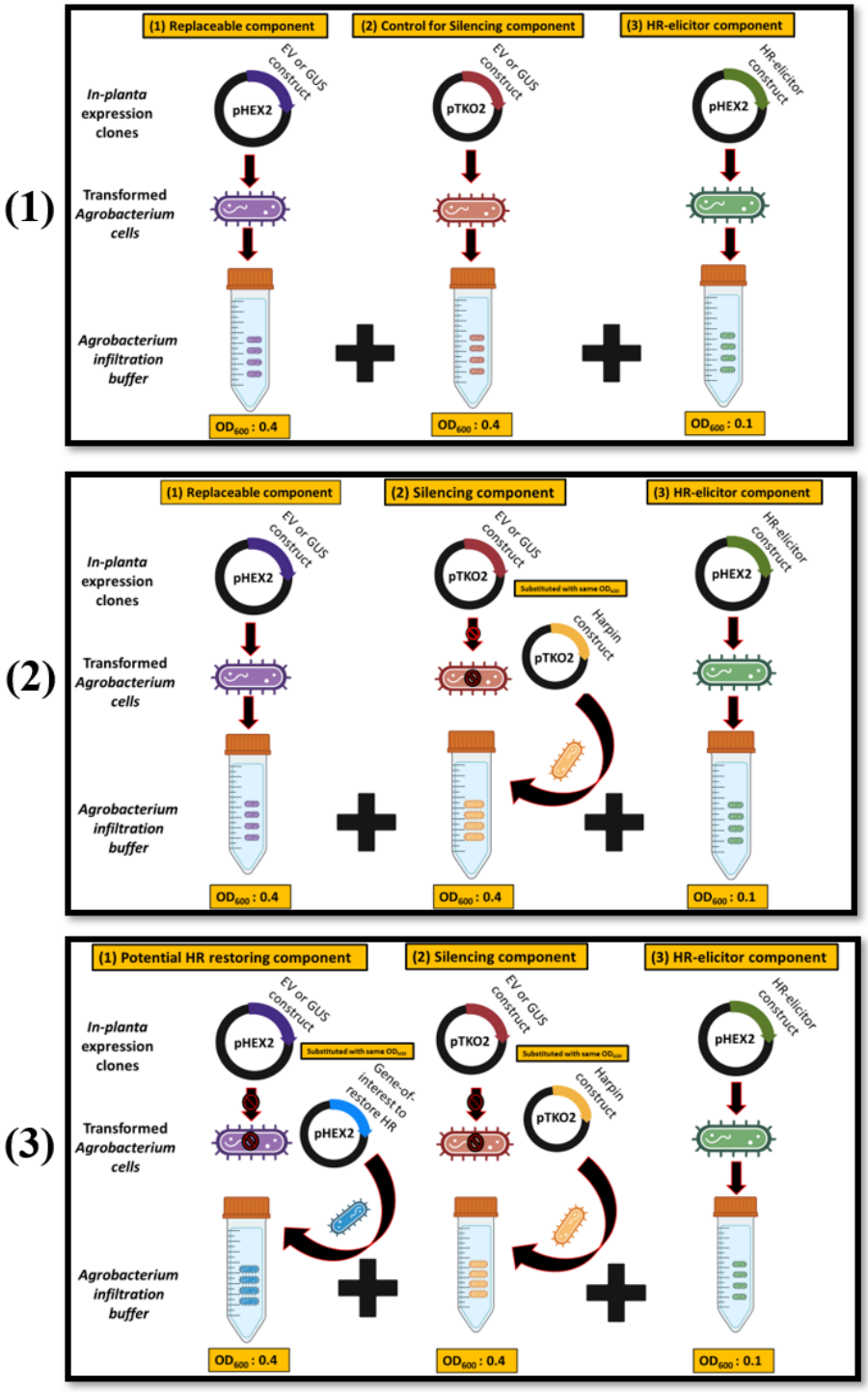

Figure 4.2: Concept of the 'three-component co-infiltration system'. (1) 'Three-component co-infiltration combination' used as a control to test the HR eliciting ability of the effector at a particular *Agrobacterium* concentration of the components; (2) 'Three-component co-infiltration

combination' employed to test the involvement of the 'gene-of-interest' in the effector induced HR activity by silencing it via hairpin construct produced through silencing vector: pTKO2, and screening for HR reduction or its absence; (3) Following hairpin-mediated silencing and HR reduction, the involvement of 'gene-of-interest' can be validated by restoring HR by replacing the 'replaceable component' in the co-infiltration system with the exogenous form of 'gene-of-interest' expressed under an appropriate promoter such as 35S CaMV promoter.

4.2.4 Molecular methods

4.2.4.1 Formation of GUS expression clones of the silencing vector (pTKO2) and expression vector (pHEX2)

The GUS expression clones of the silencing vector (pTKO2) and expression vector (pHEX2) used as controls in the study were made by employing the Gateway® LR reaction protocol described in section 2.2.3.2.1. The entry clones carrying the GUS construct used in the LR reaction were provided in the Gateway® cloning kit [Life Technologies, CA, USA].

4.3 Results

4.3.1 *Agrobacterium*-mediated transient expression of Eop1 variants in *Nicotiana benthamiana*

The previous study discovered that the Eop1 effector from *E. amylovora* and related species trigger HR in the non-host plant *Nicotiana tabacum*. *N. tabacum* and *N. benthamiana* are related tetraploid species that share roughly 2026 protein clusters (Sierro et al., 2014) and have *N. sylvestris* (2n = 24) as a common progenitor (Schiavinato et al., 2020; Sierro et al., 2014). Additionally, NLR genes are often conserved between *N. tabacum* and *N. benthamiana* (Yoon & Rikkerink, 2020). Therefore, transient expression analysis of Eop1s was performed in *N. benthamiana* to determine if Eop1s would likewise elicit HR in the tobacco-related non-host plant *N. benthamiana*.

Agrobacterium tumefaciens (GV3101) harbouring expression clones carrying the *eop1* gene under CaMV 35S promoter were infiltrated in 3-4 weeks old *Nicotiana benthamiana* leaves. Additionally, HopZ3 and HopZ5 were employed as negative and positive controls for HR phenotype, respectively. HopZ3 and HopZ5 are *Pseudomonas syringae* YopJ effectors (Bundalovic-Torma et al., 2022; Ma & Ma, 2016). HopZ3 was chosen as a negative control as it does not trigger HR in *N. benthamiana* (Vinatzer et al., 2006), whereas HopZ5 (Cordially provided by Jay Jayaraman) was chosen as a positive control because of its ability to trigger a robust HR in *N. benthamiana* (Jayaraman et al., 2017).

Interestingly, Eop1 variants that triggered HR in *N. tabacum* did not elicit HR in *N. benthamiana* (Figure 4.3). However, chlorosis independent of HR[47] at 6 dpi was observed in *N.*

[47] The *Erwinia tasmanensis* (*Et*1/99) Eop1 induced 'HR-independent chlorosis' was verified by bleaching the leaf infiltrated with *Agrobacterium harbouring the expression clone carrying the E. tasmaniensis* str. Et1/99 *eop1* gene with methanol at 6 dpi (Figure 4.5), a methodology adopted from Adlung et al. (2016).

benthamiana leaves infiltrated with *Agrobacterium* harbouring gene encoding for Eop1 homolog from *Erwinia tasmanensis* (*Et*1/99) (Figure 4.4 and Figure 4.5). Moreover, HopZ5-induced HR was also found to be less robust as it did not cause complete cell death in the infiltrated region, which contrasted with its usual response of robust HR at 2-3 dpi, as reported by Jayaraman et al. (2017).

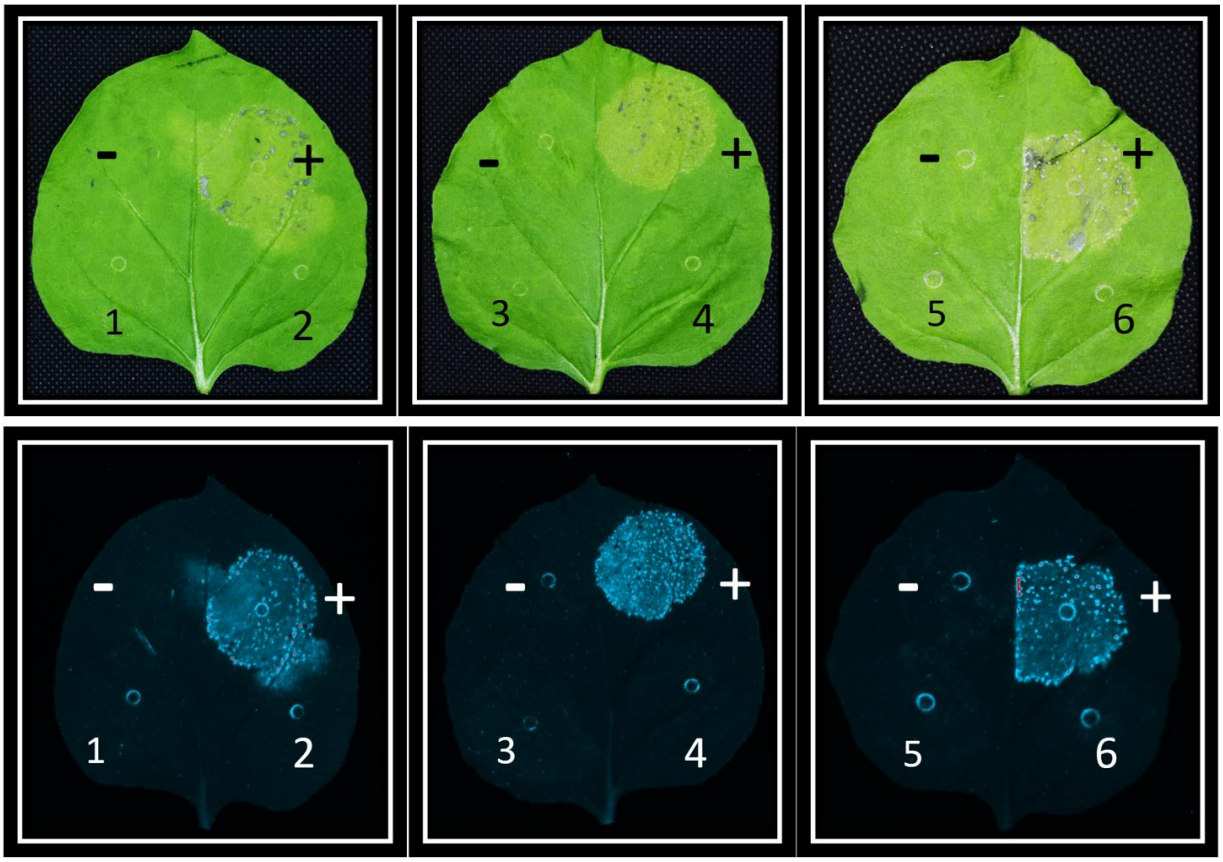

Figure 4.3: *Agrobacterium*-mediated transient expression analysis of Eop1 variants in *Nicotiana benthamiana* (upper panel). The same leaves were visualised in the ChemiDoc™ Gel Imaging System under the Pro-Q Emerald 488 (stain-free) (bottom panel); the luminous patch signifies HR-induced cell death in the leaves. The annotations are as follows: '-' = HopZ3 (negative control for HR), '+' = HopZ5 (positive control for HR), 1 = Eop1: *E. pyrifoliae* str. *Ep*1/96; 2 = Eop1: *E. amylovora* str. *Ea*246; 3 = Eop1: *E. amylovora* str. *Ea*262; 4 = Eop1: *E. tasmaniensis* str. *Et*1/99; 5 = Eop1: *E. tracheiphila* str. MDcuke; 6 = Eop1: *P. vagans* str. C9-1. The presented results were validated by repeating the experiment three times with three replications with similar results. The images were taken at 3 dpi.

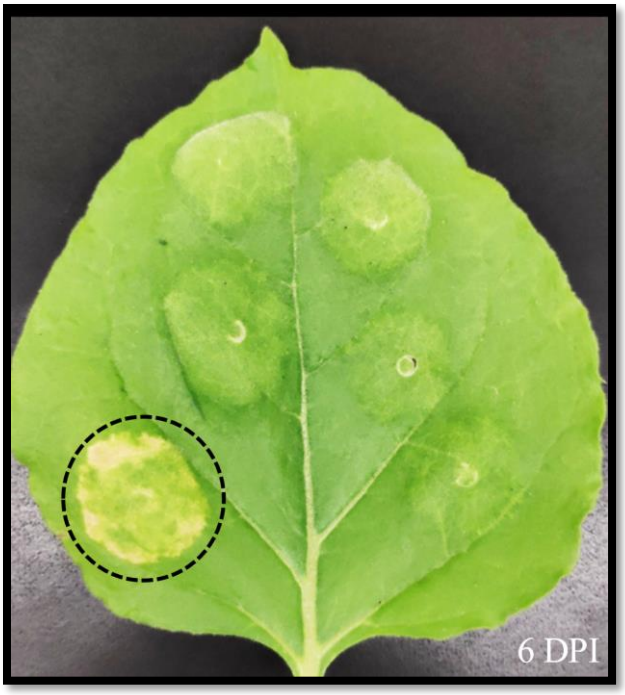

Figure 4.4: *E. tasmaniensis* str. Et1/99 Eop1 induced 'HR-independent chlorosis' in *N. benthamiana* (encircled region). The experiment was repeated thrice with similar results. The image was taken at 6 dpi.

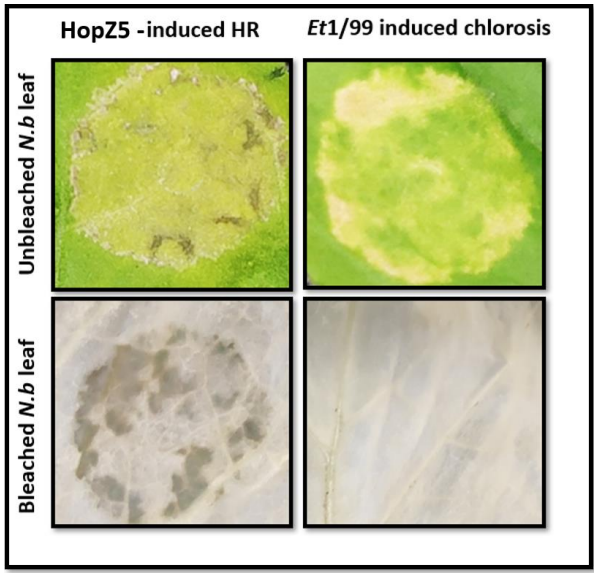

Figure 4.5: Methanol facilitated bleaching assay of HopZ5 induced HR and Eop1: *Et*1/99 induced 'HR-independent chlorosis' in *N. benthamiana*. The experiment was repeated twice with similar results. The images of the unbleached leaf segments were taken at 6 dpi; the leaf was then bleached by submerging it in methanol, and an image was taken 24 hours later.

4.3.2 Analysis of RPA1 participation in molecular recognition of Eop1 variants via transient expression in *Nicotiana benthamiana*

In the previous experiment, the Eop1 variants HR assay performed in *N. benthamiana* demonstrated that none of the tested Eop1s triggered HR. Therefore, a forward genetics approach was adopted to investigate RPA1's involvement in the molecular recognition of Eop1 variants. In this approach, the functional allele of RPA1 cloned in an expression clone was transiently expressed (under CaMV 35S promoter) in the *N. benthamiana* plant in combination with Eop1s via *Agrobacterium*. The screening strategy involved the induction of HR in the *N. benthamiana* leaves infiltrated with *Agrobacterium* carrying the expression clones for RPA1 and Eop1.

4.3.2.1 Analysis of RPA1 autoimmunity in *N. benthamiana*

Heterologous expression of R-genes in non-native plants can induce autoimmunity because of the lack of regulatory components (Li et al., 2010; van Wersch et al., 2020). Therefore, the autoimmune activity of RPA1 R-protein in *N. benthamiana* was investigated by delivering different concentrations of *Agrobacterium* carrying exogenous RPA1 in an expression clone under the CaMV 35S promoter. The *Agrobacterium* concentrations evaluated ranged from 8.0 x 10^6 CFU/mL to 4.8 x 10^8 CFU/mL, corresponding to an OD_{600} range of 0.01 to 0.6.

Different concentrations of *Agrobacterium* (OD_{600} ranging from 0.01 to 0.6) carrying the *RPA1* gene in an expression vector: pGWB20[48] (Nakagawa et al., 2007) were infiltrated in the leaves of 3-4 weeks old *N. benthamiana* plants. Interestingly, no autoimmune response was observed in *N. benthamiana* leaves infiltrated with *RPA1*-harbouring *Agrobacterium* cells in concentration levels ranging from 8.0 x 10^6 CFU/mL to 1.6 x 10^8 CFU/mL (OD_{600} from 0.01 to

[48] The expression clone of RPA1 (pGWB20: *RPA1*) was cordially provided by Minsoo Yoon and had been previously used in a study by Yoon & Rikkerink (2020).

0.2) (Figure 4.6). However, occasional moderate autoimmunity, signified by mild cell death, was observed in leaves infiltrated with a concentration above 1.6 x 10^8 CFU/mL (OD_{600}: 0.2), which varied in replication. As a result, *Agrobacterium* cell suspension with a concentration of 1.6 x 10^8 CFU/mL (OD_{600}: 0.2) was considered optimal and was employed in the co-infiltration experiment to investigate Eop1s' interaction with RPA1.

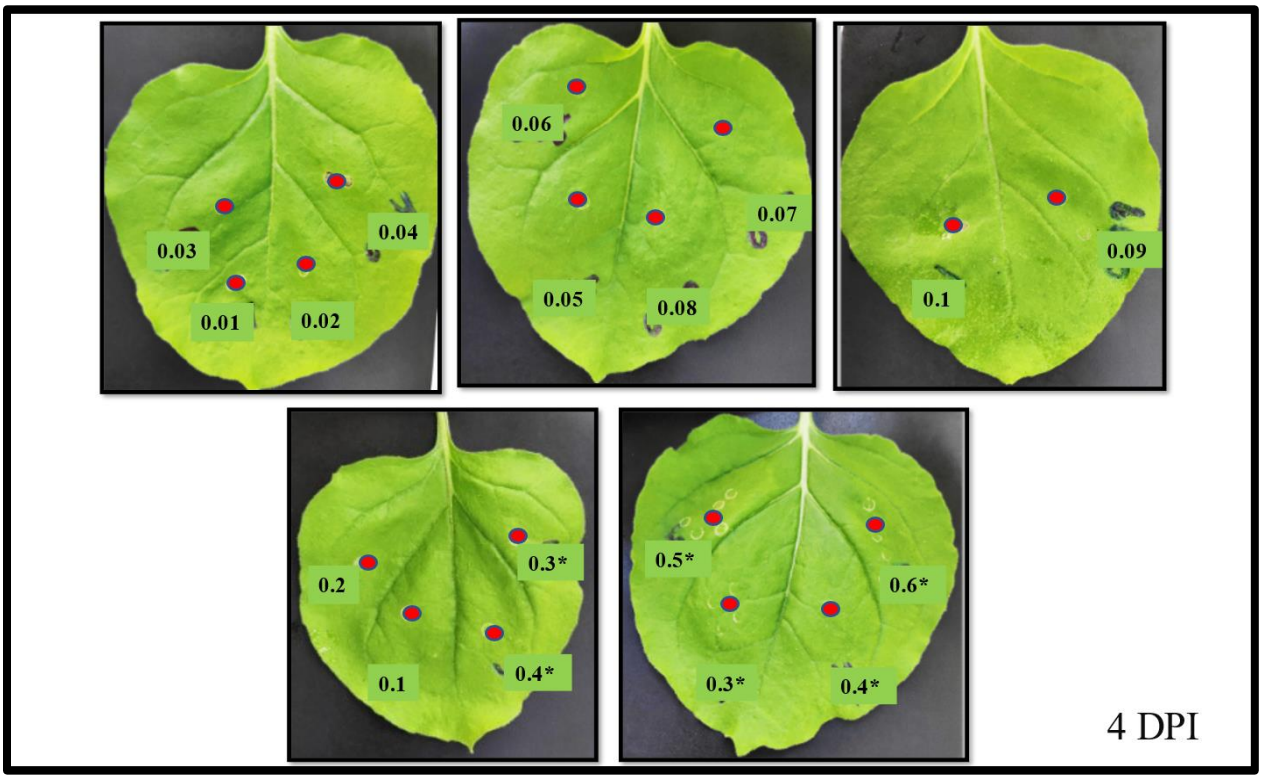

Figure 4.6: RPA1 autoimmunity analysis in *N. benthamiana*. The *Agrobacterium* cells harbouring the expression clones carrying the *RPA1* gene were infiltrated in 3-4 weeks old *N. benthamiana* leaves. The red dots on the leaf represent the infiltration sites, with the corresponding *Agrobacterium* concentration (OD_{600}) infiltrated annotated below it. The experiment was repeated three times with two replications. The OD_{600} marked with an asterisk (*) signifies the occurrence of occasional HR in the replications. The images were taken at 4 dpi.

4.3.2.2 RPA1 and Eop1s interaction analysis in *Nicotiana benthamiana* through co-infiltration

In the RPA1 autoimmunity analysis, it was found that *Agrobacterium* harbouring RPA1 expression clones infiltrated at a concentration of 1.6 x 10^8 CFU/mL (OD_{600}: 0.2) was the 'threshold level' of RPA1 that did not elicit an autoimmune response in the *N. benthamiana* plant. As a result, co-infiltration analysis with Eop1 variants was conducted at the RPA1 concentration of 1.6 x 10^8 CFU/mL (OD_{600}: 0.2). The screening strategy was based on the induction of HR phenotype upon infiltration of RPA1 with Eop1s in *N. benthamiana.* HopZ5 and RPA1 (RPA1 without the Eop1 effectors[49]) were employed as the positive and negative control for HR phenotype, respectively.

An infiltration pre-mix composed of *Agrobacterium* cells harbouring expression clones for RPA1 and Eop1 variants at the concentration of 1.6 x 10^8 CFU/mL (OD_{600}: 0.2) and 8.0 x 10^7 CFU/mL (OD_{600}: 0.1), respectively, suspended in 10 mL of infiltration buffer (10 mM MES and 10 mM MgCl2) were infiltrated in the leaves of 3-4 weeks old *N. benthamiana*. Interestingly, All the tested Eop1 variants triggered moderate HR when co-expressed with RPA1 (Figure 4.7). However, the replication exhibited high variation in which occasionally extreme HR and sometimes no visual HR was observed. Furthermore, HopZ5-induced HR was also observed to be weak.

[49] Infiltration of *Agrobacterium* harbouring the expression clones carrying the *RPA1* gene at OD_{600} of 0.2 did not trigger HR in *N. benthamiana*; consequently, it was used as a negative control for HR in the analysis.

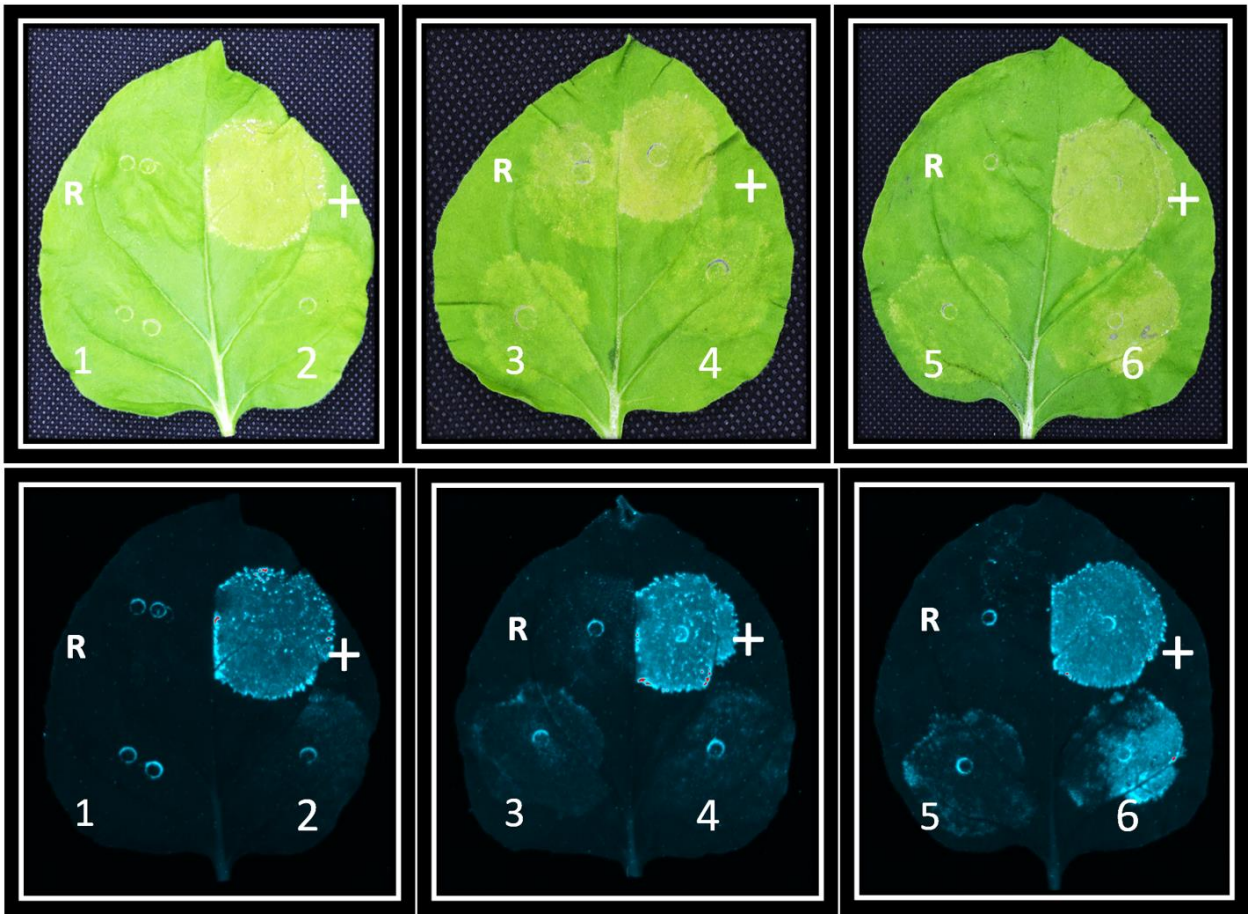

Figure 4.7: Co-infiltration assay of Eop1 variants (OD_{600}: 0.1) with RPA1 (OD_{600}: 0.2) in *Nicotiana benthamiana*. The same leaves were visualised in the ChemiDoc™ Gel Imaging System under the Pro-Q Emerald 488 (stain-free) (bottom panel); the luminous patch signifies HR-induced cell death in the leaves. The *Agrobacterium* harbouring the expression clones carrying the gene for RPA1 and Eop1 variants were co-infiltrated in 3-4 weeks old *N. benthamiana* leaves. The annotations are as follows: 'R' = RPA1 exclusively (negative control[50] for HR; OD_{600}: 0.2), '+' = HopZ5 (positive control for HR; OD_{600}: 0.1); 1 = Eop1: *E. pyrifoliae* str. *Ep*1/96; 2 = Eop1: *E. amylovora* str. *Ea*246; 3 = Eop1: *E. amylovora* str. *Ea*262; 4 = Eop1: *E. tasmaniensis* str. *Et*1/99; 5 = Eop1: *E. tracheiphila* str. MDcuke; 6 = Eop1: *P. vagans* str. C9-1*;* The images were taken at 4 dpi; The presented results exhibited variations in the replications conducted at different time points.

[50] Exclusive infiltration of *Agrobacterium* harbouring the 'RPA1' expression clones at OD_{600} of 0.2 did not trigger HR in *N. benthamiana* and was thus used as a negative control for HR in the analysis.

4.3.2.3 RPA1 and Eop1: *Ea*246 interaction analysis in *Nicotiana benthamiana* through sequential infiltration

Preliminary screening of Eop1s co-infiltration with RPA1 in *N. benthamiana* revealed that Eop1 variants induced mild HR when co-expressed with RPA1. However, the results were observed to vary during the replications. Therefore, an alternate strategy involving sequential infiltration was used to find the optimal and compatible concentration of RPA1 with Eop1 that would trigger HR in *N. benthamiana*. The experiment was conducted with Eop1: *Ea*246 as an archetype of Eop1s.

Different concentrations of *Agrobacterium* cells harbouring expression clones for RPA1 (OD_{600} ranging from 0.01 to 0.6) were first delivered in *N. benthamiana* leaves to promote abundant expression of RPA1 protein. Then, the *eop1: Ea246* harbouring *Agrobacterium* cells were successively infiltrated (OD_{600}: 0.1) at a two-day interval. In contrast to the co-infiltration assay, the HR was observed at much lower concentrations of supplemented RPA1, ranging from 8.0×10^6 CFU/mL to 3.2×10^7 CFU/mL ($OD_{600:}$ 0.01 to 0.04) (Figure 4.8), which was amusingly absent at higher concentrations. Nevertheless, the finding remained unreplaceable and varied among replications.

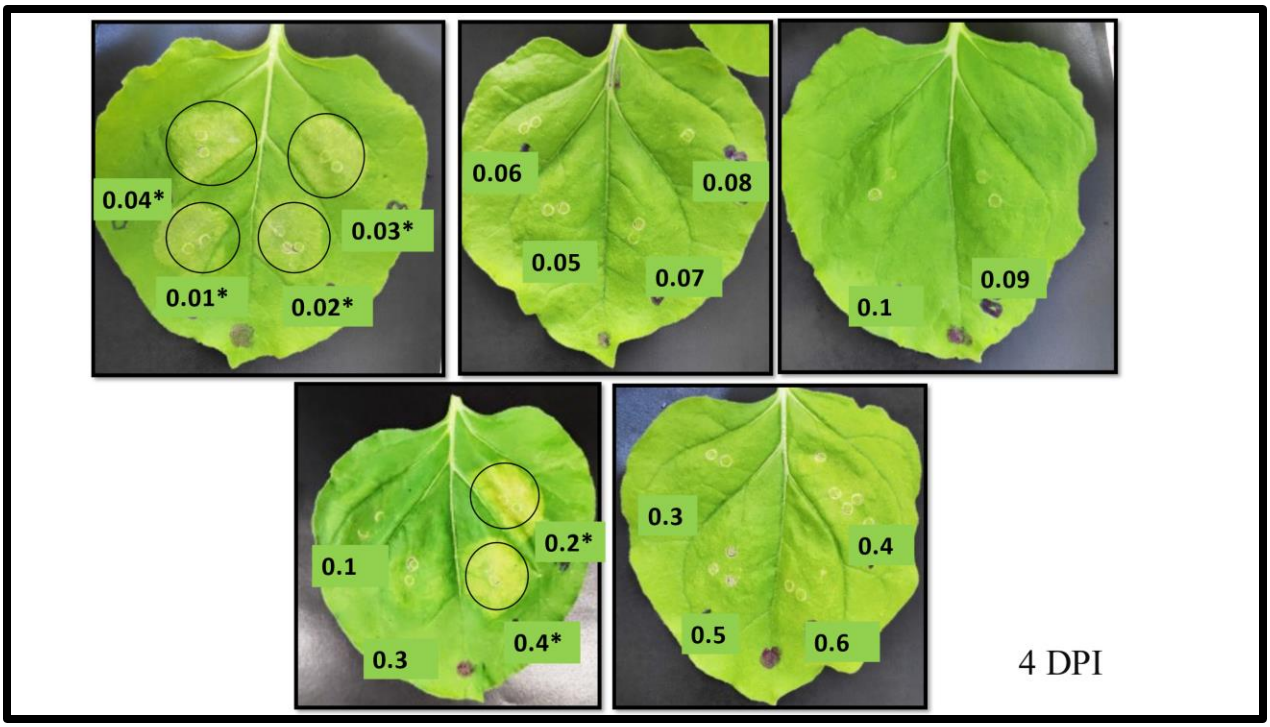

Figure 4.8: RPA1-Eop1: *Ea*246 interaction analysis via sequential infiltration in *Nicotiana benthamiana*. The annotations in the figures correspond to the concentration (OD_{600}) of *Agrobacterium* harbouring the expression clones carrying the *RPA1* gene, administered in the *N. benthamiana* leaves 2 days prior to the infiltration of *Agrobacterium* carrying *eop1*: *Ea*246 expression clones (OD_{600}: 0.1). The encircled regions represent observed HR. The presented results were validated by repeating the experiment three times with three replications; however, the OD_{600} annotations marked with an asterisk (*) signify that the presented phenotype was not reproducible during the replications. The images were taken at 4 dpi.

4.3.2.4 Environmentally stressed *N. benthamiana* plants potentially failed to trigger a replicable immune response

The positive control for HR in *N. benthamiana*, HopZ5, was examined to determine the reason for inconsistency in the results. It was discovered that HopZ5 could not induce a robust HR even at a concentration of 2.4 x 10^8 CFU/mL (OD_{600}: 0.3) after 6 dpi (Figure 4.9). This observed phenomenon starkly contrasted with its usual response of strong HR characterised by complete cell death of the infiltrated region at 2 dpi (Jayaraman et al., 2017). Thus, it was concluded that the *N. benthamiana* plants employed in the study were already stressed and were not used for further

experiments for interaction analysis. Furthermore, efforts were made to grow more stable *N. benthamiana* plants by changing the environment. However, no effect on the obtained result was observed. Consequently, the experimental strategy of investigating RPA1 involvement in Eop1-induced HR via *RPA1* supplementation in *N. benthamiana* was changed to a reverse genetic technique of silencing the resident *RPA1* in *N. tabacum*.

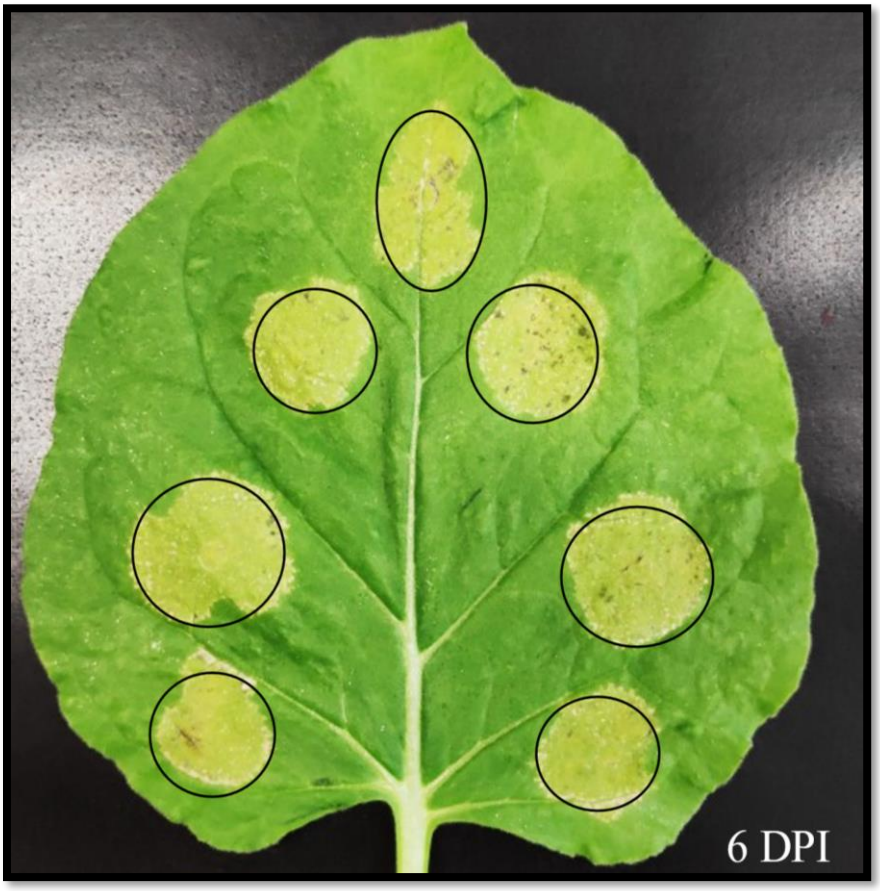

Figure 4.9: Analysis of HopZ5-induced HR in *Nicotiana benthamiana*. The *Agrobacterium* cells harbouring the *hopZ5* gene expression clones were infiltrated at the OD_{600} of 0.3. The presented result was validated by repeating the experiment 3 times with similar results. The encircled regions represent HR-induced cell death. The image was taken at 6 dpi.

4.3.3 Analysis of RPA1 involvement in molecular recognition of Eop1 variants in *Nicotiana tabacum*

In contrast to the previous strategy, which employed a forward genetics approach, the following procedure entails a reverse genetics method to investigate the involvement of RPA1 R-protein in the Eop1-triggered HR in *N. tabacum*. The fundamental notion behind using a reverse genetics approach was that the Eop1 effectors-induced HR would be significantly reduced upon silencing the implicated R-protein. Consequently, the screening strategy was based on the reduction of HR in *N. tabacum* upon silencing RPA1 R-protein in the presence of an Eop1 effector. For *RPA1* silencing, an RNAi-inducing hairpin construct (hp*RPA1*) targeting the 3'-untranslated region (UTR) of *RPA1*, cloned into a hairpin-producing expression vector: pTKO2 was used in the study[51].

4.3.3.1 Analysis of RPA1 involvement in Eop1 variants induced HR via RPA1 silencing in *Nicotiana tabacum* through co-infiltration

An infiltration pre-mix comprised of *Agrobacterium* cells harbouring expression clones for the Eop1 variant (separately) and *RPA1* hairpin (pTKO2: hp*RPA1*) at the concentration of $8.0x10^7$ CFU/mL ($OD_{600:}$ 0.1) and 1.6 x 10^8 CFU/mL ($OD_{600:}$ 0.2), respectively, suspended in 10 mL of infiltration buffer (10 mM MES and 10 mM MgCl2) was infiltrated in the 3-4 weeks old *N. tabacum* plant leaves. Contrary to anticipation, all the Eop1 variants still induced HR (Figure 4.10) in the same manner as observed and reported in the preliminary HR assay of Eop1s in section 2.3.3.1.

[51] The *RPA1* hairpin, cloned in the silencing vector pTKO2, i.e., pTKO2: hp*RPA1*, was genially provided by Minsoo Yoon and had been used in Yoon and Rikkerink (2020).

Upon further analysis of the work conducted by Yoon & Rikkerink on RPA1 (Yoon & Rikkerink, 2020), it was deduced that simultaneous infiltration and expression of the HR-inducing effector Eop1 and RPA1 silencing construct (hp*RPA1*) did not allow enough time for the hairpin to silence the *RPA1* gene effectively. Additional evidence supporting this hypothesis was the induction of a full-fledged HR by HopZ3*psa*_V1 in the presence of the silencing construct 'hp*RPA1*' (positive control for silencing), which contrasted the 'unpublished' result reported by Yoon & Rikkerink.

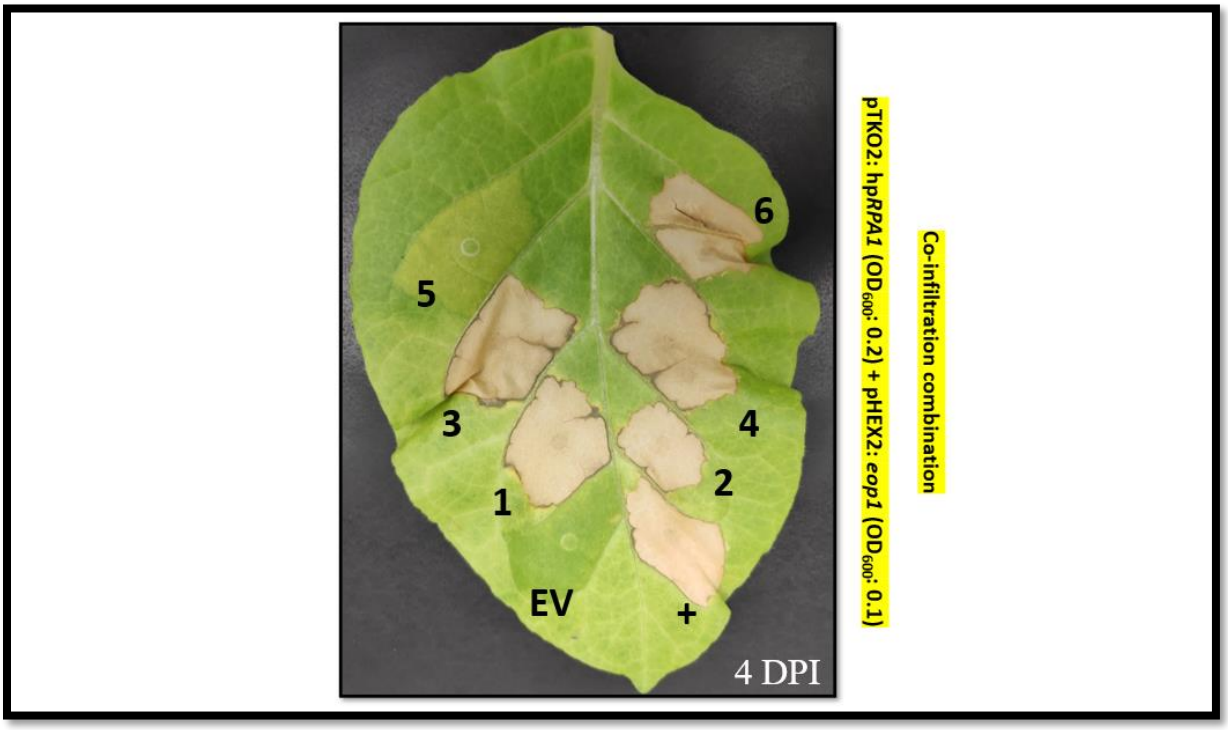

Figure 4.10: Analysis of RPA1 involvement in Eop1-induced HR via co-infiltration. The infiltrated *Agrobacterium* co-infiltration combination is highlighted on the right side of the leaf's image. The annotations are: EV = pHEX2: Empty Vector (negative control for HR), '+' = HopZ3*psa*_V1 in combination with pTKO2: hp*RPA1* (positive control for hairpin-induced silencing), 1 = Eop1: *E. pyrifoliae* str. *Ep*1/96; 2 = Eop1: *E. amylovora* str. *Ea*246; 3 = Eop1: *E. amylovora* str. *Ea*262; 4 = Eop1: *E. tasmaniensis* str. *Et*1/99; 5 = Eop1: *E. tracheiphila* str. MDcuke; 6 = Eop1: *P. vagans str. C9-1*; The experiment was repeated thrice with three replications with similar results. The image was taken at 4 dpi.

4.3.3.2 *Nicotiana tabacum* leaves pre-exposed to the *Agrobacterium* cells fail to trigger HR upon delivering HR-eliciting effectors

The previous experiment discovered that co-expression of the RPA1 silencing construct (hp*RPA1*) with Eop1s via *Agrobacterium* in *N. tabacum* still elicits HR (as described in the above section 4.3.3.2). Furthermore, it was deduced that simultaneous delivery and expression of the effector and silencing gene construct was ineffective as the effector triggers an HR before the silencing could be effective. Therefore, to address this problem, the approach of sequential infiltration was adopted. However, it had been reported that *N. tabacum* leaves already challenged with *Agrobacterium* did not exhibit HR upon delivering the HR-eliciting effector (Klement et al., 2003; Rico et al., 2010; Szatmari et al., 2014; Yoon & Rikkerink, 2020). Consequently, considering all the aforementioned factors, the sequential infiltration experiment was carried out to determine whether the involvement of RPA1 in Eop1-triggered HR can be investigated through sequential infiltration in *N. tabacum* or whether pre-exposure of the *N. tabacum* leaf with *Agrobacterium* would result in HR loss, as previously reported.

Agrobacterium cells harbouring empty expression vectors, i.e., 'pHEX2: Empty Vector' and 'pTKO2: Empty Vector' at the concentration of 1.6 x 10^8 CFU/mL (OD_{600}: 0.2) suspended separately in 10 mL infiltration buffer (10 mM MES and 10 mM MgCl2) were first infiltrated in two separate leaves. The *Agrobacterium* cells harbouring gene for the Eop1 variant were delivered at two days intervals at the concentration of 1.6 x 10^8 CFU/mL (OD_{600}: 0.2).

Interestingly, in parallel with the results reported in other research (Klement et al., 2003; Rico et al., 2010; Szatmari et al., 2014; Yoon & Rikkerink, 2020), none of the tested Eop1s elicited HR upon infiltration in the *N. tabacum* leaves preexposed with *Agrobacterium* (Figure 4.11). Thus, it was deduced that the co-expression of *RPA1* hairpin and *eop1* via co-infiltration is the only

approach that can be employed in *Nicotiana tabacum* to study RPA1 interaction with Eop1. However, as observed in the preliminary analysis, co-expression of *eop1* with the *RPA1* silencing construct jeopardises the screening since the rapidly responding R-protein triggers HR before effective silencing (section 4.3.3.1). Thus, to counter this problem, a strategy was devised that employed 'ethylene glycol-bis (β-aminoethyl ether)-N,N,N′,N′-tetraacetic acid' (EGTA) to slow down the rapid immune response.

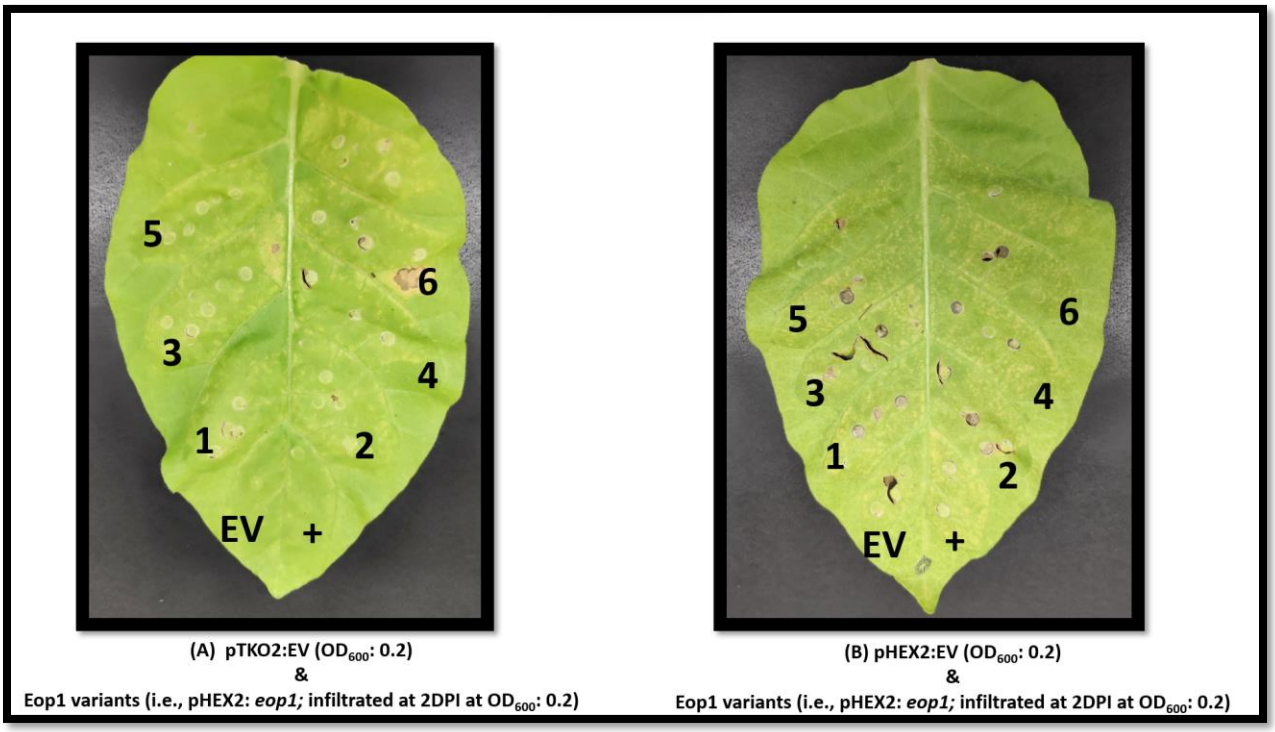

Figure 4.11: Analysis of Eop1 variants HR elicitation activity in *Nicotiana tabacum* leaves pre-exposed to *Agrobacterium*. The expression clones administered via *Agrobacterium* in the leaves are annotated below the images. The annotations are as follows: EV = Empty Vectors (negative control for HR); '+' = HopZ3*psa*_V1 (positive control for HR); 1 = Eop1: *E. pyrifoliae* str. Ep1/96; 2 = Eop1: *E. amylovora* str. Ea246; 3 = Eop1: *E. amylovora* str. Ea262; 4 = Eop1: *E. tasmaniensis* str. Et1/99; 5 = Eop1: *E. tracheiphila* str. MDcuke; 6 = Eop1: *Pantoea vagans* str. C9-1. The experiment was repeated thrice with three replications with similar results. The images were taken at 4 dpi.

4.3.4 EGTA differential analysis in *Nicotiana tabacum*

From the experiments conducted in section 4.3.3.1, it was deduced that Eop1 variants triggered HR before the *RPA1* hairpin-induced silencing could be effective. As a result, an intervention was considered necessary to slow down the effector-triggered immune response and provide some time for effective silencing. Therefore, the chemical 'EGTA', which had been reported to delay the HR (Yoon & Rikkerink, 2020), was employed in the experiments.

Yoon & Rikkerink (2020) utilised a 5 mM concentration of EGTA to delay the RPA1-mediated immune response in *N. tabacum*; however, the effector under investigation in the study was different. Therefore, the effect of EGTA at two different concentrations (10 mM and 5 mM) was examined separately under the Eop1: *Ea*246 effector-mediated HR in *N. tabacum.*

Different concentrations of *Agrobacterium* (OD_{600} range from 0.02 to 0.1), harbouring expression clones for Eop1: *Ea*246, suspended in 10 mL infiltration buffer composed of 5 mM and 10 mM EGTA separately along with 10 mM MgCl2, were infiltrated in 3-4 weeks old *N. tabacum* leaves. The *N. tabacum* leaves infiltrated with *eop1: Ea246* harbouring *Agrobacterium* cells in 10 mM EGTA infiltration buffer (Figure 4.12) started to exhibit drooping and shrivelling symptoms 4-5 hours post-infiltration, which lasted the duration of the experiment. Interestingly, cell necrosis in the tissues of non-infiltrated and Empty Vector (EV) infiltrated leaf regions was also observed (Figure 4.12). In addition, hindrance in the Eop1: *Ea*246 induced HR was also observed, which resulted in mosaic pattern-like HR cell death on the leaf 36-42 hours post infiltration.

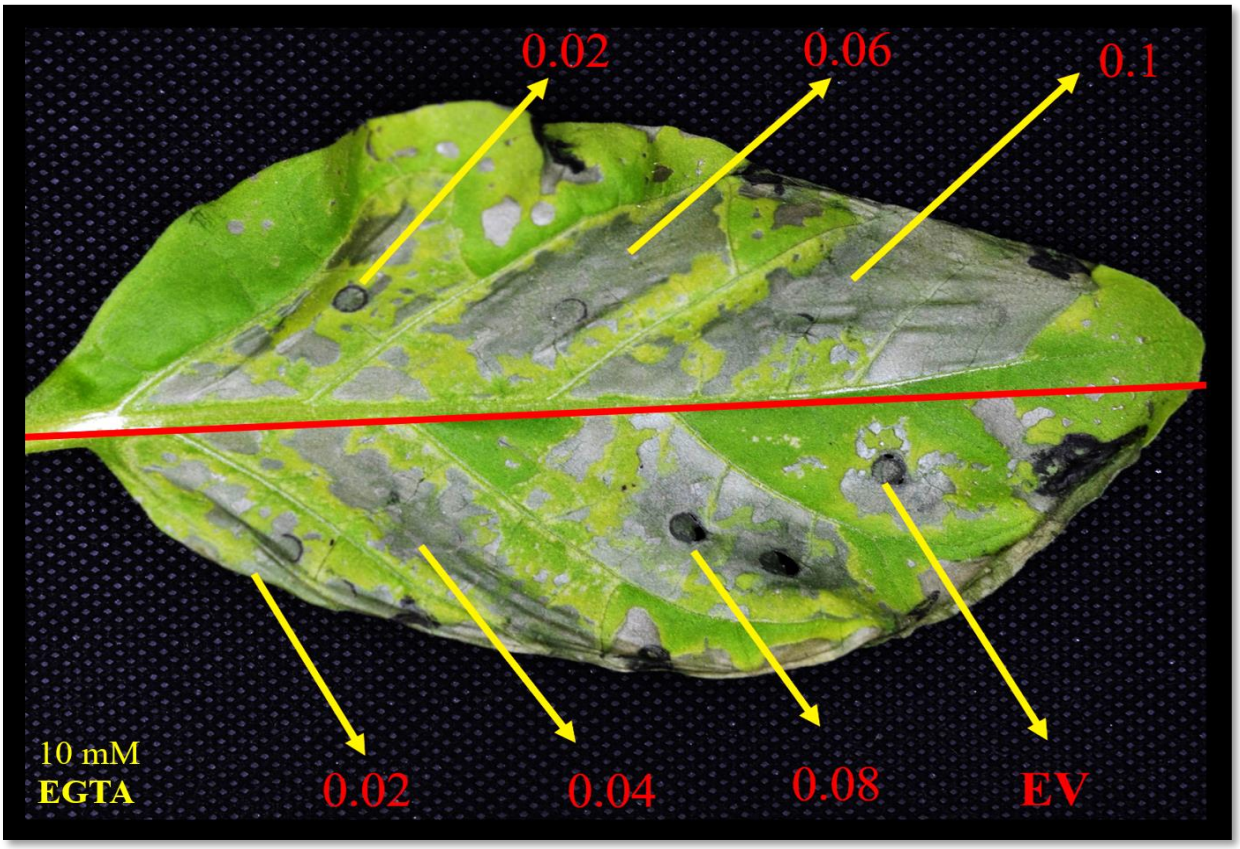

Figure 4.12: Analysis of 10 mM EGTA effect on *Nicotiana tabacum* leaves. The effect was assessed by infiltrating different concentrations of *Agrobacterium* harbouring the Eop1: *Ea*246 expression clones (OD_{600} range from 0.02 to 0.1) with 10 mM EGTA infiltration buffer. The numeric annotations in the image correspond to the *Agrobacterium* concentration (OD_{600}) administered in the corresponding leaf segment. The Empty Vector (EV) was employed as a negative control for HR and infiltrated at the OD_{600}: 0.1 with 10 mM EGTA. The experiment was repeated thrice with similar results. The image was taken at 4 dpi.

In contrast, the *N. tabacum* leaves infiltrated with *eop1: Ea246* harbouring *Agrobacterium* cells in 5 mM EGTA infiltration buffer (Figure 4.13) exhibited mild drooping and shrivelling symptoms, with no hindrance in the occurrence of HR. Furthermore, leaf regions infiltrated with *Agrobacterium* cells (harbouring *eop1: Ea246*) at the concentration of 8.0 x 10^7 CFU/mL (OD_{600}: 0.1) and 4.0 x 10^7 CFU/mL (OD_{600}: 0.05) triggered HR at 36-42 hpi, as opposed to 24 hpi when infiltrated with MES buffer (see section 2.3.3.1). Therefore, considering the results mentioned above, EGTA at 5 mM concentration was chosen for subsequent co-infiltration experiments.

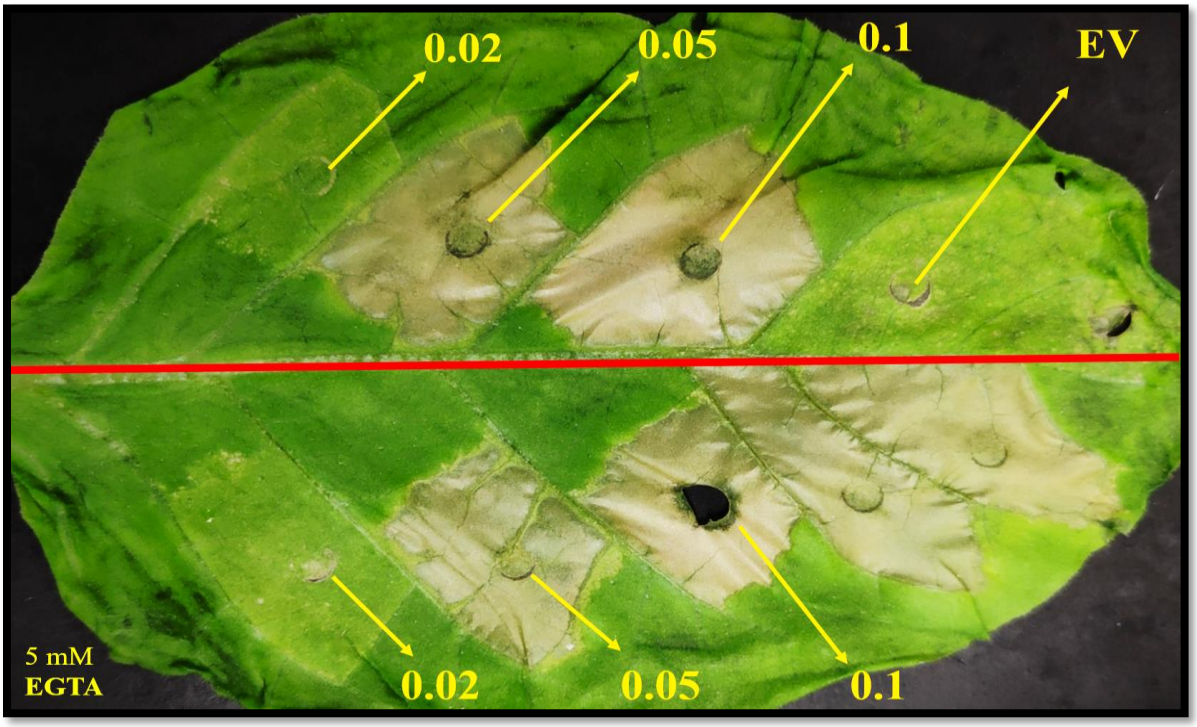

Figure 4.13: Analysis of 5 mM EGTA effect on *Nicotiana tabacum* leaves. The effect was evaluated by infiltrating different concentrations of *Agrobacterium* harbouring the Eop1: *Ea*246 expression clones (OD_{600}: 0.1, 0.05 and 0.02) with 5 mM EGTA buffer. The numeric annotations in the image correspond to the *Agrobacterium* concentration (OD_{600}) administered in the corresponding leaf segment. The Empty Vector (EV), acting as a negative control for HR, was infiltrated at the OD_{600}: 0.1, with 5 mM EGTA. The image was taken at 4 dpi. The presented result was validated by repeating the experiment twice with two replications with similar results.

4.3.5 Testing of the developed 'three-component co-infiltration system' in *N. tabacum*

Experiments conducted in section 4.3.3 indicated that co-expression of hp*RPA1* and *eop1* via co-infiltration is the only method that can be employed to test the RPA1 involvement in Eop1-induced HR in *Nicotiana tabacum*. However, EGTA intervention was inferred to be necessary for effective silencing to occur prior to Eop1-induced HR for testing RPA1 involvement. Furthermore, after testing two different EGTA concentrations (5 and 10 mM), it was observed that 5 mM concentration is ideal for the experiments as a higher concentration of EGTA (10 mM) tends to have necrogenic effects on the treated leaf and could tamper with the results (refer to section 4.3.4). Therefore, considering the results from the preceding experiments, an *Agrobacterium*-mediated 'three-component co-infiltration system' in combination with EGTA (5 mM) was developed ('conceptualisation' and 'method' explained in section 4.2.3 and Figure 4.2). The developed system was designed to determine the involvement of various proteins in the molecular recognition of Eop1s in *N. tabacum*. The foundation of the 'three-component co-infiltration system' relies on silencing the expression of the protein under investigation (possibly involved in HR) using hairpin-induced RNAi silencing and screening for HR reduction.

To find optimal conditions to investigate the involvement of RPA1 in Eop1-triggered HR, the co-infiltration combination system, developed as described in section 4.2.3, was first tested separately in the MES and EGTA buffer with different concentrations of *Agrobacterium* harbouring expression clones for Eop1: *Ea*246 (archetypal Eop1 used in the testing of the developed system). In addition, the efficacy of the proposed co-infiltration system was also tested using Empty Vector, and *GUS* construct[52], with tested combinations and their corresponding

[52] Testing the co-infiltration combinations with expression vectors containing the *'GUS'* gene was crucial because it produced the 'GUS' protein and provided an actual protein expression paradigm in plants, which was lacking in the

Agrobacterium concentrations stated as follows: (1) pHEX2: EV (OD_{600}: 0.4) + pTKO2: EV (OD_{600}: 0.4) + Eop1: *Ea*246 (OD_{600}: 0.1, 0.05, 0.01, separately), and (2) pHEX2: *GUS* (OD_{600}: 0.4) + pTKO2: *GUS* (OD_{600}: 0.4) + pHEX2: *eop1: Ea246* (OD_{600}: 0.1, 0.05, 0.01, separately). (See footnote '53' for OD_{600} to CFU/mL conversion values).

Upon infiltration of the 'three-component co-infiltration combination system' with EGTA (Figure 4.14) and MES (Figure 4.15) infiltration buffers in 3-4 weeks old *Nicotiana tabacum* plant leaves, it was found that the combinations carrying *Agrobacterium* cells (harbouring *eop1: Ea246*) at OD_{600}: 0.1 and 0.05 concentration (0.05 not tested in the MES) in the premix triggered strong HR. However, the leaf region infiltrated with the combinations carrying *Agrobacterium* cells at OD_{600}: 0.01 concentration induced weak HR. The occurrence of the weak HR was not surprising as the same phenotype was observed when *Agrobacterium* carrying *eop1: Ea246* was solely infiltrated at the concentration of 1.6 x 10^7 CFU/mL (OD_{600}: 0.02) concentration in *Nicotiana tabacum* (Figure 4.13). Interestingly, the tested co-infiltration combination in the MES buffer triggered HR at 24-30 hpi, whereas the co-infiltration combination in EGTA triggered HR at 36-40 hpi, thus providing 12-18 hours extra for effective silencing to occur.

'empty' expression vectors co-infiltration combinations tests. Additionally, this strategy enables testing the impact of the hairpin-induced silencing of the GUS protein via X-Gluc staining (5-bromo-4-chloro-3-indolyl glucuronide).

[53] Approx. OD_{600} to CFU/mL values: (0.4 = 3.2 x 10^8 CFU/mL; 0.1 = 8.0 x 10^7 CFU/mL; 0.05 = 4.0 x 10^7 CFU/mL; 0.01 = 8.0 x 10^6 CFU/mL)

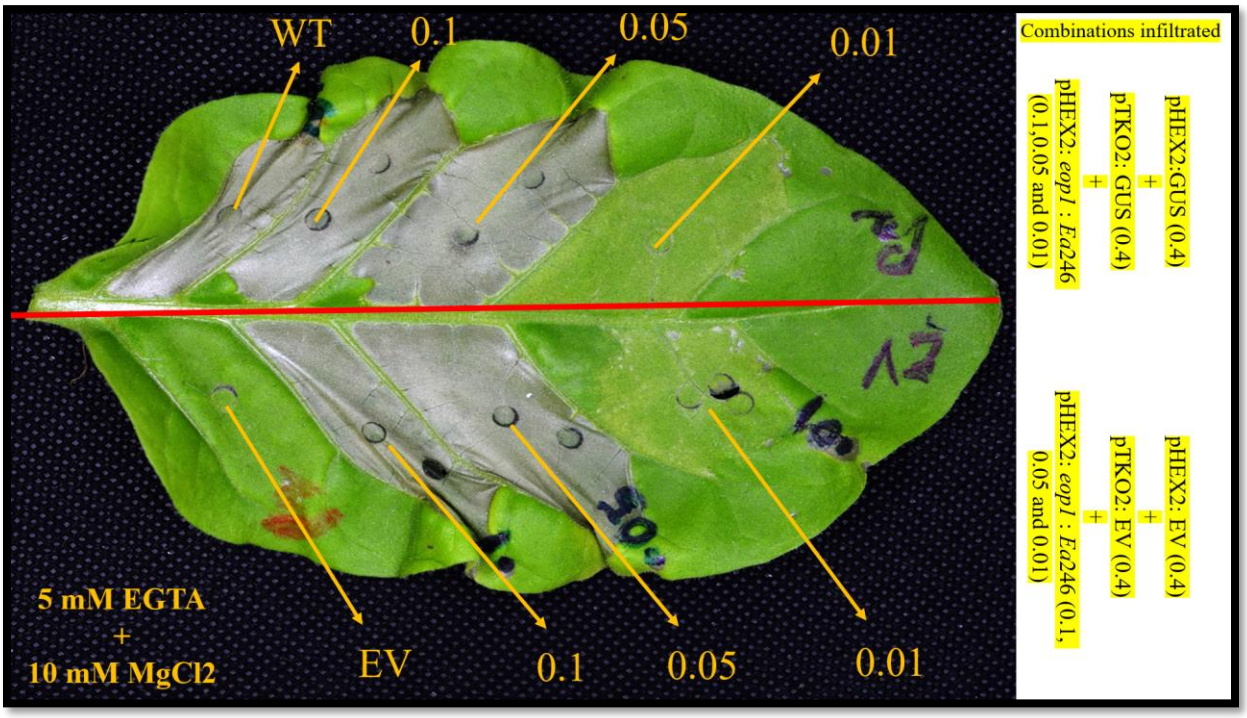

Figure 4.14: Testing of the three-component co-infiltration combination system with EGTA buffer. The co-infiltration premixes administered in the leaf, along with the *Agrobacterium* concentration (OD_{600}) and its corresponding expression clones, are described and highlighted on the right of the image. The annotations are as follows: WT = Wildtype (Eop1: *Ea*246, infiltrated at the OD_{600} of 0.1 with EGTA buffer; employed as a positive control for HR), EV = Empty Vector (pHEX2: EV, infiltrated at the OD_{600} of 0.1 with EGTA buffer; employed as a negative control for HR); The numeric annotations in the image correspond to the concentration of Eop1: *Ea*246 (in OD_{600}) administered through the co-infiltration premix combination in the indicated leaf segment. The image was taken at 4 dpi. The presented results were validated by repeating the experiment twice with three replications with similar results.

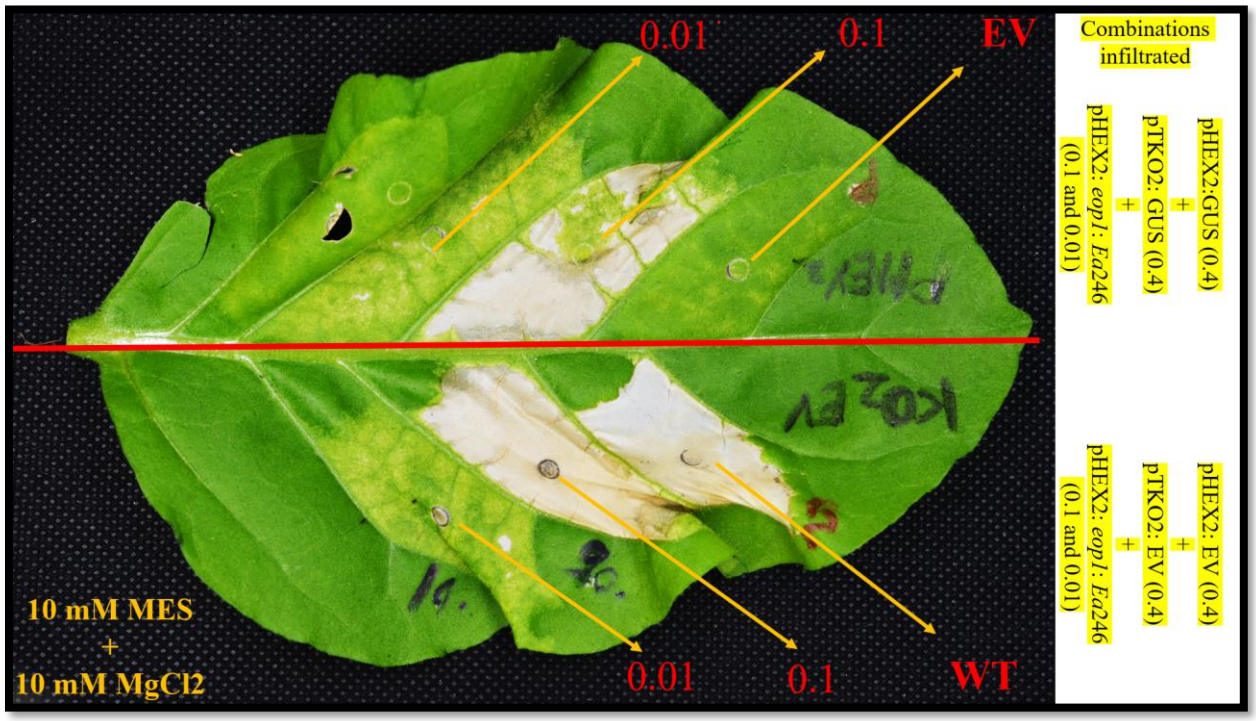

Figure 4.15: Testing of the three-component co-infiltration combination system with MES buffer. The co-infiltration premixes administered in the leaf, along with the *Agrobacterium* concentration (OD_{600}) and its corresponding expression clones, are described and highlighted on the right of the image. The annotations are as follows: WT = Wildtype (Eop1: *Ea*246, infiltrated at the OD_{600} of 0.1 with MES buffer; employed as a positive control for HR), EV = Empty Vector (pHEX2: EV, infiltrated at the OD_{600} of 0.1 with MES buffer; employed as a negative control for HR); The numeric annotations in the image correspond to the concentration of Eop1: *Ea*246 (in OD_{600}) administered through the co-infiltration premix combination in the indicated leaf segment. The image was taken at 4 dpi. The presented results were validated by repeating the experiment twice with three replications.

4.3.6 Eop1-RPA1 interaction analysis via 'three-component co-infiltration system' in combination with EGTA in *N. tabacum*

The co-infiltration premix system developed and tested as described in sections 4.2.3 and 4.3.5, respectively, was adopted to investigate the involvement of RPA1 in the HR triggered by Eop1 variants in the non-host plant *Nicotiana tabacum*. Furthermore, EGTA at a concentration of 5 mM was also employed to delay the HR for the RPA1 hairpin-induced silencing to be effective.

A premix composed of *Agrobacterium* cells harbouring pHEX2: *GUS* (OD_{600}: 0.4), pTKO2: hp*RPA1* (OD_{600}: 0.4) and pHEX2: *eop1* (OD_{600}: 0.1) suspended in 10 mL of infiltration buffer (5 mM EGTA and 10 mM MgCl2) was infiltrated in the leaves of 3-4 weeks old *Nicotiana tabacum* plants. During the preliminary investigation, it was found that the co-infiltration combinations were effective, as an absence of HR was observed for all the tested Eop1s, particularly when tested in the youngest and fully-expanded leaf of the plant. However, a high degree of variation was observed within the replicate and among the replications, as presented in Figure 4.16.

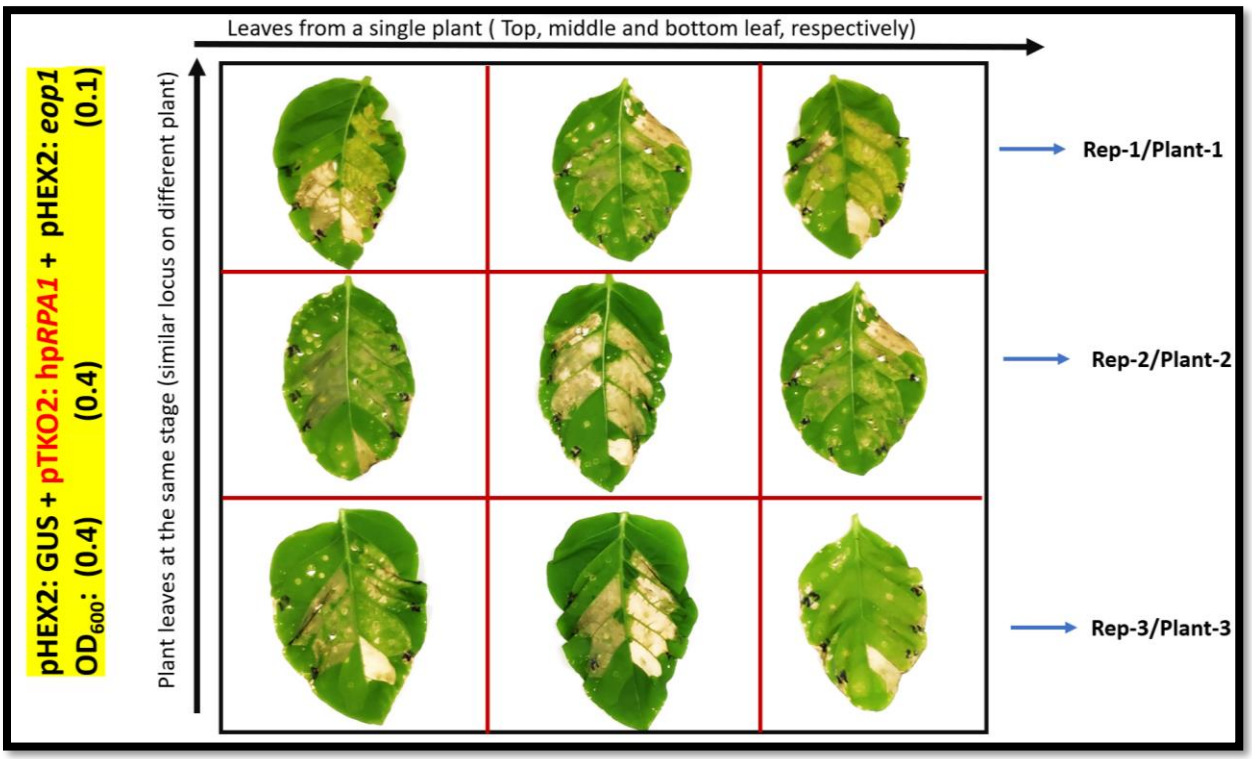

Figure 4.16: Preliminary result from Eop1-RPA1 interaction analysis. The interaction was tested by employing the three-component co-infiltration combination system (as described in Figure 4.2; sub-figure 2) with EGTA (5 mM) in *Nicotiana tabacum*. The co-infiltration premixes administered in the leaves, along with the *Agrobacterium* concentration (OD_{600}) and its corresponding expression clones, are described and highlighted on the left of the image. The Eop1 variants were infiltrated in the same patterns as illustrated in Figure 4.17. The experiment was replicated thrice with similar results. The images were taken at 4 dpi; (Note: The figure attempts to represent the variation observed within the replicate and among the replications).

To mitigate the observed high variation, the uppermost and youngest leaf of the tobacco plants were used for the co-infiltration analysis (i.e., one leaf per plant, usually 3rd leaf from the apical bud), and only two Eop1 variants were tested within one leaf along with controls for HR phenotype. Furthermore, positive controls for the 'Eop1 variants induced HR' (Figure 4.17; sub-figure 'A') and the employed 'three-component co-infiltration combination'(i.e., pHEX2: *GUS* (OD_{600}: 0.4) + pTKO2: *GUS* (OD_{600}: 0.4) + pHEX2: *eop1* (OD_{600}: 0.1)), in an infiltration buffer composed of 5 mM EGTA and 10 mM MgCl2, were also tested (Figure 4.17; sub-figure 'B').

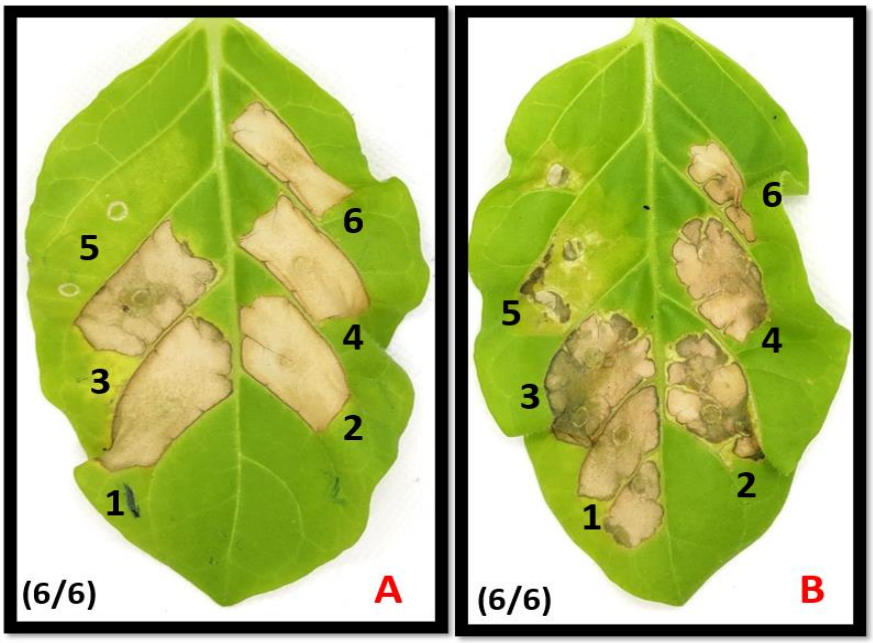

Figure 4.17: Positive controls employed in Eop1-RPA1 interaction analysis in *Nicotiana tabacum*. (A) Eop1 variants induced HR in *Nicotiana tabacum* were employed as a positive control for Eop1 activity; Eop1 variants were administered at the OD_{600}: 0.1. (B) Control for the three-component co-infiltration combination system (the administered *Agrobacterium* co-infiltration premix denoted by its corresponding expression clones is as follows: pHEX2: *GUS* (OD_{600}: 0.4) + pTKO2: *GUS* (OD_{600}: 0.4) + pHEX2: *eop1* (OD_{600}: 0.1)). The annotations are as follows: 1 = Eop1: *E. pyrifoliae* str. Ep1/96; 2 = Eop1: *E. amylovora* str. Ea246; 3 = Eop1: *E. amylovora* str. Ea262; 4 = Eop1: *E. tasmaniensis* str. Et1/99; 5 = Eop1: *E. tracheiphila* str. MDcuke; 6 = Eop1: *Pantoea vagans* str. C9-1. The ratio (6/6) in the figures indicates the number of leaves with the presented phenotype/total number of conducted replications. The images were taken at 4 dpi.

In the Eop1-RPA1 interaction analysis, tested through the 'three-component co-infiltration combination': pHEX2: *GUS* (OD_{600}: 0.4) + pTKO2: hp*RPA1* (OD_{600}: 0.4) + pHEX2: *eop1* (OD_{600}: 0.1), it was found that silencing *RPA1* gene via 'hairpin-induced silencing' results in a significant reduction in the HR induced by Eop1 variants (Figure 4.18), which contrast the full-fledged HR triggered by the Eop1 variants tested in the HR assay in section 2.3.3. Furthermore, in the replications conducted at separate time-points[54], it was observed that silencing was 'occasionally' obstructed, which resulted in partial HR, as presented in (Figure 4.18; sub-figure '1'). Moreover, upon *RPA1* silencing, the phenotype observed in the leaf segments infiltrated with the co-infiltration combination carrying HR-inducing *eop1*s was absent in the leaf region infiltrated with *eop1* from *Erwinia tracheiphila* (Figure 4.18; sub-figure '5') as it did not trigger HR in the first place. As a result, the contrast in HR phenotype observed between Eop1 from *Erwinia tracheiphila* and other Eop1 variants in *N. tabacum* also served as a model for comparing the effect of *RPA1* silencing.

[54] The phrase "separate time-point" in the text signifies the replications conducted at different moments in time, usually after 7 days interval, to account for the probable variation.

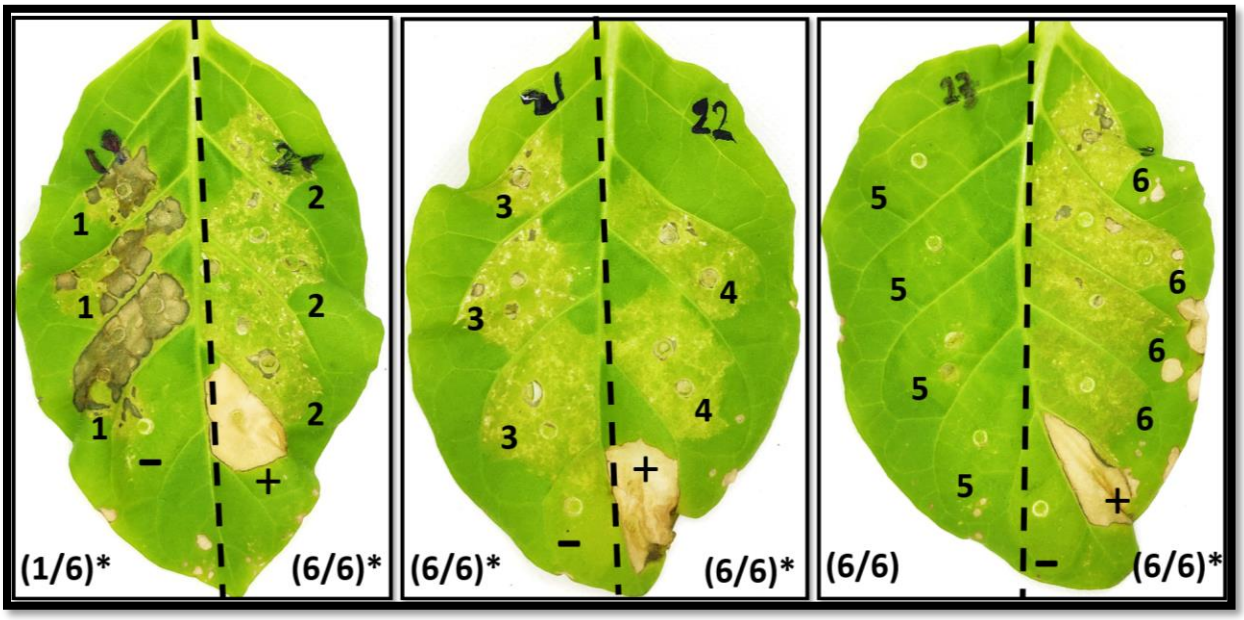

Figure 4.18: Eop1-RPA1 interaction analysis, tested via *RPA1* silencing by employing a 'three-component co-infiltration combination' system. The administered *Agrobacterium* co-infiltration premix denoted by its corresponding expression clones is as follows: pHEX2: *GUS* (OD_{600}: 0.4) + pTKO2: hp*RPA1* (OD_{600}: 0.4) + pHEX2: *eop1* (OD_{600}: 0.1). The annotations are as follows: '-' = pHEX2: Empty Vector (negative control for HR; OD_{600}: 0.1); '+' = Eop1: Ea246 (positive control for HR; OD_{600}: 0.1); 1 = Eop1: *E. pyrifoliae* str. Ep1/96; 2 = Eop1: *E. amylovora* str. Ea246; 3 = Eop1: *E. amylovora* str. Ea262; 4 = Eop1: *E. tasmaniensis* str. Et1/99; 5 = Eop1: *E. tracheiphila* str. MDcuke; 6 = Eop1: *Pantoea vagans* str. C9-1. The presented results were validated by repeating the experiment thrice with 6 replications each. The ratio (6/6) in the figures indicates the number of leaves with the presented phenotype/total number of conducted replications. The images were taken at 4 dpi. (Note: the ratios marked with an asterisk (*) represent the occasional occurrence of the opposite of the presented phenotype (i.e., HR) in replications conducted at different time points).

4.3.7 Eop1-RIN4 interaction analysis via 'three-component co-infiltration system' in combination with EGTA in *N. tabacum*

The previous experiment discovered that silencing *RPA1* via hairpin-induced silencing results in a significant reduction in the HR induced by Eop1 variants. Similarly, to investigate the involvement of *Nicotiana tabacum* RIN4 (*Nt*RIN4) in the HR triggered by Eop1 variants, the *NtRIN4* gene was silenced using a *Nicotiana benthamiana* RIN4 (*Nb*RIN4) hairpin construct (hp-*NbRIN4*) cloned into silencing vector[55] pTKO2 (pTKO2: hp-*NbRIN4*). The hp-*NbRIN4* was designed to silence the *NbRIN4* gene; however, *NtRIN4* shared 98.1% sequence identity[56] with *NbRIN4* and was inferred to be ideal for utilisation in *NtRIN4* silencing. The screening strategy was based on the reduction in HR upon silencing of *NtRIN4* in the presence of the Eop1 effector.

An infiltration premix composed of *Agrobacterium* cells carrying expression clones: pHEX2: *eop1* (OD_{600}: 0.1), pTKO2: hp-*NbRIN4* (OD_{600}: 0.4) and pHEX2: *GUS* (OD_{600}: 0.4), suspended in 10 mL of infiltration buffer (5 mM EGTA and 10 mM MgCl2) was infiltrated in the leaves of 3-4 weeks old *N. tabacum* plants. Interestingly, the variation within and among the replications, as observed and described in the Eop1-RPA1 interaction analysis (Figure 4.16), was also observed in the RIN4 involvement analysis (Supplementary Figure C4S1), which was mitigated using the same strategy of using the youngest and fully expanded leaf in the plant. Interestingly, in the Eop1-RIN4 interaction analysis, it was found that similar to the Eop1-RPA1 interaction analysis, silencing of *RIN4* also results in a significant reduction in the HR triggered by the Eop1 variants in *Nicotiana tabacum* (Figure 4.19).

[55] *NbRIN4* hairpin construct, cloned into silencing expression vector pTKO2, i.e., pTKO2: hp-*NbRIN4,* was cordially provided by Minsoo Yoon.

[56] Nucleotide sequence identity between *NtRIN4* (XM_016608203.1) & *NbRIN4* (APY20266.1) sequences was analysed through nucleotide sequence alignment.

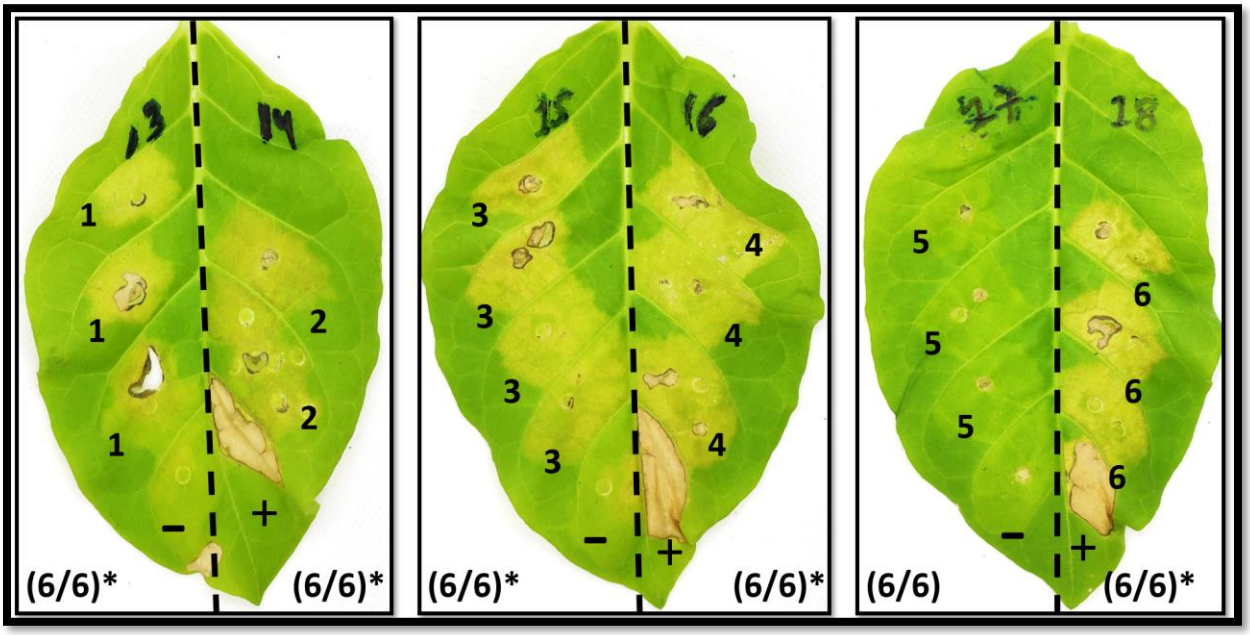

Figure 4.19: Eop1–RIN4 interaction analysis, tested via *RIN4* silencing by employing through three-component co-infiltration combination system. The administered *Agrobacterium* co-infiltration premix denoted by its corresponding expression clones is as follows: pHEX2: *GUS* (OD_{600}: 0.4) + pTKO2: hp-*NbRIN4* (OD_{600}: 0.4) + pHEX2: *eop1* (OD_{600}: 0.1). The annotations are as follows: '-' = pHEX2: Empty Vector (negative control for HR; OD_{600}: 0.1); '+' = Eop1: *Ea*246 (positive control for HR; OD_{600}: 0.1); 1 = Eop1: *E. pyrifoliae* str. Ep1/96; 2 = Eop1: *E. amylovora* str. Ea246; 3 = Eop1: *E. amylovora* str. Ea262; 4 = Eop1: *E. tasmaniensis* str. *Et*1/99; 5 = Eop1: *E. tracheiphila* str. MDcuke; 6 = Eop1: *Pantoea vagans* str. C9-1. The presented results were validated by repeating the experiment thrice with 6 replications each. The ratio (6/6) in the figures indicates the number of leaves with the presented phenotype/total number of conducted replications. The images were taken at 4 dpi. (Note: The ratios marked with an asterisk (*) represent the occasional occurrence of the opposite of the presented phenotype (i.e., HR) in replications conducted at different time points).

4.4 Discussion

4.4.1 Premature termination of R-gene results in non-recognition of the Eop1 effectors in *Nicotiana benthamiana*

Eop1 effector from *E. amylovora* and its homologs from other related species induce HR in the non-host plant *N. tabacum*. Similarly, an *Agrobacterium*-mediated transient expression was performed to investigate if Eop1 variants would trigger HR in another non-host plant, *N. benthamiana*, which is an ancestrally related plant to *N. tabacum* (Schiavinato et al., 2020; Sierro et al., 2014). Interestingly, Eop1s that induced full-fledged HR in *N. tabacum* did not induce HR in *N. benthamiana*. The inability of the Eop1s to trigger HR in *N. benthamiana* suggested that the putative R-protein that mediated the HR in *N. tabacum* is either not conserved or is non-functional in *N. benthamiana*; moreover, an alternate possibility was also deduced to be the lack of R-protein associated regulatory components in *N. benthamiana*.

AvrRpm1 effectors from *Psa*_V3 and *Psy*B728a trigger RPA1-mediated HR in *Nicotiana tabacum*; interestingly, they fail to do the same in *N. benthamiana* (Vinatzer et al., 2006; Yoon & Rikkerink, 2020). Upon further investigation, Yoon & Rikkerink observed that the RPA1 allele is also present in *N. benthamiana*; however, it remains dysfunctional due to premature termination of the open reading frame (ORF) by stop codons (premature termination at 250 aa residues compared to a full-length functional RPA1 of 903 aa residues), thus explaining the inability of the AvrRpm1 effectors to elicit HR in *N. benthamiana*. However, when both AvrRPM1 effectors were co-expressed in *N. benthamiana* with the exogenously supplemented functional form of RPA1, both AvrRPM1 effectors elicited HR (Yoon & Rikkerink, 2020).

Similar to AvrRpm1 from *Psa*_V3, HopZ3 effectors from *Psa*_V1 (unpublished data from Yoon & Rikkerink; also investigated in this study) and *Psy*B728a trigger HR in *N. tabacum* but not in *N. benthamiana* (Vinatzer et al., 2006). Yoon & Rikkerink also discovered that *Psa*_V1 HopZ3 induced HR in *N. tabacum*, like AvrRpm1, can be attributed to RPA1 (unpublished data from Yoon & Rikkerink). Furthermore, HopZ3 homologs include Eop1 effectors from *E. amylovora* and related species, with *E. amylovora* Eop1 as its putative functional homologue (Ma & Ma, 2016; Ma et al., 2006). Therefore, considering multiple factors such as HopZ3's and Eop1s' ability to elicit HR in *N. tabacum* but not in *N. benthamiana* and the phylogenetic relationship of HopZ3 with Eop1, RPA1 R-protein was deduced to be the 'putative' R-protein responsible for the Eop1 induced HR activity in *N. tabacum*.

Furthermore, to verify the proposed hypothesis of RPA1 participation in the Eop1 triggered HR. The Eop1s were co-infiltrated and sequentially infiltrated with the exogenously supplied functional allele of RPA1 in *N. benthamiana.* The co-expression resulted in moderate HR (Figure 4.7), in contrast to Eop1 expression without RPA1 (Figure 4.3), indicating RPA1 involvement in HR. However, the findings varied greatly throughout replications. As a result, the strategy of assessing RPA1 involvement in *N. benthamiana* by exogenous supplementation and screening for HR induction was switched to a counterstrategy of RPA1 silencing via the RNAi hairpin construct and screening for the loss or reduction of HR in the presence of Eop1 effectors.

4.4.2 RPA1 R-protein drives the recognition of Eop1 effectors in *Nicotiana tabacum*

NB-LRR proteins are special sensor proteins that can perceive effectors delivered by bacterial pathogens and initiate a robust immune response (ETI) involving HR cell death (Dodds & Rathjen, 2010; Jones & Dangl, 2006). RPA1, an R-protein discovered in *Nicotiana tabacum*, perceives the AvrRpm1 effector from *Psa*_V3 and *Psy*B728a and triggers HR in *N. tabacum* (Yoon & Rikkerink, 2020).

The preliminary investigation conducted to test the Eop1 effector activity in the non-host plants, *Nicotiana tabacum* and *N. benthamiana*, suggested the involvement of RPA1 R-protein (see sections 4.3.6, 4.4.1 and 4.4.2). Consequently, an RNAi-based silencing technique was adopted to test the participation of RPA1 in Eop1-induced HR. The screening strategy was based on the loss or significant reduction in HR caused by *RPA1* silencing in the presence of HR-inducing Eop1 effectors. The *RPA1* hairpin (hp*RPA1*) used in the study was constructed from 295 bp long DNA fragment in the 3'-untranslated region (UTR) of the *RPA1* gene (Yoon & Rikkerink, 2020).

The analysis was carried out on the *Nicotiana tabacum* plant through co-expression via sequential and co-infiltration. However, both strategies were inconclusive as simultaneous delivery and expression of the *RPA1* silencing construct and *eop1*s unexpectedly resulted in HR, which was inferred to be due to the lack of adequate time for the silencing to be effective. Furthermore, silencing via sequential infiltration was also ineffective as the *N. tabacum* leaves pre-exposed to *Agrobacterium* lost the ability to trigger HR, perhaps due to PTI[57] (Klement et al., 2003; Rico et al., 2010; Szatmari et al., 2014; Yoon & Rikkerink, 2020).

[57] If a successful PTI has already been initiated before an ETI triggering effector is delivered, it can stop the development of subsequent ETI and HR. This acts as a defence mechanism against unnecessary damage and yield losses instigated by ETI, sparing the plants from the "unnecessary cost of resistance" (Rico et al., 2010; Szatmári et al., 2014; Tian et al., 2003).

EGTA at a concentration of 5 mM was employed to mitigate the issue of early HR in co-expression via co-infiltration. Interestingly, higher concentrations of EGTA (tested at 10 mM concentration) caused wilting and loss of structural rigidity in the treated leaves. EGTA acts as a calcium chelator which leads to the loss of Ca^{2+} ions essential for biochemical activity (White & Broadley, 2003), maintaining structural rigidity[58] (Hepler, 2005; Hepler & Winship, 2010) and PTI and ETI-triggered immune response (Thor et al., 2020; Wang et al., 2019). Consequently, the loss of structural rigidity specifically can be ascribed to the calcium-chelating property of EGTA from the plant's cell walls (Tang et al., 2019). Moreover, a calcium-deficient environment in the leaf affects water absorption and regulation abilities, resulting in wilting symptoms. Additionally, the delay in HR can also be attributed to the calcium-deficient environment caused by EGTA treatment (Atkinson et al., 1990).

Finally, this study found that simultaneous transient expression of Eop1 and *RPA1*-hairpin via co-infiltration with 5 mM EGTA buffer results in the significant reduction of HR triggered by Eop1 variants in *Nicotiana tabacum* (see section 4.3.6). The significant HR reduction suggests that the RPA1 R-protein is crucial in mediating HR in response to Eop1 transient expression in *N. tabacum*. Therefore, considering the moderate HR triggered by RPA1 upon co-expression with Eop1s in *N. benthamiana* and the absence of HR caused by RPA1 silencing in *N. tabacum*, RPA1 is deduced to be the R-Protein responsible for the Eop1 effector's recognition in *N. tabacum.*

[58] Calcium aids in maintaining the structural rigidity of the leaf by binding with structurally important polysaccharides such as pectin.

4.4.3 A plant immune regulator protein, RIN4, is crucial for the Eop1 effectors-triggered HR in *Nicotiana tabacum*

RIN4 is a conserved 'plant immune regulator protein' that regulates innate immunity in a variety of host plants, including tomato (Luo et al., 2009), apple (Vogt et al., 2013), soybean (Selote & Kachroo, 2010), lettuce (Jeuken et al., 2009), and *Arabidopsis* (Belkhadir et al., 2004). Consequently, the RIN4 protein is targeted by effectors from several bacterial pathogens, which modifies RIN4 post-translation via several mechanisms, including acetylation (Lee et al., 2015), phosphorylation (Chung et al., 2011; Chung et al., 2014; Mackey et al., 2002), and cleavage (Afzal et al., 2011; Axtell & Staskawicz, 2003), to tackle the host plant defences effectively and enhance virulence.

In the catalytic triad mutation analysis, it was discovered that Eop1: *Ea*246 probably functions via its catalytic activity (refer to section 3.4.3), which was proposed to be the acetylation of the host target. Moreover, HopZ3, a putative functional-homolog effector of Eop1 (Ma et al., 2006), acetylates RIN4 (Lee et al., 2015). Therefore, considering all these factors together, the involvement of RIN4 protein in the Eop1-induced HR was investigated by screening for the absence or significant reduction in HR upon RNAi-induced silencing of *N. tabacum* RIN4.

Interestingly, a significant reduction in the Eop1 variants induced HR in *N. tabacum* was observed upon silencing the expression of the RIN4 protein. Thus, indicating the potential involvement of the RIN4 protein in the Eop1-induced HR. Additionally, RIN4 is known to be guarded by several R-proteins that evolved independently in various plant species (Afzal et al., 2013). Co-immunoprecipitation assays also suggest that RIN4 protein can physically associate with RPA1 R-protein (Yoon & Rikkerink, 2020). Thus, it is very likely that the RIN4 protein interacts with RPA1 R-protein to mediate resistance to the Eop1 effector in *N. tabacum*.

4.5 Conclusion

In conclusion, findings from a series of experiments conducted in this study to investigate the participation of RPA1 and RIN4 proteins in the Eop1 effectors-elicited HR in the non-host plant *Nicotiana tabacum* suggest that they are crucial for HR. Therefore, it can be hypothesised that all three proteins, namely, Eop1, RIN4, and RPA1, are associated in a classic 'guard' paradigm of effector recognition in which RIN4 would act as a 'guardee' to trigger RPA1-mediated defence response in response to the Eop1 induced modification in *N. tabacum*. However, the alternate 'decoy model' with RIN4 acting as a decoy protein is implausible as RIN4 is involved in plant immune and stomata regulation activities during pathogen invasion (Afzal et al., 2013; Elmore & Coaker, 2011; Ray et al., 2019; Sun et al., 2014). In contrast, a decoy protein evolves as a 'target mimic' bait for effector perception with no function of its own in the absence of the cognate R protein (van der Hoorn & Kamoun, 2008). Additionally, results from the catalytic triad mutation experiment (section 3.3.3) suggest the role of Eop1 as an enzyme, most likely for acetylation, consequently reducing the possibility of direct interaction with the R-protein to nil. Therefore, it is highly probable that similar to HopZ3 (Lee et al., 2015), Eop1s also acetylate the RIN4 protein, which eventually results in RPA1 triggered immune response of HR. Nevertheless, more research utilising Yeast-2-hybrid assays, *in-vitro* acetylation assays and co-immunoprecipitations would be necessary to confirm the hypothesised interaction of all these proteins.

5 Chapter 5: Discussion of the Research

5.1 Synopsis of major findings from the current research

The primary focus of the work conducted in this study was on Eop1, a widely conserved effector delivered by *E. amylovora* and many other related species in plants during pathogenesis (X. C. Yuan et al., 2021; Zhao, 2014). A series of experiments were conducted to understand the effectors' reactions in the non-host tobacco plant, its function, mechanism, and potential host-target proteins.

First, the Eop1 effectors' reaction in the non-host plant *Nicotiana tabacum* was assessed. Eop1 effector from *E. amylovora* and its sequence homologs from other related species were selected for analysis based on differences in the protein sequence identity and then transiently expressed via agroinfiltration (refer to 'Figure 5.1' for the pictorial summary of the steps involved in the process). Based on the analysis of obtained qualitative and quantitative data of the HR elicited by Eop1 variants, it was concluded that Eop1s act as a 'putative' avirulence factor in *Nicotiana tabacum* (Chapter 2) and hypothesised the involvement of RPA1 R-protein (Yoon & Rikkerink, 2020) in the HR triggering event.

Second, the functional mechanism of Eop1 was deciphered by mutating the predicted functionally important catalytic triad residues: cysteine, histidine, and glutamic acid in the genetic background of Eop1 from *E. amylovora* '*Ea*246' (Chapter 3). The results from the analysis indicated that Eop1 utilises a conserved histidine residue for its function. Based on that, it was hypothesised that Eop1 has an associated enzymatic function, probably involving the host protein's acetylation (Chapter 3). Additionally, *in-silico* tertiary structure models of Eop1 variants were produced using AlphaFold2 to understand the essential structural details of the Eop1 effectors. The analysis of the models revealed that, despite varying degrees of protein sequence differences, all

of the tested Eop1 shared a high structural and catalytic motif homology. Furthermore, the potential involvement of 'IP6' and 'AcCoA' in the activation and function of Eop1s in the plant cells was also hypothesised.

Finally, experiments focused on identifying the host-target(s) of Eop1s and the R-protein responsible for the induction of HR in *N. tabacum* were performed (Chapter 4). The findings from the experiments supported the hypothesis that RIN4 and RPA1 are crucial for HR induction by Eop1 variants, as silencing of either of the two significantly reduced the ability of Eop1 to induce a full-fledged HR in *Nicotiana tabacum.* Consequently, it was hypothesised that the host target of Eop1 could be RIN4, the perturbation of which is detected by its guard protein, RPA1, resulting in HR in the tobacco plant. In addition, an '*Agrobacterium*-mediated co-infiltration system' was also developed, which can be used to test the involvement of different R-proteins and host-origin accessory proteins with Eop1 in the non-host plant *Nicotiana tabacum*.

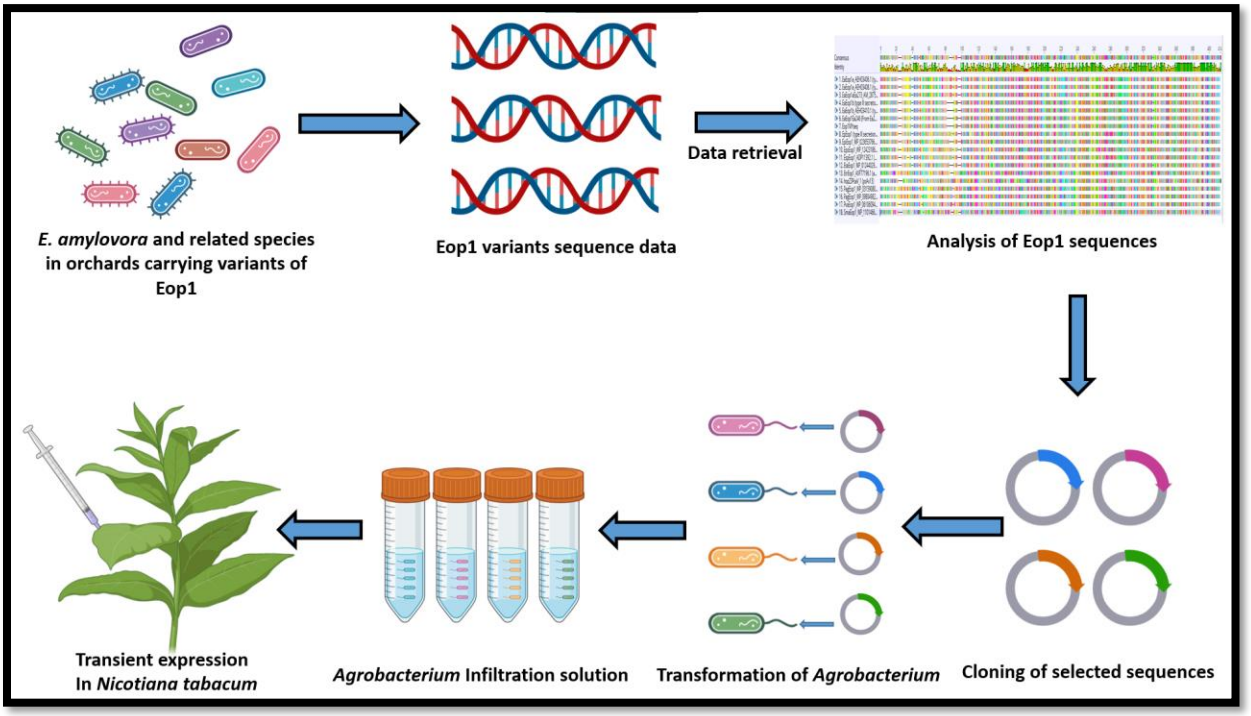

Figure 5.1: Pictorial summary of the processes involved in transient expression analysis of Eop1 variants in *Nicotiana tabacum*.

5.2 Putative models for Eop1s' recognition in *Nicotiana tabacum*

A thorough analysis of the data obtained from the experiments performed in this study suggests that the Eop1 effector potentially targets RIN4 protein using its enzymatic property and possibly acetylates it. The induced perturbation of the RIN4 protein is then perceived by RPA1, triggering the HR. This proposed mechanism of effector detection indicates that the Eop1s' recognition in *N. tabacum* follows the 'guard hypothesis' proposed by Jones & Dangl (2006).

The guard hypothesis suggests that the pathogen's effectors are recognised indirectly by the R-protein by perceiving the effector-induced perturbation in the host-target protein (guardee protein). However, as described in section 4 and Figure 4.1 (sub-figures 2.1 and 2.2), 'guard hypothesis' based recognition events can occur via two mechanisms. Consequently, Eop1-induced HR, facilitated by RPA1, is explained using both mechanisms in Figure 5.2 and Figure 5.3. Additionally, it is also proposed that the recognition is more likely to occur via 'GH model 2' (as proposed in 'Figure 5.3'), as co-immunoprecipitation pull-down experiments conducted by Yoon & Rikkerink (2020) suggest that *Nb*RIN4 (98.1% sequence homolog of *Nt*RIN4) is also pulled down in complex with RPA1, suggesting that the RIN4 and RPA1 potentially exist together maintaining an *in-planta* protein-protein complex (as portrayed in Figure 5.3; sub-figure 1). Moreover, it is crucial to note that, based on *in-silico* structure analysis, the Eop1 effector may interact with the IP6 and AcCoA for their activation before the acetylation activity.

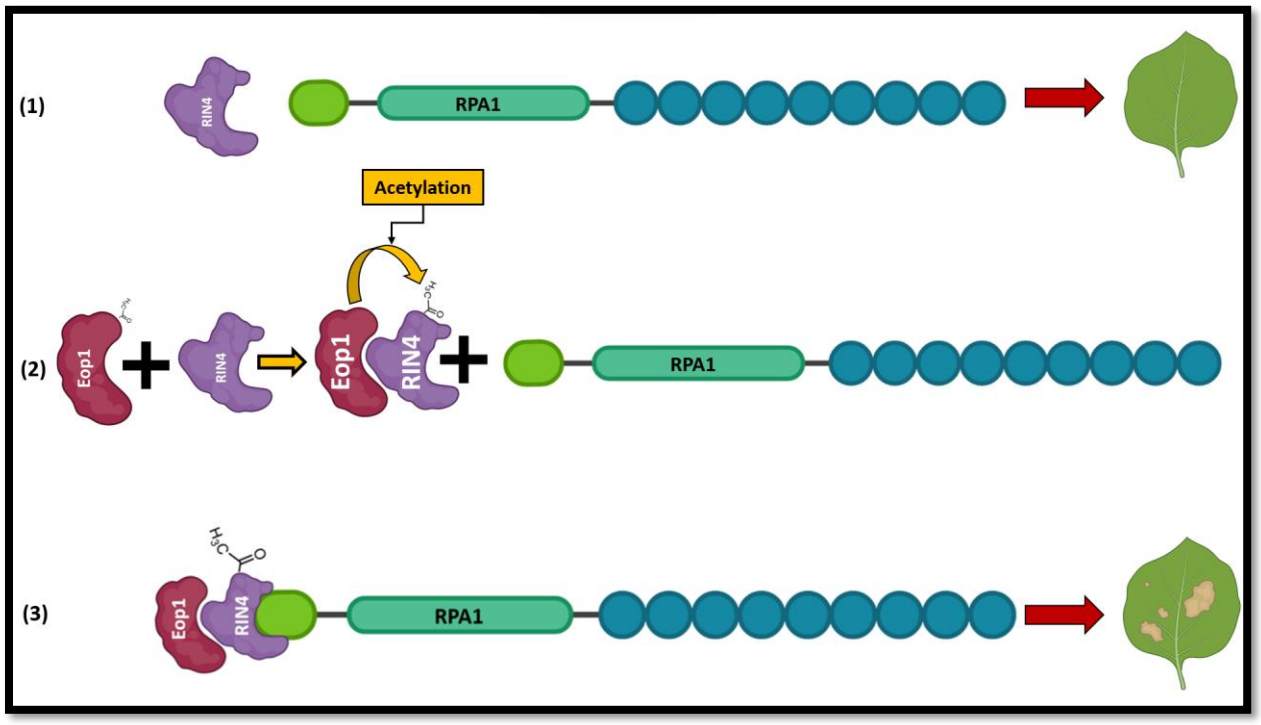

Figure 5.2: Putative model '1' of Eop1 interaction with RIN4 and RPA1, resulting in its recognition in *N. tabacum*. The presented model corresponds to 'GH model 1' described in Figure 4.1 (sub-figure 2.1). The proposed recognition mechanism is as follows: (1) before the *in-planta* transient expression of the Eop1 effector via *Agrobacterium*, the RIN4 protein remains unmodified and does not trigger HR; (2) Upon encountering the RIN4 protein, the Eop1 effector acetylates it; (3) acetylation results in the perturbation of the RIN4 protein, which is recognised by RPA1, triggering ETI and resulting in HR.

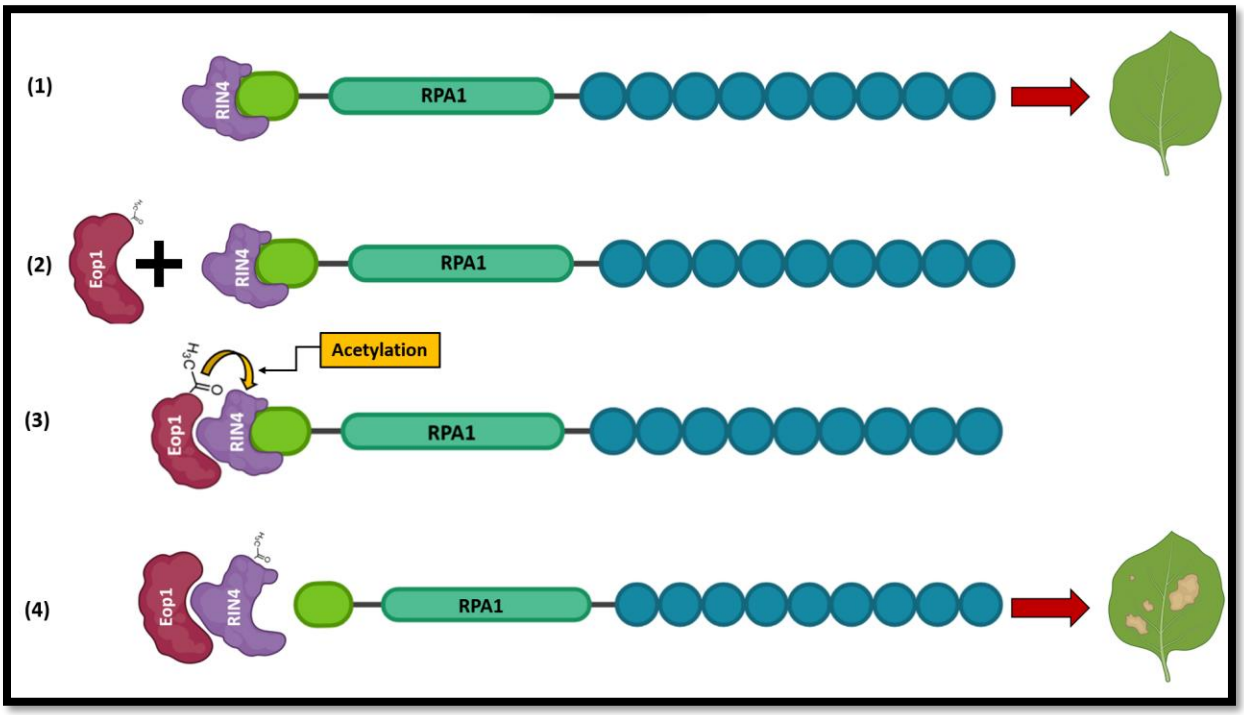

Figure 5.3: Putative model '2' of Eop1 interaction with RIN4 and RPA1, resulting in its recognition in *N. tabacum*. The presented model corresponds to 'GH model 2' described in Figure 4.1 (sub-figure 2.2). The proposed recognition mechanism is as follows: (1) the R-protein RPA1 and RIN4 co-exist in a healthy state, maintaining a protein-protein complex and repressing the immune response; (2) & (3) upon encountering the RPA1-RIN4 protein complex (guard and guardee complex), the Eop1 effector acetylates RIN4; (4) acetylation modifies the RIN4 protein, liberating RPA1 from the 'guard and guardee' complex and allowing it to engage in the immune signalling activities, resulting in HR.

One vital question that must be addressed is: what could be the impact of potential acetylation by Eop1 in the absence of the cognate R-protein in the host or non-host plants? RIN4 protein acts as a trigger for the multiple R-proteins such as RPM1 (Belkhadir et al., 2004), RPS2 (Axtell & Staskawicz, 2003), Fb_MR5 (Broggini et al., 2014) and RPA1 (Yoon & Rikkerink, 2020). Most importantly, it functions as a negative regulator of plant immunity (Sun et al., 2014). Therefore, in the absence of a cognate R-protein, it is proposed that the pathogen would employ the effector-driven acetylation activity in suppressing the plant immunity, making the *in-planta* environment conducive to the pathogen proliferation. However, this area demands more research.

5.3 Future research prospectus

Science is an ever-evolving discipline, and the research conducted in the presented work has opened multiple streams that can be explored to corroborate various hypotheses proposed in this study or explore entirely new research areas based on the findings of this research. Some research areas that can be investigated are listed as follows:

1. Identification of the putative 'secondary nucleophile' that can compensate for the loss of the 'primary nucleophile' in Eop1: *Ea*246.
2. Analysis of Eop1-induced RIN4 acetylation via *in-vitro* acetylation assays using the protocol described by Jeleńska et al. (2021). Following a positive acetylation result, mass-spectrometry analysis can be performed to pinpoint the acetylation sites in the RIN4 protein.
3. Analysis of RPA1 and RIN4 *in-planta* interaction with Eop1 through Co-immunoprecipitation (Co-IP) and protein-protein interactions via Yeast-2-hybrid assay, using the protocol described by Yoon & Rikkerink (2020) and Lee et al. (2015), respectively.

4. Analysis of the complementation ability of the *Malus* and *Pyrus* RIN4s with Eop1 in *N. tabacum* using the co-infiltration system developed in this study, followed by Co-IP analysis [59].
5. Also, another interesting 'side project' could be the investigation of the escape mechanism of Eop1 from *Erwinia tracheiphila* from RPA1 recognition in *N. tabacum.* Research in this area can provide insight into the evolution of Eop1s in *Erwinia* species targeting different hosts apart from the Rosaceae members.

Having listed all the potential future research, it is crucial to account their relevance to the current study and their impact on the future R-gene deployment strategies in pome fruit cultivars. The aforementioned points 1, 2, and 3 are pertinent to the 'functional understanding' of the effector Eop1, which will corroborate the hypothesis proposed in the current study, such as Eop1s' acetylation activity and targeting of the RIN4 protein. Furthermore, the discovery of a 'secondary nucleophile' would be an international first and will shed light on the evolutionary conservation of Eop1 residues and their function.

It is proposed that a positive interaction in the analysis described in the above-mentioned 4th point can lead to another study involving the introgression of the RPA1 encoding gene into the genomes of commercial cultivars of pears and apples in order to generate transgenic resistant cultivars. Interestingly, developing *RPA1*-integrated transgenic cultivars is an excellent approach for studying Eop1 interaction directly in pome fruit cultivars; however, its acceptance as a breeding line would be limited due to strict regulation in the development, use, and release of transgenic cultivars.

[59] Note: The phylogenetic analyses and some preliminary experiments relevant to the proposed research were carried out; the methodology and results for the same are presented in 'Chapter 6'.

5.4 A potential challenge to encounter

Additional studies conducted by Yoon & Rikkerink on RPA1 suggest that it belongs to the 'NLR required for cell death' (NRC) clade of NLRs (unpublished data from Yoon & Rikkerink). However, the NRC clade is absent in Rosid dicots and is only present in Asterid (Supplementary Figure C5S1) (Wu et al., 2017). Consequently, the likelihood of using phylogeny to find an RPA1 functional orthologue in apple and pear (which belong to the Rosids) is remote to absent altogether; nonetheless, the potential existence of another R-protein perceiving Eop1 in *Malus floribunda* 851 and *Malus* 'Evereste' genomes cannot be denied because of their gene-for-gene resistance corresponding to Eop1 (Wöhner et al., 2018). Consequently, alternate strategies based on advanced biotech tools such as 'Resistance gene enrichment sequencing' (RenSeq) (Jupe et al., 2013) can be employed to search for R-protein in *Malus floribunda* 851 and *Malus* 'Evereste' that recognises Eop1. A Positive discovery can then lead to the identification of the gene imparting resistance, followed by its introduction into commercial cultivars through 'molecular cloning backed' breeding efforts using the protocol described by Broggini et al. (2014).

5.5 A 'putative model' for durable resistance to fire blight in pome fruits

Finally, based on the available literature and analysis of the findings from the current study, a model for durable resistance to fire blight in pome fruits is proposed, which functions through the deployment of R-genes that recognise Eop1 and AvrRpt2$_{Ea}$ separately. Results from the research conducted in the current study suggest that the RIN4 protein is more likely to be the host target of Eop1. This hypothesis is also supported by the research on Eop1's putative functional homologue, HopZ3 (Lee et al., 2015; Ma et al., 2006). Furthermore, RIN4 is also targeted and cleaved by another *E. amylovora* effector, AvrRpt2$_{Ea}$ (Prokchorchik et al., 2020; Vogt et al., 2013). Thus, both

effectors could compete for the same host target. As a result, Eop1's interaction with RIN4 may be compromised, affecting the recognition and resistance imparted by it. However, an alternate possibility could also be true, in which AvrRpt2$_{Ea}$ does not interfere with Eop1 activity. In such a situation, the recognition of Eop1 could maintain resistance to *E. amylovora* where AvrRpt2$_{Ea}$ recognition-mediated resistance would fail, as previously observed in the case of *Mr*5 resistance breakdown (Figure 5.4) (Vogt et al., 2013). Consequently, it is crucial to understand the relationships between these two effectors and determine whether they are 'competing' for RIN4 recognition or if they work independently of each other. The knowledge from that can then be used to design a strategy in which the pathogen is 'forced' to lose both AvrRpt2$_{Ea}$ and Eop1 and thus lose a significant component of its pathogenicity in order to escape recognition by the R genes; however, before exploring the potential Eop1 and AvrRpt2$_{Ea}$ interactions, it is necessary to experimentally prove that Eop1 does interact with RIN4 at the molecular level.

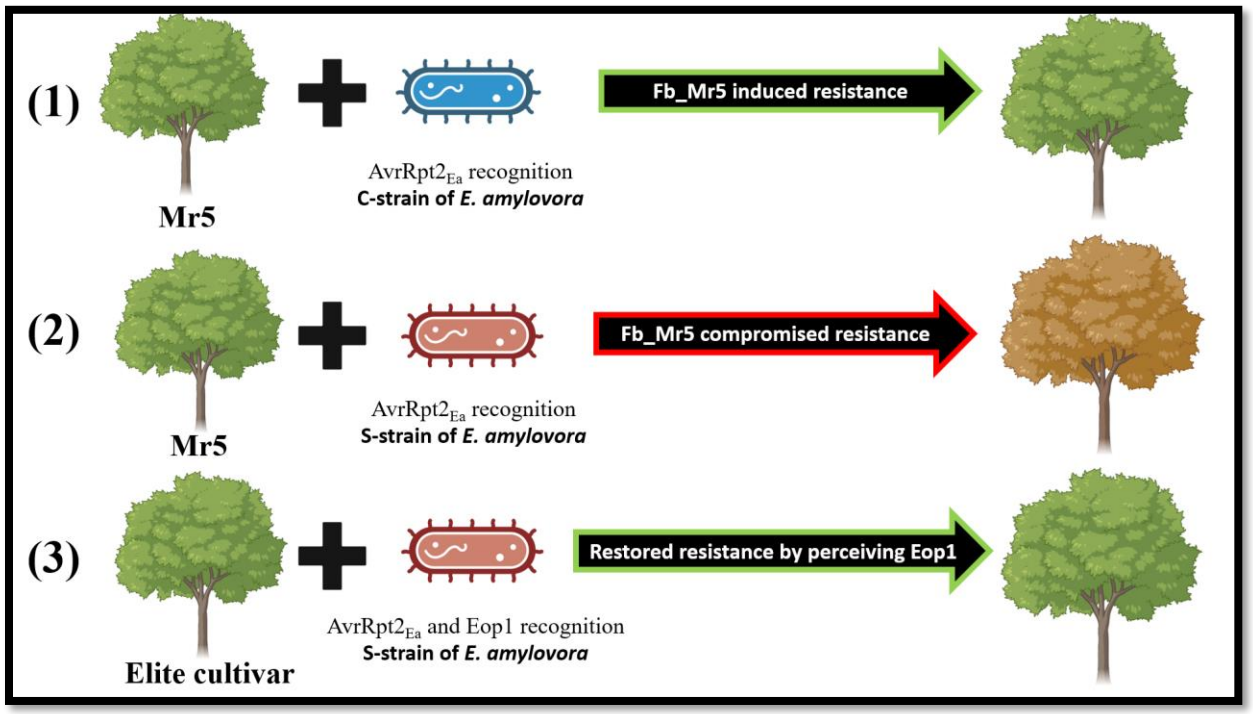

Figure 5.4: 'Putative model' for the durable resistance to fire blight in pome fruits through pyramiding of R-genes separately recognising Eop1 and AvrRpt2$_{Ea}$ effectors. The notion behind the model for durable resistance is as follows: (1) *Malus robusta* 5 (*Mr*5) is a wild *Malus* species resistant to *E. amylovora*. The R-protein 'Fb_MR5' confers the resistance to *E. amylovora* upon recognition of the RIN4 protein cleavage induced by AvrRpt2$_{Ea}$ effector; (2) The Fb_MR5 imparted resistance in *Mr*5 is overcome by *E. amylovora* strains carrying 'C156S' mutation in the AvrRpt2$_{Ea}$ effector, making the *Mr*5 species susceptible to the mutant strains; (3) an elite cultivar harbouring the *Fb_MR5* gene would be susceptible to C156S mutant strains of *E. amylovora*; however, if the elite cultivar also harbours the gene encoding for R-protein recognising Eop1 effector[60] (which also potentially targets the RIN4 protein), then it is likely to compensate for the collapse of Fb_MR5 imparted resistance. Thus, maintaining resistance to the *E. amylovora* C156S mutant strains and imparting durable resistance.

[60] Based on the available literature, *Malus* 'Evereste' and *Malus floribunda* 821 are the most potent sources of the R-protein recognising Eop1 effector (Wöhner et al., 2018).

6 Chapter 6: Analysis of the complementation ability of *Malus* and *Pyrus* RIN4s in Eop1-induced HR in *Nicotiana tabacum* (Additional Research)

6.1 Brief Introduction

The experiments conducted in the previous studies discovered that RPA1 and RIN4 proteins are crucial for the Eop1-elicited HR in the non-host plant *Nicotiana tabacum* (see sections 4.3.6 and 4.3.7). Additionally, results also indicated that Eop1 could be targeting and potentially acetylating the RIN4 protein in *N. tabacum* (see sections 3.5 and 4.3.7), which led to the hypothesis that Eop1 might also target RIN4 proteins in its host species. Consequently, RIN4 homologs from the *Malus* and *Pyrus* species (major host species of *E. amylovora*) were selected to test if the *Malus* and *Pyrus* RIN4s could interact with RPA1 to elicit the Eop1-triggered HR in *Nicotiana tabacum* when the resident RIN4 (*Nt*RIN4) is silenced through hp-*NbRIN4*. This experiment was considered vital as the results obtained from this would not only provide information about the interaction ability of the *Malus* and *Pyrus* RIN4s with Eop1 but also with RPA1 protein, which upon positive interaction, could be a valuable source of R-protein from a non-host species. Therefore, the succeeding research focuses on selecting the *Malus* and *Pyrus* RIN4 candidates and testing their complementation ability with RPA1 to trigger the Eop1-induced resistance.

6.2 Material and Methods

6.2.1 Total RNA Extraction

First, the harvested young plant leaves were immersed in liquid nitrogen and ground to fine powder consistency using a mortar and pestle. The pulverised leaf samples were then weighed, divided into 100 mg aliquots, and stored in a -80℃ freezer. Next, the total RNA was extracted using materials and 'protocol A' instructions guided by Spectrum™ Plant Total RNA kit [Sigma, NZ]. Finally, the concentration and quality of extracted RNA samples were evaluated using a Nanodrop® ND-1000 spectrophotometer and running 5 µL of the samples on 1% agarose gel.

6.2.2 DNase treatment

Extracted RNA from the leaves was made DNA-free by deoxyribonuclease (DNase) treatment with DNase I, Amplification Grade (DNase I, Amp Grade) [Invitrogen; San Diego, CA, USA]. First, 2 µg of RNA sample was put in a pre-chilled RNase-free 1.5 mL Eppendorf® tube, followed by the addition of 2 µL 10X DNase I Reaction Buffer, 2 µL DNase I, Amp Grade (1 U/µL), and PCR-grade water to the final volume of 20 µL. The mixture was then incubated for 15 minutes at room temperature. The DNase treatment was terminated by adding 2 µL of 25 mM EDTA solution to the reaction mix and heating for 10 minutes at 65℃. The quality of RNA post-DNase treatment was assessed by running and visualising 5 µL of DNase I-treated RNA sample on a 1% agarose gel. The remaining volume (15 µL) of the RNA sample was used in reverse transcription PCR (RT-PCR) to produce single-stranded cDNA.

6.2.3 Making cDNA through RT-PCR

Single-stranded cDNA was generated from DNase-treated RNA using the High-Capacity cDNA Reverse Transcription Kit [Applied Biosystems, Vilnius, Lithuania]. First, a 15 µL master mix

was prepared in a pre-chilled 0.2 mL nuclease-free PCR tube. The master mix consisted of 3 µL of 10X RT Buffer, 3 µL 25X RT Random Primers, 1.2 µL dNTP Mix (0.75 mM), 1.5 µL Reverse Transcriptase (50 U/µL), and 6.3 µL of nuclease-free PCR-grade water. To this master mix, 5 µL of DNase-treated RNA was added, totalling the reaction mix to 20 µL. The components in the reaction mix were mixed by gentle pipetting, followed by a brief micro-centrifuge to bring the content together at the bottom of the tube. The reaction mix was then put in a Mastercycler® X50s thermocycler [Eppendorf; Hamburg, Germany] for reverse transcription to generate cDNA. The thermocycler conditions for RT–PCR were set as recommended in the High-Capacity cDNA Reverse Transcription Kit guide.

6.2.4 Amplification of *Pyrus communis* L. cv. 'Conference' *RIN4* gene using cDNA

The *Pyrus communis* L. cv. 'Conference' *RIN4* gene was amplified by employing cDNA generated in section 6.2.3 as a template. First, a 20 µL master mix was prepared in a pre-chilled 0.2 mL nuclease-free PCR tube by combining 2.5 µL 10X PCR buffer [Invitrogen], 1.5 µL (3 mM) MgCl2 [Invitrogen], 1.5 µL (0.6 mM) dNTPs mix, 1.5 µL (0.6 µM) of each forward and reverse primer (Table 6.1), 11 µL nuclease-free PCR-grade water, and 0.5 µL of Platinum™ Taq DNA Polymerase. To this master mix, 5 µL of cDNA was added, bringing the final volume of the PCR reaction mix to 25 µL. The PCR mix was then run in Mastercycler®X50s thermocycler [Eppendorf; Hamburg, Germany] for gene amplification under three-step PCR conditions. First, initial denaturation was performed at 95℃ for 4 minutes, followed by 35 sequentially ran successive cycles of denaturation at 95℃ for 30 seconds, annealing at 58℃ for 30 seconds and extension at 68℃ for 2 minutes; final extension was carried out at 68℃ for 10 minutes followed by a final hold of the samples at 4℃. 5 µL of the PCR product was then checked on 1 % agarose gel to confirm the gene amplification.

Table 6.1: Primer sequences used in the PCR-driven gene amplification of *Pyrus communis* L. cv. 'Conference' *RIN4*.

Amplified gene	Primer type	Primer sequences
Pyrus communis L. cv. 'Conference' *RIN4* gene	Forward	5'—ATGGACTACAAAGACGATGACGACAAGATGGCACAACGTTCACATGTACCAAAG—3'
	Reverse: *Ppy*RIN4-1	3'—TCATTTTCTGCTCCATGGAAAGCAG—5'
	Reverse: *Ppy*RIN4-2	3'—TCATTTTCTGCCCCATGGAAAGCAG—5'
Note: see footnote '61' for information on the two reverse primers		

6.2.5 Isolation of the amplified product through gel purification

The amplified gene was isolated and purified from the PCR product using the agarose gel DNA recovery method. First, 5 volumes of the PCR product were combined with 1 volume of gel loading dye (6X) and loaded onto a 1% (w/v) agarose gel prepared using the method described in section 2.2.6. The gel was then run for 40 minutes at 110 volts. Next, the DNA bands were visualised and captured in an image using GelDoc XR+ [Bio-Rad; Hercules, CA, USA]. Following that, the bands were illuminated again by placing the gel on a UV box, and DNA fragments were sliced out from the gel. Finally, the DNA from the sliced gel fragments was isolated and purified using materials and instructions as guided by the Zymoclean^{TM} Gel DNA recovery kit [Zymo Research, USA].

[61] The primer pair used in the study for *Pyrus communis* L. cv. 'Conference' *RIN4* gene amplification employed the same forward primer but different reverse primers. This was done because the sequence alignment analysis showed that both 'putative' *Pyrus* homologs share the same sequence at the N-terminus end while differing at the C-terminus end (Data for the sequence alignment is not shown; however, the protein and FASTA DNA sequence provided in the appendix section can be used to verify the aforementioned statement). Consequently, the reverse primers were specifically designed to amplify different 'allelic versions' of the *Pyrus* RIN4s, namely *PpyRIN4-1* and *PpyRIN4-2*.

6.2.6 Nucleotide sequence alignment

The nucleotide sequences were aligned using Genious software, Version 10.2.5. Geneious alignment algorithm combined with alignment type: Global alignment with free end gaps; Cost matrix: 65% similarity (5.0/- 4.0); Gap open penalty: 12; Gap extension penalty: 3 and Refinement iterations: 2, were used in the analysis.

6.3 Results

6.3.1 Protein sequence alignment analysis of *Malus* and *Pyrus* RIN4 variants

Malus and *Pyrus* RIN4 variants [62] employed in the analysis were selected using a combination of protein sequence alignment and Phylogenetic analysis. A protein sequence alignment of *Malus* and *Pyrus* RIN4s was first produced by employing the sequence alignment parameters described in section 2.2.1.1. The protein sequence alignment analysis revealed that all the analysed RIN4s share more than 90% sequence identity and form two separate groups in the alignment matrix (Figure 6.1). The sequences were also analysed using a phylogenetic tree generated using the UPGMA method, which led to the identification of 2 separate clades in the phylogenetic tree, annotated as 'Clade: 1' and 'Clade: 2' (Figure 6.2).

Interestingly, the two identified clades harboured *Mxd*RIN4-1 (FJ265821.1) and *Mxd*RIN4-2 (FJ265822.1), identified by Cui & Rikkerink (2008) (Figure 6.2). Further analysis conducted by the same researchers found the alleles' loci on the homoeologous chromosome pair of linkage groups (LG) LG5 (*Mxd*RIN4-2) and LG10 (*Mxd*RIN4-1), proposed to be derived from the 'whole genome duplication' (WGD) event that occurred in the progenitor of both apple and pear (Sanzol, 2010). Consequently, RIN4 variants tested in the experiment were selected from the 2 separate clades, i.e., two RIN4 variants from the *Malus* genus and two RIN4 variants from the *Pyrus* genus, as shown in Table 6.2.

[62] The RIN4 sequence homologs were retrieved via BLAST search with *Mxd*RIN4-1 (FJ265821.1) and *Mxd*RIN4-2 (FJ265822.1) sequences against apple and pear genome and cDNA databases.

	1-MxdRIN4-1	2-PbRIN4-1...	3-PpyRIN4-1...	4-PbRIN4-1B...	5-PcoRIN4-1_	6-PcRIN4-1	7-PuPcRIN4-1	8-MxdRIN4-2	9-PbRIN4-2_...	10-PpyRIN4-2	11-PuPcRIN4-2
1-MxdRIN4-1		94.2%	94.2%	93.4%	94.2%	94.2%	93.8%	90.9%	91.3%	91.3%	90.0%
2-PbRIN4-1A_XP_0093706...	94.2%		100%	97.9%	97.9%	97.9%	96.7%	92.5%	92.9%	92.9%	91.7%
3-PpyRIN4-1_cDNA_GALR...	94.2%	100%		97.9%	97.9%	97.9%	96.7%	92.5%	92.9%	92.9%	91.7%
4-PbRIN4-1B_XP_0093349...	93.4%	97.9%	97.9%		97.5%	97.5%	97.1%	91.7%	92.1%	92.1%	90.9%
5-PcoRIN4-1_	94.2%	97.9%	97.9%	97.5%		100%	98.8%	92.9%	93.4%	93.4%	92.1%
6-PcRIN4-1	94.2%	97.9%	97.9%	97.5%	100%		98.8%	92.9%	93.4%	93.4%	92.1%
7-PuPcRIN4-1	93.8%	96.7%	96.7%	97.1%	98.8%	98.8%		92.5%	92.9%	92.9%	91.7%
8-MxdRIN4-2	90.9%	92.5%	92.5%	91.7%	92.9%	92.9%	92.5%		96.3%	96.3%	95.0%
9-PbRIN4-2_XP_00937188...	91.3%	92.9%	92.9%	92.1%	93.4%	93.4%	92.9%	96.3%		100%	97.9%
10-PpyRIN4-2	91.3%	92.9%	92.9%	92.1%	93.4%	93.4%	92.9%	96.3%	100%		97.9%
11-PuPcRIN4-2	90.0%	91.7%	91.7%	90.9%	92.1%	92.1%	91.7%	95.0%	97.9%	97.9%	

Figure 6.1: Protein sequence alignment matrix of *Malus* and *Pyrus* RIN4 variants. The red boxes represent the two identified groups.

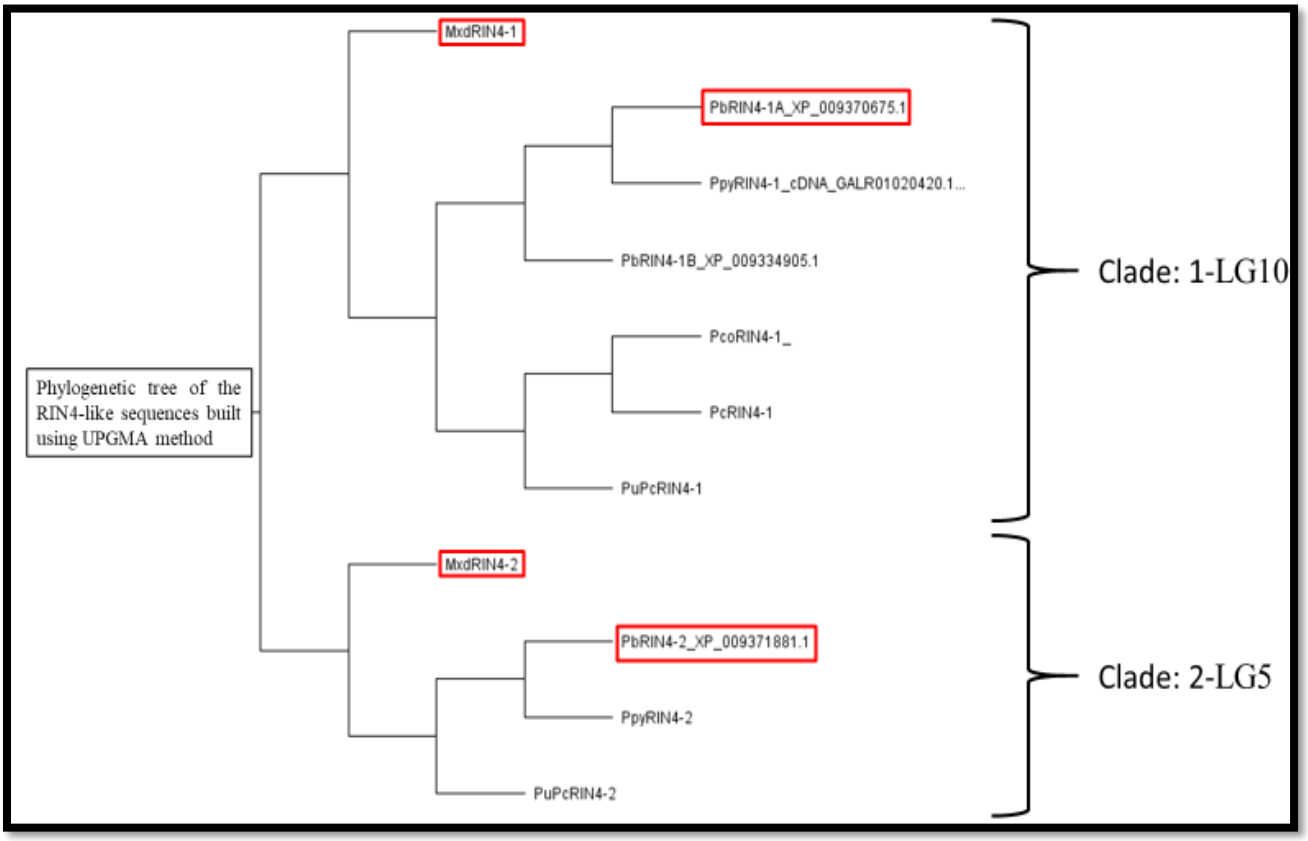

Figure 6.2: Phylogenetic tree of the *Malus* and *Pyrus* RIN4 variants. The tree was built using the UPGMA method with Geneious software V10.2.5. The identified clades and their corresponding linkage groups are annotated on the right side of the figure, and the red boxes represent the RIN4 variants selected for the analysis.

Table 6.2: An overview of essential details of *Malus* and *Pyrus* RIN4 variants selected for the interaction analysis.

S. No	Sequence name	NCBI accession No.	Resident species of the RIN4 variant	Additional information
1.	*Mxd*RIN4-1	NP_001280923.1 (FJ265821.1)	*Malus domestica*	*Malus domestica* RIN4 – 1; resident to *Malus* linkage group 10
2.	*Mxd*RIN4-2	NP_001280834.1 (FJ265822.1)	*Malus domestica*	*Malus domestica* RIN4 – 2: resident to *Malus* linkage group 5
3.	*Pb*RIN4-1A	XP_009370675.1	*Pyrus bretschneideri*	Predicted *Pyrus* RIN4; s*hares* 100% and > 90 % sequence identity with *Pyrus pyrifolia and Pyrus communis* cv. Conference, respectively (verified in this study); homolog to *Mxd*RIN4-1.
4.	*Pb*RIN4-2	XM_009373606.1	*Pyrus bretschneideri*	Predicted *Pyrus* RIN4; s*hares* 100% and > 90 % sequence identity with *Pyrus pyrifolia* cv. Nijisseiki and *Pyrus communis* cv. Conference, respectively (verified in this study); homolog to *Mxd*RIN4-2.
Note: The protein and FASTA DNA sequences of the above-mentioned RIN4 variants are presented in the 'appendix section'.				

6.3.2 Validation of the predicted *Pyrus* RIN4 sequences

The *Malus* RIN4s selected for the study were chosen based on the 'cloned cDNA' from *Malus* species identified by Cui & Rikkerink (2008); In contrast, the selected *Pyrus* RIN4s were computationally predicted from the *Pyrus* genome sequence data and, therefore, required confirmation by cloning the cDNA from the *Pyrus* species. Hence, the predicted *Pyrus* RIN4s selected for the study were first validated by comparing them with the *Pyrus communis* L. cv. 'Conference' *RIN4* sequence cloned through extracted mRNA.

Total RNA was isolated from fresh leaves of micro-propagated *Pyrus communis* L. cv. 'Conference' plantlets (cordially provided by Sumathi Thomas, PFR, Auckland) by employing the methodology described in section 6.2.1. The purity and integrity of the isolated RNA samples were assessed by analysis on a Nanodrop® ND-1000 spectrophotometer and visualising it on the 1% agarose gel. The 28S and 18S ribosomal RNA bands were used as a quality parameter as they remain intact in high-quality RNA (Figure 6.3). The extracted RNA was then treated with DNase according to the methodology described in section 6.2.2 and again tested for quality on 1 % agarose gel.

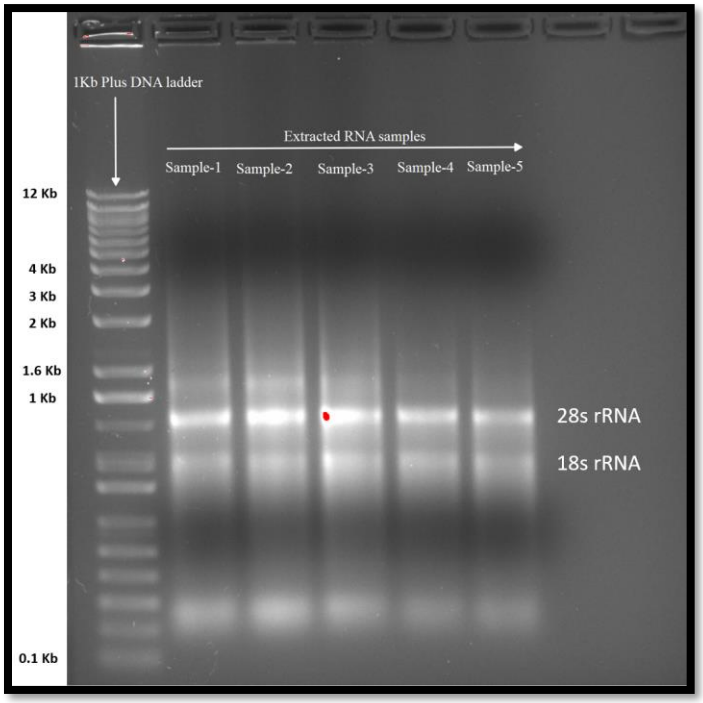

Figure 6.3: Gel electrophoresis of *Pyrus communis* L. cv. 'Conference' extracted RNA on 1 % agarose gel. Each sample corresponds to the RNA extracted from 100 mg leaves sample.

The DNase-free extracted RNA was then used to generate cDNA by employing the protocol described in section 6.2.3. Following that, the *Pyrus RIN4* gene was amplified using cDNA as a template and *Pyrus RIN4* specific primers for both the homologs (Table 6.1) in a PCR-

driven gene amplification by employing the protocol described in section 6.2.4. The PCR product was then visualised on 1 % agarose gel (Figure 6.4). Next, the PCR-amplified *RIN4* gene was extracted from the bands visualised on the gel using materials from the Zymoclean™ Gel DNA recovery kit [Zymo Research, USA] in accordance with the kit's instructions. Before sequencing, the sample's quality was assessed on the Nanodrop® ND-1000 spectrophotometer. It is also essential to note that out of the two tested reverse primers (one reverse primer amplifying each *RIN4* homolog), only the *PpyRIN4-1* specific reverse primer (Table 6.1) produced a positive result when the *RIN4* gene was amplified from the cDNA obtained from *Pyrus* communis L. cv. 'Conference', indicating that the 'Conference' cultivar possibly harbours only the *PpyRIN4-1* homolog of the RIN4.

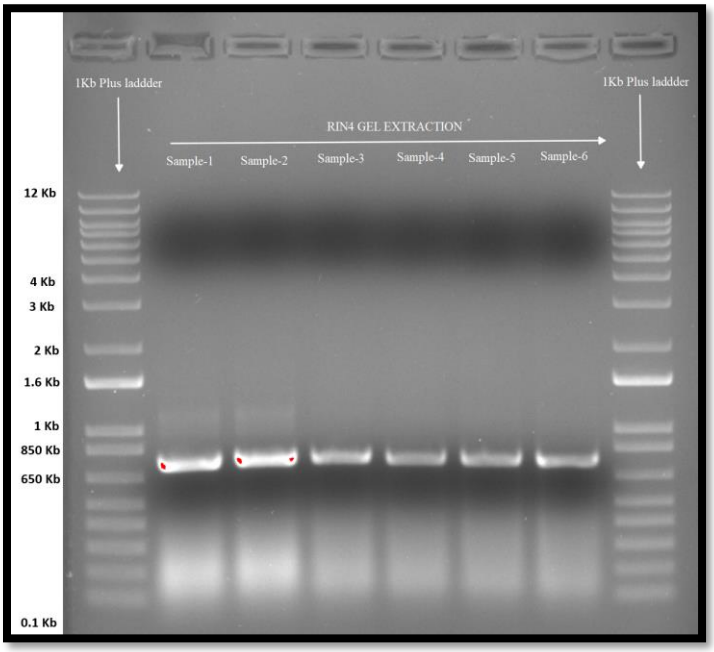

Figure 6.4: Gel electrophoresis of PCR amplified *Pyrus communis* L. cv. 'Conference' *RIN4* gene[63].

[63] Note: each sample presented in the 'Figure 6.4' was amplified using primers mentioned in 'Table 6.1', with reverse primer specifically from '*PpyRIN4*-1'. Also, the '*PpyRIN4-2*' reverse primer failed to produce the PCR-amplified product (result not shown).

The PCR-amplified *Pyrus communis* L. cv. 'Conference' *RIN4* gene was sequenced by Macrogen (Seoul, South Korea) using the primers mentioned in Table 6.1. The obtained sequencing result was analysed via nucleotide sequence alignment. The nucleotide sequence of the selected *Pyrus* RIN4s was individually aligned with the sequenced *Pyrus communis* L. cv. 'Conference' *RIN4* sequence by employing the parameters described in section 6.2.6. The analysis discovered that the *Pyrus communis* L. cv. 'Conference' *RIN4* shares 98.1 % and 93.4 % nucleotide sequence identity with the predicted *RIN4s*: *PbRIN4-1A* and *PbRIN4-2*, respectively; consequently, sharing the same percentage of nucleotide sequence identity with *Pyrus pyrifoliae RIN4s*: *PpyRIN4-1* and *PpyRIN4-2*, respectively as *PbRIN4*s shares 100 % sequence homology with *PpyRIN4s*. Consequently, this suggests that the computationally predicted sequences of the selected *Pyrus* RIN4s are accurate and can be employed in subsequent experiments.

Following validation of the *Pyrus RIN4* sequences, the selected *Malus* and *Pyrus RIN4* sequences tagged with the FLAG-tag gene at the N-terminus end were synthesised into a Gateway® cloning compatible entry vector by Twist Bioscience (See section 2.2.3.1.1). To generate RIN4s' expression clones, the entry clones harbouring the *RIN4* sequence were Gateway® cloned with the destination vector (pHEX2) by employing the LR Gateway® cloning protocol described in section 2.2.3.2.1.

Following Gateway® cloning, the expression clones were checked for the presence of RIN4 genes via *Pst*I-HF® restriction digest by employing the protocol described in sections 2.2.7 (Figure 6.5 A). The restriction digest result was then compared with an *in-silico*-generated restriction digest template of RIN4 expression clones produced using the method described in section 2.2.8 (Figure 6.5; sub-figure 'B').

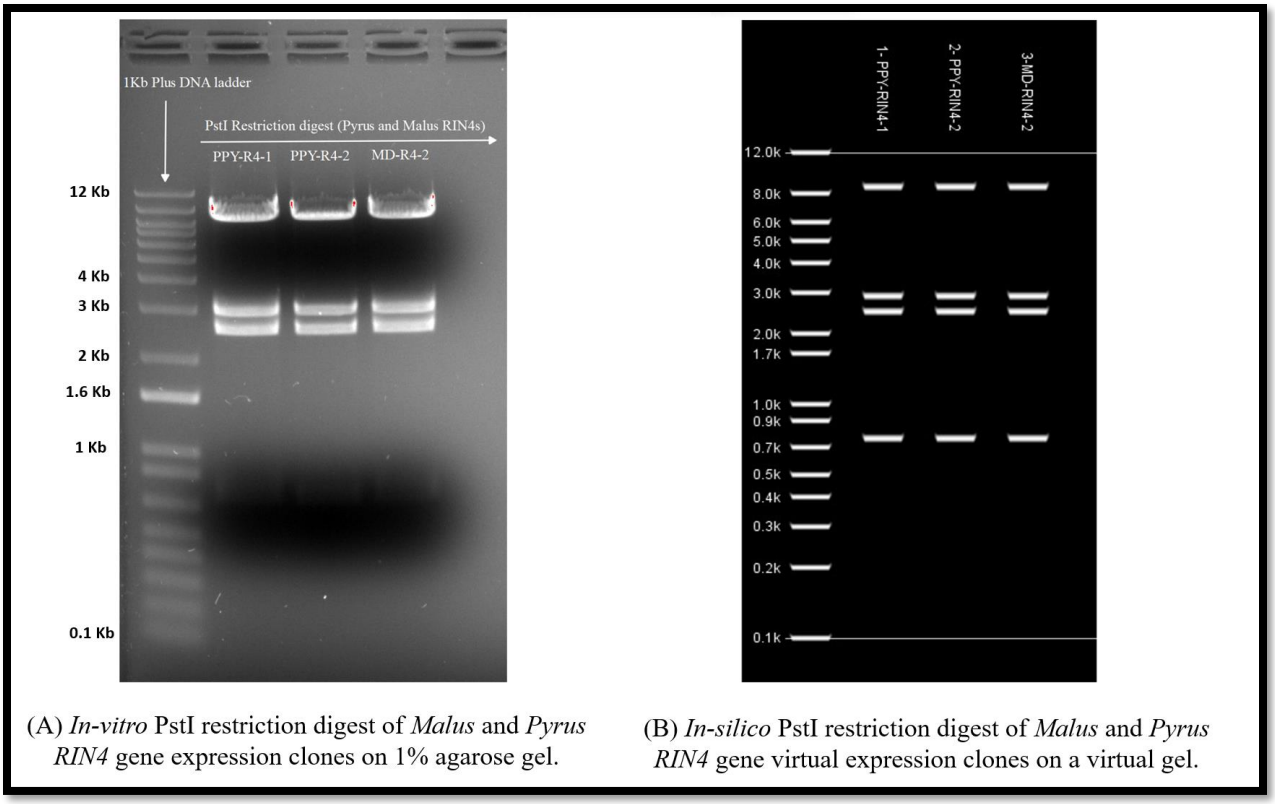

(A) *In-vitro* PstI restriction digest of *Malus* and *Pyrus RIN4* gene expression clones on 1% agarose gel.

(B) *In-silico* PstI restriction digest of *Malus* and *Pyrus RIN4* gene virtual expression clones on a virtual gel.

Figure 6.5: Comparison of the *in-vitro Pst*I restriction digest result of expression clones carrying *Malus* and *Pyrus RIN4* with *in-silico* generated restriction digest template. The remarkable similarity confirms the positive cloning of *Malus* and *Pyrus RIN4* in the expression clones[64]. (See footnote '64' for information on the *Mxd*RIN4-1 expression clones).

The expression clones harbouring the *RIN4* gene were then used to transform *Agrobacterium* for *in-planta* expression by employing the protocol described in section 2.2.4. Finally, glycerol stocks from the *Agrobacterium* cells harbouring RIN4 expression clones were made (as described in section 2.2.10) after the presence of the *RIN4* gene in the *Agrobacterium* was verified through M13 universal primers driven colony PCR (Figure 6.6) by employing the protocol as described in the section 2.2.9. Next, the *Agrobacterium* harbouring *Malus* and *Pyrus* RIN4s were employed for the analysis in *N. tabacum*.

[64] *MxdRIN4-1* expression clone was not assessed as it was already provided in *Agrobacterium* by Minsoo Yoon.

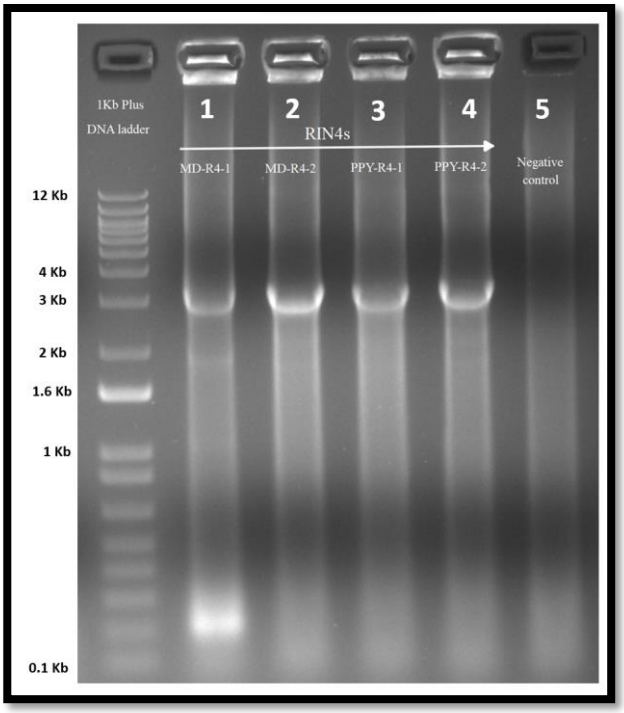

Figure 6.6: Gel electrophoresis of colony PCR of *Agrobacterium* colonies harbouring *Malus* and *Pyrus* RIN4 expression clones. The annotations are as follows: 1 = *Mxd*RIN4-1, 2 = *Mxd*RIN4-2, 3 = *Pb*RIN4-1; 4 = *Pb*RIN4-2, 5 = Negative control.

6.3.3 Analysis of RPA1 HR triggering ability with *Malus* and *Pyrus* RIN4s and Eop1s in *Nicotiana tabacum* via sequential and co-infiltration

In the previous experiments, it was discovered that both co-infiltration and sequential infiltration with the MES buffer could not be used for the interaction analysis (see section 4.3.3); however, the complementation ability of the *Malus* and *Pyrus* RIN4 was assessed with Eop1s in *Nicotiana tabacum* through sequential and co-infiltration[65] before employing the three-component co-infiltration combination system that was conceptualised and developed, as described in section 4.2.3 and tested to be effective in section 4.3.5.

[65] Note: The analysis was performed before developing the 'three component co-infiltration combination system'.

6.3.3.1 Analysis of the complementation ability of *Malus* and *Pyrus* RIN4 in RPA1-mediated HR in *N. tabacum* via sequential infiltration

First, a nucleotide sequence alignment analysis (as described in section 6.2.6) was performed to analyse if the 'hp-*NbRIN4'* hairpin construct could target and silence the *Malus* or *Pyrus RIN4* gene, which could jeopardise the results obtained from the analysis. The analysis revealed that the hp-*NbRIN4* sequence share less than 54% sequence identity with *Malus* or *Pyrus RIN4* genes, with no continuous segment in the gene matching for more than 10 bp (Supplementary Figure ACF1). Consequently, it was deduced that hp-*NbRIN4* would not silence the *Malus* and *Pyrus RIN4s*. Following this, *Malus* and *Pyrus* RIN4 complementation analysis was performed.

In sequential infiltration, the *Agrobacterium* harbouring expression clones for the *Nt*RIN4 silencing construct (pTKO2: hp-*NbRIN4*) were first administered into the *N. tabacum* leaves at the concentration of 3.2 x 10^8 CFU/mL (OD_{600}: 0.4). Next, a premix of *Agrobacterium* harbouring expression clones for Eop1 at 8 x 10^7 CFU/mL (OD_{600}: 0.1), and *Malus* and *Pyrus* RIN4 separately at 3.2 x 10^8 CFU/mL (OD_{600}: 0.4) concentration was infiltrated at two days interval. The *Agrobacterium* cells in both infiltrations were suspended in 10 mL of infiltration buffer composed of 10 mM of MES and MgCl2. As observed in the results from previously conducted sequential infiltration experiments described in section 4.3.3.2, no HR was observed upon infiltrating the *RIN4* and *Eop1 Agrobacterium* premix at 2 dpi after primary infiltration of *Agrobacterium* carrying pTKO2: hp-*NbRIN4* (Figure 6.7).

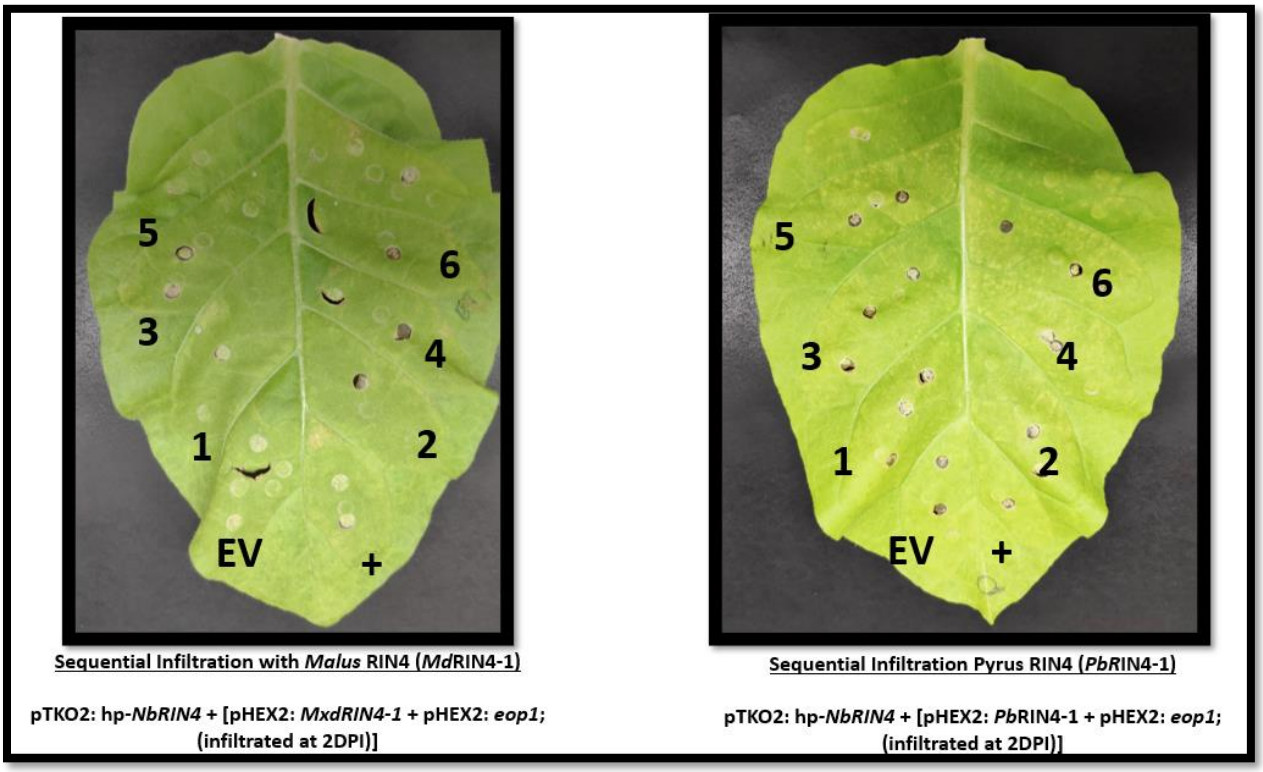

Figure 6.7: Analysis of RPA1 HR triggering ability with *Malus* and *Pyrus* RIN4s via sequential infiltration. The infiltrations administered in the leaf segments are mentioned below the leaf images. The annotations are as follows: EV = pHEX2: Empty Vector (negative control for HR; OD_{600}: 0.1); '+' = Eop1: *Ea*246 (positive control for HR; OD_{600}: 0.1); 1 = Eop1: *E. pyrifoliae* str. Ep1/96; 2 = Eop1: *E. amylovora* str. Ea246; 3 = Eop1: *E. amylovora* str. Ea262; 4 = Eop1: *E. tasmaniensis* str. Et1/99; 5 = Eop1: *E. tracheiphila* str. MDcuke; 6 = Eop1: *Pantoea vagans* str. C9-1. The presented results were validated by repeating the experiment twice with 3 replications. The image was taken at 4 dpi.

6.3.3.2 Analysis of the complementation ability of *Malus* and *Pyrus* RIN4 in RPA1-mediated HR in *N. tabacum* via co-infiltration

In the co-infiltration analysis with *Malus* and *Pyrus* RIN4 (Figure 6.8), a premix composed of *Agrobacterium* harbouring expression clones for *Nb*RIN4 silencing construct (pTKO2: hp-*NbRIN4*) at the concentration of 3.2 x 10^8 CFU/mL (OD_{600}: 0.4), Eop1 at 8 x 10^7 CFU/mL (OD_{600}: 0.1), and *Malus* and *Pyrus* RIN4 separately at 3.2 x 10^8 CFU/mL (OD_{600}: 0.4) concentration, suspended in 10 mL infiltration buffer (10 mM MES and 10 mM MgCl2) was infiltrated in 3-4 weeks old leaves of *N. tabacum*. The Eop1 variants that triggered HR, as described in section 2.3.3.1, also elicited HR in the current co-infiltration analysis (Figure 6.8). However, as described in section 4.3.3.1, the HR is more likely due to ineffective silencing of the resident *NtRIN4*. Thus, it was deduced that it would be necessary to replicate the co-infiltration experiment by employing the 'three-component co-infiltration system' in combination with EGTA (5 mM) infiltration buffer as described in section 4.2.3 (Figure 4.2; sub-figure 3); however, these experiments were not performed due to a limited time frame.

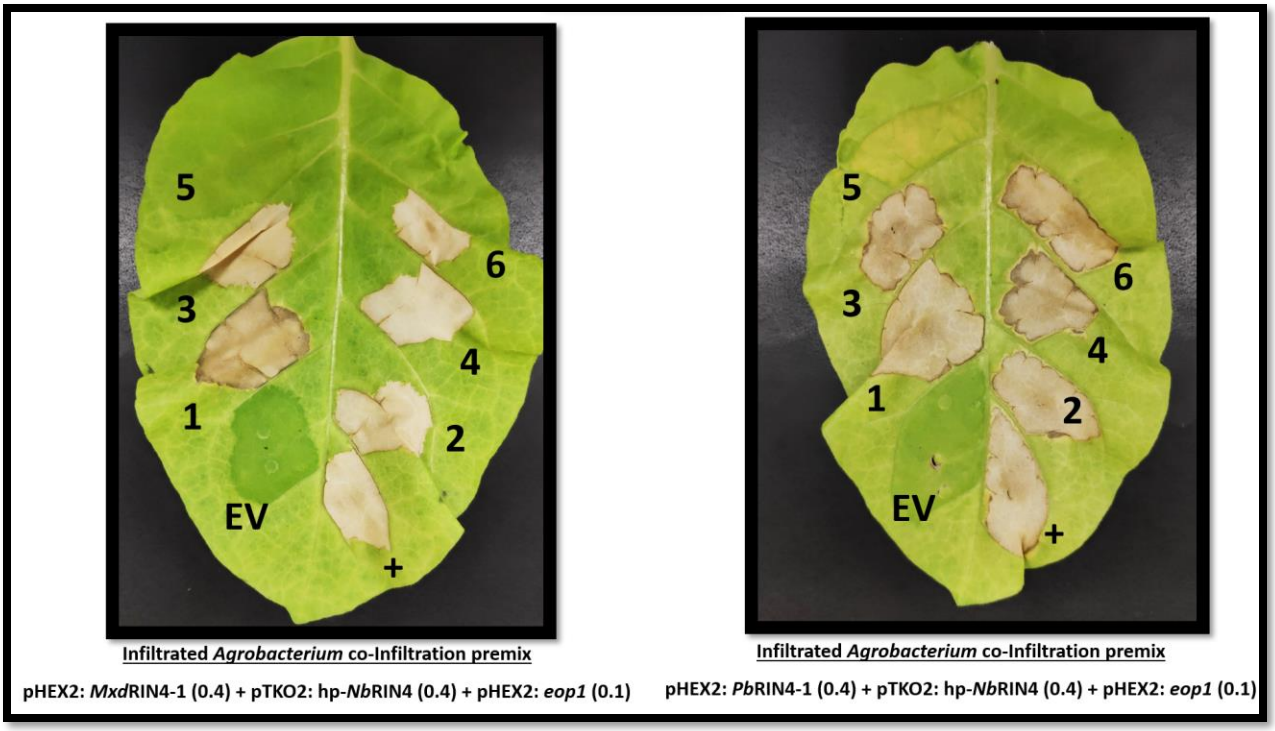

Figure 6.8: Analysis of RPA1 HR triggering ability with *Malus* and *Pyrus* RIN4s via co-infiltration. The infiltration combinations administered in the leaf are mentioned below the images. The annotations are as follows: EV = pHEX2: Empty Vector (negative control for HR; OD_{600}: 0.1); '+' = Eop1: *Ea*246 (positive control for HR; OD_{600}: 0.1); 1 = Eop1: *E. pyrifoliae* str. *Ep*1/96; 2 = Eop1: *E. amylovora* str. *Ea*246; 3 = Eop1: *E. amylovora* str. *Ea*262; 4 = Eop1: *E. tasmaniensis* str. *Et*1/99; 5 = Eop1: *E. tracheiphila* str. MDcuke; 6 = Eop1: *Pantoea vagans* str. C9-1. The presented results were validated by repeating the experiment twice with 3 replications. The image was taken at 4 dpi.

Note: Since the research presented in the current chapter was only partially completed and required additional experiments, no 'major deductions or conclusions' were made; however, the main findings have been reported in the results, along with a brief description of the significance of the findings.

Appendix

Supplementary material: Chapter 2

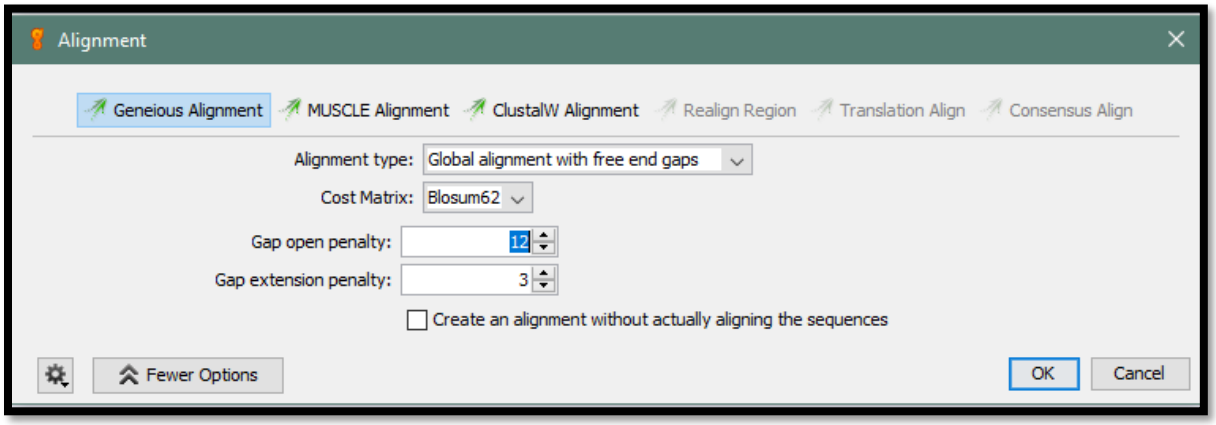

Figure C2S1: The protein sequence alignment parameter used in Geneious software Version 10.2.5.

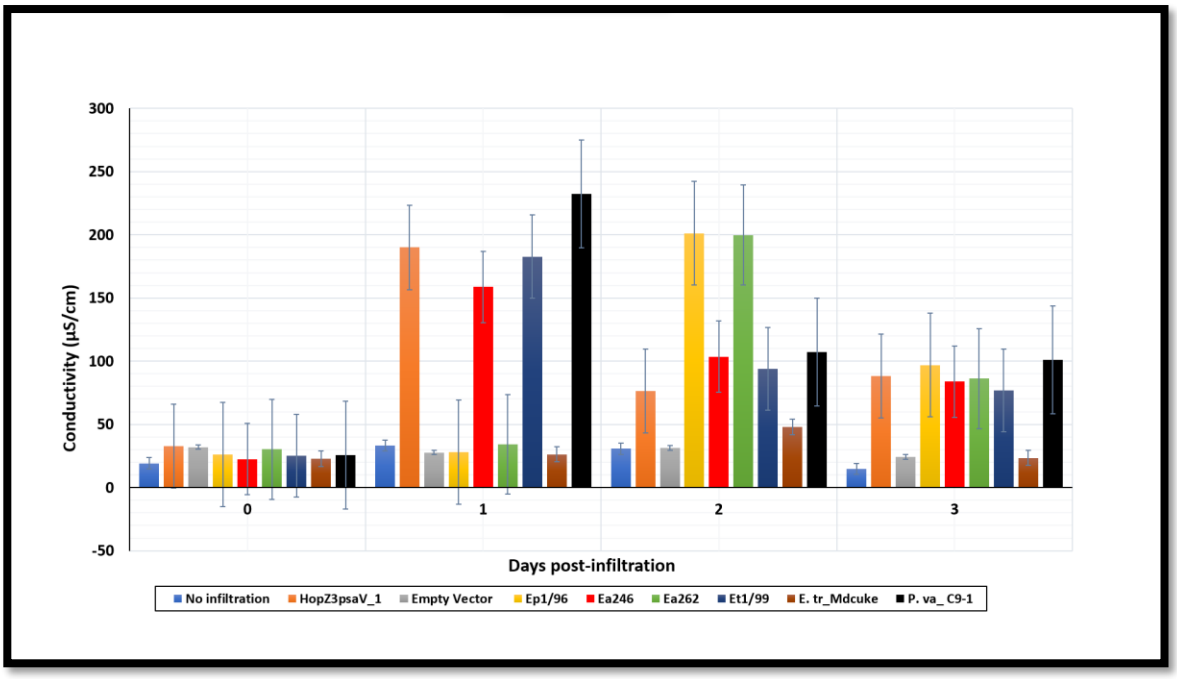

Figure C2S2: Bar chart of electrolyte leakage data from *N. tabacum* leaf discs infiltrated with *Agrobacterium tumefaciens* (OD_{600}: 0.1) carrying the *eop1* gene in an expression clone. The graph is plotted based on the mean value from four replicates for each tested sample on the

indicated days; error bars indicate the standard error from the replicates (see section 2.2.11.3 for the procedure).

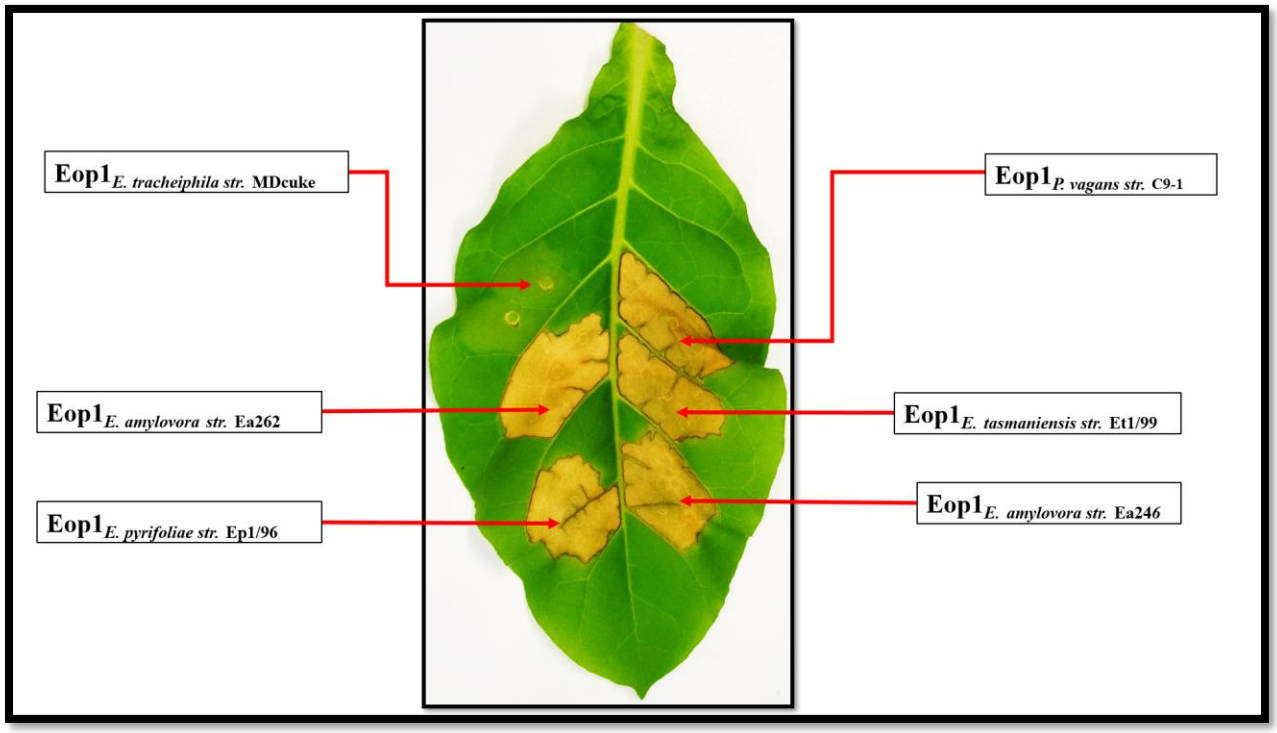

Figure C2S3: Transient expression analysis of the Eop1 variants in *N. tabacum* cv. W38. The Eop1-induced HR followed the same trend as described in section 2.3.3.

Supplementary material: Chapter 3

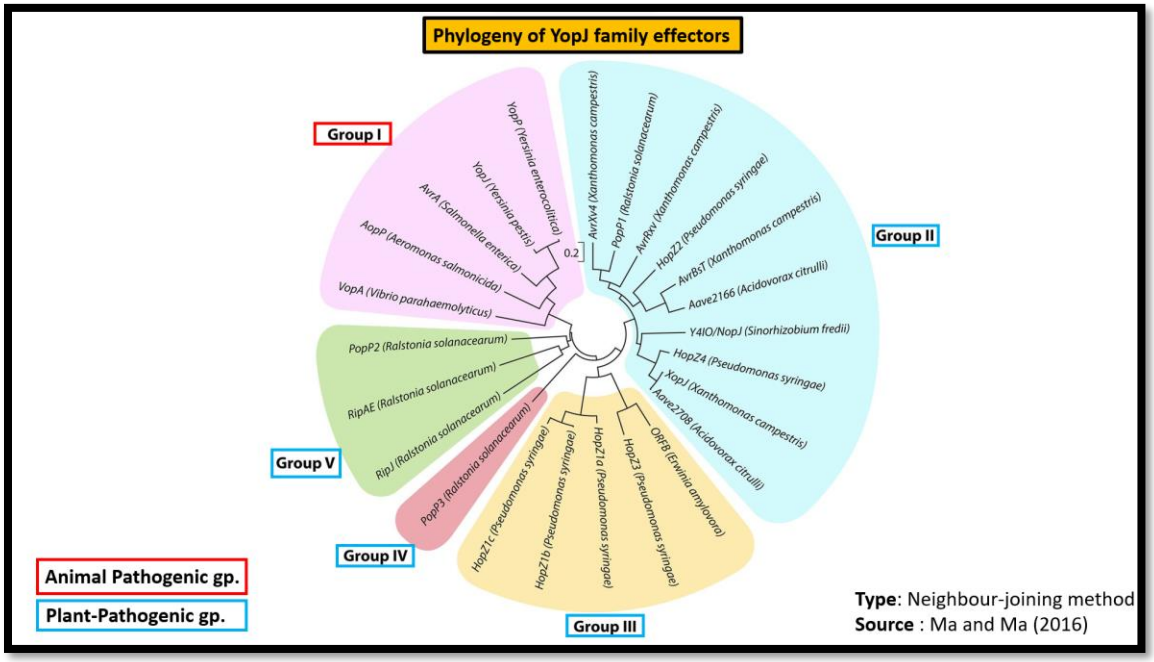

Figure C3S1: YopJ family effectors phylogeny. The phylogenetic tree was generated with MEGA7 using the neighbour-joining method with full-length protein sequences of 24 YopJ family effectors. The image was adapted from Ma & Ma (2016) and slightly modified.

Figure C3S2: Protein sequence alignment of Eop1 variants and the controls: HopZ1a and HopZ3*psa*_V1. The catalytic residues are colour coded and annotated as histidine (H) = red, glutamic acid (E) = green, cysteine (C) = yellow, and putative cysteine-substituting 'secondary nucleophile' = black (S249, S281 and S289).

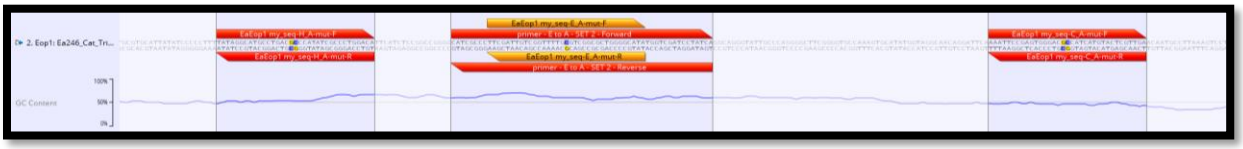

Figure C3S3: GC graph representing GC content of the mutagenic primers and region surrounding the catalytic triad residues. The blue line in the graph corresponds to the GC content.

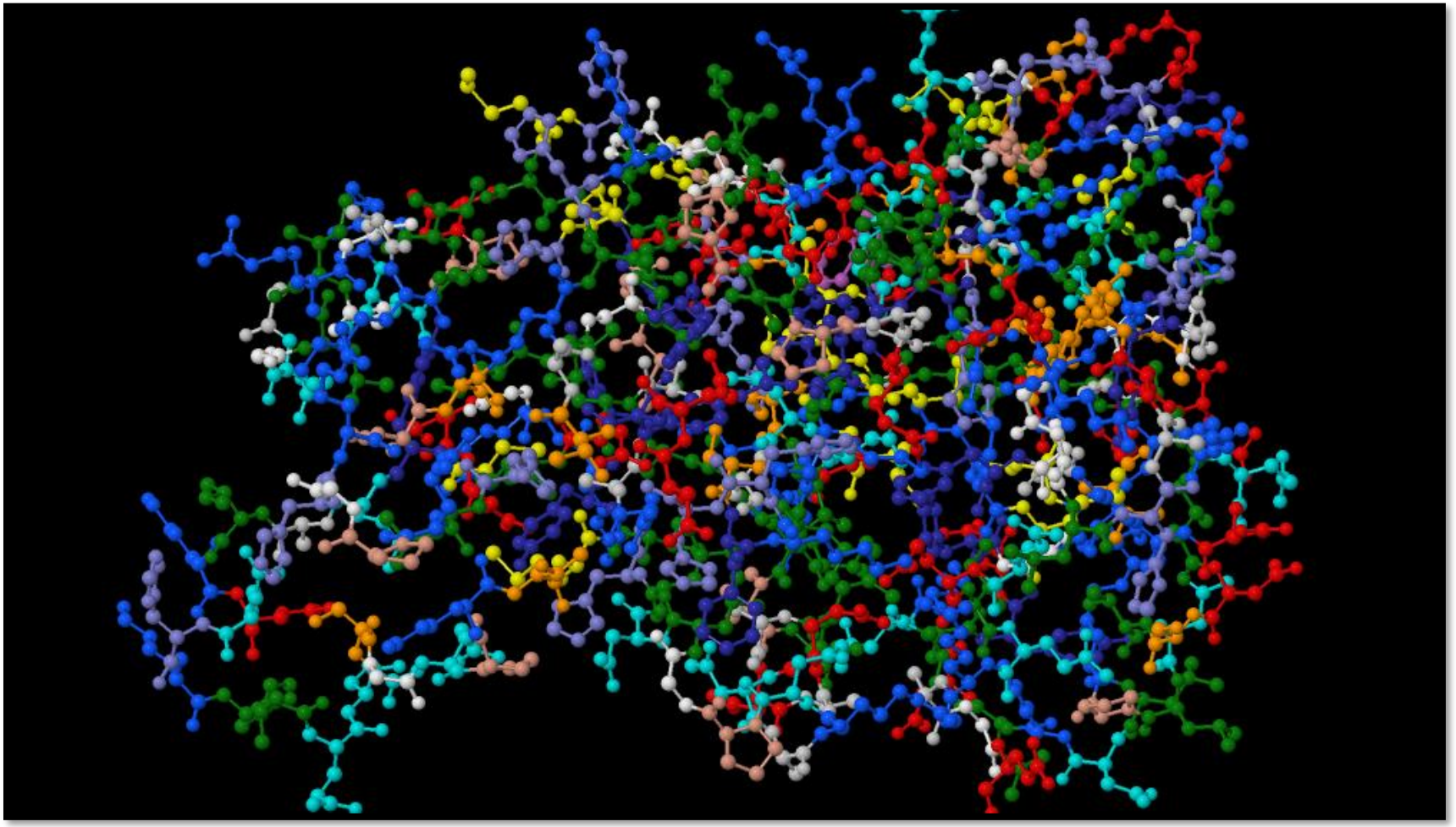

Figure C3S4: Phyre2 predicted model of Eop1: *Ea*246.

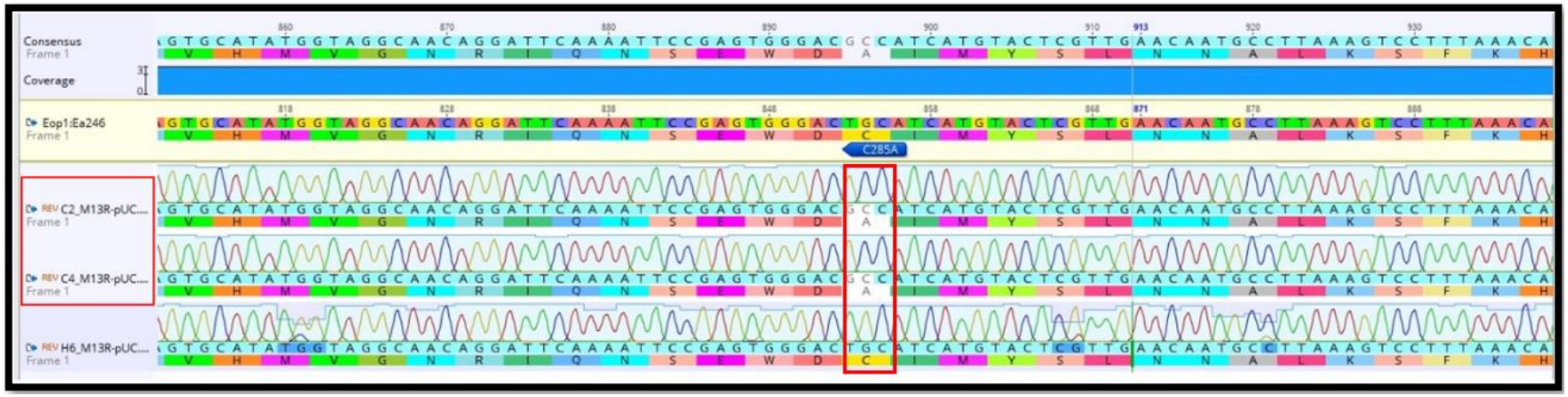

Figure C3S5: Analysis of *Ea*246: C285A mutation sequencing results. The relevant mutated sequences and residue (C285A) are enclosed in the red box.

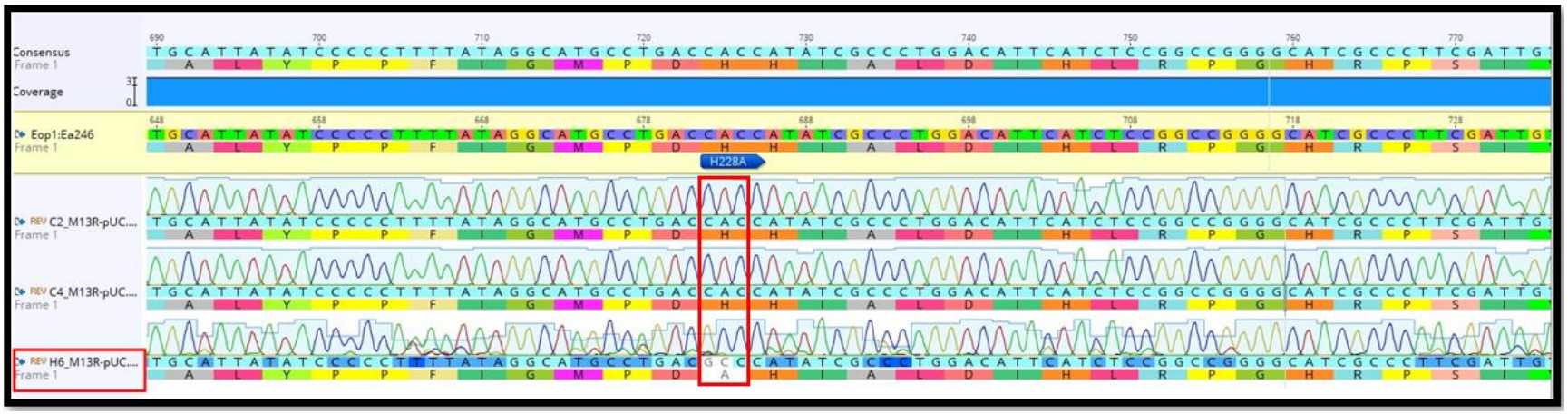

Figure C3S6: Analysis of *Ea*246: H228A mutation sequencing results. The relevant mutated sequence and residue (H228A) are enclosed in the red box.

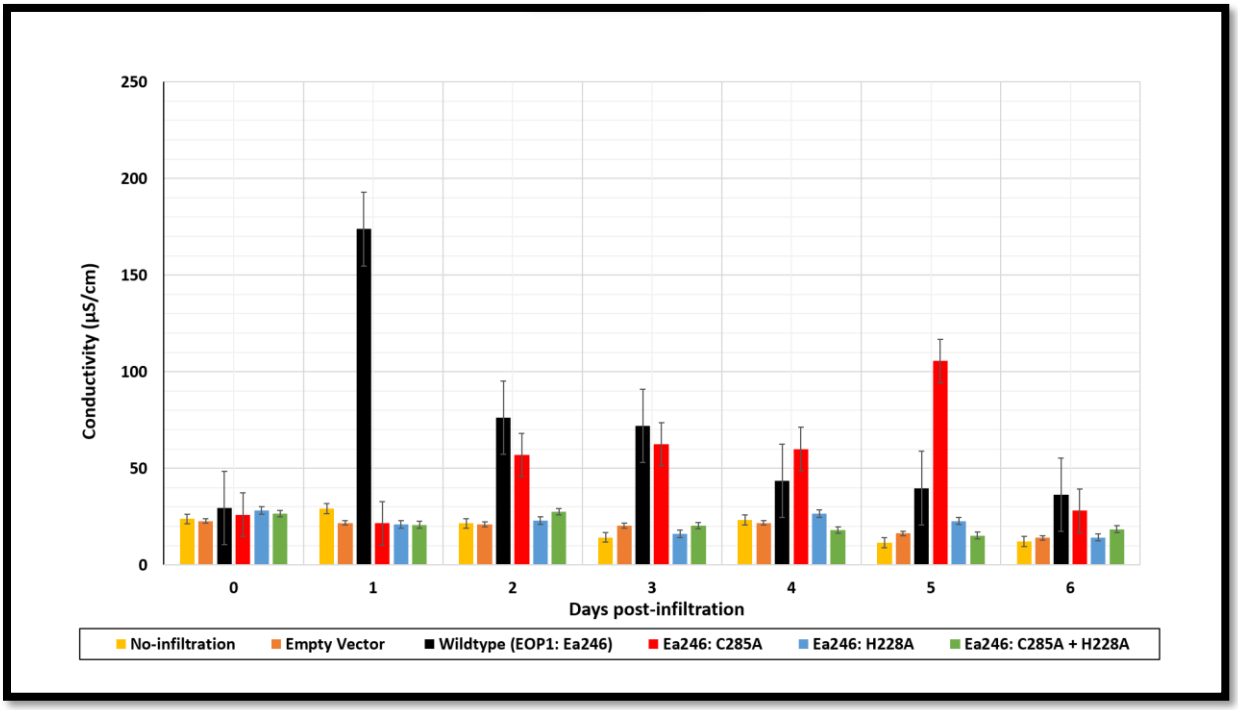

Figure C3S7: Bar chart of electrolyte leakage data from *N. tabacum* leaf discs infiltrated with *Agrobacterium tumefaciens* harbouring the expression clones for Eop1: *Ea*246 catalytic triad mutants. *Agrobacterium* was infiltrated at the OD_{600} of 0.1 (approx. 1 x 10^8 CFU/mL). The graph was plotted based on the mean value of four replicates from different leaves for each sample on the indicated days. MS Excel 2019 software was used for the plotting; error bars indicate the standard error from the replicates.

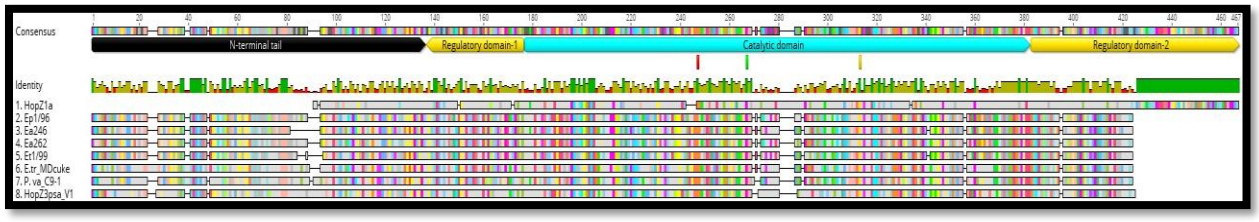

Figure C3S8: Analysis of the conserved domains in the tested Eop1 variants and the controls: HopZ1a and HopZ3*psa*_V1. The domains are annotated above the sequences and colour-coded as follows: Black = N-terminal tail; Yellow = Regulatory domains 1 and 2 (at far left and right, respectively); Cyan = catalytic domain. The catalytic triad residues are annotated below the domain annotations and are colour-coded: histidine = red, glutamic acid = green, and cysteine = yellow.

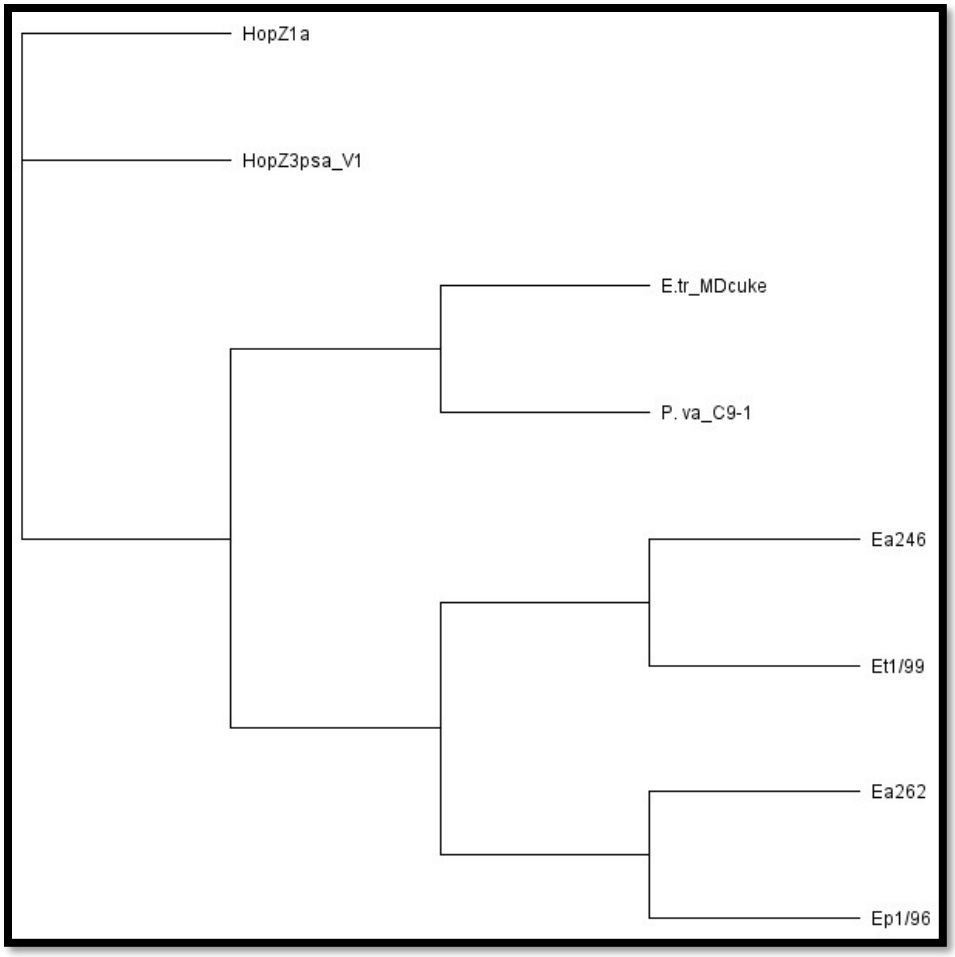

Figure C3S9: Phylogenetic tree of the tested Eop1 variants and the controls: HopZ1a and HopZ3*psa*_V1. The tree was generated using Genious 2018: V10.2.5 using the neighbour-joining method with full-length protein sequences.

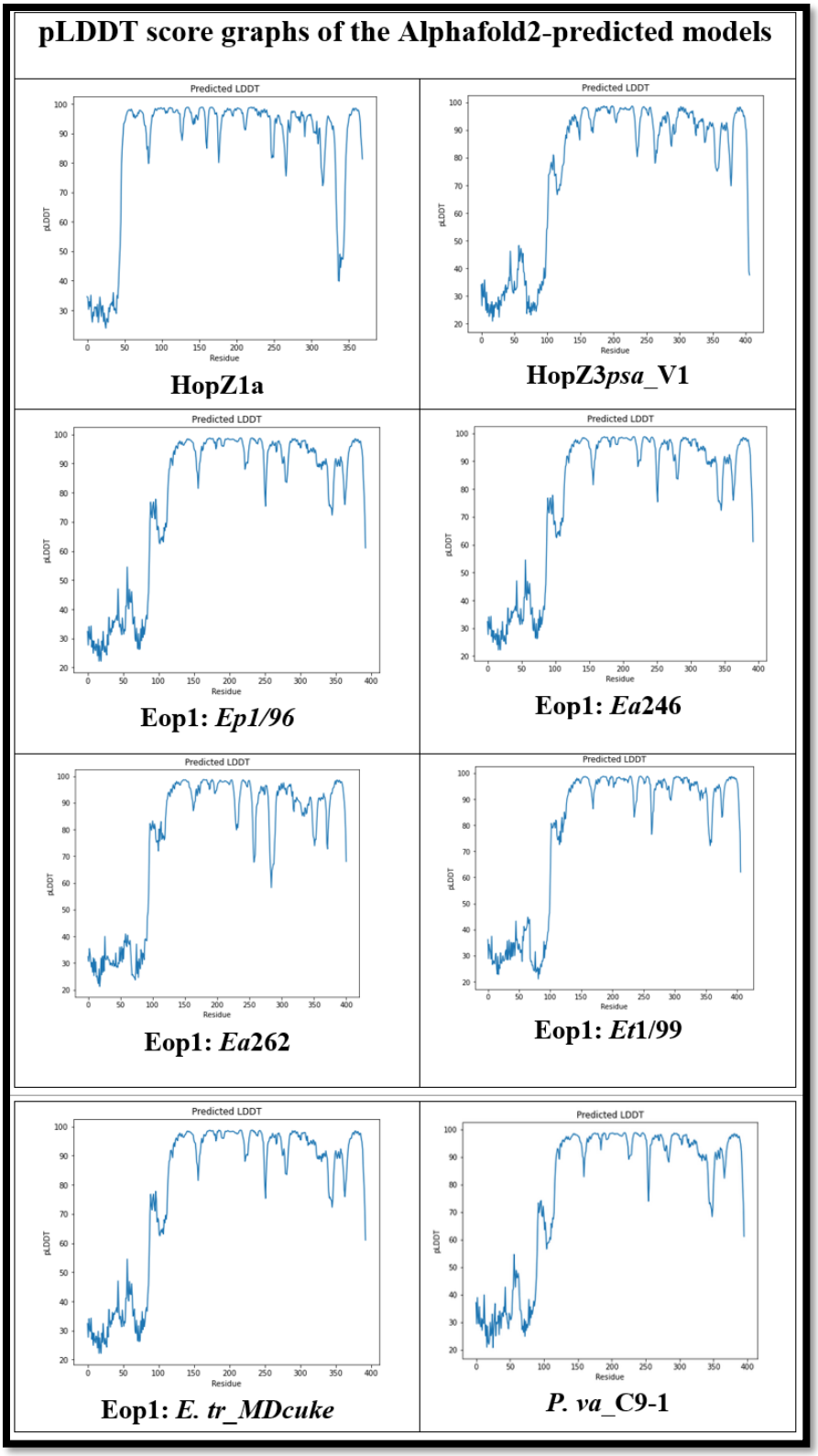

Figure C3S10: The pLDDT score graphs of the AlphaFold2 predicted *in-silico* models of Eop1 variants, HopZ1a and HopZ3*psa*_V1.

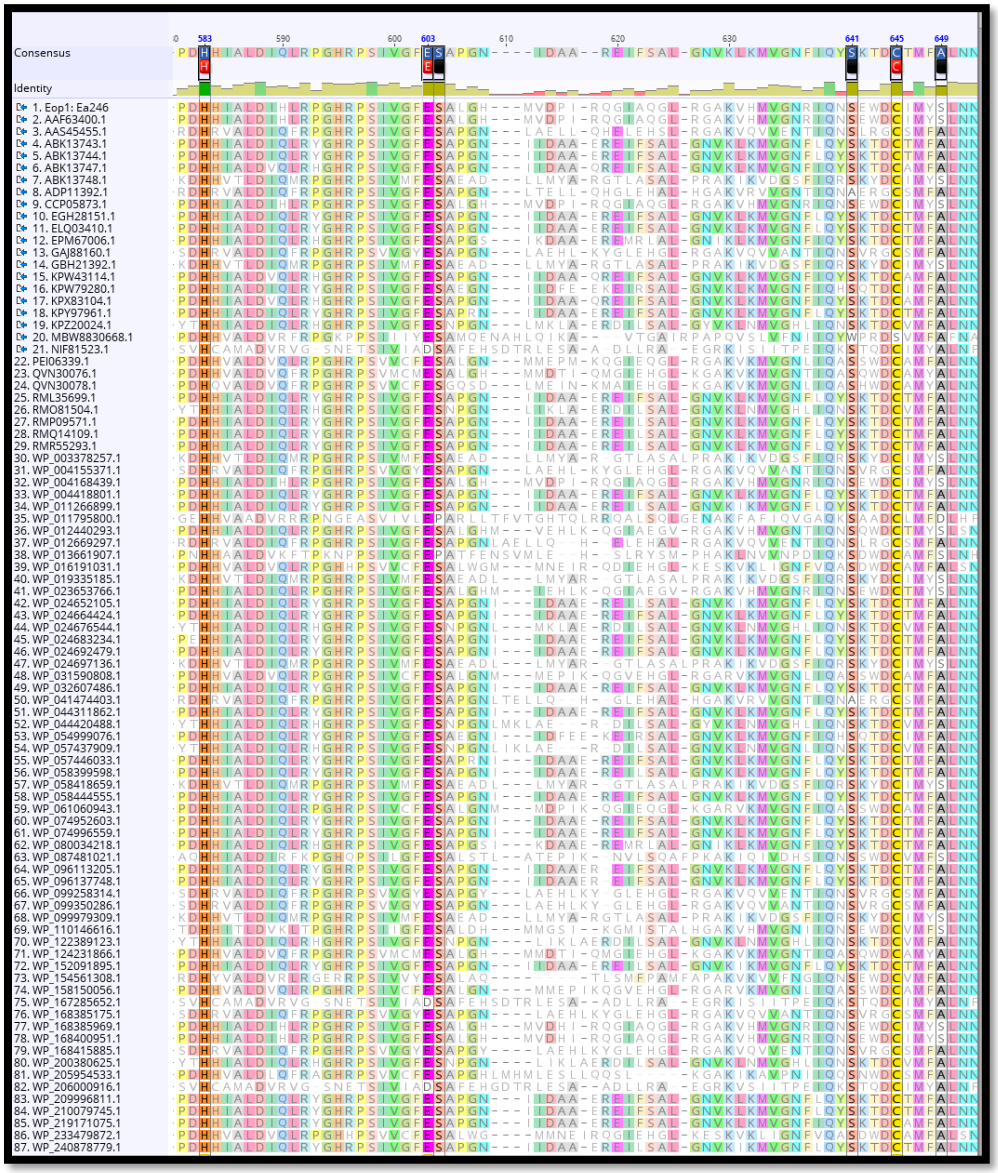

Figure C3S11: Conservation analysis of the 'putative secondary nucleophile' residues in Eop1: *Ea*246 protein sequence homologs retrieved from the NCBI database through BLASTp. The red boxes in the image below the consensus sequence represent the catalytic triad residues: H/E/C, from left to right, respectively. The black boxes represent 'putative secondary nucleophiles', with conservation rates[66] as follows: 97.6% (S249), 96.5% (S281), and 22% (S289) (see footnote '66' for the equation used to calculate the conservation rates of the residues).

[66] **Equation:** sequences with conserved residues / total no. of sequences X 100
[Sequences with Conserved residues = Total number of sequences – sequences with unconserved residues].

Supplementary material: Chapter 4

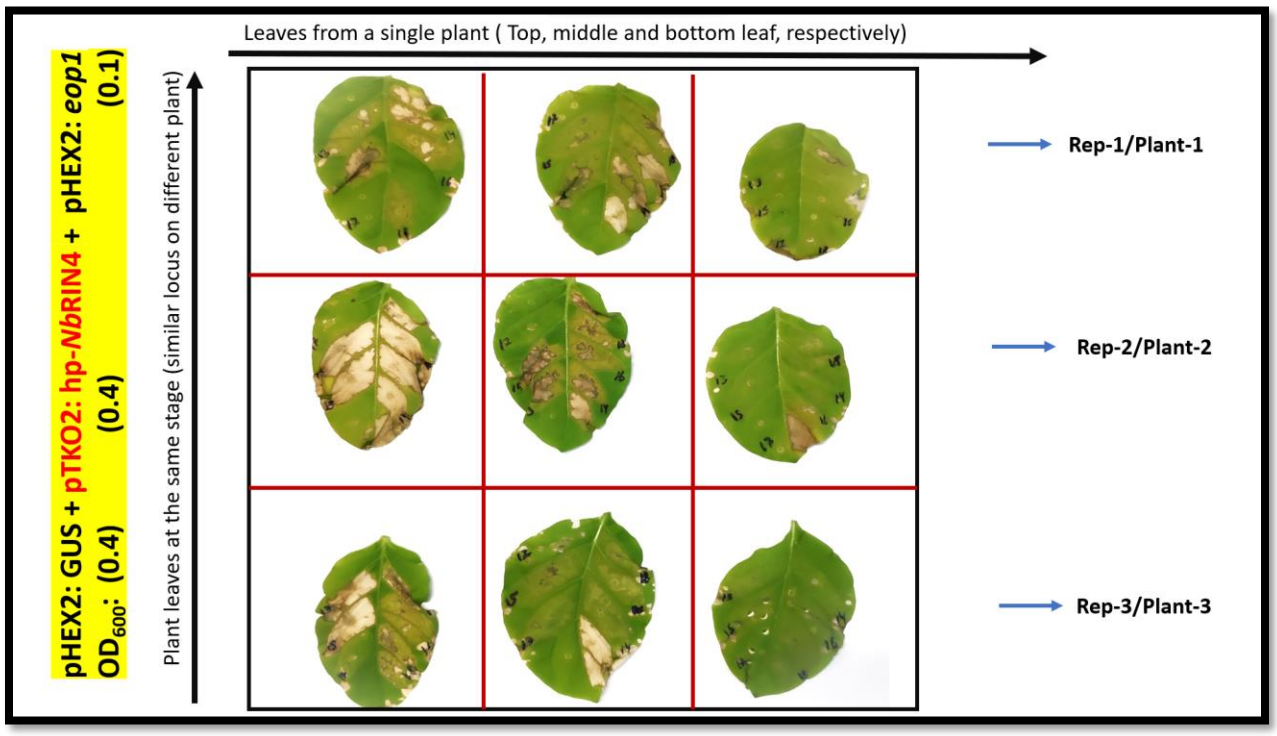

Figure C4S*1*: Preliminary result of Eop1-RIN4 interaction analysis, tested by employing the three-component co-infiltration combination system (as described in Figure 4.2; sub-figure 2) with EGTA (5 mM) in *Nicotiana tabacum*. The co-infiltration premixes administered in the leaves, along with the *Agrobacterium* concentration (OD_{600}) and its corresponding expression clones, are described and highlighted on the left of the image. The Eop1 variants were infiltrated in the same patterns as illustrated in Figure 4.17. The experiment was replicated thrice with similar results. The images were taken at 4 dpi; (Note: The figure attempts to represent the variation observed within the replicate and among the replications).

Supplementary material: Chapter 5

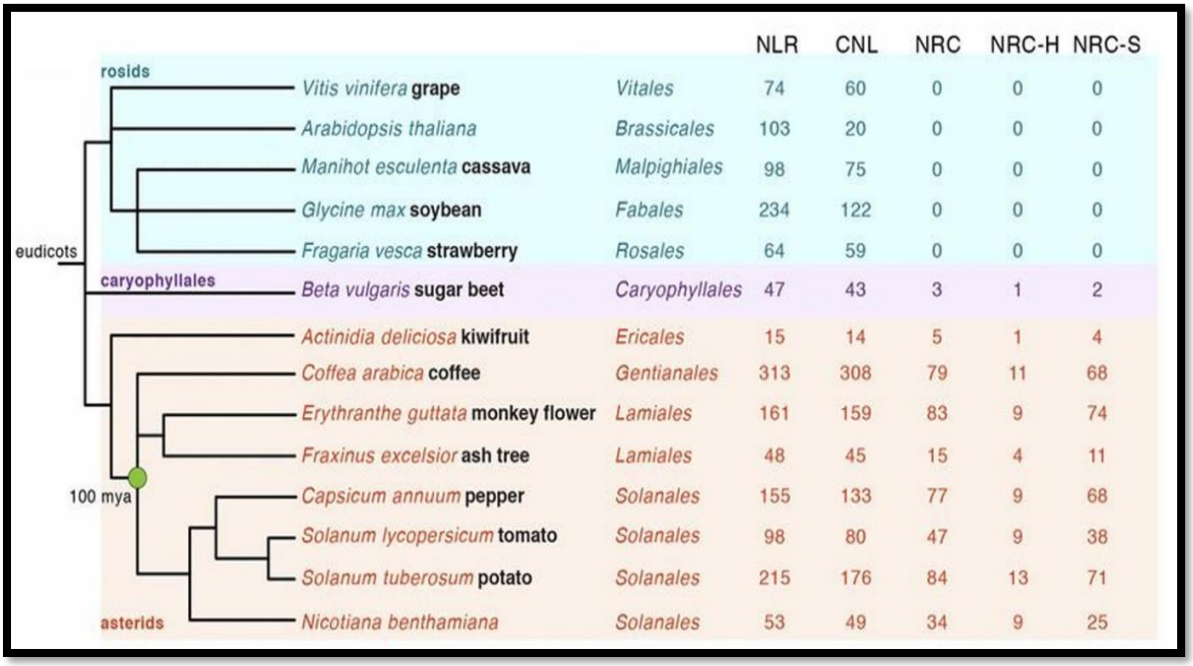

		NLR	CNL	NRC	NRC-H	NRC-S
Vitis vinifera **grape**	*Vitales*	74	60	0	0	0
Arabidopsis thaliana	*Brassicales*	103	20	0	0	0
Manihot esculenta **cassava**	*Malpighiales*	98	75	0	0	0
Glycine max **soybean**	*Fabales*	234	122	0	0	0
Fragaria vesca **strawberry**	*Rosales*	64	59	0	0	0
Beta vulgaris **sugar beet**	*Caryophyllales*	47	43	3	1	2
Actinidia deliciosa **kiwifruit**	*Ericales*	15	14	5	1	4
Coffea arabica **coffee**	*Gentianales*	313	308	79	11	68
Erythranthe guttata **monkey flower**	*Lamiales*	161	159	83	9	74
Fraxinus excelsior **ash tree**	*Lamiales*	48	45	15	4	11
Capsicum annuum **pepper**	*Solanales*	155	133	77	9	68
Solanum lycopersicum **tomato**	*Solanales*	98	80	47	9	38
Solanum tuberosum **potato**	*Solanales*	215	176	84	13	71
Nicotiana benthamiana	*Solanales*	53	49	34	9	25

Figure C5S1: An account of the phylogeny of the identified NLRs in different plant species. The image was reproduced from Wu et al. (2017).

Supplementary material: Chapter 6 (Additional research)

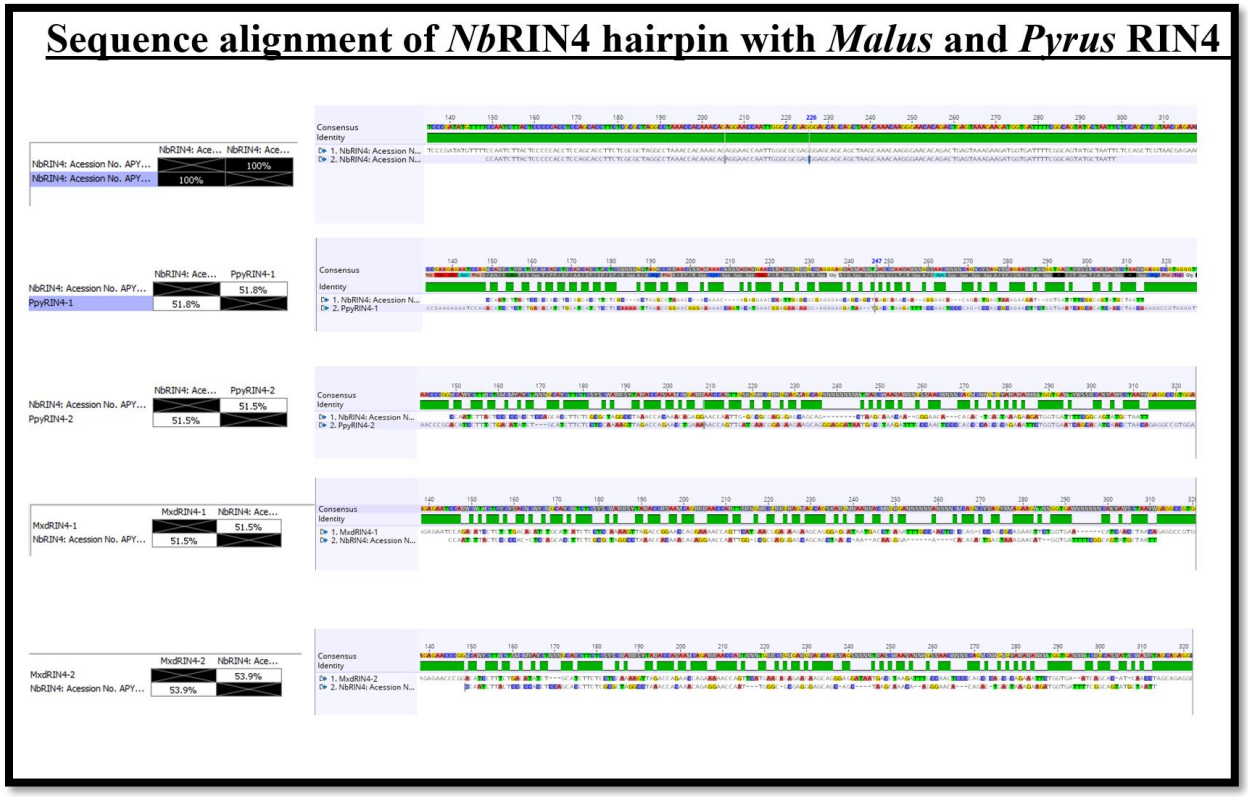

Figure ACF1: Sequence homology analysis between *NbRIN4* hairpin sequence and *Malus* and *Pyrus RIN4s*. The analysis provided information regarding the potential silencing of the *Malus* and *Pyrus RIN4s* in the co-infiltration analysis (performed as described in section 6.3.3.2). The investigation revealed that the 'hp-*NbRIN4'* sequence has less than 54% sequence identity with the *Malus* and *Pyrus RIN4s*, and no segment in the gene matches continuously for more than 10 bp. Consequently, it was deduced that the 'hp-*NbRIN4'* sequence is not likely to silence the *Malus* and *Pyrus* RIN4s.

Research reports

Based on the presented research work, two research reports[67] were submitted to the Pear Research Institute, RDA, Republic of Korea (the funding agency). The research reports can be provided upon request.

[67] One of the two research reports provided to Pear Research Institute was solely drafted by the author of the thesis. However, another report was drafted via collective efforts from Erik HA Rikkerink, Vincent GM Bus and Vishant Tomar.

Vector maps

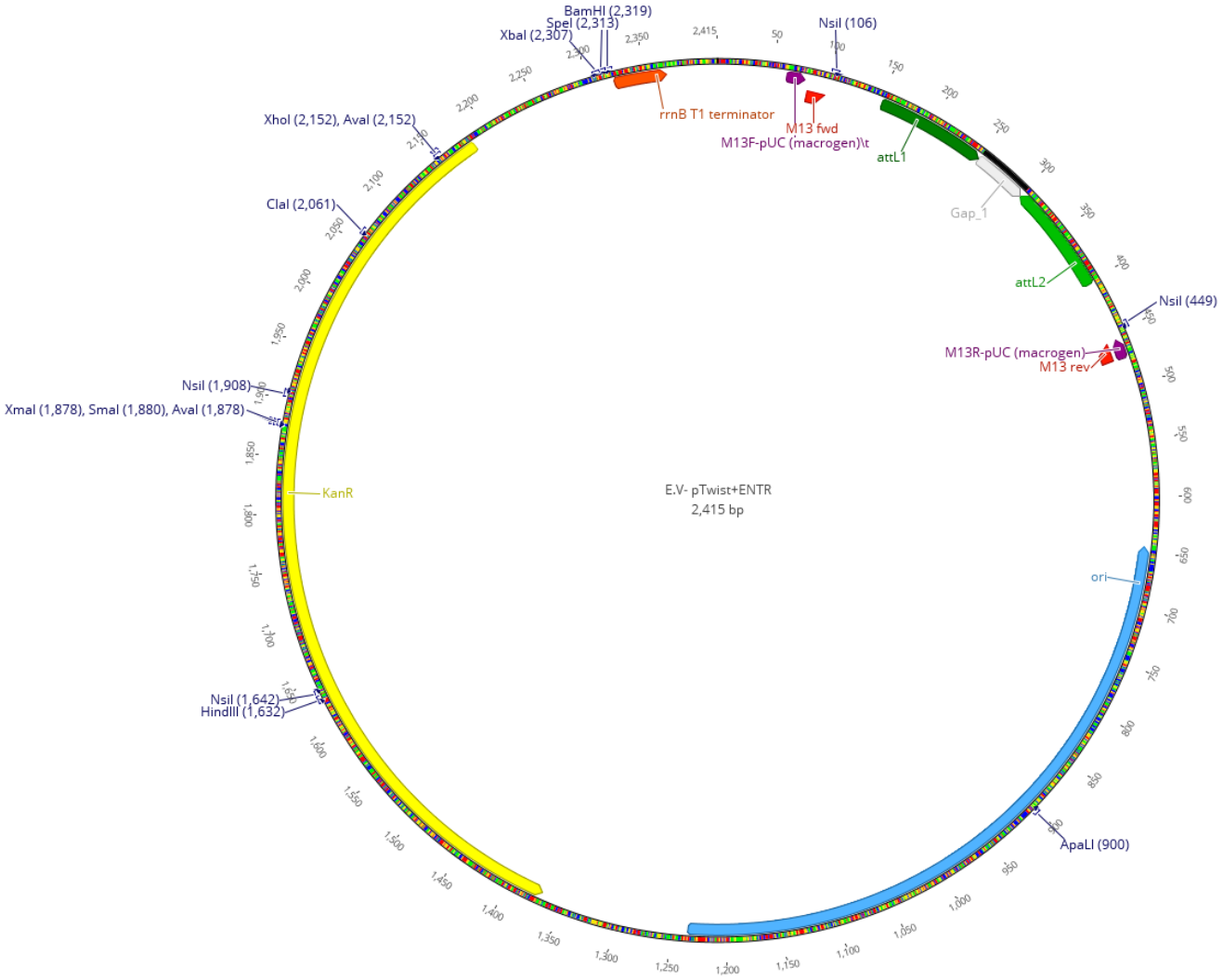

Figure VM1: Plasmid map of Entry Vector (pTwist+ENTR)

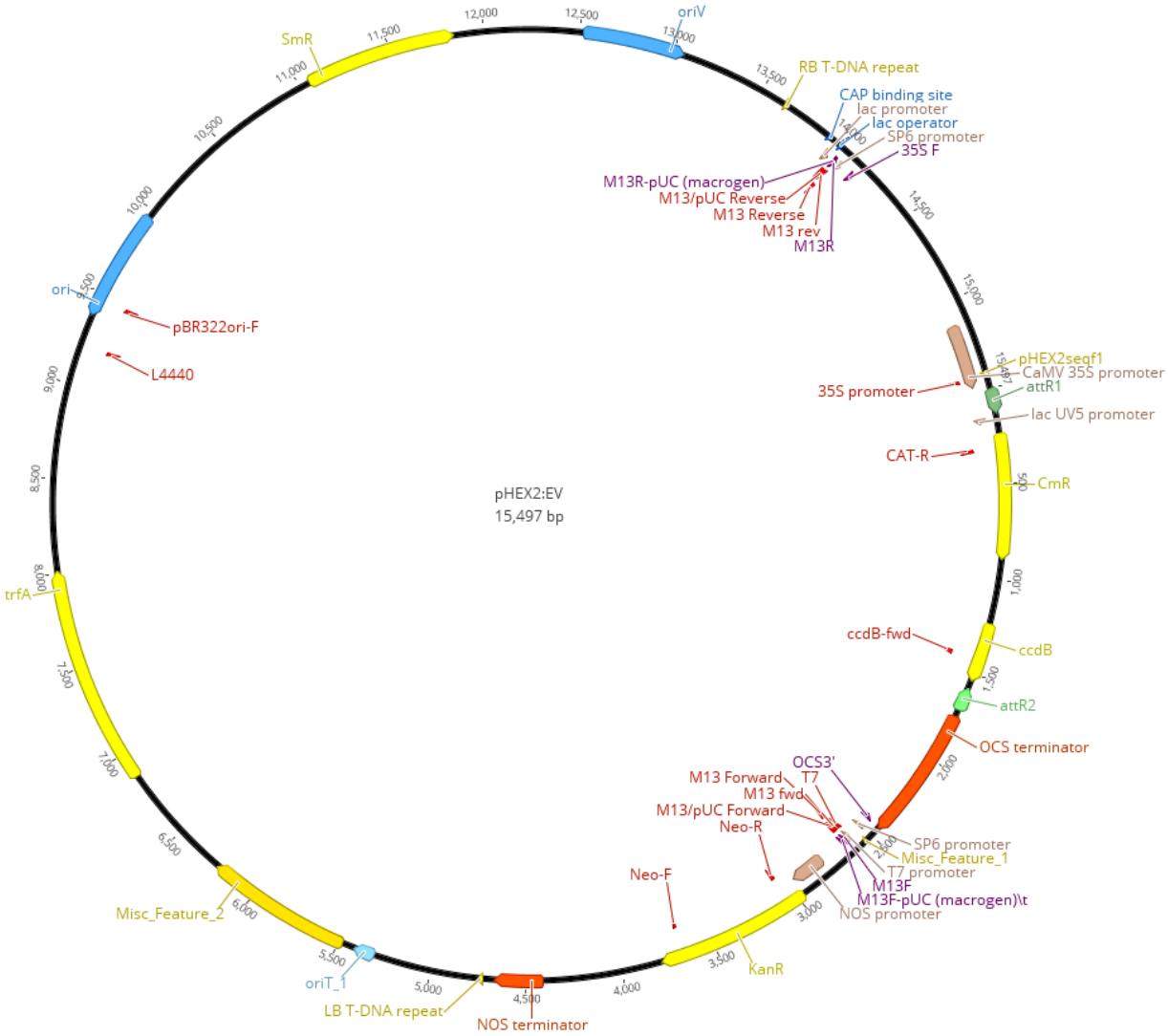

Figure VM2: Plasmid map of Expression Vector (pHEX2)

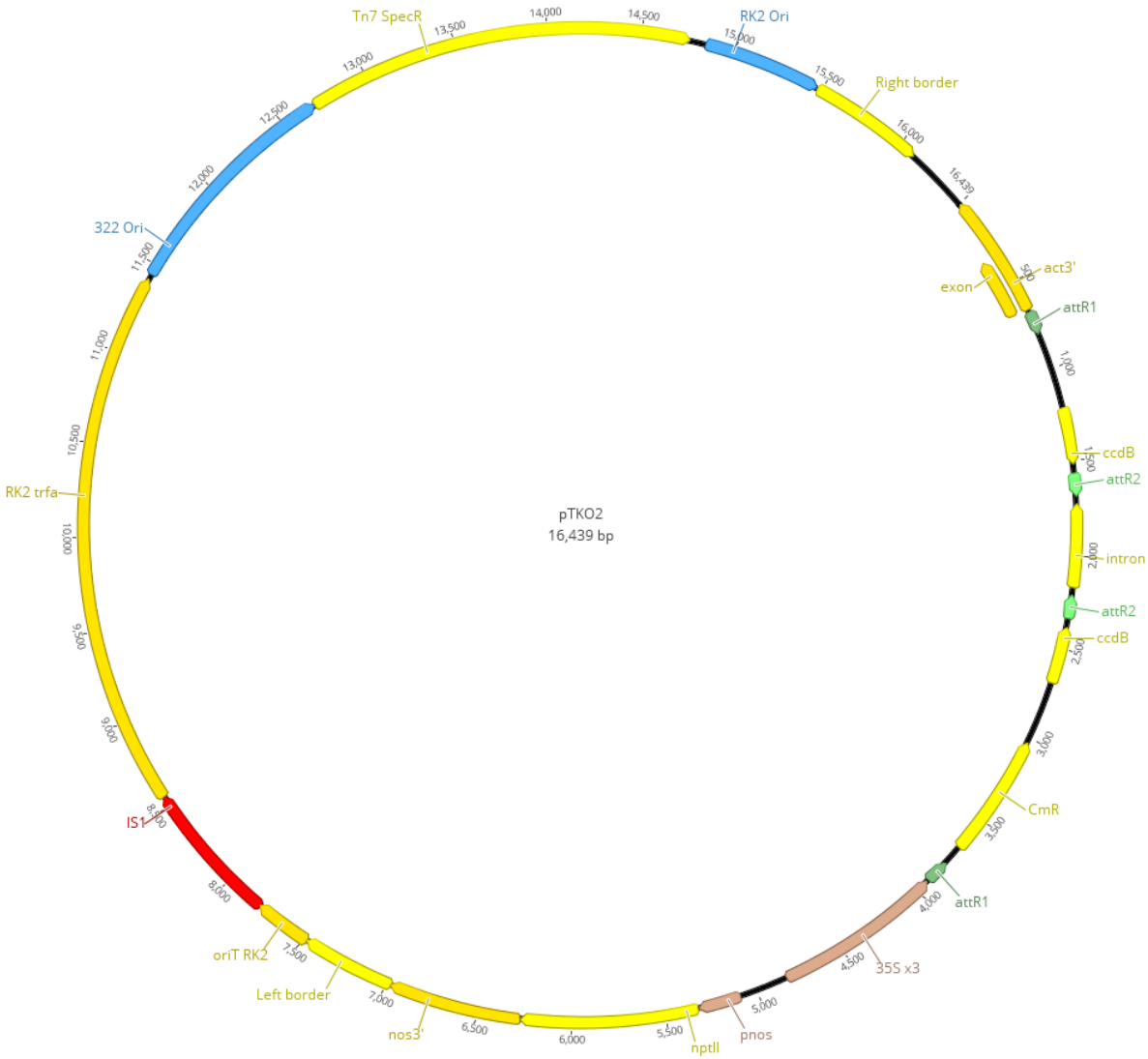

Figure VM3: Plasmid map of the Silencing Vector (pTKO2)

Protein and DNA sequence of the Eop1 variants tested in the study

Erwinia pyrifoliae strain *Ep*1/96 *Eop1* Protein and DNA sequence.

EpEop1	**WP_012669297.1**	***Erwinia pyrifoliae* str. *Ep*1/96**

Protein sequence-

MNVSGLRAGQRSPSQQADHAPSSSTQASPAQTGRRLQRQDALPANNRYHASQTPATPDRARAAARYASGA
SSSAAPAAGPAGPSMALSRQHANRENPTFARFHDAMQQSPKMLRASPVPEKPEKIPERLQQKADAIDLPG
LKKLDKSLYEYAKLATELVKEGAGPDNDLADMDRKLLPLLADAENARNPGLNLRTFKSSEECYRAIKDQN
KSVQQSRQPMSMRVLYPPLKGARDHRVALDIQFRPGHRPSIVGFESAPGNLAELLQHELEHALRGAKVQV
VENTIQNSLRGCSMFALNNALKSFKHHDEYTARLHSGEKQVPVPAEFLKHAHSKALVEGHRHQDAIVSKD
KGGLHAETLLHRNLAYRADRINHSYSTSIEGFRLQEIQRAGEFLAARKQRR

DNA sequence

ATGAATGTATCTGGTTTGAGGGCTGGGCAAAGAAGCCCGTCCCAGCAAGCGGATCACGCTCCTTCTTCAT
CGACACAGGCCTCACCGGCGCAGACGGGCAGACGGTTGCAGCGGCAGGACGCGCTGCCTGCTAACAACCG
CTATCATGCCAGCCAGACGCCCGCGACGCCGGATCGTGCGCGCGCAGCCGCCAGATACGCATCGGGGGCC
AGCTCTTCGGCGGCGCCTGCTGCCGGGCCCGCTGGCCCATCTATGGCGCTATCTCGTCAGCACGCTAACC
GTGAAAACCCGACGTTTGCCCGTTTTCATGATGCGATGCAGCAGTCCCCTAAAATGTTGCGCGCCAGCCC
CGTGCCGGAAAAGCCGGAGAAGATCCCCGAGCGCCTGCAGCAAAAGGCCGACGCCATCGATTTGCCAGGG
TTAAAGAAACTGGATAAAAGCCTGTACGAATATGCCAAACTGGCGACCGAACTGGTCAAGGAAGGAGCGG
GACCCGATAACGACCTCGCTGATATGGATAGAAAGCTACTGCCGCTGCTGGCCGATGCGGAAAACGCGCG
TAACCCGGGGCTGAATCTGCGCACTTTTAAGAGCAGCGAAGAGTGCTACCGGGCGATAAAGGATCAGAAT
AAAAGCGTACAGCAGTCCAGGCAGCCGATGTCTATGCGCGTGCTCTATCCGCCCTTGAAGGGCGCGCGTG
ACCATCGCGTGGCGTTGGACATCCAGTTCCGGCCGGGCCATCGTCCTTCGATTGTGGGTTTTGAGTCCGC
GCCGGGCAATTTGGCTGAGCTTTTGCAACACGAACTTGAACACGCCTTGCGCGGAGCCAAAGTGCAGGTG
GTGGAAAATACGATTCAAAACTCCCTAAGAGGCTGCTCAATGTTTGCTTTGAATAATGCCCTGAAGTCCT
TTAAGCATCATGATGAATACACTGCGCGGCTGCACAGCGGTGAAAAACAGGTTCCCGTTCCCGCCGAATT
TTTAAAGCATGCGCATTCGAAAGCCCTGGTTGAAGGGCACCGGCATCAGGACGCTATCGTCAGCAAAGAT
AAAGGCGGGCTGCATGCCGAAACCCTGCTGCACAGAAACCTGGCCTATCGTGCCGACAGGATCAACCACT
CTTACAGTACCTCGATTGAAGGTTTCCGCCTGCAGGAGATACAGCGGGCAGGTGAATTTTTGGCCGCGCG
AAAACAAAGAAGATAG

Erwinia amylovora strain *Ea*246 Eop1 Protein and DNA sequence		
Eop1Ea246	**AAF63400.1**	***Erwinia amylovora* str. *Ea*246**

Protein sequence

MNISGLRGGYKSQAQQADNASSSSTQGSPAPTGRRLQRQDALPANYRYHASQMPATPERARVAARYASQA
SSSAGPSILLSRQSGHRENPSLVRFHETMQQSPKMSRGDPLPEKPEIVPKRLQEKIDSVNLPRLNKLDKN
LYEYGKMATELAKEGSGSSVALMRMDKKVLPLLADAENARNPGLNLHVYKRGEECYQAIKEQHKIVQQSG
QPKTMRALYPPFIGMPDHHIALDIHLRPGHRPSIVGFESALGHMVDPIRQGIAQGLRGAKVHMVGNRIQN
SEWDCIMYSLNNALKSFKHHDEYTARLHKGEKIPVPAEFFKHAQSKSMVEGLPHQDAIVTKDKGGLHAET
LLHRNLAYRADRFDHACNTSIEGFRMQEIQRAGEFLSAQNRKS

DNA sequence

ATGAATATATCTGGTCTGAGAGGCGGGTACAAAAGCCAGGCACAGCAGGCGGATAACGCCTCTTCCTCAT
CGACACAAGGCTCACCTGCACCGACGGGCAGACGGTTACAGCGGCAGGATGCGCTGCCGGCCAACTATCG
CTATCACGCCAGCCAAATGCCCGCGACGCCGGAACGCGCGCGCGTAGCCGCCAGATATGCATCGCAGGCC
AGCTCTTCGGCGGGCCCTTCGATATTGCTGTCCCGTCAGTCTGGCCATCGCGAGAATCCATCGCTTGTCA
GATTCCATGAAACGATGCAGCAATCCCCTAAGATGTCGCGTGGCGATCCTCTGCCGGAAAAACCAGAGAT
CGTGCCAAAACGTCTGCAGGAGAAGATAGATTCCGTTAATCTGCCACGGTTAAATAAACTGGATAAAAAC
CTGTACGAATACGGCAAAATGGCGACCGAACTGGCAAAAGAAGGATCGGGATCCAGCGTTGCACTGATGC
GCATGGATAAAAAGGTCCTGCCGCTGTTGGCCGATGCGGAAAATGCGCGCAATCCCGGACTCAACCTGCA
TGTCTATAAGCGGGGTGAAGAGTGTTATCAGGCGATAAAGGAGCAGCATAAGATCGTACAGCAGTCCGGG
CAGCCAAAGACGATGCGTGCATTATATCCCCCTTTTATAGGCATGCCTGACCACCATATCGCCCTGGACA
TTCATCTCCGGCCGGGGCATCGCCCTTCGATTGTCGGTTTTGAGTCGGCGCTGGGGCATATGGTCGATCC
TATCAGGCAGGGTATTGCCCAGGGGCTTCGGGGTGCCAAAGTGCATATGGTAGGCAACAGGATTCAAAAT
TCCGAGTGGGACTGCATCATGTACTCGTTGAACAATGCCTTAAAGTCCTTTAAACATCATGATGAGTACA
CGGCCCGCCTGCATAAGGGCGAAAAGATCCCCGTCCCTGCAGAATTCTTTAAACATGCTCAATCGAAATC
AATGGTTGAGGGACTACCGCATCAGGACGCCATTGTGACTAAAGATAAAGGCGGGCTGCATGCCGAAACC
TTGCTGCACAGAAATCTGGCCTATCGCGCCGACAGGTTCGATCACGCTTGCAACACCTCGATTGAGGGCT
TCCGCATGCAGGAAATTCAGCGTGCGGGTGAGTTTCTGTCCGCGCAAAATCGCAAAAGTTAG

Erwinia amylovora strain *Ea*262 Eop1 Protein and DNA sequence

EaEop1a	**AEH03408.1**	***Erwinia amylovora: Ea*262**

Protein sequence

MKLSGLSSGQKSPAQQTDQASSSSTRPSPPPAGRRLQRQDALPTNIRYHAIQVPGTPDRARVATRNASEA
SSSAAPASEHAGPSMALSRQFGNRESPALARFHDALQQSPKTLRANPAPEKPEKVPDRLQQKADAINLPQ
LKKLDKSLYEYAKMATELIKEGAGPDGDLTAMDRKLLPLLADAENARNPGLNLRTFHKTDECYQAIKAQN
KKVQESRQPMSMRAIYPPMRGMSDHRVALDIQFRPGHRPSVVGYESAPGNLAEHLKYGLEHGLRGAKVQV
VANTIQNSVRGCSMFALNNALKSFKHQDEYTARLHSGEKQVPIPAEFFKHAHSKTLIEGHPHKDAIVSKD
KGGLHAETLLHRNLAYRADRTNHSYSTSIEGFRLQEIQRAGEFLAARKQRK

DNA sequence

ATGAAATTATCTGGACTGAGTAGCGGGCAAAAAAGCCCGGCCCAGCAAACGGATCAAGCTTCCTCCTCTT
CAACACGCCCCTCACCTCCACCGGCGGGAAGGCGCTTACAGCGGCAGGACGCGCTGCCCACCAACATCCG
CTATCATGCCATACAGGTACCGGGTACGCCGGATCGCGCGCGCGTAGCCACCCGAAATGCATCGGAGGCC
AGCTCTTCTGCGGCGCCTGCTTCTGAGCACGCTGGCCCATCTATGGCACTATCTCGTCAGTTCGGTAACC
GTGAGAGCCCAGCGCTTGCCCGTTTTCATGATGCGCTGCAGCAATCTCCCAAAACGTTGCGCGCCAACCC
CGCGCCGGAAAAGCCGGAGAAAGTCCCGGATCGCCTGCAGCAAAAGGCAGACGCCATCAATTTGCCACAG
TTAAAGAAACTGGATAAAAGCCTGTACGAATACGCCAAAATGGCGACCGAACTCATAAAAGAAGGAGCGG
GACCCGACGGCGATCTTACTGCAATGGATAGAAAGCTATTGCCGCTACTGGCCGATGCGGAAAACGCACG
TAACCCGGGGCTGAATCTGCGCACTTTTCACAAAACCGATGAGTGCTATCAGGCGATAAAGGCGCAAAAT
AAAAAAGTACAGGAGTCCAGACAGCCAATGTCTATGCGCGCGATTTATCCGCCCATGAGGGGCATGAGTG
ACCATCGCGTTGCGTTGGACATCCAGTTCCGACCGGGTCATCGCCCTTCGGTTGTGGGTTATGAGTCCGC
GCCGGGCAATTTGGCTGAGCATTTGAAATACGGACTTGAGCATGGATTGCGCGGGGCTAAGGTGCAGGTG
GTGGCAAATACGATTCAAAACTCCGTAAGAGGCTGCTCCATGTTTGCCTTGAATAATGCCCTGAAGTCCT
TTAAGCATCAAGATGAGTACACTGCGCGGCTGCATAGCGGTGAAAAACAGGTTCCCATCCCCGCCGAATT
TTTCAAACATGCGCATTCGAAAACCCTGATTGAGGGGCACCCGCATAAGGACGCTATTGTCTCTAAAGAT
AAAGGCGGGCTGCATGCAGAAACATTGCTGCACAGAAATCTGGCCTATCGTGCTGACAGGACTAACCACT
CTTACAGTACCTCGATTGAAGGTTTCCGCCTGCAGGAAATACAGCGGGCAGGTGAATTTCTGGCCGCAAG
AAAACAAAGAAAGTAG

Erwinia tasmaniensis strain *Et*1/99 Eop1 Protein and DNA sequence

EtaEop1	***WP_012440293.1***	***Erwinia tasmaniensis str. Et*1/99**

Protein sequence

MNISGLRAGQGSPSQQTDRAASSSTQASPAPAGRRLQRQDALPTNTRYQASQMPATPERARVAARNSAGA
SSSAAHAQPSLSLSRQNAHREDPALARFHHQMQQSTKMSRADPLPEKPQVVPKRLQEKIDAINLPRLKKL
DNNLHEYGKMATELAKEGSGSSSALTRMDKKVLPLLADAENARHPGLNLHVYKKGEECYQAIKDQHKSVQ
QSGQPKTMRALYPPFKGMPDHHIALDIQLRPGHRPSIVGFESALGHMVEHLKQGIAEGVRGAKVHMVGNT
IQNSQWDCTMYSLSNALKSFKHHDEYTARLHKGEKVPVPAEFFKHAQSKSSVEGKPHQDAVVTKDKGGLH
AETLLHRNLAYRADRFDRAYSTSIEGFRMQEIQRAGEHLAAKKHKS

DNA sequence

ATGAATATATCGGGTTTGCGAGCCGGGCAGGGGAGCCCATCGCAGCAAACGGATCGGGCTGCTTCCTCAT
CGACCCAGGCCTCACCGGCCCCGGCGGGCAGACGGTTACAGCGCCAGGACGCGCTGCCCACCAACACTCG
TTATCAGGCCAGCCAGATGCCCGCTACGCCGGAGCGTGCGCGCGTCGCCGCCAGAAACAGCGCGGGGGCG
AGCTCTTCAGCGGCGCATGCGCAACCCTCCCTGTCTTTGTCACGCCAGAACGCGCATCGTGAGGATCCAG
CGCTCGCCCGTTTTCATCACCAGATGCAGCAGTCGACAAAAATGTCGCGCGCCGATCCTCTGCCGGAAAA
GCCGCAGGTCGTGCCAAAACGCCTACAGGAAAAGATAGACGCCATTAACCTGCCACGATTAAAAAAGCTG
GATAACAACCTACACGAATACGGCAAAATGGCGACCGAACTGGCAAAAGAAGGTTCGGGCTCCAGCAGCG
CACTGACGCGCATGGATAAAAAGGTCCTGCCGCTATTGGCCGATGCGGAAAATGCGCGTCATCCCGGCCT
CAACCTGCATGTTTATAAGAAGGGTGAAGAGTGTTATCAGGCGATAAAGGATCAGCATAAAAGCGTACAG
CAGTCCGGGCAGCCAAAGACGATGCGTGCGCTATATCCTCCTTTCAAGGGCATGCCAGACCACCACATTG
CTCTGGATATTCAGCTCCGGCCGGGCCATCGCCCCTCGATTGTCGGCTTTGAGTCGGCTTTGGGGCATAT
GGTCGAGCATCTCAAACAGGGTATTGCCGAAGGGGTACGTGGGGCTAAAGTGCATATGGTGGGCAATACG
ATTCAAAATTCCCAGTGGGATTGCACCATGTATTCGTTGAGTAATGCTTTAAAATCTTTTAAGCATCATG
ACGAATATACGGCCCGCCTGCACAAGGGGGAAAAGGTTCCTGTGCCCGCGGAGTTCTTCAAACATGCGCA
GTCGAAATCATCCGTCGAGGGTAAACCGCATCAGGATGCCGTTGTCACCAAAGATAAAGGCGGGCTGCAT
GCCGAAACCCTGCTGCACAGAAACCTGGCCTATCGCGCCGACAGGTTCGACCGCGCTTACAGCACCTCGA
TTGAGGGCTTCCGCATGCAGGAGATCCAGCGTGCCGGCGAGCATCTGGCGGCGAAAAAACACAAAAGCTA
G

Erwinia tracheiphila strain MDcuke Eop1 Protein and DNA sequence

EtrEop1	***AXF77196.1***	***Erwinia tracheiphila* str. MDcuke**

Protein sequence

MNVFGVRIGRKSSSQQEEQTPSSSPLASPQSSPLPAGRAGRLQRQNATLSNNTRYNARSTPGTPDRARAT
SRHSGEGSSSSAYSTGPASSSRAVLVRQGGNREHSQLAQFHEMMQVSPKISRNDPLPETPESIPRRLQEK
MDTVNLPELEKLDGGLYEYAKMAIERVNEKKGADKQLSELDKKMLPLFAEAENARHPDLNLHVFRGPEAC
YKAIKEQNKKAWDSRQPMNMRVVFSPSRGIPDHHVALDVQLRPGHHPSVVCFESALWGMMNEIRQGIEHG
LKESKVKLIGNFVQASDWDCAMFALSNALKLYKHHDEYTSRLHAGEENVRIPSELIKHAQSKGHAERQGR
RNDIVTKDKGGLHAETLLHRNLAYRAQRFDKAYSTSIEGFRFQEIQRAGDYLAAQRGRK

DNA sequence

ATGAACGTATTTGGCGTCAGAATAGGGCGTAAAAGCAGTTCACAACAGGA
AGAGCAAACGCCATCCTCCTCGCCGCTGGCGTCGCCACAGTCATCCCCAC
TGCCTGCGGGCCGAGCTGGACGTCTTCAGCGGCAAAATGCCACCTTGTCT
AATAACACCCGCTACAATGCCCGCTCCACACCCGGCACGCCTGATCGTGC
GCGTGCGACCTCAAGGCACAGTGGCGAAGGGAGCAGCTCGTCGGCGTATT
CTACAGGGCCGGCCAGTTCATCAAGGGCAGTATTAGTGCGCCAGGGCGGC
AATCGCGAGCATTCACAGCTGGCACAATTCCACGAGATGATGCAGGTGTC
ACCGAAGATCTCACGTAACGATCCGCTGCCGGAAACGCCGGAGAGCATCC
CCAGGCGTTTGCAGGAAAAGATGGATACCGTCAACCTGCCGGAGCTGGAA
AAGCTGGACGGGGGACTCTATGAATACGCCAAAATGGCTATCGAACGGGT
CAATGAGAAAAAAGGTGCCGATAAACAGCTGTCGGAACTGGATAAAAAAA
TGTTGCCGCTGTTCGCCGAAGCCGAAAACGCGCGTCATCCTGACCTGAAC
CTGCACGTTTTCCGCGGACCGGAGGCGTGTTATAAAGCGATCAAAGAGCA
GAACAAAAAGGCATGGGACAGTAGGCAGCCAATGAATATGCGCGTGGTCT
TCAGCCCGTCCAGAGGCATACCCGATCACCATGTTGCCCTCGACGTACAG
TTGCGTCCCGGCCATCACCCCTCGGTGGTGTGTTTTGAGTCAGCACTGTG
GGGTATGATGAATGAGATTCGGCAGGGTATCGAACACGGGCTTAAAGAGA
GCAAAGTGAAGTTGATAGGCAACTTTGTTCAGGCTTCAGACTGGGACTGT
GCTATGTTTGCGCTGAGTAATGCGCTGAAATTATATAAGCATCACGATGA
ATACACCTCACGTCTTCACGCTGGTGAAGAAAATGTGCGGATCCCGTCAG
AGCTTATCAAACATGCGCAGTCAAAAGGCCATGCCGAAAGGCAGGGGCGC
CGAAACGACATTGTTACTAAAGATAAAGGTGGCCTGCATGCGGAAACTCT
GCTGCACCGCAACCTTGCTTACCGCGCCCAGCGGTTTGATAAAGCCTACA
GCACCTCCATTGAGGGGTTCCGCTTCCAGGAAATCCAGCGGGCCGGTGAC
TATCTCGCCGCACAGCGAGGACGAAAATAA

Pantoea vagans strain C9-1 Eop1 Protein and DNA sequence

PvaEop1	**WP_061060943.1**	***Pantoea vagans* str. C9-1**

Protein sequence

MNIFRAITGNKSPSQQPERTPTASPQASPLPAGRAGRLQRQNAMSPDVRYNASATQSTPDRARATTRHRG
EASSSSAQSAGEGSMSTGSSLGLIRQSGRRENTELVQFHDMMQSSSKMSRSDPLPQNPERLPGRLQQKMD
TVNLPKLKKLDKDLYDYAKLATDLVKDNSGTNVLLTRLDKKMMPLIADAENARHPDLNLHVFKGPDECYK
AIKEQNKQVWNSRQPGNMRVVFAPAKGMPDHHIALDIQLRPGHRPSIVCFESALGNMMDPIKQGIEQGLK
GARVKMVGNFIQASSWDCAMFALNNALKSFKHYDDYTSRLHAGEQNVPKPSEFFKHAQSKSHIEGGPREN
DIVSKDKGGLHAETLLHRNLAYRAQRFDKAYSTSIEGFRFQEIERAGEYLAAQRGRR

DNA sequence

ATGAATATTTTTCGTGCGATAACGGGCAATAAAAGCCCGTCTCAGCAGCCCGAACGCACGCCGACTGCGT
CACCTCAGGCGTCACCATTACCGGCAGGCAGAGCCGGACGATTACAGCGTCAAAATGCCATGTCCCCTGA
TGTTCGCTACAATGCCAGCGCCACCCAAAGCACGCCGGATCGCGCTCGTGCCACCACCAGGCATCGTGGT
GAAGCGAGCAGCTCTTCGGCGCAATCCGCTGGCGAGGGCAGTATGTCGACCGGTTCATCATTGGGCTTGA
TTCGTCAAAGCGGCCGTCGTGAGAATACTGAATTGGTCCAGTTCCACGACATGATGCAGTCTTCATCAAA
AATGTCGCGTAGCGATCCCCTGCCGCAGAACCCGGAGAGATTACCGGGACGACTCCAGCAGAAGATGGAT
ACTGTTAACCTGCCGAAGCTTAAGAAACTGGATAAAGATTTATACGATTACGCCAAACTGGCTACCGATC
TGGTGAAGGACAACTCCGGTACAAATGTACTGCTCACCCGGCTGGATAAAAAGATGATGCCGCTCATTGC
CGATGCAGAAAATGCCCGTCATCCAGACTTGAATCTGCATGTCTTTAAAGGACCGGATGAATGTTATAAG
GCCATCAAAGAGCAAAATAAACAGGTCTGGAACAGCAGACAGCCCGGGAATATGCGCGTGGTCTTTGCGC
CTGCGAAGGGGATGCCAGATCACCATATTGCACTTGATATCCAGTTACGCCCGGGTCATCGTCCATCAAT
CGTGTGTTTCGAGTCAGCGCTGGGAAATATGATGGATCCAATAAAACAGGGAATTGAGCAGGGTCTAAAG
GGAGCCAGAGTGAAGATGGTAGGTAACTTTATTCAGGCCTCATCATGGGATTGTGCGATGTTTGCGCTGA
ATAATGCGCTGAAAAGCTTTAAGCATTATGACGACTATACATCGCGTCTTCATGCAGGCGAACAGAATGT
GCCGAAGCCGTCTGAGTTTTTTAAACATGCGCAATCTAAATCTCATATTGAGGGTGGACCTCGTGAGAAC
GACATCGTTTCGAAAGACAAAGGCGGCCTGCATGCTGAAACGCTACTGCACCGCAATCTGGCCTATCGCG
CACAACGCTTTGATAAAGCCTATAGCACCTCGATTGAAGGCTTTCGCTTTCAGGAGATCGAGCGCGCCGG
TGAATACCTTGCTGCGCAAAGAGGCAGAAGATAA

Protein and DNA sequence of *Malus* and *Pyrus* RIN4 variants tested in the study

Malus domestica RIN4: allele 1 protein and DNA sequence

***Mxd*RIN4-1**	**NP_001280923.1**	***Malus domestica*: RIN4-1**

Protein sequence

MAQRSHVPKFGNWEDQESVPYTAYFDKARKGRTGVGGKMINPNDPEENPDILSDTSASSPPKVRPEPGKP
VHERRRSREDNDLRFANSPAQRRSSGEHQPNRGRGVSSGETHRRAARPSAGSENSVERSPLHRNARVSGR
DSPSWEGKASYESSHGTPARSRLKPRDESPEKGAAVPKFGEWDENDPASADGFTHIFNKVREEKAGKAPG
TPSHPSYQDARKQGSNDSAKCCCFPWGRK

DNA sequence

ATGGCACAACGTTCACATGTACCAAAGTTTGGCAATTGGGAAGACCAAGAAAGTGTTCCTTACACTGCCT
ATTTTGATAAGGCCCGTAAGGGTCGAACTGGTGTTGGGGGAAAGATGATTAATCCTAATGACCCCGAAGA
GAATCCAGACATCCTCTCTGACACATCTGCATCATCTCCTCCAAAAGTTAGACCGGAACCAGGAAAACCA
GTTCATGAACGGAGAAGAAGCAGGGAGGATAATGACCTGAGATTTGCCAACTCCCCAGCCCAGCGCAGAA
GTTCTGGTGAACATCAACCTAACAGAGGCCGTGGGGTTAGTTCTGGTGAAACCCATCGAAGAGCTGCACG
ACCAAGTGCTGGGTCTGAGAACAGTGTTGAACGTTCACCTCTCCATCGCAATGCAAGGGTCTCAGGAAGA
GATTCACCCTCCTGGGAAGGAAAGGCGTCATATGAAAGTAGCCATGGCACTCCTGCAAGATCCCGCCTCA
AACCTCGTGATGAAAGTCCTGAGAAAGGTGCTGCTGTTCCCAAATTTGGCGAGTGGGATGAGAACGACCC
GGCATCAGCTGATGGTTTCACTCATATATTCAACAAAGTGCGGGAGGAGAAGGCGGGAAAAGCACCAGGG
ACTCCTTCTCATCCGTCTTACCAAGATGCAAGGAAGCAGGGTTCCAATGACAGTGCCAAGTGTTGCTGCT
TTCCATGGGGCAGAAAATGA

Malus domestica RIN4: allele 2 protein and DNA sequence

***Mxd*RIN4-2**	**NP_001280834.1**	***Malus domestica*: RIN4-2**

Protein sequence

MAQRSHVPKFGNWEGEESVPYTAYFDKARKDRTGVGGKMINPNDPQENPDILSDISASSPPKVRPEPEKP
VHEQRRSREDNDLRFANSPAQRRNSGESAHQPSRGRGVSSGETRRRPARPSAGSENSVERSPLHRNARVT
GRDSPSWEGKASYETSHGTPGRSRLKPRDESPEKGAAVPKFGEWDENDPASADGFTHIFNKVREERAGKV
PGTPSQPSYQDARRQGSNDSAKSCCFPWSRK

DNA sequence

ATGGCACAACGTTCACATGTACCAAAGTTTGGCAATTGGGAAGGCGAAGAAAGTGTTCCTTACACAGCCT
ATTTTGATAAGGCCCGTAAGGATCGAACTGGTGTCGGGGGAAAGATGATTAATCCAAATGACCCCCAAGA
GAACCCGGACATCCTTTCTGACATATCTGCATCTTCTCCTCCAAAAGTTAGACCAGAACCAGAAAAACCA
GTTCATGAACAGAGAAGAAGCAGGGAGGATAATGACCTAAGATTTGCCAACTCCCCAGCCCAGCGCAGAA
ATTCTGGTGAATCAGCACATCAACCTAGCAGAGGCCGTGGAGTTAGTTCTGGTGAAACCCGTCGAAGGCC
TGCACGGCCAAGTGCTGGGTCTGAGAACAGTGTTGAGCGTTCACCTCTCCATCGCAATGCGAGGGTCACA
GGACGAGATTCACCCTCCTGGGAAGGAAAGGCTTCATACGAAACTAGCCATGGCACTCCTGGAAGGTCCC
GCCTCAAACCTCGTGATGAAAGTCCTGAGAAAGGTGCTGCTGTTCCGAAATTTGGCGAGTGGGATGAAAA
CGACCCGGCATCAGCTGATGGTTTCACTCACATATTCAACAAAGTGCGGGAGGAGCGGGCGGGAAAAGTAC
CAGGGACTCCTTCTCAGCCGTCTTACCAGGATGCCAGAAGGCAGGGTTCCAATGACAGTGCCAAGAGTT
GCTGCTTTCCATGGAGCAGAAAATGA

Pyrus bretschneideri RIN4: allele 1 protein and DNA sequence

***Pb*RIN4-1A**	**XP_009370675.1**	***Pyrus bretschneideri*: RIN4-1**

Protein sequence

MAQRSHVPKFGNWESQESVPYTAYFDKARKGKTGVGGKMINPNDPEENPDILSDTSASSPPKVRPEREK
PVHERRRSREDNDLRFANSPAQRRTSGESAHQPNRGRGVSSGETHRRPARPSGGSENSVERSPLHRNAR
VSGRDSPSWEGKASYESSHGTPARSRLKPRDESPEKGAAVPKFGEWDENDPASADGFTHIFNKVREERA
GKVPGTPSQPSYQDARKQGSNDRAKSCCFPWGRK

DNA sequence

ATGGCACAACGTTCACATGTACCAAAGTTTGGCAATTGGGAAAGCCAAGAAAGTGTTCCTTACACTGC
CTATTTTGATAAGGCCCGTAAGGGTAAAACTGGTGTTGGGGGAAAGATGATTAATCCAAATGACCCC
GAAGAGAATCCAGACATCCTCTCTGACACATCTGCATCATCTCCTCCAAAAGTTAGACCGGAACGGGA
AAAACCAGTACATGAACGGAGAAGAAGCAGGGAGGATAATGACCTAAGATTTGCCAACTCCCCAGCC
CAGCGCAGAACTTCTGGTGAATCAGCACATCAACCTAACAGAGGCCGTGGGGTTAGTTCTGGTGAAA
CCCATCGAAGACCTGCACGACCAAGTGGTGGGTCTGAGAACAGCGTTGAACGTTCACCTCTCCATCGC
AATGCAAGGGTCTCAGGAAGAGATTCACCCTCCTGGGAAGGAAAGGCGTCATATGAAAGTAGCCAT
GGCACTCCTGCAAGATCCCGCCTCAAACCTCGCGATGAAAGTCCTGAGAAAGGTGCTGCTGTTCCCAA
ATTTGGCGAGTGGGATGAGAACGACCCGGCATCAGCTGATGGTTTCACTCATATATTCAACAAAGTG
CGGGAGGAGAGGGCGGGAAAAGTACCAGGGACTCCTTCTCAGCCGTCTTACCAAGATGCAAGGAAG
CAGGGTTCCAATGACAGGGCCAAGAGTTGCTGCTTTCCGTGGGGCAGAAAATGA

Pyrus bretschneideri allele 2 protein and DNA sequence

***Pb*RIN4-1**	**XM_009373606.1**	***Pyrus bretschneideri*: RIN4 - 2**

Protein sequence

MAQRSHVPKFGNWEGEESVPYTAYFDKARKDRTGVGGKMINPNDPQENPDILSDISASSPPKVRPEPEKP
VDERRRSREDNDLRFANSPAQRRNSGESAHQPNRGRGVSSGDTHQRPARPSAGSENSVERSPLHRNARVT
GRNSPSWEGKASYESSHGTPGRSRLKPRDESPEKGAAVPKFGEWDENDPASADGFTHIFNKVREERAGKV
PGTPSQPSYQDARKQGSNDSAKSCCFPWSRK

DNA sequence

ATGGCACAACGTTCACATGTACCAAAGTTTGGCAATTGGGAAGGCGAAGAAAGTGTTCCTTACACAGCCT
ATTTTGATAAGGCCCGTAAGGATCGAACTGGTGTCGGTGGAAAGATGATTAATCCAAATGACCCCCAAGA
GAACCCGGACATCCTTTCTGACATATCTGCATCTTCTCCTCCAAAAGTTAGACCAGAACCTGAAAAACCA
GTTGATGAACGGAGAAGAAGCAGGGAGGATAATGACCTAAGATTTGCCAACTCCCCAGCCCAGCGCAGAA
ATTCTGGTGAATCAGCACATCAACCTAACAGAGGCCGTGGAGTTAGTTCTGGGGATACCCATCAAAGGCC
TGCACGACCAAGTGCTGGGTCTGAGAACAGTGTTGAGCGTTCACCTCTCCATCGCAATGCGAGGGTCACA
GGACGAAATTCACCCTCCTGGGAAGGAAAGGCTTCATATGAATCTAGCCATGGCACTCCTGGAAGGTCCC
GCCTCAAACCTCGCGATGAAAGTCCTGAGAAAGGTGCTGCTGTTCCGAAATTTGGCGAGTGGGATGAAAA
TGACCCGGCATCAGCTGATGGTTTCACTCACATATTCAACAAAGTGCGGGAGGAGCGGGCGGGAAAAGTA
CCAGGGACTCCTTCTCAGCCGTCTTACCAAGATGCAAGAAAGCAGGGTTCCAATGACAGTGCCAAGAGTT
GCTGCTTTCCATGGAGCAGAAAATGA

References

Adeolu, M., Alnajar, S., Naushad, S., & R, S. G. (2016). Genome-based phylogeny and taxonomy of the 'Enterobacteriales': proposal for Enterobacterales ord. nov. divided into the families Enterobacteriaceae, Erwiniaceae fam. nov., Pectobacteriaceae fam. nov., Yersiniaceae fam. nov., Hafniaceae fam. nov., Morganellaceae fam. nov., and Budviciaceae fam. nov. *Int J Syst Evol Microbiol*, *66*(12), 5575-5599. https://doi.org/10.1099/ijsem.0.001485

Adlung, N., Prochaska, H., Thieme, S., Banik, A., Bluher, D., John, P., Nagel, O., Schulze, S., Gantner, J., Delker, C., Stuttmann, J., & Bonas, U. (2016). Non-host Resistance Induced by the Xanthomonas Effector XopQ Is Widespread within the Genus Nicotiana and Functionally Depends on EDS1. *Front Plant Sci*, *7*, 1796. https://doi.org/10.3389/fpls.2016.01796

Afunian, M. R., & Rahimian, H. (1996). Investigation on the Characteristics of Iranian Isolates of *Erwinia Amylovora*. *Acta horticulturae*(411), 187-188. https://doi.org/10.17660/ActaHortic.1996.411.38

Afzal, A. J., da Cunha, L., & Mackey, D. (2011). Separable fragments and membrane tethering of Arabidopsis RIN4 regulate its suppression of PAMP-triggered immunity. *Plant Cell*, *23*(10), 3798-3811. https://doi.org/10.1105/tpc.111.088708

Afzal, A. J., Kim, J. H., & Mackey, D. (2013). The role of NOI-domain containing proteins in plant immune signaling. *BMC Genomics*, *14*(1), 327. https://doi.org/10.1186/1471-2164-14-327

Agrios, G. N. (2005a). Genetics of Plant Disease. In G. N. Agrios (Ed.), *Plant Pathology* (pp. 124-174). Academic Press. https://doi.org/10.1016/b978-0-08-047378-9.50010-5

Agrios, G. N. (2005b). Plant Diseases Caused by Prokaryotes: Bacteria and Mollicutes. In G. N. Agrios (Ed.), *Plant Pathology* (pp. 615-703). Academic Press. https://doi.org/10.1016/b978-0-08-047378-9.50018-x

Anand, A., Vaghchhipawala, Z., Ryu, C. M., Kang, L., Wang, K., del-Pozo, O., Martin, G. B., & Mysore, K. S. (2007). Identification and characterization of plant genes involved in Agrobacterium-mediated plant transformation by virus-induced gene silencing. *Molecular plant-microbe interactions : MPMI*, *20*(1), 41-52. https://doi.org/10.1094/MPMI-20-0041

Arnold, D. L., Jackson, R. W., Fillingham, A. J., Goss, S. C., Taylor, J. D., Mansfield, J. W., & Vivian, A. (2001). Highly conserved sequences flank avirulence genes: isolation of novel avirulence genes from *Pseudomonas syringae* pv. pisi. *Microbiology (Reading)*, *147*(Pt 5), 1171-1182. https://doi.org/10.1099/00221287-147-5-1171

Asselin, J. E., Bonasera, J. M., Kim, J. F., Oh, C. S., & Beer, S. V. (2011). Eop1 from a *Rubus* strain of *Erwinia amylovora* functions as a host-range limiting factor. *Phytopathology*, *101*(8), 935-944. https://doi.org/10.1094/PHYTO-12-10-0339

Asselin, J. E., Yip, K. N., & Beer, S. V. (2008). eop1 DIFFERS IN STRAINS OF ERWINIA AMYLOVORA THAT DIFFER IN HOST SPECIFICITY.

Atkinson, M. M., Keppler, L. D., Orlandi, E. W., Baker, C. J., & Mischke, C. F. (1990). Involvement of plasma membrane calcium influx in bacterial induction of the k/h and hypersensitive responses in tobacco. *Plant Physiol*, *92*(1), 215-221. https://doi.org/10.1104/pp.92.1.215

Ausubel, F. M. (2005). Are innate immune signaling pathways in plants and animals conserved? *Nat Immunol*, *6*(10), 973-979. https://doi.org/10.1038/ni1253

Axtell, M. J., Chisholm, S. T., Dahlbeck, D., & Staskawicz, B. J. (2003). Genetic and molecular evidence that the *Pseudomonas syringae* type III effector protein AvrRpt2 is a cysteine protease. *Mol Microbiol*, *49*(6), 1537-1546. https://doi.org/10.1046/j.1365-2958.2003.03666.x

Axtell, M. J., & Staskawicz, B. J. (2003). Initiation of RPS2-specified disease resistance in Arabidopsis is coupled to the AvrRpt2-directed elimination of RIN4. *Cell*, *112*(3), 369-377. https://doi.org/10.1016/s0092-8674(03)00036-9

Baker, K. F. (1971). Fire blight of pome fruits: The genesis of the concept that bacteria can be pathogenic to plants. *Hilgardia*, *40*(18), 603-633. https://doi.org/10.3733/hilg.v40n18p603

Balint-Kurti, P. (2019). The plant hypersensitive response: concepts, control and consequences [10.1111/mpp.12821]. *Mol Plant Pathol*, *20*(8), 1163-1178. https://doi.org/10.1111/mpp.12821

Baltrus, D. A., Nishimura, M. T., Dougherty, K. M., Biswas, S., Mukhtar, M. S., Vicente, J., Holub, E. B., & Dangl, J. L. (2012). The molecular basis of host specialization in bean pathovars of Pseudomonas syringae. *Molecular plant-microbe interactions : MPMI*, *25*(7), 877-888. https://doi.org/10.1094/MPMI-08-11-0218

Belkhadir, Y., Nimchuk, Z., Hubert, D. A., Mackey, D., & Dangl, J. L. (2004). Arabidopsis RIN4 negatively regulates disease resistance mediated by RPS2 and RPM1 downstream or independent of the NDR1 signal modulator and is not required for the virulence functions of bacterial type III effectors AvrRpt2 or AvrRpm1. *Plant Cell*, *16*(10), 2822-2835. https://doi.org/10.1105/tpc.104.024117

Bertani, G. (1951). Studies on lysogenesis. I. The mode of phage liberation by lysogenic Escherichia coli. *J Bacteriol*, *62*(3), 293-300. https://doi.org/10.1128/jb.62.3.293-300.1951

Bio-Rad. *Gene Pulser Xcell Total System (1652660)*. https://www.bio-rad.com/en-nz/product/gene-pulser-xcell-electroporation-systems?ID=b1a35eb3-d55c-47b3-aaf3-95e4d1d85848

Bio-Rad. *Gene Pulser/MicroPulser Electroporation Cuvettes, 0.1 cm gap (1652089)*. https://www.bio-rad.com/en-nz/sku/1652089-gene-pulser-micropulser-electroporation-cuvettes-0-1-cm-gap?ID=1652089

Biochemie, D. (2017). Rifampicin (R0146). https://www.duchefa-biochemie.com/product/details/number/R0146/name/rifampicin

Biochemie, D. (2018). Carbenicilllin disodium (C0109). https://www.duchefa-biochemie.com/product/details/number/C0109/name/carbenicillin-disodium

Biochemie, D. (2020). *Gentamicin sulfate (GO124)*. https://www.duchefa-biochemie.com/product/details/number/G0124

Bliven, K. A., & Maurelli, A. T. (2012). Antivirulence genes: insights into pathogen evolution through gene loss. *Infect Immun*, *80*(12), 4061-4070. https://doi.org/10.1128/IAI.00740-12

Bocsanczy, A. M., Schneider, D. J., DeClerck, G. A., Cartinhour, S., & Beer, S. V. (2012). HopX1 in Erwinia amylovora functions as an avirulence protein in apple and is regulated by HrpL. *J Bacteriol*, *194*(3), 553-560. https://doi.org/10.1128/JB.05065-11

Bogdanove, A. J., Bauer, D. W., & Beer, S. V. (1998). Erwinia amylovora secretes DspE, a pathogenicity factor and functional AvrE homolog, through the Hrp (type III secretion) pathway. *J Bacteriol*, *180*(8), 2244-2247. https://doi.org/10.1128/JB.180.8.2244-2247.1998

Bogdanove, A. J., Kim, J. F., Wei, Z., Kolchinsky, P., Charkowski, A. O., Conlin, A. K., Collmer, A., & Beer, S. V. (1998). Homology and functional similarity of an hrp-linked pathogenicity locus, dspEF, of Erwinia amylovora and the avirulence locus avrE of Pseudomonas syringae pathovar tomato. *Proc Natl Acad Sci U S A*, *95*(3), 1325-1330. https://doi.org/10.1073/pnas.95.3.1325

Bonn, W. G., & Zwet, T. v. d. (2000). *Distribution and economic importance of fire blight*. CABI International. https://doi.org/10.1079/9780851992945.0037

Boureau, T., ElMaarouf-Bouteau, H., Garnier, A., Brisset, M. N., Perino, C., Pucheu, I., & Barny, M. A. (2006). DspA/E, a type III effector essential for Erwinia amylovora pathogenicity and growth in planta, induces cell death in host apple and nonhost tobacco plants. *Molecular plant-microbe interactions : MPMI*, *19*(1), 16-24. https://doi.org/10.1094/MPMI-19-0016

Braun, P. G., & Hildebrand, P. D. (2005). Infection, carbohydrate utilization, and protein profiles of apple, pear, and raspberry isolates ofErwinia amylovora. *Canadian Journal of Plant Pathology*, *27*(3), 338-346. https://doi.org/10.1080/07060660509507231

Brendolise, C., Montefiori, M., Dinis, R., Peeters, N., Storey, R. D., & Rikkerink, E. H. (2017). A novel hairpin library-based approach to identify NBS-LRR genes required for effector-triggered hypersensitive response in Nicotiana benthamiana. *Plant Methods*, *13*, 32. https://doi.org/10.1186/s13007-017-0181-7

Broggini, G. A., Wohner, T., Fahrentrapp, J., Kost, T. D., Flachowsky, H., Peil, A., Hanke, M. V., Richter, K., Patocchi, A., & Gessler, C. (2014). Engineering fire blight resistance into the apple cultivar 'Gala' using the FB_MR5 CC-NBS-LRR resistance gene of Malus x robusta 5. *Plant Biotechnol J*, *12*(6), 728-733. https://doi.org/10.1111/pbi.12177

Bundalovic-Torma, C., Lonjon, F., Desveaux, D., & Guttman, D. S. (2022). Diversity, Evolution, and Function of Pseudomonas syringae Effectoromes. *Annu Rev Phytopathol*, *60*, 211-236. https://doi.org/10.1146/annurev-phyto-021621-121935

Burrill, T. J., Griffith, C. S., Arthur, J. C., & Waite, M. B. (2003). *Fire Blight: The Foundation of Phytobacteriology*. APS Press. https://my.apsnet.org/APSStore/Product-Detail.aspx?WebsiteKey=2661527A-8D44-496C-A730-8CFEB6239BE7&iProductCode=43097

Buttner, D., & He, S. Y. (2009). Type III protein secretion in plant pathogenic bacteria. *Plant Physiol*, *150*(4), 1656-1664. https://doi.org/10.1104/pp.109.139089

Callu, D. (1984). Situation du feu bactérien en France (1982-Août 1983). *Acta horticulturae*(151), 317-323.

Calzolari, A., Finelli, F., & Mazzoli, G. L. (1999). A Severe Unforeseen Outbreak of Fire Blight in the Emilia-Romagna Region. *Acta horticulturae*(489), 171-176. https://doi.org/10.17660/ActaHortic.1999.489.26

Campbell, J. (1920). The orchard: the outbreak of fire blight. *New Zealand Journal of Agriculture*, *20*, 181-182.

Carrigan, P. E., Ballar, P., & Tuzmen, S. (2011). Site-Directed Mutagenesis. In J. K. DiStefano (Ed.), *Disease Gene Identification: Methods and Protocols* (pp. 107-124). Humana Press. https://doi.org/10.1007/978-1-61737-954-3_8

Carter, P., & Wells, J. A. (1988). Dissecting the catalytic triad of a serine protease. *Nature*, *332*(6164), 564-568. https://doi.org/10.1038/332564a0

Chakraborty, J. (2021). In-silico structural analysis of Pseudomonas syringae effector HopZ3 reveals ligand binding activity and virulence function. *J Plant Res*, *134*(3), 599-611. https://doi.org/10.1007/s10265-021-01274-8

Chang, M., Chen, H., Liu, F., & Fu, Z. Q. (2022). PTI and ETI: convergent pathways with diverse elicitors. *Trends Plant Sci*, *27*(2), 113-115. https://doi.org/10.1016/j.tplants.2021.11.013

Chen, Z., Agnew, J. L., Cohen, J. D., He, P., Shan, L., Sheen, J., & Kunkel, B. N. (2007). Pseudomonas syringae type III effector AvrRpt2 alters Arabidopsis thaliana auxin physiology. *Proc Natl Acad Sci U S A*, *104*(50), 20131-20136. https://doi.org/10.1073/pnas.0704901104

Cheong, M. S., Kirik, A., Kim, J. G., Frame, K., Kirik, V., & Mudgett, M. B. (2014). AvrBsT acetylates Arabidopsis ACIP1, a protein that associates with microtubules and is required for immunity. *PLoS Pathog*, *10*(2), e1003952. https://doi.org/10.1371/journal.ppat.1003952

Chiew Foan Chin, J. Y. C. (2015). Gateway Cloning Technology: Advantages and Drawbacks. *Cloning & Transgenesis*, *04*(01), 138. https://doi.org/10.4172/2168-9849.1000138

Chisholm, S. T., Dahlbeck, D., Krishnamurthy, N., Day, B., Sjolander, K., & Staskawicz, B. J. (2005). Molecular characterization of proteolytic cleavage sites of the Pseudomonas syringae effector AvrRpt2. *Proc Natl Acad Sci U S A*, *102*(6), 2087-2092. https://doi.org/10.1073/pnas.0409468102

Chung, E. H., da Cunha, L., Wu, A. J., Gao, Z., Cherkis, K., Afzal, A. J., Mackey, D., & Dangl, J. L. (2011). Specific threonine phosphorylation of a host target by two unrelated type III effectors activates a host innate immune receptor in plants. *Cell Host Microbe*, *9*(2), 125-136. https://doi.org/10.1016/j.chom.2011.01.009

Chung, E. H., El-Kasmi, F., He, Y., Loehr, A., & Dangl, J. L. (2014). A plant phosphoswitch platform repeatedly targeted by type III effector proteins regulates the output of both tiers of plant immune receptors. *Cell Host Microbe*, *16*(4), 484-494. https://doi.org/10.1016/j.chom.2014.09.004

Coaker, G., Zhu, G., Ding, Z., Van Doren, S. R., & Staskawicz, B. (2006). Eukaryotic cyclophilin as a molecular switch for effector activation. *Mol Microbiol*, *61*(6), 1485-1496. https://doi.org/10.1111/j.1365-2958.2006.05335.x

Coburn, B., Sekirov, I., & Finlay, B. B. (2007). Type III secretion systems and disease. *Clin Microbiol Rev*, *20*(4), 535-549. https://doi.org/10.1128/CMR.00013-07

Cockayne, A. (1921). Fire blight and its control: the hawthorn question. *New Zealand Journal of Agriculture*, *23*, 30-36.

Collier, S. M., & Moffett, P. (2009). NB-LRRs work a "bait and switch" on pathogens. *Trends Plant Sci*, *14*(10), 521-529. https://doi.org/10.1016/j.tplants.2009.08.001

Cook, D. E., Mesarich, C. H., & Thomma, B. P. (2015). Understanding plant immunity as a surveillance system to detect invasion. *Annu Rev Phytopathol*, *53*(1), 541-563. https://doi.org/10.1146/annurev-phyto-080614-120114

Crosse, J. E., Bennett, M., & Garrett, C. M. E. (1958). Fire-blight of Pear in England. *Nature*, *182*(4648), 1530-1530. https://doi.org/10.1038/1821530a0

Cuesta, S. A., Mora, J. R., Zambrano, C. H., Torres, F. J., & Rincon, L. (2020). Comparative study of the nucleophilic attack step in the proteases catalytic activity: A theoretical study. *Molecular Physics*, *118*(14), e1705412. https://doi.org/10.1080/00268976.2019.1705412

Cui, F., Wu, S., Sun, W., Coaker, G., Kunkel, B., He, P., & Shan, L. (2013). The *Pseudomonas syringae* type III effector AvrRpt2 promotes pathogen virulence via stimulating Arabidopsis auxin/indole acetic acid protein turnover. *Plant Physiol*, *162*(2), 1018-1029. https://doi.org/10.1104/pp.113.219659

Cui, H., Tsuda, K., & Parker, J. E. (2015). Effector-triggered immunity: from pathogen perception to robust defense. *Annu Rev Plant Biol*, *66*(1), 487-511. https://doi.org/10.1146/annurev-arplant-050213-040012

Dangl, J. L., & Jones, J. D. (2001). Plant pathogens and integrated defence responses to infection. *Nature*, *411*(6839), 826-833. https://doi.org/10.1038/35081161

De la Cruz Blanco, J. (1996). Incidentias climaticas y fitosanitarias en los cultivos espanoles durante 1995. *Phytoma-Espana*, *78*, 22-27.

Degrave, A., Fagard, M., Perino, C., Brisset, M. N., Gaubert, S., Laroche, S., Patrit, O., & Barny, M. A. (2008). Erwinia amylovora type three-secreted proteins trigger cell death and defense responses in Arabidopsis thaliana. *Molecular plant-microbe interactions : MPMI*, *21*(8), 1076-1086. https://doi.org/10.1094/MPMI-21-8-1076

Degrave, A., Siamer, S., Boureau, T., & Barny, M. A. (2015). The AvrE superfamily: ancestral type III effectors involved in suppression of pathogen-associated molecular pattern-triggered immunity. *Mol Plant Pathol*, *16*(8), 899-905. https://doi.org/10.1111/mpp.12237

Demidchik, V., Straltsova, D., Medvedev, S. S., Pozhvanov, G. A., Sokolik, A., & Yurin, V. (2014). Stress-induced electrolyte leakage: the role of K+-permeable channels and involvement in programmed

cell death and metabolic adjustment. *J Exp Bot*, *65*(5), 1259-1270. https://doi.org/10.1093/jxb/eru004

Denning, W. (1794). On the decay of apple trees. *New York Society for the Promotion of Agricultural Arts and Manufacturers Transaction*, *2*, 219-222.

Dodds, P. N., & Rathjen, J. P. (2010). Plant immunity: towards an integrated view of plant-pathogen interactions. *Nat Rev Genet*, *11*(8), 539-548. https://doi.org/10.1038/nrg2812

Doolotkeldieva, T., & Bobusheva, S. (2016). Fire Blight Disease Caused by *Erwinia amylovora* on Rosaceae Plants in Kyrgyzstan and Biological Agents to Control This Disease. *Advances in Microbiology*, *06*(11), 831-851, Article 70568. https://doi.org/10.4236/aim.2016.611080

Dowen, R. H., Engel, J. L., Shao, F., Ecker, J. R., & Dixon, J. E. (2009). A family of bacterial cysteine protease type III effectors utilizes acylation-dependent and -independent strategies to localize to plasma membranes. *J Biol Chem*, *284*(23), 15867-15879. https://doi.org/10.1074/jbc.M900519200

Drenova, N. V., Isin, M. M., Dzhaimurzina, A. A., Zharmukhamedova, G. A., & Aitkulov, A. K. (2013). BAcTeriAL fire BLighTin the repuBliC of KazaKhstan. *Карантин растений. Наука и практика*(1), 44-48. https://www.elibrary.ru/item.asp?id=25051586

Du, J., & Vleeshouwers, V. G. (2014). The do's and don'ts of effectoromics. *Methods Mol Biol*, *1127*, 257-268. https://doi.org/10.1007/978-1-62703-986-4_19

Dubin, M. J., Bowler, C., & Benvenuto, G. (2008). A modified Gateway cloning strategy for overexpressing tagged proteins in plants. *Plant Methods*, *4*(1), 3. https://doi.org/10.1186/1746-4811-4-3

Dye, D. W. (2012). A numerical taxonomic study of the genus *Erwinia*. *New Zealand Journal of Agricultural Research*, *24*(2), 223-229. https://doi.org/10.1080/00288233.1981.10420894

Earley, K. W., Haag, J. R., Pontes, O., Opper, K., Juehne, T., Song, K., & Pikaard, C. S. (2006). Gateway-compatible vectors for plant functional genomics and proteomics. *Plant J*, *45*(4), 616-629. https://doi.org/10.1111/j.1365-313X.2005.02617.x

Ellingboe, A. H. (1981). Changing Concepts in Host-Pathogen Genetics. *Annual Review of Phytopathology*, *19*(1), 125-143. https://doi.org/10.1146/annurev.py.19.090181.001013

Elmore, J. M., & Coaker, G. (2011). The role of the plasma membrane H+-ATPase in plant-microbe interactions. *Mol Plant*, *4*(3), 416-427. https://doi.org/10.1093/mp/ssq083

Emeriewen, O. F., Wohner, T., Flachowsky, H., & Peil, A. (2019). Malus Hosts-Erwinia amylovora Interactions: Strain Pathogenicity and Resistance Mechanisms [Mini Review]. *Front Plant Sci*, *10*, 551. https://doi.org/10.3389/fpls.2019.00551

Eschen-Lippold, L., Jiang, X., Elmore, J. M., Mackey, D., Shan, L., Coaker, G., Scheel, D., & Lee, J. (2016). Bacterial AvrRpt2-Like Cysteine Proteases Block Activation of the Arabidopsis Mitogen-Activated Protein Kinases, MPK4 and MPK11. *Plant Physiol*, *171*(3), 2223-2238. https://doi.org/10.1104/pp.16.00336

Fahrentrapp, J., Broggini, G. A. L., Kellerhals, M., Peil, A., Richter, K., Zini, E., & Gessler, C. (2012). A candidate gene for fire blight resistance in Malus × robusta 5 is coding for a CC–NBS–LRR. *Tree Genetics & Genomes*, *9*(1), 237-251. https://doi.org/10.1007/s11295-012-0550-3

Fischer, H., & Meyer, J. (1972). Praktische Erfahrungen bei der Bekampfung der Feuerbrandkrankheit (Erwinia amylovora) 1971. *Bienenzucht*.

Flor, H. H. (1971). Current Status of the Gene-For-Gene Concept. *Annual Review of Phytopathology*, *9*(1), 275-296. https://doi.org/10.1146/annurev.py.09.090171.001423

Fonseca, J. P., & Mysore, K. S. (2019). Genes involved in nonhost disease resistance as a key to engineer durable resistance in crops. *Plant Sci*, *279*, 108-116. https://doi.org/10.1016/j.plantsci.2018.07.002

Galan, J. E., Lara-Tejero, M., Marlovits, T. C., & Wagner, S. (2014). Bacterial type III secretion systems: specialized nanomachines for protein delivery into target cells. *Annu Rev Microbiol*, *68*(1), 415-438. https://doi.org/10.1146/annurev-micro-092412-155725

Gardner, J. M., & Kado, C. I. (1972). Comparative Base Sequence Homologies of the Deoxyribonucleic Acids of *Erwinia* Species and Other Enterobacteriaceae. *International Journal of Systematic Bacteriology*, *22*(4), 201-209. https://doi.org/10.1099/00207713-22-4-201

Gelvin, S. B. (2003). Agrobacterium-mediated plant transformation: the biology behind the "gene-jockeying" tool. *Microbiol Mol Biol Rev*, *67*(1), 16-37, table of contents. https://doi.org/10.1128/MMBR.67.1.16-37.2003

Gimenez-Ibanez, S., Boter, M., Fernandez-Barbero, G., Chini, A., Rathjen, J. P., & Solano, R. (2014). The bacterial effector HopX1 targets JAZ transcriptional repressors to activate jasmonate signaling and promote infection in Arabidopsis. *PLoS Biol*, *12*(2), e1001792. https://doi.org/10.1371/journal.pbio.1001792

Glowacki, S., Macioszek, V. K., & Kononowicz, A. K. (2011). R proteins as fundamentals of plant innate immunity. *Cell Mol Biol Lett*, *16*(1), 1-24. https://doi.org/10.2478/s11658-010-0024-2

Grimm, R., & Vogelsanger, J. (1989). First record of fire blight in Switzerland. *Schweizerische Zeitschrift für Obst- und Weinbau*, *125*(18), 514-516. https://www.cabdirect.org/cabdirect/abstract/19901148338

Hacker, J., & Kaper, J. B. (2000). Pathogenicity islands and the evolution of microbes. *Annu Rev Microbiol*, *54*(1), 641-679. https://doi.org/10.1146/annurev.micro.54.1.641

Hauben, L., Moore, E. R., Vauterin, L., Steenackers, M., Mergaert, J., Verdonck, L., & Swings, J. (1998). Phylogenetic position of phytopathogens within the Enterobacteriaceae. *Syst Appl Microbiol*, *21*(3), 384-397. https://doi.org/10.1016/S0723-2020(98)80048-9

Henry, E., Yadeta, K. A., & Coaker, G. (2013). Recognition of bacterial plant pathogens: local, systemic and transgenerational immunity. *New Phytol*, *199*(4), 908-915. https://doi.org/10.1111/nph.12214

Hepler, P. K. (2005). Calcium: a central regulator of plant growth and development. *Plant Cell*, *17*(8), 2142-2155. https://doi.org/10.1105/tpc.105.032508

Hepler, P. K., & Winship, L. J. (2010). Calcium at the cell wall-cytoplast interface. *J Integr Plant Biol*, *52*(2), 147-160. https://doi.org/10.1111/j.1744-7909.2010.00923.x

Hevesi, M. (1996). Az *Erwinia amylovora* (Burill) Winslow et al. hazai megjelenése almán. *Növényvédelem*, *32*(5), 225-228.

Holt, J. G., Krieg, N. R., Sneath, P. H., Staley, J. T., & Williams, S. T. (1994). *Bergey's Manual of determinate bacteriology* (9 ed.). Williams & Wilkins.

Ishimaru, C. A., Klos, E. J., & Brubaker, R. R. (1988). Multiple Antibiotic Production by Erwinia-Herbicola. *Phytopathology*, *78*(6), 746-750. https://doi.org/10.1094/Phyto-78-746

Janda, J. M., & Abbott, S. L. (2021). The Changing Face of the Family Enterobacteriaceae (Order: "Enterobacterales"): New Members, Taxonomic Issues, Geographic Expansion, and New Diseases and Disease Syndromes. *Clin Microbiol Rev*, *34*(2), e00174-00120. https://doi.org/10.1128/CMR.00174-20

Jayaraman, J., Choi, S., Prokchorchik, M., Choi, D. S., Spiandore, A., Rikkerink, E. H., Templeton, M. D., Segonzac, C., & Sohn, K. H. (2017). A bacterial acetyltransferase triggers immunity in Arabidopsis thaliana independent of hypersensitive response. *Sci Rep*, *7*(1), 3557. https://doi.org/10.1038/s41598-017-03704-x

Jeuken, M. J., Zhang, N. W., McHale, L. K., Pelgrom, K., den Boer, E., Lindhout, P., Michelmore, R. W., Visser, R. G., & Niks, R. E. (2009). Rin4 causes hybrid necrosis and race-specific resistance in an interspecific lettuce hybrid. *Plant Cell*, *21*(10), 3368-3378. https://doi.org/10.1105/tpc.109.070334

Jiang, S., Yao, J., Ma, K. W., Zhou, H., Song, J., He, S. Y., & Ma, W. (2013). Bacterial effector activates jasmonate signaling by directly targeting JAZ transcriptional repressors. *PLoS Pathog*, *9*(10), e1003715. https://doi.org/10.1371/journal.ppat.1003715

Jock, S., Donat, V., Lopez, M. M., Bazzi, C., & Geider, K. (2002). Following spread of fire blight in Western, Central and Southern Europe by molecular differentiation of *Erwinia amylovora* strains with PFGE analysis. *Environ Microbiol*, *4*(2), 106-114. https://doi.org/10.1046/j.1462-2920.2002.00277.x

Jock, S., Rodoni, B., Gillings, M., Kim, W. S., Copes, C., Merriman, P., & Geider, K. (2000). Screening of ornamental plants from the Botanic Gardens of Melbourne and Adelaide for the occurrence of *Erwinia amylovora*. *Australasian Plant Pathology*, *29*(2), 120-128. https://doi.org/10.1071/ap00020

Johnson, K. B., Stockwell, V. O., & Sawyer, T. L. (2004). Adaptation of Fire Blight Forecasting to Optimize the Use of Biological Controls. *Plant Dis*, *88*(1), 41-48. https://doi.org/10.1094/PDIS.2004.88.1.41

Jones, J. D., & Dangl, J. L. (2006). The plant immune system. *Nature*, *444*(7117), 323-329. https://doi.org/10.1038/nature05286

Jumper, J., Evans, R., Pritzel, A., Green, T., Figurnov, M., Ronneberger, O., Tunyasuvunakool, K., Bates, R., Zidek, A., Potapenko, A., Bridgland, A., Meyer, C., Kohl, S. A. A., Ballard, A. J., Cowie, A., Romera-Paredes, B., Nikolov, S., Jain, R., Adler, J., . . . Hassabis, D. (2021). Highly accurate protein structure prediction with AlphaFold. *Nature*, *596*(7873), 583-589. https://doi.org/10.1038/s41586-021-03819-2

Jupe, F., Witek, K., Verweij, W., Sliwka, J., Pritchard, L., Etherington, G. J., Maclean, D., Cock, P. J., Leggett, R. M., Bryan, G. J., Cardle, L., Hein, I., & Jones, J. D. (2013). Resistance gene enrichment sequencing (RenSeq) enables reannotation of the NB-LRR gene family from sequenced plant genomes and rapid mapping of resistance loci in segregating populations. *Plant J*, *76*(3), 530-544. https://doi.org/10.1111/tpj.12307

Kapila, J., De Rycke, R., Van Montagu, M., & Angenon, G. (1997). An Agrobacterium-mediated transient gene expression system for intact leaves. *Plant Science*, *122*(1), 101-108. https://doi.org/10.1016/s0168-9452(96)04541-4

Keck, M., Reich, H., Chartier, R., & Paulin, J. P. (1996). First Record of Fire Blight (*Erwinia Amylovora*) in Austria Preliminary Experiments on the Survival on Fruit Boxes. *Acta horticulturae*(411), 9-12. https://doi.org/10.17660/ActaHortic.1996.411.3

Khan, M. A., Zhao, Y., & Korban, S. S. (2011). Molecular Mechanisms of Pathogenesis and Resistance to the Bacterial Pathogen Erwinia amylovora, Causal Agent of Fire Blight Disease in Rosaceae. *Plant Molecular Biology Reporter*, *30*(2), 247-260. https://doi.org/10.1007/s11105-011-0334-1

Kim, W. S., Hildebrand, M., Jock, S., & Geider, K. (2001). Molecular comparison of pathogenic bacteria from pear trees in Japan and the fire blight pathogen *Erwinia amylovora*. *Microbiology (Reading)*, *147*(Pt 11), 2951-2959. https://doi.org/10.1099/00221287-147-11-2951

Kim, W. S., Jock, S., Paulin, J. P., Rhim, S. L., & Geider, K. (2001). Molecular Detection and Differentiation of Erwinia pyrifoliae and Host Range Analysis of the Asian Pear Pathogen. *Plant Dis*, *85*(11), 1183-1188. https://doi.org/10.1094/PDIS.2001.85.11.1183

Klarup, J. (1969). Fire blight'en pa Nordfalster. *Erhversfrugt*, *36*, 143-146.

Klement, Z., Bozso, Z., Kecskes, M. L., Besenyei, E., Arnold, C., & Ott, P. G. (2003). Local early induced resistance of plants as the first line of defence against bacteria. *Pest Manag Sci*, *59*(4), 465-474. https://doi.org/10.1002/ps.694

Koczan, J. M., McGrath, M. J., Zhao, Y., & Sundin, G. W. (2009). Contribution of Erwinia amylovora exopolysaccharides amylovoran and levan to biofilm formation: implications in pathogenicity. *Phytopathology*, *99*(11), 1237-1244. https://doi.org/10.1094/PHYTO-99-11-1237

Kourelis, J., & van der Hoorn, R. A. L. (2018). Defended to the Nines: 25 Years of Resistance Gene Cloning Identifies Nine Mechanisms for R Protein Function. *Plant Cell*, *30*(2), 285-299. https://doi.org/10.1105/tpc.17.00579

Kube, M., Migdoll, A. M., Muller, I., Kuhl, H., Beck, A., Reinhardt, R., & Geider, K. (2008). The genome of Erwinia tasmaniensis strain Et1/99, a non-pathogenic bacterium in the genus Erwinia. *Environ Microbiol*, *10*(9), 2211-2222. https://doi.org/10.1111/j.1462-2920.2008.01639.x

Kůdela, V. (1988). Erwinia amylovora - causal agent of fireblight on rosaceous plants in Czechoslovakia. *Sborník ÚVTIZ, Ochrana Rostlin*, *24*(3), 173-182.

Kunkel, T. A. (1985). The mutational specificity of DNA polymerase-beta during in vitro DNA synthesis. Production of frameshift, base substitution, and deletion mutations. *J Biol Chem*, *260*(9), 5787-5796. https://doi.org/10.1016/S0021-9258(18)89090-1

Laflamme, B., Dillon, M. M., Martel, A., Almeida, R. N. D., Desveaux, D., & Guttman, D. S. (2020). The pan-genome effector-triggered immunity landscape of a host-pathogen interaction. *Science*, *367*(6479), 763-768. https://doi.org/10.1126/science.aax4079

Le Roux, C., Huet, G., Jauneau, A., Camborde, L., Tremousaygue, D., Kraut, A., Zhou, B., Levaillant, M., Adachi, H., Yoshioka, H., Raffaele, S., Berthome, R., Coute, Y., Parker, J. E., & Deslandes, L. (2015). A receptor pair with an integrated decoy converts pathogen disabling of transcription factors to immunity. *Cell*, *161*(5), 1074-1088. https://doi.org/10.1016/j.cell.2015.04.025

Lee, A. H., Hurley, B., Felsensteiner, C., Yea, C., Ckurshumova, W., Bartetzko, V., Wang, P. W., Quach, V., Lewis, J. D., Liu, Y. C., Bornke, F., Angers, S., Wilde, A., Guttman, D. S., & Desveaux, D. (2012). A bacterial acetyltransferase destroys plant microtubule networks and blocks secretion. *PLoS Pathog*, *8*(2), e1002523. https://doi.org/10.1371/journal.ppat.1002523

Lee, B., Park, Y. S., Lee, S., Song, G. C., & Ryu, C. M. (2016). Bacterial RNAs activate innate immunity in Arabidopsis. *New Phytol*, *209*(2), 785-797. https://doi.org/10.1111/nph.13717

Lee, G. M., Ko, S., Oh, E. J., Song, Y. R., Kim, D., & Oh, C. S. (2020). Comparative Genome Analysis Reveals Natural Variations in the Genomes of Erwinia pyrifoliae, a Black Shoot Blight Pathogen in Apple and Pear. *Plant Pathol J*, *36*(5), 428-439. https://doi.org/10.5423/PPJ.OA.06.2020.0097

Lee, J., Manning, A. J., Wolfgeher, D., Jelenska, J., Cavanaugh, K. A., Xu, H., Fernandez, S. M., Michelmore, R. W., Kron, S. J., & Greenberg, J. T. (2015). Acetylation of an NB-LRR Plant Immune-Effector Complex Suppresses Immunity. *Cell Rep*, *13*(8), 1670-1682. https://doi.org/10.1016/j.celrep.2015.10.029

Lelliott, R. A. (1984). Genus Erwinia. *Bergey's manual of systematic bacteriology*, *1*, 469-476.

Lemieux, M. G. (2016). *Plasmids 101: ccdB-The toxic key to efficient cloning*. https://blog.addgene.org/plasmids-101-ccdb-the-toxic-key-to-efficient-cloning

Lewis, J. D., Lee, A., Ma, W., Zhou, H., Guttman, D. S., & Desveaux, D. (2011). The YopJ superfamily in plant-associated bacteria. *Mol Plant Pathol*, *12*(9), 928-937. https://doi.org/10.1111/j.1364-3703.2011.00719.x

Lewis, J. D., Lee, A. H., Hassan, J. A., Wan, J., Hurley, B., Jhingree, J. R., Wang, P. W., Lo, T., Youn, J. Y., Guttman, D. S., & Desveaux, D. (2013). The Arabidopsis ZED1 pseudokinase is required for ZAR1-mediated immunity induced by the Pseudomonas syringae type III effector HopZ1a. *Proc Natl Acad Sci U S A*, *110*(46), 18722-18727. https://doi.org/10.1073/pnas.1315520110

Lewis, J. D., Wilton, M., Mott, G. A., Lu, W., Hassan, J. A., Guttman, D. S., & Desveaux, D. (2014). Immunomodulation by the Pseudomonas syringae HopZ type III effector family in Arabidopsis. *PLOS ONE*, *9*(12), e116152. https://doi.org/10.1371/journal.pone.0116152

Lewis, J. D., Wu, R., Guttman, D. S., & Desveaux, D. (2010). Allele-specific virulence attenuation of the Pseudomonas syringae HopZ1a type III effector via the Arabidopsis ZAR1 resistance protein. *PLoS Genet*, *6*(4), e1000894. https://doi.org/10.1371/journal.pgen.1000894

Li, Y., Li, S., Bi, D., Cheng, Y. T., Li, X., & Zhang, Y. (2010). SRFR1 negatively regulates plant NB-LRR resistance protein accumulation to prevent autoimmunity. *PLoS Pathog*, *6*(9), e1001111. https://doi.org/10.1371/journal.ppat.1001111

Lindgren, P. B., Peet, R. C., & Panopoulos, N. J. (1986). Gene cluster of Pseudomonas syringae pv. "phaseolicola" controls pathogenicity of bean plants and hypersensitivity of nonhost plants. *J Bacteriol*, *168*(2), 512-522. https://doi.org/10.1128/jb.168.2.512-522.1986

Lopez, M. M., Rosello, M., Llop, P., Ferrer, S., Christen, R., & Gardan, L. (2011). *Erwinia piriflorinigrans* sp. nov., a novel pathogen that causes necrosis of pear blossoms. *Int J Syst Evol Microbiol*, *61*(Pt 3), 561-567. https://doi.org/10.1099/ijs.0.020479-0

Luo, Y., Caldwell, K. S., Wroblewski, T., Wright, M. E., & Michelmore, R. W. (2009). Proteolysis of a negative regulator of innate immunity is dependent on resistance genes in tomato and Nicotiana benthamiana and induced by multiple bacterial effectors. *Plant Cell*, *21*(8), 2458-2472. https://doi.org/10.1105/tpc.107.056044

Ma, K. W., Jiang, S., Hawara, E., Lee, D., Pan, S., Coaker, G., Song, J., & Ma, W. (2015). Two serine residues in Pseudomonas syringae effector HopZ1a are required for acetyltransferase activity and association with the host co-factor. *New Phytol*, *208*(4), 1157-1168. https://doi.org/10.1111/nph.13528

Ma, K. W., & Ma, W. (2016). YopJ Family Effectors Promote Bacterial Infection through a Unique Acetyltransferase Activity. *Microbiol Mol Biol Rev*, *80*(4), 1011-1027. https://doi.org/10.1128/MMBR.00032-16

Ma, W., Dong, F. F., Stavrinides, J., & Guttman, D. S. (2006). Type III effector diversification via both pathoadaptation and horizontal transfer in response to a coevolutionary arms race. *PLoS Genet*, *2*(12), e209. https://doi.org/10.1371/journal.pgen.0020209

Macho, A. P., & Zipfel, C. (2015). Targeting of plant pattern recognition receptor-triggered immunity by bacterial type-III secretion system effectors. *Curr Opin Microbiol*, *23*, 14-22. https://doi.org/10.1016/j.mib.2014.10.009

Mackey, D., Holt, B. F., 3rd, Wiig, A., & Dangl, J. L. (2002). RIN4 interacts with Pseudomonas syringae type III effector molecules and is required for RPM1-mediated resistance in Arabidopsis. *Cell*, *108*(6), 743-754. https://doi.org/10.1016/s0092-8674(02)00661-x

Maes, M., Orye, K., Bobev, S., Devreese, B., Van Beeumen, J., De Bruyn, A., Busson, R., Herdewijn, P., Morreel, K., & Messens, E. (2001). Influence of amylovoran production on virulence of Erwinia

amylovora and a different amylovoran structure in E-amylovora isolates from Rubus. *European Journal of Plant Pathology*, *107*(8), 839-844. https://doi.org/10.1023/A:1012215201253

Malnoy, M., Martens, S., Norelli, J. L., Barny, M. A., Sundin, G. W., Smits, T. H., & Duffy, B. (2012). Fire blight: applied genomic insights of the pathogen and host. *Annu Rev Phytopathol*, *50*(1), 475-494. https://doi.org/10.1146/annurev-phyto-081211-172931

Maltseva, E. R., Zharmukhamedova, G. A., Jumanova, Z. K., Naizabayeva, D. A., Berdygulova, Z. A., Dmitriyeva, K. A., Soltanbekov, S. S., Argynbayeva, A. M., Skiba, Y. A., Malakhova, N. P., Rezzonico, F., & Smits, T. H. M. (2022). Assessment of fire blight introduction in the wild apple forests of Kazakhstan. *Biodiversity*, 1-6. https://doi.org/10.1080/14888386.2022.2141880

Mansfield, J., Genin, S., Magori, S., Citovsky, V., Sriariyanum, M., Ronald, P., Dow, M., Verdier, V., Beer, S. V., Machado, M. A., Toth, I., Salmond, G., & Foster, G. D. (2012). Top 10 plant pathogenic bacteria in molecular plant pathology. *Mol Plant Pathol*, *13*(6), 614-629. https://doi.org/10.1111/j.1364-3703.2012.00804.x

Mansfield, J., Jenner, C., Hockenhull, R., Bennett, M. A., & Stewart, R. (1994). Characterization of avrPphE, a gene for cultivar-specific avirulence from Pseudomonas syringae pv. phaseolicola which is physically linked to hrpY, a new hrp gene identified in the halo-blight bacterium. *Molecular plant-microbe interactions : MPMI*, *7*(6), 726-739. https://doi.org/10.1094/mpmi-7-0726

Manual, I. QuikChange II XL Site-Directed Mutagenesis Kit. In.

Marinus, M. G., & Lobner-Olesen, A. (2014). DNA Methylation. *EcoSal Plus*, *6*(1). https://doi.org/10.1128/ecosalplus.ESP-0003-2013

Mayerhofer, R., Koncz-Kalman, Z., Nawrath, C., Bakkeren, G., Crameri, A., Angelis, K., Redei, G. P., Schell, J., Hohn, B., & Koncz, C. (1991). T-DNA integration: a mode of illegitimate recombination in plants. *Embo j*, *10*(3), 697-704. https://doi.org/10.1002/j.1460-2075.1991.tb07999.x

Mergaert, J., Verdonck, L., Kersters, K., Swings, J., Boeufgras, J. M., & De Ley, J. (1984). Numerical Taxonomy of Erwinia Species Using API Systems. *Microbiology*, *130*(8), 1893-1910. https://doi.org/10.1099/00221287-130-8-1893

Mittal, R., Peak-Chew, S. Y., Sade, R. S., Vallis, Y., & McMahon, H. T. (2010). The acetyltransferase activity of the bacterial toxin YopJ of Yersinia is activated by eukaryotic host cell inositol hexakisphosphate. *J Biol Chem*, *285*(26), 19927-19934. https://doi.org/10.1074/jbc.M110.126581

Mizuno, A., Sato, S., & Kawai, A. (2002). Serological Differences among *Erwinia amylovora* Biovars. *Journal of General Plant Pathology*, *68*(4), 350-355. https://doi.org/10.1007/pl00013102

Mizuno, A., Tsukamoto, T., Shimizu, Y., Ooya, H., Matsuura, T., Saito, N., Sato, S., Kikuchi, S., Uzuki, T., & Azegami, K. (2009). Occurrence of bacterial black shoot disease of European pear in Yamagata Prefecture. *Journal of General Plant Pathology*, *76*(1), 43-51. https://doi.org/10.1007/s10327-009-0215-8

Mohan, S. K., & Bijman, V. P. (1999). Susceptibility of prunus species to Erwinia amylovora. *Proceedings of the Eighth International Workshop on Fire Blight*, *489*(489), 145-148. https://doi.org/10.17660/ActaHortic.1999.489.21

Mooney, B. C., Mantz, M., Graciet, E., & Huesgen, P. F. (2021). Cutting the line: manipulation of plant immunity by bacterial type III effector proteases. *J Exp Bot*, *72*(9), 3395-3409. https://doi.org/10.1093/jxb/erab095

Mukherjee, S., Keitany, G., Li, Y., Wang, Y., Ball, H. L., Goldsmith, E. J., & Orth, K. (2006). Yersinia YopJ Acetylates and Inhibits Kinase Activation by Blocking Phosphorylation. *Science*, *312*(5777), 1211-1214. https://doi.org/10.1126/science.1126867

Murray, M. B., Cape, J. N., & Fowler, D. (1989). Quantification of frost damage in plant tissues by rates of electrolyte leakage. *New Phytol*, *113*(3), 307-311. https://doi.org/10.1111/j.1469-8137.1989.tb02408.x

Nakagawa, T., Kurose, T., Hino, T., Tanaka, K., Kawamukai, M., Niwa, Y., Toyooka, K., Matsuoka, K., Jinbo, T., & Kimura, T. (2007). Development of series of gateway binary vectors, pGWBs, for realizing efficient construction of fusion genes for plant transformation. *J Biosci Bioeng*, *104*(1), 34-41. https://doi.org/10.1263/jbb.104.34

Naveed, Z. A., Wei, X., Chen, J., Mubeen, H., & Ali, G. S. (2020). The PTI to ETI Continuum in Phytophthora-Plant Interactions [Review]. *Front Plant Sci*, *11*, 593905. https://doi.org/10.3389/fpls.2020.593905

Nazareno, E. S., Kersey, C. M., & Dumenyo, C. K. (2016). Characterization of the incompatible interaction between Erwinia tracheiphila and non-host tobacco (Nicotiana tabacum). *Physiological and Molecular Plant Pathology*, *96*, 85-93. https://doi.org/10.1016/j.pmpp.2016.10.001

Ngou, B. P. M., Ahn, H. K., Ding, P., & Jones, J. D. G. (2021). Mutual potentiation of plant immunity by cell-surface and intracellular receptors. *Nature*, *592*(7852), 110-115. https://doi.org/10.1038/s41586-021-03315-7

Nimchuk, Z. L., Fisher, E. J., Desveaux, D., Chang, J. H., & Dangl, J. L. (2007). The HopX (AvrPphE) family of Pseudomonas syringae type III effectors require a catalytic triad and a novel N-terminal domain for function. *Molecular plant-microbe interactions : MPMI*, *20*(4), 346-357. https://doi.org/10.1094/MPMI-20-4-0346

Nissan, G., Gershovits, M., Morozov, M., Chalupowicz, L., Sessa, G., Manulis-Sasson, S., Barash, I., & Pupko, T. (2018). Revealing the inventory of type III effectors in *Pantoea agglomerans* gall-forming pathovars using draft genome sequences and a machine-learning approach. *Mol Plant Pathol*, *19*(2), 381-392. https://doi.org/10.1111/mpp.12528

Nissinen, R. M., Ytterberg, A. J., Bogdanove, A. J., KJ, V. A. N. W., & Beer, S. V. (2007). Analyses of the secretomes of Erwinia amylovora and selected hrp mutants reveal novel type III secreted proteins and an effect of HrpJ on extracellular harpin levels. *Mol Plant Pathol*, *8*(1), 55-67. https://doi.org/10.1111/j.1364-3703.2006.00370.x

Norelli, J. L., Jones, A. L., & Aldwinckle, H. S. (2003). Fire Blight Management in the Twenty-first Century: Using New Technologies that Enhance Host Resistance in Apple. *Plant Dis*, *87*(7), 756-765. https://doi.org/10.1094/PDIS.2003.87.7.756

Oh, C. S., & Beer, S. V. (2005). Molecular genetics of Erwinia amylovora involved in the development of fire blight. *FEMS Microbiol Lett*, *253*(2), 185-192. https://doi.org/10.1016/j.femsle.2005.09.051

Olawole, O. I., Liu, Q., Chen, C., Gleason, M. L., & Beattie, G. A. (2021). The Contributions to Virulence of the Effectors Eop1 and DspE Differ Between Two Clades of *Erwinia tracheiphila* Strains. *Molecular plant-microbe interactions : MPMI*, *34*(12), 1399-1408. https://doi.org/10.1094/MPMI-06-21-0149-R

Orth, K., Xu, Z., Mudgett, M. B., Bao, Z. Q., Palmer, L. E., Bliska, J. B., Mangel, W. F., Staskawicz, B., & Dixon, J. E. (2000). Disruption of signaling by Yersinia effector YopJ, a ubiquitin-like protein protease. *Science*, *290*(5496), 1594-1597. https://doi.org/10.1126/science.290.5496.1594

Palacio-Bielsa, A., Roselló, M., Llop, P., & López, M. M. (2011). Erwinia spp. from pome fruit trees: similarities and differences among pathogenic and non-pathogenic species. *Trees*, *26*(1), 13-29. https://doi.org/10.1007/s00468-011-0644-9

Panstruga, R., & Moscou, M. J. (2020). What is the Molecular Basis of Nonhost Resistance? *Molecular plant-microbe interactions : MPMI*, *33*(11), 1253-1264. https://doi.org/10.1094/MPMI-06-20-0161-CR

Paulin, J. (2000). *Erwinia amylovora: general characteristics, biochemistry and serology*. CABI International. https://doi.org/10.1079/9780851992945.0087

Peil, A., Bus, V., Geider, K., Richter, K., Flachowsky, H., & Hanke, M.-V. (2009). Improvement of fire blight resistance in apple and pear. *International journal of plant breeding*, *3*, 1-27. http://www.globalsciencebooks.info/Online/GSBOnline/images/0906/IJPB_3(1)/IJPB_3(1)1-27o.pdf

Pierce, N. B. (1902). Pear Blight in California. *Science*, *16*(396), 193-194. https://doi.org/10.1126/science.16.396.193

Pique, N., Minana-Galbis, D., Merino, S., & Tomas, J. M. (2015). Virulence Factors of Erwinia amylovora: A Review. *Int J Mol Sci*, *16*(6), 12836-12854. https://doi.org/10.3390/ijms160612836

Potter, D., Eriksson, T., Evans, R. C., Oh, S., Smedmark, J. E. E., Morgan, D. R., Kerr, M., Robertson, K. R., Arsenault, M., Dickinson, T. A., & Campbell, C. S. (2007). Phylogeny and classification of Rosaceae. *Plant Systematics and Evolution*, *266*(1-2), 5-43. https://doi.org/10.1007/s00606-007-0539-9

Prokchorchik, M., Choi, S., Chung, E. H., Won, K., Dangl, J. L., & Sohn, K. H. (2020). A host target of a bacterial cysteine protease virulence effector plays a key role in convergent evolution of plant innate immune system receptors. *New Phytol*, *225*(3), 1327-1342. https://doi.org/10.1111/nph.16218

Psallidas, P. G. (1990). Fire Blight of Pomaceous Trees in Greece-Evolution of the Disease and Characteristics of the Pathogen *Erwinia amylovora*. *Acta horticulturae*, *273*(273), 25-32. https://doi.org/10.17660/ActaHortic.1990.273.1

Psallidas, P. G., & Dimova, M. (1986). Occurrence of the disease fire-blight of pomaceous trees in Cyprus. Characteristics of the pathogen *Erwinia amylovora*. *Annales de l'Institut Phytopathologique Benaki*, *15*(1), 61-70. https://www.cabdirect.org/cabdirect/abstract/19881341632

Pusey, P. L. (2002). Biological Control Agents for Fire Blight of Apple Compared Under Conditions Limiting Natural Dispersal. *Plant Dis*, *86*(6), 639-644. https://doi.org/10.1094/PDIS.2002.86.6.639

Rathore, J. S., & Ghosh, C. (2018). Pathogen-Associated Molecular Patterns and Their Perception in Plants. In A. Singh & I. K. Singh (Eds.), *Molecular Aspects of Plant-Pathogen Interaction* (pp. 79-113). Springer Singapore. https://doi.org/10.1007/978-981-10-7371-7_4

Ray, S. K., Macoy, D. M., Kim, W. Y., Lee, S. Y., & Kim, M. G. (2019). Role of RIN4 in Regulating PAMP-Triggered Immunity and Effector-Triggered Immunity: Current Status and Future Perspectives. *Mol Cells*, *42*(7), 503-511. https://doi.org/10.14348/molcells.2019.2433

Rhim, Volksch, Gardan, Paulin, Langlotz, Kim, & Geider. (1999). *Erwinia pyrifoliae*, an *Erwinia* species different from *Erwinia amylovora*, causes a necrotic disease of Asian pear trees. *Plant Pathology*, *48*(4), 514-520. https://doi.org/10.1046/j.1365-3059.1999.00376.x

Rico, A., Bennett, M. H., Forcat, S., Huang, W. E., & Preston, G. M. (2010). Agroinfiltration reduces ABA levels and suppresses Pseudomonas syringae-elicited salicylic acid production in Nicotiana tabacum. *PLOS ONE*, *5*(1), e8977. https://doi.org/10.1371/journal.pone.0008977

Rojas, E. S., Batzer, J. C., Beattie, G. A., Fleischer, S. J., Shapiro, L. R., Williams, M. A., Bessin, R., Bruton, B. D., Boucher, T. J., Jesse, L. C. H., & Gleason, M. L. (2015). Bacterial Wilt of Cucurbits: Resurrecting a Classic Pathosystem. *Plant Dis*, *99*(5), 564-574. https://doi.org/10.1094/PDIS-10-14-1068-FE

Roselló, M., Peñalver, J., Llop, P., Gorris, M. T., Cambra, M., López, M. M., Chartier, R., García, F., & Montón, C. (2006). Identification of anErwiniasp. different fromErwinia amylovoraand responsible for necrosis on pear blossoms. *Canadian Journal of Plant Pathology*, *28*(1), 30-41. https://doi.org/10.1080/07060660609507268

Russell, A. R., Ashfield, T., & Innes, R. W. (2015). Pseudomonas syringae Effector AvrPphB Suppresses AvrB-Induced Activation of RPM1 but Not AvrRpm1-Induced Activation. *Molecular plant-microbe interactions : MPMI*, *28*(6), 727-735. https://doi.org/10.1094/MPMI-08-14-0248-R

Sahdev, S., Saini, S., Tiwari, P., Saxena, S., & Singh Saini, K. (2007). Amplification of GC-rich genes by following a combination strategy of primer design, enhancers and modified PCR cycle conditions. *Mol Cell Probes*, *21*(4), 303-307. https://doi.org/10.1016/j.mcp.2007.03.004

Sang, Y., Yu, W., Zhuang, H., Wei, Y., Derevnina, L., Yu, G., Luo, J., & Macho, A. P. (2020). Intra-strain Elicitation and Suppression of Plant Immunity by Ralstonia solanacearum Type-III Effectors in Nicotiana benthamiana. *Plant Commun*, *1*(4), 100025. https://doi.org/10.1016/j.xplc.2020.100025

Sanzol, J. (2010). Dating and functional characterization of duplicated genes in the apple (Malus domestica Borkh.) by analyzing EST data. *BMC Plant Biol*, *10*(1), 87. https://doi.org/10.1186/1471-2229-10-87

Sarris, P. F., Duxbury, Z., Huh, S. U., Ma, Y., Segonzac, C., Sklenar, J., Derbyshire, P., Cevik, V., Rallapalli, G., Saucet, S. B., Wirthmueller, L., Menke, F. L. H., Sohn, K. H., & Jones, J. D. G. (2015). A Plant Immune Receptor Detects Pathogen Effectors that Target WRKY Transcription Factors. *Cell*, *161*(5), 1089-1100. https://doi.org/10.1016/j.cell.2015.04.024

Schiavinato, M., Marcet-Houben, M., Dohm, J. C., Gabaldon, T., & Himmelbauer, H. (2020). Parental origin of the allotetraploid tobacco Nicotiana benthamiana. *Plant J*, *102*(3), 541-554. https://doi.org/10.1111/tpj.14648

Selote, D., & Kachroo, A. (2010). RPG1-B-derived resistance to AvrB-expressing Pseudomonas syringae requires RIN4-like proteins in soybean. *Plant Physiol*, *153*(3), 1199-1211. https://doi.org/10.1104/pp.110.158147

Senthil-Kumar, M., & Mysore, K. S. (2013). Nonhost resistance against bacterial pathogens: retrospectives and prospects. *Annu Rev Phytopathol*, *51*(1), 407-427. https://doi.org/10.1146/annurev-phyto-082712-102319

Serrano, M., Coluccia, F., Torres, M., L'Haridon, F., & Metraux, J. P. (2014). The cuticle and plant defense to pathogens [Review]. *Front Plant Sci*, *5*, 274. https://doi.org/10.3389/fpls.2014.00274

Shabi, E., & Zutra, D. (1987). Outbreaks of Fire Blight in Israel in 1985 and 1986. *Acta horticulturae*(217), 23-32. https://doi.org/10.17660/ActaHortic.1987.217.2

Shapiro, L. R., Paulson, J. N., Arnold, B. J., Scully, E. D., Zhaxybayeva, O., Pierce, N. E., Rocha, J., Klepac-Ceraj, V., Holton, K., & Kolter, R. (2018). An Introduced Crop Plant Is Driving Diversification of the Virulent Bacterial Pathogen Erwinia tracheiphila. *mBio*, *9*(5), e01307-01318. https://doi.org/10.1128/mBio.01307-18

Shrestha, R., Koo, J.-H., Park, D.-H., Hwang, I.-G., Hur, J.-H., & Lim, C.-K. (2003). *Erwinia pyrifoliae*, a Causal Endemic Pathogen of Shoot Blight of Asian Pear Tree in Korea. *Plant Pathol J*, *19*(6), 294-300. https://doi.org/10.5423/ppj.2003.19.6.294

Sierro, N., Battey, J. N., Ouadi, S., Bakaher, N., Bovet, L., Willig, A., Goepfert, S., Peitsch, M. C., & Ivanov, N. V. (2014). The tobacco genome sequence and its comparison with those of tomato and potato. *Nat Commun*, *5*(1), 3833. https://doi.org/10.1038/ncomms4833

Smits, T. H. M., Duffy, B., Blom, J., Ishimaru, C. A., & Stockwell, V. O. (2019). Pantocin A, a peptide-derived antibiotic involved in biological control by plant-associated Pantoea species. *Arch Microbiol*, *201*(6), 713-722. https://doi.org/10.1007/s00203-019-01647-7

Stockwell, V. O., Johnson, K. B., Sugar, D., & Loper, J. E. (2011). Mechanistically compatible mixtures of bacterial antagonists improve biological control of fire blight of pear. *Phytopathology*, *101*(1), 113-123. https://doi.org/10.1094/PHYTO-03-10-0098

Strachan, T., & Read, A. P. (1999). Human molecular genetics. In: BIOS Scientific Publishers, Oxford.

Stuart, L. M., Paquette, N., & Boyer, L. (2013). Effector-triggered versus pattern-triggered immunity: how animals sense pathogens. *Nat Rev Immunol*, *13*(3), 199-206. https://doi.org/10.1038/nri3398

Sugimoto, M., Esaki, N., Tanaka, H., & Soda, K. (1989). A simple and efficient method for the oligonucleotide-directed mutagenesis using plasmid DNA template and phosphorothioate-modified nucleotide. *Anal Biochem*, *179*(2), 309-311. https://doi.org/10.1016/0003-2697(89)90134-6

Sun, X., Greenwood, D. R., Templeton, M. D., Libich, D. S., McGhie, T. K., Xue, B., Yoon, M., Cui, W., Kirk, C. A., Jones, W. T., Uversky, V. N., & Rikkerink, E. H. (2014). The intrinsically disordered structural platform of the plant defence hub protein RPM1-interacting protein 4 provides insights into its mode of action in the host-pathogen interface and evolution of the nitrate-induced domain protein family. *FEBS J*, *281*(17), 3955-3979. https://doi.org/10.1111/febs.12937

Sundin, G. W., Mayfield, C. T., Zhao, Y., Gunasekera, T. S., Foster, G. L., & Ullrich, M. S. (2004). Complete nucleotide sequence and analysis of pPSR1 (72,601 bp), a pPT23A-family plasmid from Pseudomonas syringae pv. syringae A2. *Mol Genet Genomics*, *270*(6), 462-476. https://doi.org/10.1007/s00438-003-0945-9

Szatmari, A., Zvara, A., Moricz, A. M., Besenyei, E., Szabo, E., Ott, P. G., Puskas, L. G., & Bozso, Z. (2014). Pattern triggered immunity (PTI) in tobacco: isolation of activated genes suggests role of the phenylpropanoid pathway in inhibition of bacterial pathogens. *PLOS ONE*, *9*(8), e102869. https://doi.org/10.1371/journal.pone.0102869

Szczesny, R., Buttner, D., Escolar, L., Schulze, S., Seiferth, A., & Bonas, U. (2010). Suppression of the AvrBs1-specific hypersensitive response by the YopJ effector homolog AvrBsT from Xanthomonas depends on a SNF1-related kinase. *New Phytol*, *187*(4), 1058-1074. https://doi.org/10.1111/j.1469-8137.2010.03346.x

Tang, Y., Zhao, D., Meng, J., & Tao, J. (2019). EGTA reduces the inflorescence stem mechanical strength of herbaceous peony by modifying secondary wall biosynthesis. *Hortic Res*, *6*, 36. https://doi.org/10.1038/s41438-019-0117-7

Tao, Y., Xie, Z., Chen, W., Glazebrook, J., Chang, H. S., Han, B., Zhu, T., Zou, G., & Katagiri, F. (2003). Quantitative nature of Arabidopsis responses during compatible and incompatible interactions with the bacterial pathogen Pseudomonas syringae. *Plant Cell*, *15*(2), 317-330. https://doi.org/10.1105/tpc.007591

Tasset, C., Bernoux, M., Jauneau, A., Pouzet, C., Briere, C., Kieffer-Jacquinod, S., Rivas, S., Marco, Y., & Deslandes, L. (2010). Autoacetylation of the Ralstonia solanacearum effector PopP2 targets a lysine residue essential for RRS1-R-mediated immunity in Arabidopsis. *PLoS Pathog*, *6*(11), e1001202. https://doi.org/10.1371/journal.ppat.1001202

Tasset, C., Bernoux, M., Jauneau, A., Pouzet, C., Briere, C., Kieffer-Jacquinod, S., Rivas, S., Marco, Y., & Deslandes, L. (2022). Correction: Autoacetylation of the Ralstonia solanacearum Effector PopP2 Targets a Lysine Residue Essential for RRS1-R-Mediated Immunity in Arabidopsis. *PLoS Pathog*, *18*(3), e1010368. https://doi.org/10.1371/journal.ppat.1010368

Taylor, J. W., Ott, J., & Eckstein, F. (1985). The rapid generation of oligonucleotide-directed mutations at high frequency using phosphorothioate-modified DNA. *Nucleic Acids Res*, *13*(24), 8765-8785. https://doi.org/10.1093/nar/13.24.8765

Tehabsim, A., Masannat, K., & Janse, J. D. (1992). Fireblight (*Erwinia amylovora*) on pome fruits in Jordan. *Phytopathologia Mediterranea*, *31*(2), 117-118.

Thieme, F., Szczesny, R., Urban, A., Kirchner, O., Hause, G., & Bonas, U. (2007). New type III effectors from Xanthomonas campestris pv. vesicatoria trigger plant reactions dependent on a conserved N-myristoylation motif. *Molecular plant-microbe interactions : MPMI*, *20*(10), 1250-1261. https://doi.org/10.1094/MPMI-20-10-1250

Thomson, S. V. (1986). The Role of the Stigma in Fire Blight Infections. *Phytopathology*, *76*(5), 476-482. https://doi.org/10.1094/Phyto-76-476

Thor, K., Jiang, S., Michard, E., George, J., Scherzer, S., Huang, S., Dindas, J., Derbyshire, P., Leitao, N., DeFalco, T. A., Koster, P., Hunter, K., Kimura, S., Gronnier, J., Stransfeld, L., Kadota, Y., Bucherl, C. A., Charpentier, M., Wrzaczek, M., . . . Zipfel, C. (2020). The calcium-permeable channel OSCA1.3 regulates plant stomatal immunity. *Nature*, *585*(7826), 569-573. https://doi.org/10.1038/s41586-020-2702-1

Tian, D., Traw, M. B., Chen, J. Q., Kreitman, M., & Bergelson, J. (2003). Fitness costs of R-gene-mediated resistance in Arabidopsis thaliana. *Nature*, *423*(6935), 74-77. https://doi.org/10.1038/nature01588

Tian, H., Wu, Z., Chen, S., Ao, K., Huang, W., Yaghmaiean, H., Sun, T., Xu, F., Zhang, Y., Wang, S., Li, X., & Zhang, Y. (2021). Activation of TIR signalling boosts pattern-triggered immunity. *Nature*, *598*(7881), 500-503. https://doi.org/10.1038/s41586-021-03987-1

Toruno, T. Y., Stergiopoulos, I., & Coaker, G. (2016a). Plant-Pathogen Effectors: Cellular Probes Interfering with Plant Defenses in Spatial and Temporal Manners. *Annu Rev Phytopathol*, *54*(1), 419-441. https://doi.org/10.1146/annurev-phyto-080615-100204

Toruno, T. Y., Stergiopoulos, I., & Coaker, G. (2016b). Plant-Pathogen Effectors: Cellular Probes Interfering with Plant Defenses in Spatial and Temporal Manners. *Annu Rev Phytopathol*, *54*, 419-441. https://doi.org/10.1146/annurev-phyto-080615-100204

Triplett, L. R., Zhao, Y., & Sundin, G. W. (2006). Genetic differences between blight-causing Erwinia species with differing host specificities, identified by suppression subtractive hybridization. *Appl Environ Microbiol*, *72*(11), 7359-7364. https://doi.org/10.1128/AEM.01159-06

Trosky, J. E., Li, Y., Mukherjee, S., Keitany, G., Ball, H., & Orth, K. (2007). VopA inhibits ATP binding by acetylating the catalytic loop of MAPK kinases. *J Biol Chem*, *282*(47), 34299-34305. https://doi.org/10.1074/jbc.M706970200

Tunyasuvunakool, K., Adler, J., Wu, Z., Green, T., Zielinski, M., Zidek, A., Bridgland, A., Cowie, A., Meyer, C., Laydon, A., Velankar, S., Kleywegt, G. J., Bateman, A., Evans, R., Pritzel, A., Figurnov, M., Ronneberger, O., Bates, R., Kohl, S. A. A., . . . Hassabis, D. (2021). Highly accurate protein structure

prediction for the human proteome. *Nature*, *596*(7873), 590-596. https://doi.org/10.1038/s41586-021-03828-1

Ustun, S., & Bornke, F. (2015). The Xanthomonas campestris type III effector XopJ proteolytically degrades proteasome subunit RPT6. *Plant Physiol*, *168*(1), 107-119. https://doi.org/10.1104/pp.15.00132

Uyeda, E. (1903). The causal bacterium of apple blight. *Dai-Nippon No-Kaiho*, *260*, 1-3.

van der Hoorn, R. A., & Kamoun, S. (2008). From Guard to Decoy: a new model for perception of plant pathogen effectors. *Plant Cell*, *20*(8), 2009-2017. https://doi.org/10.1105/tpc.108.060194

Van Der Zwet, T., & Beer, S. V. (1999). *Fire Blight--its Nature, Prevention, and Control: A Practical Guide to Integrated Disease Management* (309584). (Agricultural Information Bulletins, Issue. E. R. S. United States Department of Agriculture. https://ideas.repec.org/p/ags/uersab/309584.html

Van Der Zwet, T., & Keil, H. L. (1979). *Fire blight: A bacterial disease of rosaceous plants* (Vol. 510). USDA Agriculture Handbook https://www.cabdirect.org/cabdirect/abstract/19790375755

van der Zwet, T., Orolaza-Halbrendt, N., & Zeller, W. (2016a). CHAPTER 2: Spread and Current Distribution of Fire Blight. In *Fire Blight: History, Biology, and Management* (pp. 15-36). The American Phytopathological Society. https://doi.org/10.1094/9780890544839.003

van der Zwet, T., Orolaza-Halbrendt, N., & Zeller, W. (2016b). CHAPTER 10: The Disease Cycle of Fire Blight. In *Fire Blight: History, Biology, and Management* (pp. 155-182). The American Phytopathological Society. https://doi.org/10.1094/9780890544839.012

van Wersch, S., Tian, L., Hoy, R., & Li, X. (2020). Plant NLRs: The Whistleblowers of Plant Immunity. *Plant Commun*, *1*(1), 100016. https://doi.org/10.1016/j.xplc.2019.100016

Vandeyar, M. A., Weiner, M. P., Hutton, C. J., & Batt, C. A. (1988). A simple and rapid method for the selection of oligodeoxynucleotide-directed mutants. *Gene*, *65*(1), 129-133. https://doi.org/10.1016/0378-1119(88)90425-8

Vanneste, J. (2000). *What is fire blight? Who is Erwinia amylovora? How to control it?* CABI International. https://doi.org/10.1079/9780851992945.0001

VÉGh, A., & Palkovics, L. (2013). First Occurence of Fire Blight on Apricot (*Prunus armeniaca*) in Hungary. *Notulae Botanicae Horti Agrobotanici Cluj-Napoca*, *41*(2), 440-443. https://doi.org/10.15835/nbha4129183

Veldeman, R. (1972). La découverte d'*Erwinia amylovora* (Burril) Winslow et al.(feu bactérien du poirier) en Belgique. *Revue l'Agriculture, Brussels*, *25*, 1587-1594.

Vieira, R. D. A., Zambolim, L., Ramos, R. S., da Silva, R. S., Ebel, J., & Borba, P. T. D. d. (2020). Potential Risk Levels of Invasive Fire Blight in Apple Orchards Around the World. *Journal of Agricultural Science*, *12*(11), 17. https://doi.org/10.5539/jas.v12n11p17

Vinatzer, B. A., Teitzel, G. M., Lee, M. W., Jelenska, J., Hotton, S., Fairfax, K., Jenrette, J., & Greenberg, J. T. (2006). The type III effector repertoire of Pseudomonas syringae pv. syringae B728a and its role

in survival and disease on host and non-host plants. *Mol Microbiol*, *62*(1), 26-44. https://doi.org/10.1111/j.1365-2958.2006.05350.x

Vleeshouwers, V. G., Rietman, H., Krenek, P., Champouret, N., Young, C., Oh, S. K., Wang, M., Bouwmeester, K., Vosman, B., Visser, R. G., Jacobsen, E., Govers, F., Kamoun, S., & Van der Vossen, E. A. (2008). Effector genomics accelerates discovery and functional profiling of potato disease resistance and phytophthora infestans avirulence genes. *PLOS ONE*, *3*(8), e2875. https://doi.org/10.1371/journal.pone.0002875

Vogt, I., Wohner, T., Richter, K., Flachowsky, H., Sundin, G. W., Wensing, A., Savory, E. A., Geider, K., Day, B., Hanke, M. V., & Peil, A. (2013). Gene-for-gene relationship in the host-pathogen system Malus x robusta 5-Erwinia amylovora. *New Phytol*, *197*(4), 1262-1275. https://doi.org/10.1111/nph.12094

Walterson, A. M., & Stavrinides, J. (2015). Pantoea: insights into a highly versatile and diverse genus within the Enterobacteriaceae. *FEMS Microbiol Rev*, *39*(6), 968-984. https://doi.org/10.1093/femsre/fuv027

Wang, J., Liu, X., Zhang, A., Ren, Y., Wu, F., Wang, G., Xu, Y., Lei, C., Zhu, S., Pan, T., Wang, Y., Zhang, H., Wang, F., Tan, Y. Q., Wang, Y., Jin, X., Luo, S., Zhou, C., Zhang, X., . . . Wan, J. (2019). A cyclic nucleotide-gated channel mediates cytoplasmic calcium elevation and disease resistance in rice. *Cell Res*, *29*(10), 820-831. https://doi.org/10.1038/s41422-019-0219-7

White, P. J., & Broadley, M. R. (2003). Calcium in plants. *Ann Bot*, *92*(4), 487-511. https://doi.org/10.1093/aob/mcg164

Wilson, A. J., & Seller, S. E. (1977). Reaction time to scotopic flashes of light. *Am J Optom Physiol Opt*, *54*(12), 845-848. https://doi.org/10.1097/00006324-197712000-00007

Wilson, J. (1906). Investigations by the pathologists. *USDA Yearbook*, *1907*, 41.

Winslow, C. E., Broadhurst, J., Buchanan, R. E., Krumwiede, C., Rogers, L. A., & Smith, G. H. (1920). The Families and Genera of the Bacteria: Final Report of the Committee of the Society of American Bacteriologists on Characterization and Classification of Bacterial Types. *J Bacteriol*, *5*(3), 191-229. https://doi.org/10.1128/jb.5.3.191-229.1920

Wöhner, T. W., Richter, K., Sundin, G. W., Zhao, Y., Stockwell, V. O., Sellmann, J., Flachowsky, H., Hanke, M. V., & Peil, A. (2018). Inoculation of *Malus* genotypes with a set of *Erwinia amylovora* strains indicates a gene-for-gene relationship between the effector gene *eop1* and both *Malus floribunda* 821 and *Malus* 'Evereste'. *Plant Pathology*, *67*(4), 938-947. https://doi.org/10.1111/ppa.12784

Wu, C. H., Abd-El-Haliem, A., Bozkurt, T. O., Belhaj, K., Terauchi, R., Vossen, J. H., & Kamoun, S. (2017). NLR network mediates immunity to diverse plant pathogens. *Proc Natl Acad Sci U S A*, *114*(30), 8113-8118. https://doi.org/10.1073/pnas.1702041114

Xin, X. F., Nomura, K., Ding, X., Chen, X., Wang, K., Aung, K., Uribe, F., Rosa, B., Yao, J., Chen, J., & He, S. Y. (2015). Pseudomonas syringae Effector Avirulence Protein E Localizes to the Host Plasma Membrane and Down-Regulates the Expression of the NONRACE-SPECIFIC DISEASE

RESISTANCE1/HARPIN-INDUCED1-LIKE13 Gene Required for Antibacterial Immunity in Arabidopsis. *Plant Physiol*, *169*(1), 793-802. https://doi.org/10.1104/pp.15.00547

Yanisch-Perron, C., Vieira, J., & Messing, J. (1985). Improved M13 phage cloning vectors and host strains: nucleotide sequences of the M13mp18 and pUC19 vectors. *Gene*, *33*(1), 103-119. https://doi.org/10.1016/0378-1119(85)90120-9

Yoon, M., & Rikkerink, E. H. A. (2020). Rpa1 mediates an immune response to avrRpm1(Psa) and confers resistance against Pseudomonas syringae pv. actinidiae. *Plant J*, *102*(4), 688-702. https://doi.org/10.1111/tpj.14654

Yuan, M., Jiang, Z., Bi, G., Nomura, K., Liu, M., Wang, Y., Cai, B., Zhou, J. M., He, S. Y., & Xin, X. F. (2021). Pattern-recognition receptors are required for NLR-mediated plant immunity. *Nature*, *592*(7852), 105-109. https://doi.org/10.1038/s41586-021-03316-6

Yuan, X. C., Hulin, M. T., & Sundin, G. W. (2021). Effectors, chaperones, and harpins of the Type III secretion system in the fire blight pathogen *Erwinia amylovora*: a review. *Journal of Plant Pathology*, *103*(Suppl 1), 25-39. https://doi.org/10.1007/s42161-020-00623-1

Zhang, Y., & Geider, K. (1997). Differentiation of *Erwinia amylovora* strains by pulsed-field gel electrophoresis. *Appl Environ Microbiol*, *63*(11), 4421-4426. https://doi.org/10.1128/aem.63.11.4421-4426.1997

Zhang, Y., & Qiu, S. (2015). Examining phylogenetic relationships of *Erwinia* and *Pantoea* species using whole genome sequence data. *Antonie van Leeuwenhoek*, *108*(5), 1037-1046. https://doi.org/10.1007/s10482-015-0556-6

Zhang, Z. M., Ma, K. W., Yuan, S., Luo, Y., Jiang, S., Hawara, E., Pan, S., Ma, W., & Song, J. (2016). Structure of a pathogen effector reveals the enzymatic mechanism of a novel acetyltransferase family. *Nat Struct Mol Biol*, *23*(9), 847-852. https://doi.org/10.1038/nsmb.3279

Zhao, Y. (2014). Genomics of *Erwinia amylovora* and Related *Erwinia* Species Associated with Pome Fruit Trees. In D. C. Gross, A. Lichens-Park, & C. Kole (Eds.), *Genomics of Plant-Associated Bacteria* (pp. 1-36). Springer Berlin Heidelberg. https://doi.org/10.1007/978-3-642-55378-3_1

Zhao, Y., Blumer, S. E., & Sundin, G. W. (2005). Identification of Erwinia amylovora genes induced during infection of immature pear tissue. *J Bacteriol*, *187*(23), 8088-8103. https://doi.org/10.1128/JB.187.23.8088-8103.2005

Zhao, Y., He, S. Y., & Sundin, G. W. (2006). The Erwinia amylovora avrRpt2EA gene contributes to virulence on pear and AvrRpt2EA is recognized by Arabidopsis RPS2 when expressed in pseudomonas syringae. *Molecular plant-microbe interactions : MPMI*, *19*(6), 644-654. https://doi.org/10.1094/MPMI-19-0644

Zhao, Y., & Qi, M. (2011). Comparative Genomics of *Erwinia amylovora* and Related *Erwinia* Species—What do We Learn? *Genes*, *2*(3), 627-639. https://doi.org/doi:10.3390/genes2030627

Zhao, Y. Q., Tian, Y. L., Wang, L. M., Geng, G. M., Zhao, W. J., Hu, B. S., & Zhao, Y. F. (2019). Fire blight disease, a fast-approaching threat to apple and pear production in China. *Journal of Integrative Agriculture*, *18*(4), 815-820. https://doi.org/10.1016/S2095-3119(18)62033-7

Zhou, H., Lin, J., Johnson, A., Morgan, R. L., Zhong, W., & Ma, W. (2011). Pseudomonas syringae type III effector HopZ1 targets a host enzyme to suppress isoflavone biosynthesis and promote infection in soybean. *Cell Host Microbe*, *9*(3), 177-186. https://doi.org/10.1016/j.chom.2011.02.007

Zipfel, C. (2014). Plant pattern-recognition receptors. *Trends Immunol*, *35*(7), 345-351. https://doi.org/10.1016/j.it.2014.05.004

Zipfel, C., & Robatzek, S. (2010). Pathogen-associated molecular pattern-triggered immunity: veni, vidi...? *Plant Physiol*, *154*(2), 551-554. https://doi.org/10.1104/pp.110.161547

Zwet, T. v. d., & Keil, H. L. (1979). *Fire blight, a bacterial disease of Rosaceous plants*. USDA. https://www.cabdirect.org/cabdirect/abstract/19790375755